# Geotechnical Characterisation of Oil Sand Tailings Beach Deposits in Flume Tests

by

William Anglow Kouakou

A thesis submitted in partial fulfillment of the requirements for the degree of

Master of Science

in

Geotechnical Engineering

Department of Civil and Environmental Engineering
University of Alberta

## ABSTRACT

In recent years, the oil sands industry has been investigating alternatives to the conventional tailings management practice to address the accumulation of large volumes of mature fine tailings (MFT) and abide by new government regulations in the province of Alberta. The main goals are to achieve a 50% total fines capture and a minimum undrained shear strength gain of 5 kPa in one year for the deposited material in the dedicated oil sand tailings disposal area (DDA).

TOTAL E&P Canada Ltd. is performing beaching studies in test flumes using MFT based slurries with different sand to fines ratio (SFR) at the Saskatchewan Research Council (SRC) facility in Saskatoon, SK. This thesis presents the results of the field and laboratory investigations which were implemented to analyse the fines capture of the resulting flume deposits. The beach materials were essentially silty sands and captured 9% - 17% fines. Vertical sorting and the distribution of fines particle along the slope of the beach were also observed throughout the deposits. The amount of fines captured was function of the slope of the beach deposits. The flume deposit with lower slope (i.e., 0.5%) captured 17% of fines as compared to 9% for the deposit with the highest slope (i.e., 8%). Additionally, the fines content was observed to increase with increasing distance away from the discharge point towards the toe of the beach slope. The magnitudes of in-situ and laboratory hydraulic conductivities (ks) were in the range of $1\times10^{-6}$ m/s - $1\times10^{-8}$ m/s and varied with respect to the fines content distribution. In general, the magnitudes of the vertical and horizontal ks were close to each other. A comparison of results from particle size distribution (PSD), soil water characteristic curves (SWCC) and associated drying curves indicated that the behaviour of the flume deposits was within the envelope of Devon silt (upper boundary) and typical tailings beach sand (lower boundary) samples. It was observed that the flume deposits exhibited both contractile and dilatant behaviours during direct shear tests with mean peak and residual friction angles of 38° and 33° respectively. Large strain consolidation tests highlighted the low compressibility of the flume deposits with about 1% change in void ratio with little change noted in k. Results of this study are of value for the oil sands industry for the management and modelling of the behaviour of deposited tailings.

**ACKNOWLEDGEMENTS**

First and foremost, I would like to thank God, my Father and my Creator for giving me the opportunity to work on this research project and overseeing it through to its completion. Thank you Lord for everything You have given me and the expertise that you allowed me to develop through this research program. I am thankful for my family who has always supported me and never stopped pushing me forward; this is for you Mom and Mamarie!

I would like to thank Drs. Ward Wilson and Dave Sego for welcoming me in their research group and trusting me with this project. I would particularly like to extend my gratitude to Dr. Louis Kabwe for his help with field and laboratory investigations, and for his unconditional assistance and guidance every step of the way; thank you Sir for your patience, understanding and mentoring.

Thank you to Christine Hereygers and Steve Gamble at the University of Alberta for the acquisition of field supplies and their assistance with laboratory experimentations.

Thank you to Sun Ruijun, Ian Betz, Marc Monroe and the entire staff at the Saskatchewan Research Center for welcoming us and helping with the field investigations.

Special thanks to Vivian Giang at the University of Alberta for the proofing, formatting and submission of my conference paper on very short notice; thank you also to Sally Petaske for always being available whenever I had concerns or needed advice throughout my time in the department.

Finally, I would like to thank the Geotechnical group of the University of Alberta and my fellow graduate students, particularly Mathew Long, Aileen Cash and Chao Kang. It was a good run.

Olivia, Nelly and David: I did it!

## CONTENTS

## LIST OF TABLES

## LIST OF FIGURES

# I. CHAPTER 1. INTRODUCTION

## 1.1 Overview of Oil Sands Operations

Oil sands (or Tar sands) are sand deposits that are saturated with dense petroleum of very high molar mass and viscosity referred to as bitumen (Masliyah et al. 2004). The province of Alberta houses the largest bitumen deposits in the world in the Peace River, Cold Lake and Athabasca regions, where it used to produce synthetic crude oil (Chalaturnyk et al. 2002). Oil sand deposits in Alberta are variable in quality and thickness and contain water, silt and clay in various proportions. Chalaturnyk et al. (2002) characterised the overburden of the oil sand deposits in Alberta as being comprised of muskeg glacial till and Cretaceous bedrock. With increasing oil prices, it is projected that the oil sand exploitation will account for more than 50% of Canada's oil production (Masliyah et al. 2004). Because of its density and high viscosity, bitumen in its natural state is not suitable for conventional oil recovery and transport methods. The bitumen recovery process involves many treatment options for an economically viable recovery. The chemical aspects of water based bitumen separation and recovery from the sand matrix are provided by Masliyah et al. (2004) and Liu et al. (2005). More information regarding bitumen recovery processes can be found in Shah et al. (2010). Two common bitumen extraction techniques are the hot water extraction process (HWEP) and the steam assisted gravity drainage (SAGD).

### 1.1.1 Hot Water Extraction Process

The hot water extraction process (HWEP) involves the addition of hot water and a caustic agent to the mined oil sand ore to separate and release the bitumen. Camp (1977) describes four stages in the hot water extraction of bitumen; 1) the Conditioning step where the bitumen separates from sand grains forming a pulp as the oil sand ore, water and caustic agent mixture is heated with open steam;

2) the Separation step in settling vessels, where the bitumen floats to the surface forming a froth; 3) the Scavenging step in scavenger cells, where the middling stream from the primary separation vessel is treated using air flotation for the recovery of incremental amounts of bitumen; and 4) the Extraction step where the bitumen froth is diluted and treated to yield a pure bitumen which is transported to upgrading and refining facilities.

In the separation step, the bitumen froth is skimmed from the top of the settling vessel while the coarse material settles rapidly and constitutes the coarse tailings stream. The efficiency of the settling process depends on the feed fines content, viscosity of the middling and the amount of water used. After dilution of the froth in the extraction stage, pure bitumen is primarily obtained through centrifugation of the bitumen froth. Additional tailings streams produced from the froth treatment and secondary separation vessels are combined to the coarse tailings stream to form total tailings which are conveyed to disposal sites. Efficiencies of 90% or greater have been reported for recovery of bitumen from oil sand ores using the HWEP (Chalaturnyk et al. 2002, Shah et al. 2010)

### 1.1.2 Steam Assisted Gravity Drainage (SAGD) Extraction

A significant portion of the oil sand ore deposit exists at depths that are not suitable for strip mining operations. In-situ bitumen recovery methods are therefore necessary to recover bitumen from such deep oil sand deposits. SAGD is an in-situ bitumen and heavy oil recovery method which involves the use of steam for the continuous drainage of the heated oil from the reservoir to a horizontal well (Butler 1981). In the context of bitumen extraction, a set of two parallel horizontal wells are used for SAGD. Steam is injected in the deposit through the upper injection well near the bottom of the reservoir. A steam chamber will form above the well as the heated oil and heavier condensate begin to flow downwards. The liquids are collected by the bottom production well and are pumped to the surface. The steam chamber expands upwards and sideways as increasing amounts of oil and condensate are recovered, leaving space for more steam to flow in the chamber. The steam flows through the sand in the chamber and condenses at the interface with the surrounding colder oil sand ore. The heat released is then transferred to the colder deposit and the process continues with heated oil and condensates at the interface flowing downwards by gravity to the production well. Butler (1981) provides a theoretical perspective and a numerical characterisation of the SAGD process. Bitumen recovery efficiencies in the range of 40% - 60% have achieved with SAGD but the method is not applicable to thin bitumen reservoirs. Environmental and economic considerations also limit the applicability of the method (Shah et al. 2010). However a combination of the process with upgrading operations such as gasification to produce gas for the steam generation for instance, can significantly reduce operational costs associated with SAGD. A schematic representation of a typical SAGD bitumen recovery operation is presented in Figure 1.

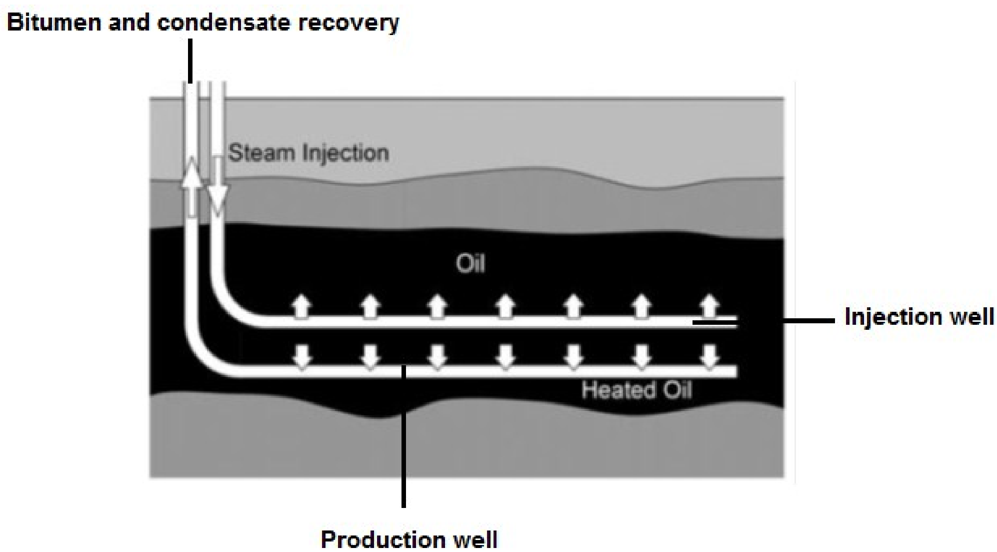


Figure I-1. Steam assisted gravity drainage (SAGD) operation for deep oil sand ore deposit (After Shah et al. 2010)

## 1.2 Oil Sand Tailings Management Issues and Presentation of the Problem

Because of its high efficiency rates, the HWEP is widely used in the processing of oil sand ores from surface mining. However, during the conditioning stage of the HWEP, deflocculation of the clay particles in the ore body is initiated. Naturally occurring clay aggregates are broken down and clays become dispersed in the resulting pulp and other process streams (Camp 1977). As a consequence, the HWEP produces high void ratio fine tailings that are very dispersed and composed primarily of silt, clay, residual bitumen and water. In the traditional discharge of oil sands total tailings streams in tailings ponds, segregation of the solids in the tailings slurry takes place. The sand fraction settles rapidly forming a gently sloping beach. The beach is typically compacted to form a containment dyke using various construction methods (Mittal and Morgenstern, 1975). Some fines in the tailings stream are captured by the beach material. The water containing suspended fines and residual bitumen flows to pond area where settling begins. These fluid fine tailings (FFT) reach a solids content of about 30% upon settling for two years and are then termed mature fine tailings (MFT). The large volumes of MFT generated exhibit low shear strength and will take years to consolidate, which increases the environmental footprint of the oil sands industry (Camp 1977, Dusseault and Scott 1983). The accumulation of MFT is a major concern as the stored MFT inventory is in the order of 720 million cubic meters (Miller 2009). This has prompted the Energy Resources and Conservation Board (ERCB, now Alberta Energy Regulator, AER) to devise stringent new regulations for the production and management of oil sands tailings. In essence, the quantity of FFT being generated must be reduced through capturing 50% of the fines in the tailings slurry feed deposited in dedicated disposal areas (ERCB 2009). Furthermore, minimum undrained shear strength of 5 kPa for the deposited tailings must be achieved within a year after deposition.

In order to meet regulatory demands, the oil sands industry has been intensively researching possible improvements to tailings management practices. Such improvements include the use of non-segregating composite and thickened tailings (TT) discharge (Matthews et al. 2002, Chalaturnyk et al. 2002) as well as heavy mineral recovery techniques from the tailings streams (Ciu et al. 2003). However, tailings are still mainly deposited as slurries, and the understanding of the depositional behaviour of the tailings slurry is of critical importance. Beach studies of deposited slurries have therefore become an integral part of tailings management practice. Such studies allow for the assessment of the fines captured, geotechnical properties and modelling of the behaviour of the deposited beach material for the safe operation and closure of the disposal facility. The reliability of flume tests for the study of tailings deposition and beach formation has been demonstrated by many authors (Blight et al. 1985, Küpper 1992, Miller et al. 2009).

In this context, TOTAL E&P Canada is conducting beach studies in test flumes using MFT with different sand to fines ratio (SFR) at the Saskatchewan Research Council (SRC) facilities in Saskatoon, SK. The resulting beach deposits in the test flumes were studied in this program.

## 1.3 Objectives and Scope of the Thesis

The main objective of this thesis was to examine the fines capture of the tailings flume deposits in TOTAL's beaching studies. For this purpose, the influence of the fines captured by the beach on the geotechnical properties of the deposited materials was evaluated through series of in-situ and laboratory investigations. In-situ tests were carried out directly in the flumes at SRC facilities. Laboratory experimentations were conducted at the University of Alberta Geotechnical Centre on undisturbed flume deposits samples obtained using an in-situ freezing technique, and on disturbed flume samples taken at key locations throughout the beach deposits. Differences between the compositions of the tailings feed slurry and their relationship with the characteristics of the resulting beach deposits were not considered in detail in this program. The specific objectives of the thesis were as follows:

- Design and completion of a testing program for the assessment of the in-situ hydraulic conductivity (k) and sampling of the beach deposits in the large scale flumes tests. Measurements of k were carried out in directions normal and parallel to the surface of the beach deposits to evaluate the vertical and horizontal ks respectively. Disturbed specimens and undisturbed frozen flume samples were acquired at specific locations in the flume deposits.

- Comparison of in-situ results with laboratory measurements of k conducted on the undisturbed flume deposits samples. The undisturbed samples were obtained upon the extraction and trimming of the frozen flume samples brought from SRC.

- Determination of the saturated and unsaturated geotechnical properties of the flume deposits in laboratory investigations. Particle size distribution, direct shear, soil water characteristic curve, drying tests and large strain consolidation were conducted on the flume specimens.

- Evaluation of the influence of the fines captured on the observed properties of the beach materials. Differences in the measured properties of the flume deposits were interpreted in terms of the changes in fines contents amongst the beach materials.

- Characterisation of the behaviour of the flume deposits. This was achieved through comparative studies with Devon silt and typical tailings beach sand samples.

## 1.4 Organisation of the Thesis

This thesis is divided in 6 chapters. In Chapter 1, an introduction to the oil sands exploitation and tailings management issues in the province of Alberta is provided. The tailings beach study topic is introduced and the thesis objectives are stated. A literature review comprising relevant background information and an overview of the previous research conducted was presented in Chapter 2. The experimental procedure was detailed in Chapter 3 with schematic representations of the flume deposits including in-situ test locations. A description and analysis of in-situ measurements of k carried out directly in the flumes at SRC were described in Chapter 4. The geotechnical properties of the flume deposits were also determined through laboratory tests. In Chapter 5, the objective was to characterise the behaviour of the tailings beach materials formed in the test flumes through comparative studies with Devon silt and typical coarse tailings beach sand samples. Large strain consolidation tests were also conducted on selected undisturbed flume samples. A summary of the main findings and suggestions for further studies were then provided in Chapter 6.

# II. CHAPTER 2. LITERATURE REVIEW AND BACKGROUND INFORMATION

## 2.1 Alternatives to Segregating Oil Sands Tailings Slurry Discharge

The generation of FFT from conventional bitumen extraction processes and new government regulations have prompted the oil sands industry to implement alternative tailings discharge methods. Such methods notably include the use of non-segregating composite and thickened tailings (TT) discharge (Matthews et al. 2002, Chalaturnyk et al. 2002) as well as heavy mineral recovery techniques from the tailings streams (Ciu et al. 2003). The main focus is to prevent or significantly reduce the generation of FFT upon deposition and maximise the amount of fines captured by the coarse fraction. Three alternative tailings management options will be considered here. The processes described below are not exclusive and can be combined with one another.

### 2.1.1 Thickened Tailings

The thickened tailings method involves the dewatering of the tailings stream to yield higher density and higher solids content materials for deposition in the disposal area. The densification of the tailings is achieved through the use of thickeners which are often installed at the disposal site to mitigate the high energy costs associated with pumping of such tailings. The technique was pioneered by Robinsky (1975), and results in a flat sloped conical tailings pile at the disposal site. A schematic representation of a typical thickened tailings conical pile is provided by Lighthall (1987).

Thickened tailings are normally discharged from a central elevated point. Low perimeter dykes are often used to contain the deposit and collect the decant water. Initially, tailings are thickened to a density which will allow the formation of flat slopes spreading to the final toe of cone. As more tailings are deposited, the thickener is operated so as to produce an underflow of increasingly higher density in order to steepen the cone. The point of discharge is thus raised as the thickened tailings accumulate and the slopes of the cone become increasingly steeper. Details of the operation of thickened tailings disposal facilities can be found in Lighthall (1987) who offers a review of the implementation of the thickened tailings discharge approach at two mine sites in Canada.

The thickened tailings discharge prevents segregation of the deposited slurry as the fine particles are trapped within the flowing tailings mass (Robinsky 1975). Other key advantages of the thickened tailings discharge include the opportunity to store larger tailings volumes, and a reduction in capital and reclamation costs of the mine operation (Robinsky 1975, Lighthall 1987). However, the adoption and application of the thickened tailings discharge are contingent upon the availability of a very flat topography and a sufficiently large containment area. It should also be ensured that the entire projected tailings volume can be stored in a cone with the maximum achievable slopes of the thickened tailings.

Modern thickening methods involving coagulants and flocculants have resulted in the emergence of paste tailings. Paste tailings refer to tailings that have been thickened to very high densities and do not release bleed water when deposited (Kwak et al. 2005). Paste tailings require a minimal amount of fines in order to retain enough water in the material for pipeline transport, and to permit flow or spreading into the disposal area. The disposal method of paste tailings follows that of thickened tailings. Once the deposited paste ceases to flow, drying and desiccation of the material occurs. Freshly deposited tailings then fill out the cracks of the underlying dry material forming a more stable structure in the conical pile. Nevertheless, the susceptibility of both thickened and paste tailing to liquefaction has been reported in the literature as a result of sufficiently high water contents (Poulos et al. 1985, Been et al. 2002).

### 2.1.2 Sub-Aerial Deposition

In the sub-aerial process, tailings are sequentially deposited in thin layers on a gently sloping beach (Lighthall 1987). The tailings slurry is discharged uniformly onto previously deposited tailings in a section of the beach, often with the use of spray bars. The newly deposited tailings layer is then allowed to settle and release water while the discharge is moved to another section of the beach. Drainage of the tailings layer occurs along the slope to a supernatant pond and through the voids and cracks of the underlying material. Further drying of the deposited tailings is achieved through evaporation as the slurry layer is exposed to atmospheric conditions. Consolidation is also enhanced due to the resulting suction that is generated during evaporation. The low gradients and resulting laminar flow of the deposited slurry layer, minimises the effects of particle segregation and transport. In other words, both coarse and fine particles are retained within the tailings deposit mass and the supernatant water collected is relatively clean.

Many factors affect the sub-aerial deposition process (Qiu and Sego, 1998). Qiu and Sego (2006) notably emphasized the need to assess the permeability, in both saturated and unsaturated conditions, compressibility and unsaturated properties to model the geotechnical behaviour of deposited tailings in sub-aerial deposition.

The higher placement density, consolidation and drainage of the tailings facilitate reclamation of the disposal site upon closure of the mining operation. The sub-aerial technique relies upon the effective drying of the deposited tailings which makes it suitable for applications in arid or semi-arid regions. Though, sub-aerial deposition has been successfully used in Canada for a long period of time as per the early report of Lighthall (1987).

### 2.1.3 Composite and Non-Segregating Tailings

Interest has grown towards the production of total oil sands tailings streams that do not segregate to ensure the continued use of hydraulic transportation, which is economically favourable. In the oil sands industry, the formation of non-segregating tailings (NST) involves the mixture of coarse and fine tailings. The relative proportions of the materials in the mixture are such that fine particles remain trapped within the coarse fraction upon deposition. The resulting tailings deposit exhibits better strength gain and consolidation as well as reduced water content in the tailings mass (Caughill 1993, Wong 2008). Furthermore, NST provides an opportunity to address the issue of the reclamation of current fine tailings inventory.

The addition of additives such as lime has been reported to yield NST mixtures (Caughill 1993, MacKinnon et al. 2001). In this regard, composite tails (CT) refer to NST mixtures often achieved with the use of coagulants and various additives. Mathews et al. (2002) defines CT technology at Syncrude, as a tailings management approach, whereby MFT is mixed with the coarse sand fraction to produce a non-segregating deposit with a coagulant aid. In general, three slurry manipulation routes were proposed to achieve a non-segregating tailings slurry: 1) an increase of the solids content through densification; 2) an increase in fines content through enrichment with settled fine tailings, i.e. MFT; 3) the use of the coagulants to shift the segregation boundary of the slurry mixture. These three options can be illustrated in Figure 1 as per the description proposed by Mathews et al. (2002). At point X, the composition of the untreated tailings slurry is below the segregation boundary, and the slurry will segregate. If the solids content of the slurry is increased without a change in the fines content (densification through thickeners or hydrocyclone), the slurry composition is be moved to point Y. the composition of the slurry at point Y is above the segregation line and the slurry will not segregate. Similarly, the enrichment of the slurry with fines without a change in the solids content will move the composition to point Z where the slurry becomes non-segregating. Finally, the use of a Gypsum coagulant will create a new segregation line for the slurry. In this scenario, the composition at point X is now above the segregation boundary and NST will be produced.

The main role of coagulants in the CT process is to change the properties of clays so as to promote their coagulation. This can be achieved through alterations of the PH, salinity and cation exchange of the CT mixture depending on the type of coagulant used (MacKinnon et al. 2001, Mathews et. al 2002).

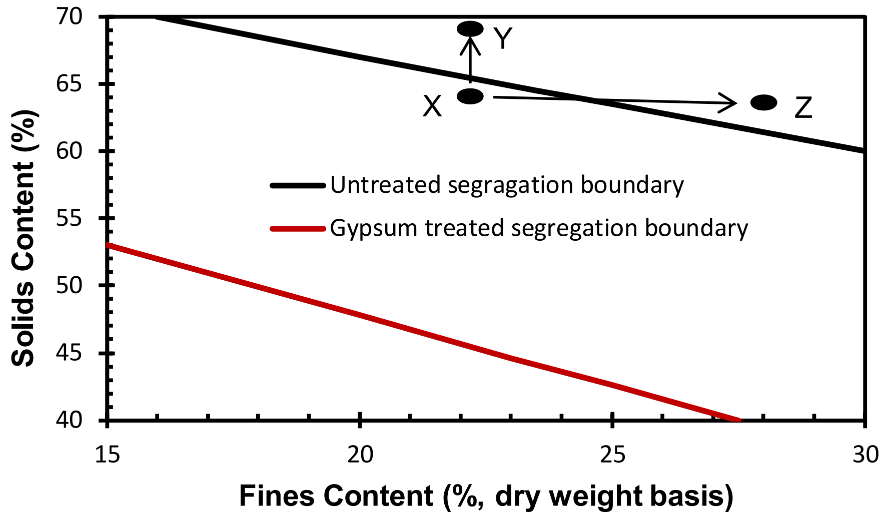


Figure II-1. Factors affecting the segregation of a tailings slurry mixture (After Mathews et al. 2002)

The discharge of CT and NST is an excellent alternative to segregating tailings slurries from the oil sand ore extraction process. Current volumes of MFT in tailing ponds can also be reduced through the use of MFT as the main constituent of the fines fraction in the NST / CT process. However the resulting deposited material remains soft for a variable period of time and requires containment. It has also been demonstrated by MacKinnon et al. (2001) that the composition of the water released from the CT deposit is affected by the nature of coagulant aid used. This may be an important issue if the water cannot be easily recycled as the water balance management is a crucial aspect of mining operations. In this project, MFT - fine sand mixtures were used as slurry feed materials for deposition in test flumes. The geotechnical properties of the resulting flume deposits will be considered in Chapters 4 and 5.

## 2.2 Factors Affecting the Permeability of Tailings

The permeability of a soil is defined as a measure of the capacity of the soil to allow fluid flow through its thickness. The permeability is often described with Darcy's law which relates the flow rate of fluid, q, travelling through a cross sectional area A of the soil, to the hydraulic gradient, i, in terms of the hydraulic conductivity, k (Head 1992):

$$q = kAi \quad [1]$$

The magnitude of k has been related to inherent properties of the soil such as mineralogy, void ratio, soil fabric, particle size and shape, as well as other factors including the nature of the fluid, temperature and degree of saturation (Head 1992, Benson and Trast 1995). An important aspect of oil sands tailings management is to assess the k of the tailings deposit to evaluate the consolidation rate and understand the consolidation behaviour of the material. The consolidation of oil sands tailings is often described in terms of the large strain consolidation theory (Gibson 1967), which requires both the void ratio-stress and void ratio-k relationships to be determined. Thus, it is crucial to understand the factors controlling k in tailings deposits. Furthermore, the evaluation of k can help the identification of potential instability issues related to increases in pore pressures at the tailings disposal site

For the purpose of improving the design of tailings dams, Mittal and Morgenstern (1975) devised laboratory and field testing procedures on tailings sands with a main focus on measurements of permeability and density. Laboratory measurements of permeability were carried out using a constant head test with a permeameter attached to a constant head source. Both, the influence of void ratio and fines content on k were investigated. Although a tendency of k to increase with respect to the void ratio could be deduced from the results, the authors observed no apparent trend between k and changes in fines content of the tailings sands. However, by plotting the permeability as a function of $D_{10}$, the particle size for which 10% of the soil is finer, a good agreement was found between the laboratory measured k and predictions made from Hazen's (1892) empirical relationship; wherein k, is related to the square of $D_{10}$ according to:

$$k = C_H \, {D_{10}}^2 \quad [2]$$

Where $C_H$ is Hazen's empirical coefficient. The authors thus reported a close correspondence between measured data and the k = $D_{10}^2$ straight line with the experimental data. As far as in situ tests were concerned, Mittal and Morgenstern used a constant head permeability apparatus feeding a piezometer standpipe to determine k for the deposited tailings sands. Results highlighted the importance of key factors such as the degree of saturation, stratification and structure of the material in situ, which are inherently linked to the method of deposition of the tailings. Further details pertaining to the test procedures and sample preparation used to yield the aforementioned results can be found in Mittal and Morgenstern (1975).

The relationship between k and particle size, especially in the fines fraction of a given soil, was further considered by Kenney et al. (1984), who investigated the effects of gradation and grain size on the permeability. With a focus on compacted granular materials, the authors identified a representative grain size $D_\alpha$, which effectively controls the size of the available flow channels in the void network of the soil, and in turn affects the magnitude of k. Other possible factors affecting k were also considered by the authors including the shape of soil particles, and the shape of the particle size distribution curve. Subsequent test results notably highlighted, that the latter had no significant influence on k, i.e. only negligible changes were observed upon measuring k for materials with distinct gradation curve shapes within the tested range of coefficient of uniformity Cu = 1 - 6. The authors concluded that the representative grain size controlling k was approximately for $D_\alpha = D_5$ or $D_{10}$, emphasising the importance of the proportion of small particles in the soil matrix, as these particles determine the size of the pore channels.

Juang and Holtz (1986a) considered the influence of the soil fabric on k in terms of the compaction effort, pore size distribution and the resulting pore size density function. Mercury intrusion porosimetry (Juang and Holtz, 1986b) was used to yield the pore size distribution of both sand and sand/clay mixtures tested, from which the pore size density function could be derived. In general, k was found to decrease with increasing compaction effort and water content from dry to optimum for the sand/clay mixtures. The large pore mode of the resulting bimodal pore size density functions was essentially found to be affected by changes in compaction variables. The large pore mode corresponded to the occurrence of a peak in the pore size density function for the larger portion of the apparent pore diameter abscissa. In contrast, a peak in the smaller apparent pore size of the density function characterised the small pore mode, thus defining a bimodal pore size distribution function. A notable observation made by the authors was, that the large pore mode of the pore size distribution function decreased with increasing clay content of the sandy mixtures whilst the small pore mode remained unaffected. This suggested the migration of clay-sized particles to the readily available space within larger pores, which affects the fluid flow channel network and subsequently the permeability.

Suthaker and Scott (1996) reported that the k of oil sand tailings is dependent upon the bitumen content and hydraulic gradient (i) in their study of both fine tailings and fine tailings-sand mixtures. Using a slurry consolidometer, the authors conducted constant head k measurements on both tailings samples with or without their bitumen content removed. It was found that the k for bitumen-removed fine tailings was an upper bound for the k of the fine tailings. This observation suggested that the k of tailings and the rate of consolidation were expected to increase with the removal of bitumen from the tailings structure. Furthermore, the authors related the deformation of bitumen from seepage forces to the influence of the gradient i on the magnitude of k. a value of i less than 0.2 was suggested for reliable measurements of k for fine tailings. Laboratory investigations undertaken by Suthaker and Scott (1996) highlighted that the k of fine tailings-sand mixes was predominantly controlled by the fines fraction (i.e. fines content). The addition of chemicals to mixtures of fine tailings and sand, such as that carried out for NST, was also identified to affect k depending on the PH and coagulation mechanisms. Suthaker and Scott (1996) also provide a review of direct and indirect measurement methods for the k of oil sand tailings.

## 2.3 The Soil Water Characteristic Curve of Sandy Materials

Unsaturated behaviour is often described in terms of the soil water characteristic curve (SWCC) which contains information pertaining to various geotechnical properties of the soil (Barbour 1998, Fredlund 2000). Fredlund (2000) identified the net normal stress (i.e., the difference between total stress and pore-air pressure $U_a$) and the matric suction (i.e., the difference between $U_a$ and the pore-water pressure $U_w$) as being the most important state variables for an unsaturated soil. The SWCC relates the water content (gravimetric or volumetric) or the degree of saturation to the soil suction. The key parameters of the SWCC are the air entry value (AEV) and the residual suction. The AEV is defined as the suction at which the soil begins to desaturate as air first enters the largest pores. The soil proceeds to drain rapidly beyond the AEV until the residual water content is reached in the residual phase (Aubertin et al. 2003, Hong et al. 2004). The suction at the residual water content is termed the residual suction, $\Psi_r$. Excessive experimental costs and a variety of factors have long plagued the study of unsaturated soil properties in engineering practice (Fredlund 2000 and 2006). The SWCC has therefore become the driving force in the implementation of unsaturated soil mechanics as it can be readily determined at reduced costs and simple laboratory settings.

A detailed review of the historical perspective and evolution of the SWCC is provided by Barbour (1998). Following pioneering from Slichter (1897-1898) and King (1899), early investigations of soil physics and unsaturated soil properties focused on the capillary potential. Richard's (1928) connected a reservoir of water to a thin soil sample through a ceramic plate using a vacuum tank to put the reservoir water under tension. Haines (1927) and Childs (1940) considered the air-water interface within soil pores, specifically the differential pressure across the meniscus at the air-water interface, to describe the capillary potential. In this approach, a stable meniscus could be achieved at the air-water interface as a result of the matric suction on the pore water being balanced by the surface tension along the air-water contractile skin. The authors envisioned the air-water interface at the soil pore level as the air-water meniscus in a glass tube. Thus, the pore water network within the soil was analogous to a series of constant diameter capillary tubes. The air entry value could then be viewed as the magnitude of the matric suction at which drainage would begin in the capillary tubes of the largest diameter.

A number of measurement techniques and experimental procedures have been devised through the years to obtain the SWCC (Fredlund and Rahardjo 1993, Carter 1993, Marshall et al. 1996). Numerical and predictive models were subsequently developed for the SWCC, which could also be related to engineering properties such as the hydraulic conductivity (Van Genuchten 1980, Bumb et al. 1992, Fredlund et al. 1994).

Fredlund et al. (2002) investigated the relationship between the particle size distribution (PSD) of the soil and its associated SWCC. More specifically, a physic-empirical model was proposed to estimate the SWCC from the PSD assuming a packing arrangement to represent the porosity for particle sizes of the soil. Such method involved the partition of the PSD into small groups of uniform particle sizes. The basis of the model resides in the hypothesis that a unique desorption SWCC exists for each increment of uniform particle size group. Results from each group are then assembled to generate the estimated SWCC. However, the effects of soil fabric, stress history and confinement were not incorporated in the model. Fredlund et al. (2002) reported that the proposed model provided more accurate predictions of the AEV and slope of the SWCC than existing models. Though, the authors conceded that the estimation of the SWCC using this approach appeared to be more reliable for sands and silts.

The accuracy in the prediction of the SWCC from the PSD for sandy soils was further demonstrated by Hong et al. (2004). The authors studied the hysteresis of the SWCC occurring between drying and wetting processes for sandy soils. It was found that the magnitude of the AEV and $\Psi_r$ of the drying SWCC of the sandy specimens varied with changes in the particle diameter, i.e. $D_{10}$. Lower AEVs and residual suctions were indeed measured for coarser soil, which have a larger $D_{10}$. Similarly, the water entry value (i.e., the suction at which the water content begins to increase significantly) of the wetting SWCC was found to be lower for the coarser materials. The authors also observed that the shapes of the SWCCs were similar to the associated PSDs of the sandy materials. A steep slope on the PSD corresponded to a steep slope on the associated SWCC for a given soil sample. Additionally, the authors found a good agreement between estimated SWCC and test data for the sandy soils using the Fredlund et al. (2002) method, which was described earlier. It was therefore concluded that the SWCC could be predicted with reasonable accuracy from the associated PSD of sandy materials.

Aubertin et al. (2003) proposed a predictive model for the SWCC labelled the MK which is essentially based on modifications made to the model developed by Kovács (1981). In agreement with the conclusions drawn by Bear (1972), the authors characterised two types of forces governing the distribution and motion of water in throughout the unsaturated porous media, namely, adhesive and capillary forces. On the on hand, adhesive forces result from adsorption processes and molecular interactions between water and the soil particles which lead to water adhering to soil surfaces. A consequence of the action of such forces in the soil matrix would be to reduce available pore space which is required for water flow, thus decreasing its permeability in a saturated environment. On the other hand, capillary forces, which originate from surface tension at the air-water interface in the porous media as previously described, will tend to disappear in the saturated soil. In the unsaturated soil these two forces become complementary and soil properties become a function of the proportion of air and water and their relative amounts in pore spaces (Aubertin et al. 2003). In the original Kovács model (1981), capillary and adhesive forces are distinct and act simultaneously to create suction in the unsaturated media. This assumption serves as the basis for the equations derived for the prediction of the SWCC. However, Aubertin et al (2003) noted that some important parameters in the Kovács model (1981) could not be completely defined limiting its practical application. By introducing modified parameters, the authors could derive the MK model (Aubertin et al. 2003) to model the SWCC and extended its use to a variety of materials, including coarse and fine grained soils. Key redefined parameters included the residual suction ($\Psi_r$), which was expressed in terms of measurable material properties (Aubertin et al. 2003):

$$\Psi_r = \frac{0.42}{(eD_H)^{1.26}} \qquad [3]$$

Where e is the void ratio and $D_H$ is an equivalent particle diameter for a heterogeneous mixture (Aubertin et al., 1998) given by:

$$D_H = [1 + 1.17\, log(C_u)]\, D_{10} \qquad [4]$$

Where $D_{10}$ is the particle size for which 10% of the soil is finer, and $C_u$ is the coefficient of uniformity**.** Specific information and a more detailed description of both Kovács and MK model alongside their respective applications can be found in Kovács 1981, Aubertin et al. 1998 and 2003.

The unsaturated behaviour as described by the SWCC can also be related to evaporation test results. An important feature of evaporation tests is the ratio of actual evaporation (AE) to potential evaporation (PE). In their characterisation of evaporative fluxes from soil surfaces, Wilson et al. (1997) proposed the following relationship between AE/PE ratio, total suction at the evaporating soil surface, Ψ and relative humidity:

$$\frac{AE}{PE} = \left[\frac{e^{\left(\frac{\Psi\, g\, W_v}{RT}\right)} - h_a}{1 - h_a}\right] \qquad [5]$$

Where $h_\alpha$ is the relative humidity of the air above the evaporating surfaces; g is the acceleration due to gravity; $W_v$ is the molecular weight of water; R is the universal gas constant (8.314 $J.mol^{-1}.K^{-1}$) and T is the absolute temperature.
The evaporation rate at the surface of an unsaturated soil is a function of the vapour pressure at the surface and the saturation vapour pressure at the surface temperature (Granger and Gray 1989). Wilson et al. (1997) observed that the relative humidity only began to decrease substantially at suctions values beyond 3000 kPa which corresponded to a 98% relative humidity. This behaviour was observed during experimentations conducted on Regina clay, Beaver Creek sand and silt samples. The authors argued that the decrease in relative humidity resulted in a decline in vapour pressure at the surface which controlled the evaporation rate, highlighting the effect of suction on the actual rate of evaporation at the soil surface. Similar observations were made for the variations of the AE/PE ratio with suction beyond a magnitude of 3000 kPa for the applied suction. Furthermore, Wilson et al. (1997) stated that the controlling effect of suction on the normalised evaporation appears to be independent of moisture content, mineralogy and soil texture. Nonetheless, the authors acknowledged that the investigations were carried out on thin soil sections which could not

account for the influence of thickness on the evaporative fluxes at the soil surface.

## 2.4 Shear Strength Characteristics of Sandy Materials

The determination of shear strength parameters of sandy materials through shearing tests is well documented, especially in the assessment of liquefaction susceptibility. Salgado et al. (2000) investigated the influence of non-plastic fines, i.e. high silt content, on the stiffness and shear strength of Ottawa sand specimens. The authors noted that the stress-strain response of sand was dependent upon the relative density, effective stress state and intrinsic variables. Such variables included particle shape/size distribution, mineralogy and surface characteristics, which are translated into the friction angle, $\phi$, dilatancy parameters and maximum/minimum void ratios. Salgado et al. (2000) reported an increase in friction angle (both peak and critical state), dilatancy and shear strength with increasing fines content for Ottawa sand with 5% - 20% silt content.

The relationship between dilatancy and shear strength of sand has also been considered by many authors who investigated the correlation between dilatancy and friction angles (Taylor 1948, Bolton 1986, Schanz and Vermeer 1996). On the assumption that friction could be considered a source of energy dissipation in simple shear, Taylor (1948) expressed $\phi$ in terms of the critical state friction angle $\phi_c$, i.e. the friction angle when shear deformation proceeds without any further change in volume at critical state, and dilatancy angle $\Psi$:

$$\tan\varphi = \tan\varphi_c + \tan\Psi \qquad [6]$$

Bolton (1986) stated that data from drained plane strain compression tests suggested sands would dilate fully in rupture zones to reach critical state. Moreover, the peak strength was associated with the point of maximum rate of dilation. The author derived the following expression upon review of extensive strength and dilatancy data for sands in plain strain conditions based on Rowe's (1962) theory:

$$\varphi = \varphi_c + 0.8\,\Psi \qquad [7]$$

The stress dilatancy theory pioneered by Rowe (1962) and plastic strain rate models both played an important role in the understanding of liquefaction and flow failures in sands. Lade (1992) proposed the use of a non-associated flow rule to characterize volume change during shearing and define an instability region from triaxial tests effective stress paths. Such region of instability was defined as that within the effective stress failure line and the lower boundary for instability, i.e. the instability line. Results also showed that drained conditions were essential to ensure the stability of soils and prevent liquefaction. Due to their relatively low permeability, small changes in the stress regime in loose, sand and silt could produce undrained conditions and initiate instability of the soil mass. The contractive nature of loose sand was also linked to its liquefaction susceptibility. However, the author noted that instability, i.e. the inability to sustain the applied load, and failure were distinct aspects of soil behaviour. The former could be initiated without causing failure, or could exist well within the failure surface. Though, instability and failure could both lead to catastrophic events.

Yamamuro and Covert (2001) investigated the effect of non-plastic silt on the susceptibility of loose sands to monotonic and cyclic liquefaction. The introduction of 5% - 20% silt to loose sand samples was found to induce contractive behaviour, but only at the initial stages of shearing, i.e. at low axial strains. However, an increase in stress and larger strains mobilized the dilatant character of the larger sand grains causing a reversal of the volume change behaviour. It was speculated by the authors that this reverse volume change could explain the occurrence of static liquefaction observed at low axial strains and stress levels in the silty sand materials. Additionally, tests on loose Nevada sand with 40% silt indicated that the introduction of larger silt contents to the sand simply extended the contractive behaviour to larger axial strains until the aforementioned reversal occurred. The authors argued that this reverse volume change behaviour could be attributed to the change in configuration and structure during shearing as a result of the introduction of silt particles. Initially, the sand is more compressible and contractive at low stress and strain due to the presence of silt particles at contact points between the larger sand grains. Further increase in applied stress and strain, would then displace the silt particles into void spaces which leads to a stiffer particle structure. This change in configuration has the effect of promoting the dilatancy of the load bearing skeleton and interlocking of the sand grains leading to higher shear strength.

Been and Jefferies (2004) emphasized the need to investigate the stress-dilatancy relationship in liquefaction studies and extended the application of dilatancy theories to loose sands. In fact, the investigators reported that loose sand showed similar stress-dilatancy behaviour to that of dense sand upon drained triaxial shear tests. Considering that the stress-dilatancy concept was based on plastic strain rates, undrained shear tests carried out by the authors identified a limiting hardening mechanism for the onset of liquefaction in loose sand.

In summary, dilatancy and shear strength parameters play an important role in the understanding and modelling of the stability of loosely deposited sand deposits. The introduction of fine particles such as silt in the sand structure has also been associated with an increase in dilatancy and shear strength. However, the susceptibility of the sandy deposit to static liquefaction may be increased at low stress-strain levels. This is due to the higher compressibility of fine particles, which promotes contractive behaviour at the initial stages of shearing before dilatant behaviour is initiated at higher applied stress/strain.

## 2.5 Flume Tests

Flume tests provide many advantages in the management of mine tailings as they allow the study of the behaviour and characteristics of the deposited material in a controlled laboratory setting. Blight et al. (1985) showed that field conditions prevailing in the tailings beach could be adequately modelled to a smaller laboratory scale with the use of flume tests. The usefulness of depositional flumes for the study and characterisation of tailings beach profiles was also demonstrated. Such flume tests would require provisions to be made for the discharge of the tailings slurry into the flume at one end, and for the decanting of water from the other. The resulting plunge pool would then overflow, forming the model beach which was found to mirror the field beach profile provided the same material was used and deposited at similar solids content. The authors noted the effects of hydraulic sorting on the distribution of particles along the beach slope upon deposition. Fine particles migrated towards the pool at the toe of the slope while coarser particles remained near the point of deposition and outer slopes. The authors thus reported a gradient of permeability along the beach deposit slope, which explained the depression of the phreatic surface observed in tailings dams.

Fan and Masliyah (1990) used depositional flumes to study the development of transient tailings beach profiles with respect to the slurry discharge solids concentration and feed flow rate. Two types of flume tests were conducted by the authors. On the one hand, a fixed slurry solids concentration was maintained in the feed while different total slurry flow rates were applied during deposition. Results showed that the slurry flow rate during discharge mainly influenced the growth rate of the beach profile, but had a negligible effect on the beach slope. On the other hand, a constant discharge flow rate was used for different feed slurry solids concentrations. The authors observed that an increase in the feed solids concentration resulted in steeper slopes and higher growth rates for the beach profiles formed. Thus, the solids concentration, which was found to control both the slope angle and growth rate of the resulting beach profile, plays a key role in the tailings beach formation.

Küpper et al. (1992) also reported on the usefulness of flume deposition tests to stimulate the phenomena associated with hydraulic fills. Results from several flume tests conducted in different parts of the world were compared by the authors in terms of the feed material characteristics, grain size distribution, density and geometry of the resulting flume deposit. The tests were predominantly carried out on sandy materials and showed a tendency of the flume deposit slopes to increase with both slurry concentration and mean grain size. The flat slopes observed in some tests were attributed to high slurry flow rates and higher fines contents. Some anisotropy between vertical and horizontal permeabilities of the sand, i.e. $k_h/k_v$ ranging from 1 - 10, was reported in one flume tests upon laboratory measurements carried out on undisturbed flume samples. In general, the similarities in the behaviour of the flume deposited hydraulic fills were found to be consistent with field observations, despite differences in the flume testing procedures and parameters used. The suitability of flume tests to model hydraulic fill deposition of sandy materials could thus be demonstrated by the authors.

Miller et al. (2009) used flume deposition tests to assess the effects of caustic and non-caustic extraction techniques on the characteristics and geotechnical properties of hydraulically deposited oil sand tailings beach deposits. Similar observations were made by the authors regarding the influence of slurry concentration, flow rate and fines content on the geometry of the newly formed beach deposits in the flumes. Furthermore, an increase in fines content was observed with increasing distance from the discharge point as a result of hydraulic sorting and ponding near the downstream end of the flume. A characterisation of the flume runoff was also undertaken to further assess the differences between the two modes of extraction studied. However, the authors emphasised that such flume test results could not be used to make quantitative predictions regarding the behaviour of oil sands tailings beach deposits in the field. This is mostly due to the complexity and inconsistent nature of the variables that prevail in the context of the field deposition of oil sands tailings at a commercial scale.

Most of the published research on tailings beach deposits in flume tests has been largely focused towards the development of predictive models for the beach profile and geometry (Blight and Bentel 1983, Fan and Masliyah 1990, Fitton et al. 2006, Miller et al. 2009). Blight and Bentel (1983) notably pioneered a “master” profile for tailings beach deposits upon the investigation of six hydraulic fill platinum tailings dam:

$$\frac{h}{H} = \frac{d}{D}\left(1 - \frac{d}{D}\right)^{n} \qquad [8]$$

Where n is an exponent characteristic of the tailings deposit and the other parameters are defined as per Figure 2 below:

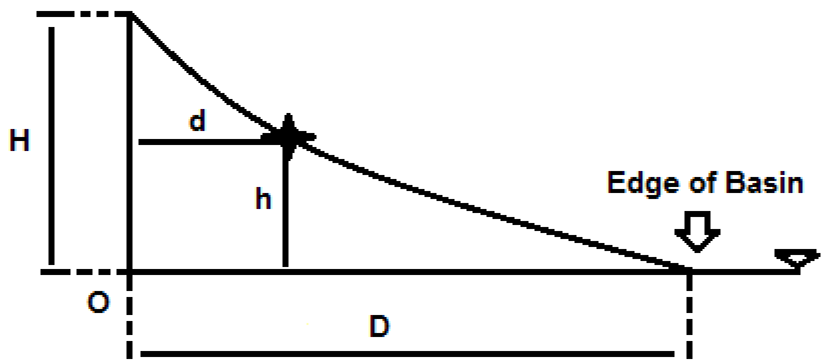


Figure II-2. Parameters in tailings beach master profile (After Blight and Bentel, 1983)

The validity and a possible application of this beach profile model were later demonstrated by Blight et al. (1985) in the comparison of laboratory deposited tailings beach profiles with those observed in actual hydraulic fill tailings dams.

Fitton et al. (2006) derived a semi-empirical beach slope model for non-segregating slurries based on channel flow behaviour and the rheological characteristics using flume tests. In sub-aerial discharge of tailings slurries, the slurry would spread into a flat sheet before forming an open channel that would flow (without deposition of particles) across previously deposited material until breaking out again into a wider sheet. It was speculated by the authors that, the slope of the self-forming channel dictated the overall slope of the tailings beach. Flume tests were devised to determine the self-forming channel equilibrium slope, defined as that at which no deposition or erosion of the underlying bed occurred. For this purpose, gold tailings slurries were discharged at various flow rates, slopes and concentrations into a 10 m long flume. From the flume test results, Fitton et al. (2006) expressed the equivalent slope percentage (s) for turbulent flow conditions using the Herschel-Bulkley rheological model:

$$s = 100 \tan \arcsin 0.073 V^2 \,/\, (Re_{HB})^{0.25} \;\; 2R_H g \qquad [9]$$

Where V is the average velocity in the channel, $Re_{HB}$ is the Reynolds number in a Herschel-Bulkley, $R_h$ is the hydraulic radius (cross-sectional area of flow divided by the wetted perimeter of that section) and g is the acceleration due to gravity. The authors also noted that the concave nature of the beach in non-segregating slurry could not be explained in terms of the effects of hydraulic sorting during deposition. Instead, it was asserted that the concavity of the beach was rather due to fluctuations in the slurry concentration or flow rate, which affected channel equilibrium slopes and in turn the overall beach profile of the deposited tailings.

In summary, general relationships between feed slurry parameters and geotechnical behaviour of hydraulically deposited materials can be qualitatively evaluated with flume deposition tests. Tailings beach studies in flume tests further highlight the possibility to design and engineer beach deposits by controlling deposition and slurry discharge parameters. However, the extrapolation of flume data to field conditions pose some challenges related to the difficulty to fully control field variables.

# III. CHAPTER 3. EXPERIMENTAL PROCEDURE

## 3.1 Flume Deposition

Mixtures of MFT, sand and process water were deposited into test flumes of rectangular cross sections at the Saskatchewan Research Council (SRC) facility in Saskatoon, SK. The tailings mixtures were discharged from spigots located at one end of the flumes. The runoff was removed from the opposite end, and the flumes were sealed afterwards. The newly formed beach deposits had slope angles between 0.5% to 9% and residual amounts of bitumen captured by the beach. Two types of flume were used in this study:

1) Type I wooden flumes, with dimensions of 0.4 m wide x 0.5 m height x 2.4 m length; 4 type I flume deposits were investigated, namely A1, A3, A5 and A13

2) Type II steel flume of dimensions 0.25 m wide x 0.5 m height x 8.0 m length. One type II flume deposit was studied and will be referred to as Pilot flume.

All five test flumes had rectangular cross sections. The flumes were saturated prior to in-situ measurements of k. Flume saturation procedures are presented in Appendix A. Test locations were selected depending on the space available along the surface of the deposit with respect to pre-existing test holes from SRC staff. A frozen flume deposit sample was obtained from each flume after in situ measurements were completed. Details regarding in-situ investigation methods are provided in Section 3.2. Locations for In-situ measurements and frozen sampling in the flume deposits will now be presented through schematic representations of the flumes.

### 3.1.1 Schematics and Test Locations in Flume A1

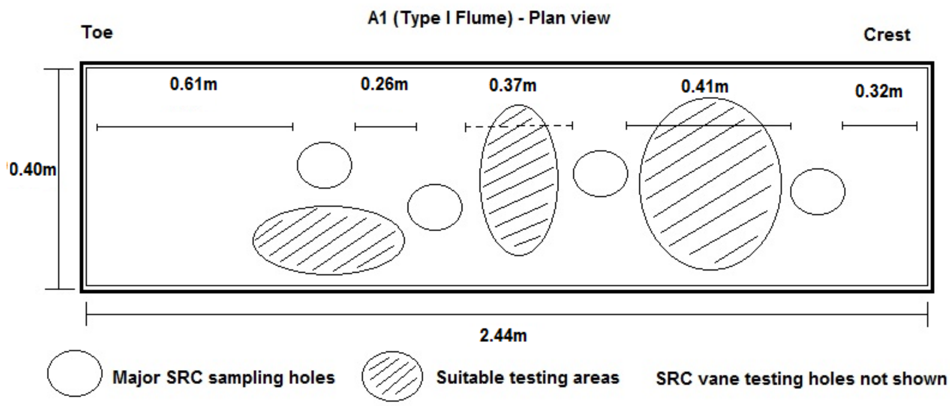


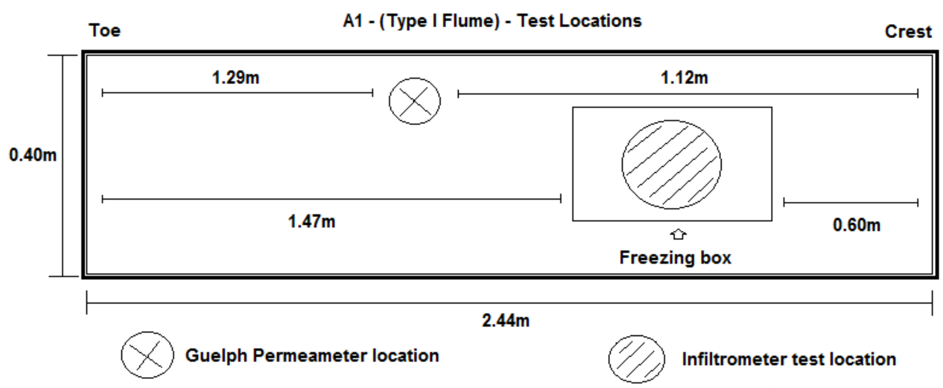


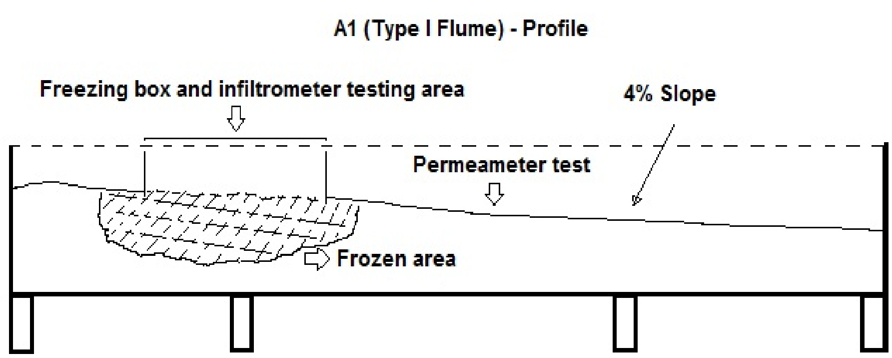


Figure III-1. Schematic representations of Flume A1 showing plan view (Top), test locations (Middle) and profile (Bottom) of the beach deposit.

### 3.1.2 Schematics and Test Locations in Flume A3

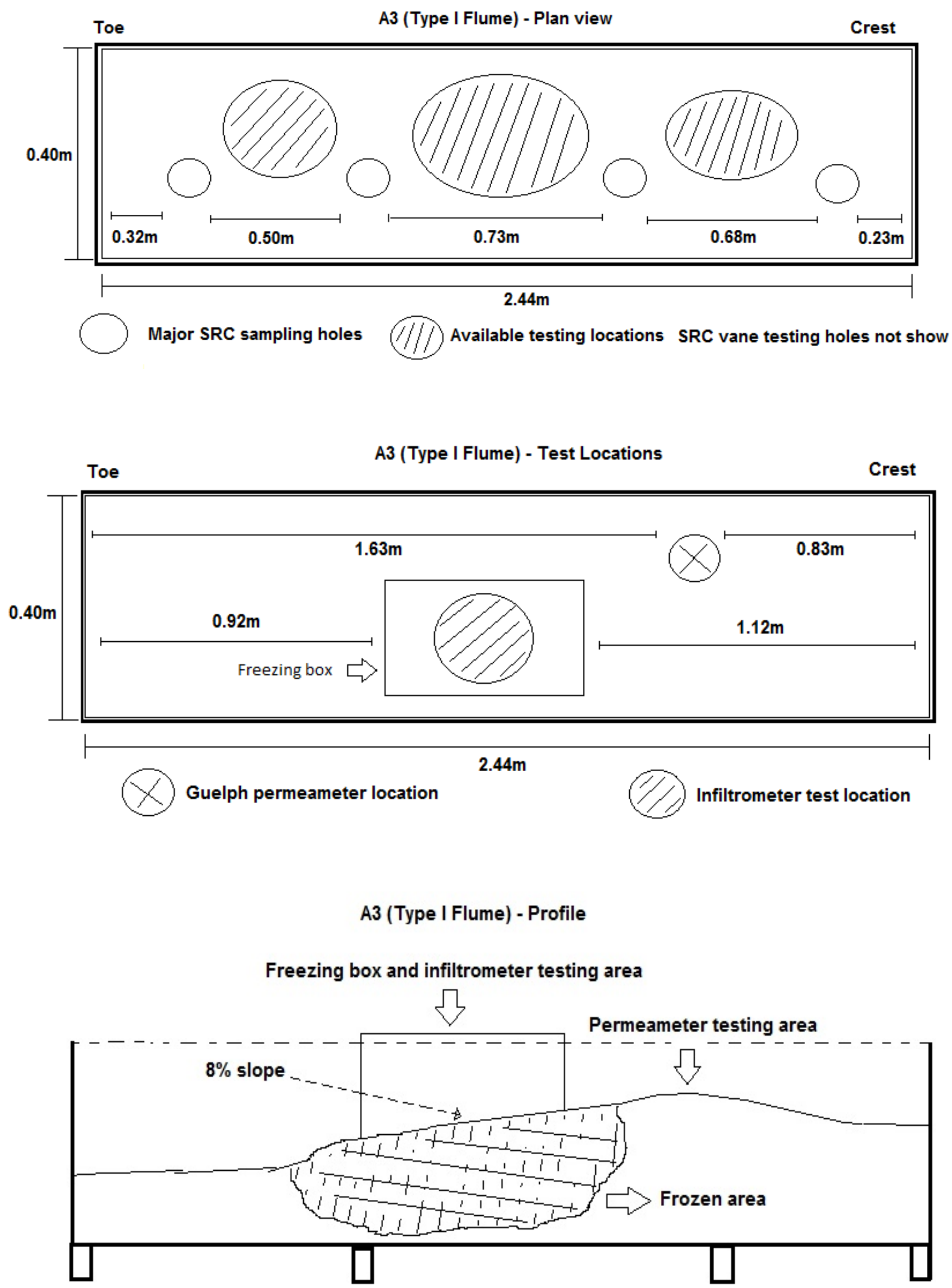


Figure III-2. Schematic representations of Flume A3 showing plan view (Top), test locations (Middle) and profile (Bottom) of the beach deposit.

### 3.1.3 Schematics and Test Locations in Flume A5

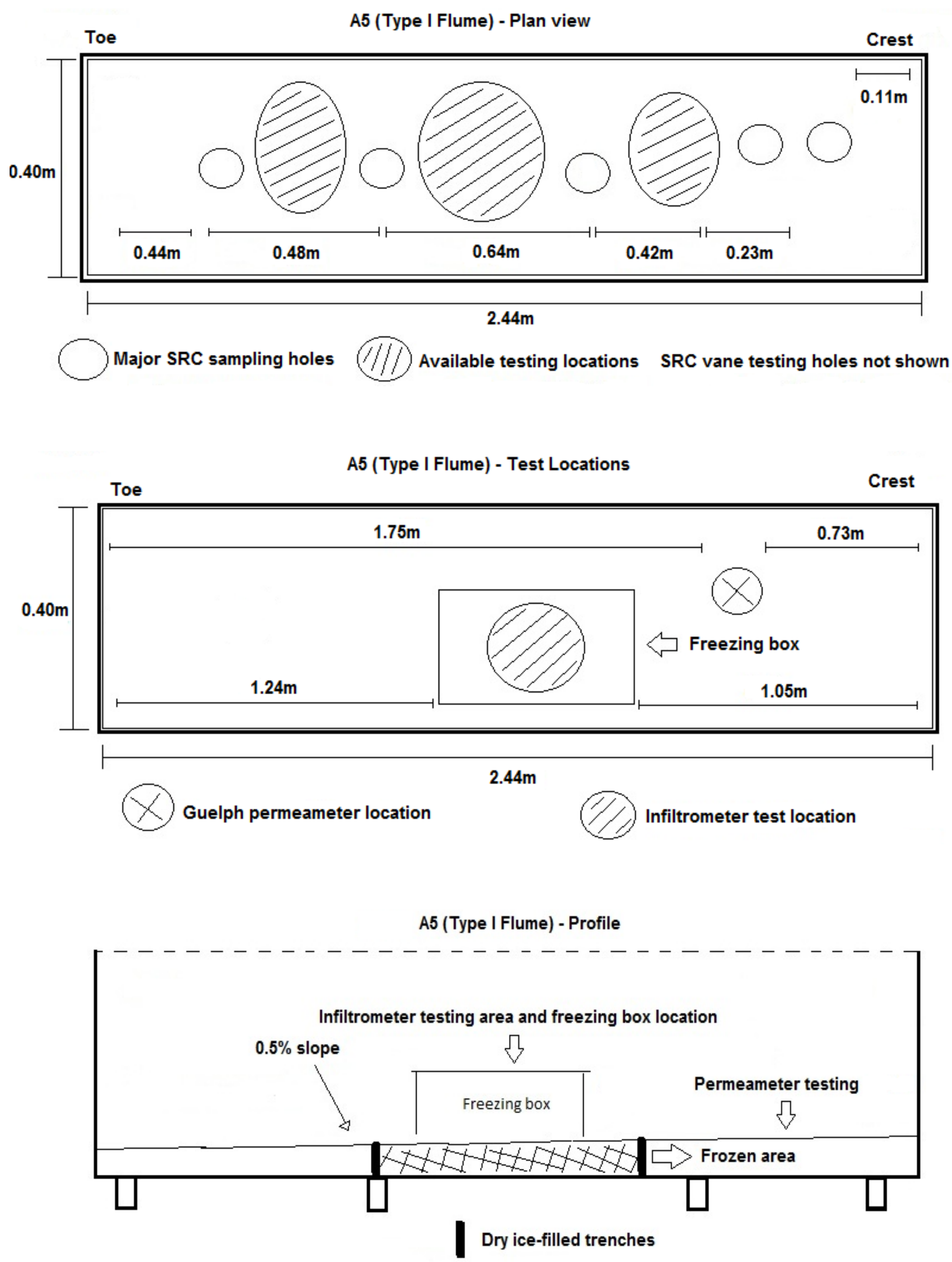


Figure III-3. Schematic representations of Flume A5 showing plan view (Top), test locations (Middle) and profile (Bottom) of the beach deposit.

### 3.1.4 Schematics and Test Locations in Flume A13

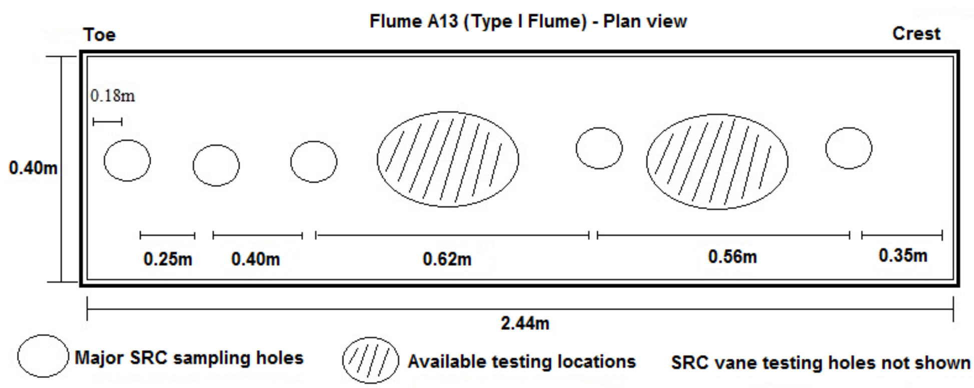


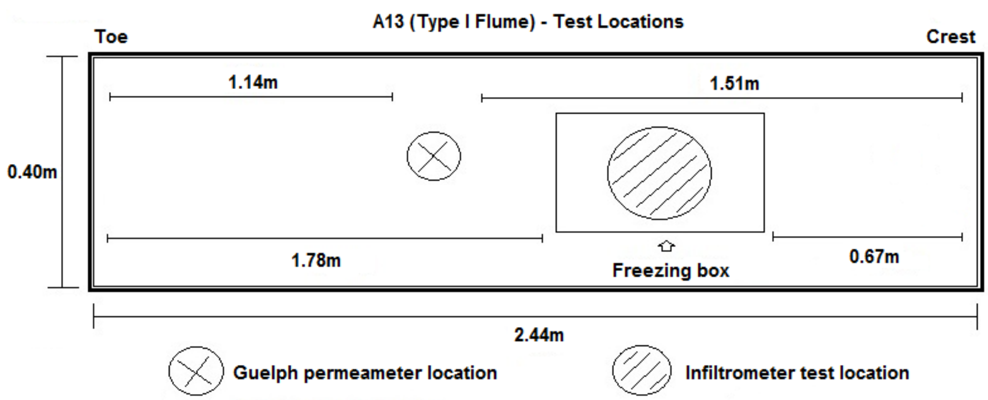


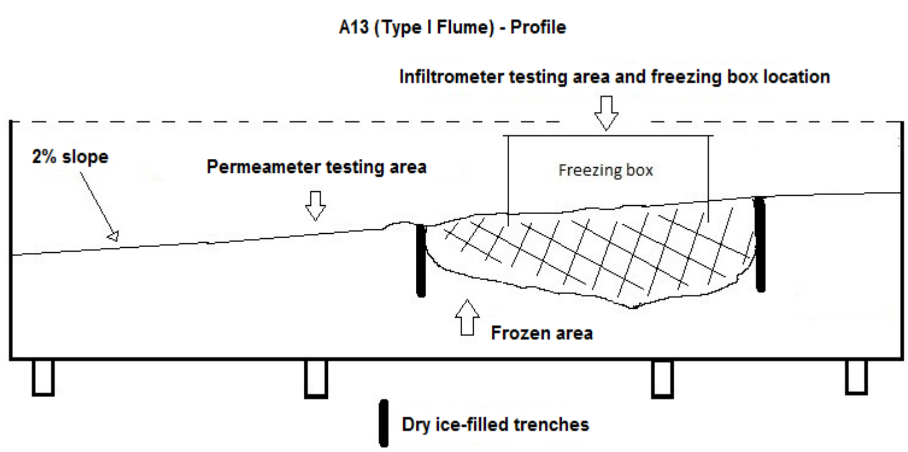


Figure III-4. Schematic representations of Flume A13 showing plan view (Top), test locations (Middle) and profile (Bottom) of the beach deposit.

3.1.5 Schematics and Test Locations in Pilot Flume

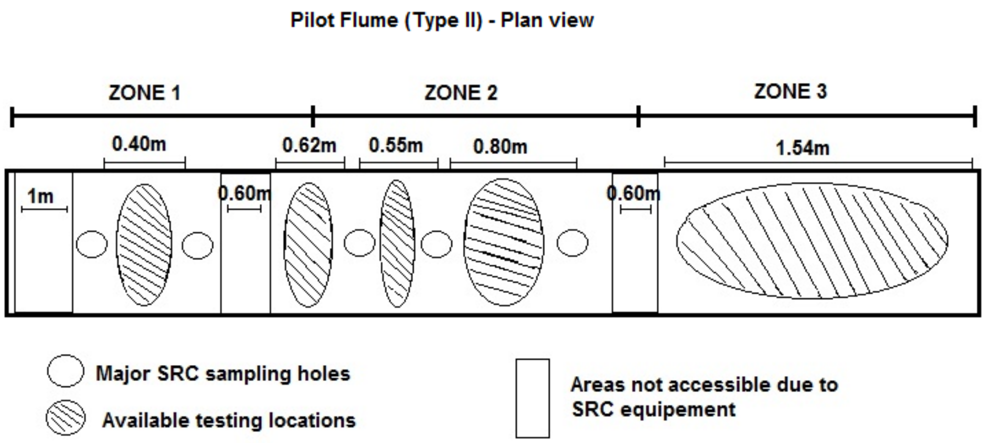


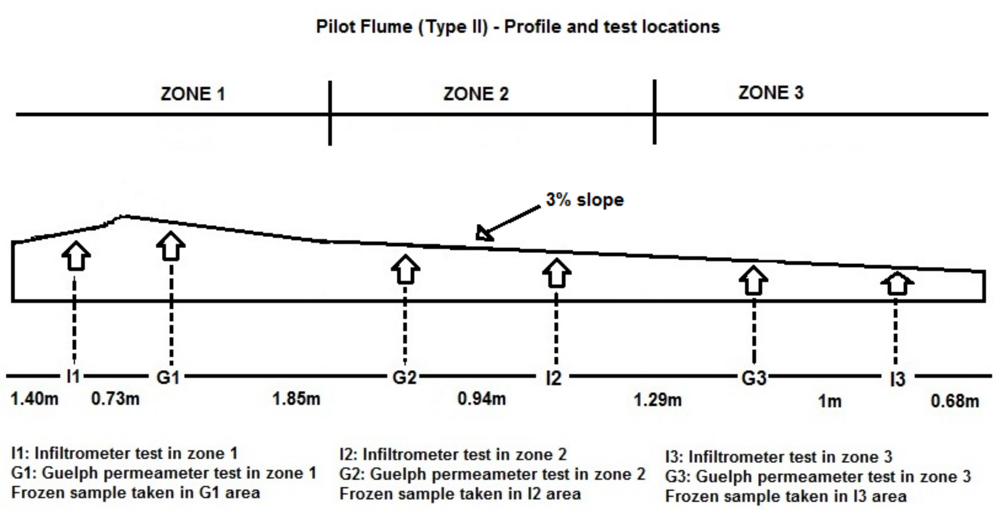


Figure III-5. Schematic representations of the Pilot flume showing plan view (Top), profile and test locations (Bottom) along the beach deposit.

## 3.2 In-Situ Investigation

### 3.2.1 Vertical Hydraulic Conductivity ($k_v$) Measurement

The double ring infiltrometer was used to measure the in-situ $k_v$ of the deposited beach materials in the direction normal to the beach surface. Measurements were carried out according to ASTM D3385. The double ring infiltrometer measures the infiltration capacity, which is an indication of the maximum infiltration rate at a given time. The infiltration capacity decreases over time until it reaches a constant value which is a measure of the saturated k of the soil tested. The infiltrometer rings are partially inserted into the soil and filled with water. The infiltration rate can therefore be monitored by recording changes in the inner ring water level over time. The larger outer ring provides a buffering effect to limit the lateral spread of water in the soil during the test, ensuring that $k_v$ is measured. Figure 6 shows a typical test setup for measurements of $k_v$ in the flumes with the double ring infiltrometer.

Figure III-6. Test setup for double ring infiltrometer measurements in Flume A5

For this testing program, a set of Mariotte bottles were used to maintain a constant water level in the rings and supply recharge water with constant head flow. The rate of infiltration of water through the flume deposits thus corresponded to changes in the water level of the bottles with time. The water level in the infiltrometer rings was monitored and recorded at regular time intervals. The infiltration capacity at a given time was obtained by dividing the water level change, i.e. the infiltration, by the corresponding time interval. The changes in infiltration capacity could then be plotted as a function of the cumulative test time. Double ring infiltrometer tests were run until steady state was reached to determine $k_v$ from the infiltration curve yielded at each test location.

### 3.2.2 Horizontal Hydraulic Conductivity ($k_h$) Measurement

The Guelph permeameter (Model 2800K1) was used to measure the $k_h$ of the deposited beach materials in the direction parallel to the beach surface. The device was inserted directly through the saturated deposit without the preparation of a borehole. This direct contact with the deposit allowed horizontal flow to be measured during the test as water was discharged radially from the sealed permeameter tip. A typical Guelph permeameter test setup in the flumes is presented in Figure 7.

The method involved measuring the steady-state rate of water recharged horizontally into the deposit while a constant head of water was maintained. Once the head of water was set by raising the air inlet tip of the permeameter, the water level was recorded at regular time intervals. The time interval between consecutive readings was gradually increased as the steady state was approached. Selected time intervals varied between 2 and 30 minutes during the test. The rate of fall of water, defined as the ratio of the change in water level to the corresponding time interval, was determined for each reading. Measurements were taken until the steady state rate of fall was reached with no further change in the rate of fall at the water head selected. The value of the steady state rate of fall was then used for calculations of the in-situ saturated $k_h$ for each flume deposit. The combined reservoirs mode and single-head procedure were used for measurements and calculations of $k_h$, which are detailed in Appendix A.

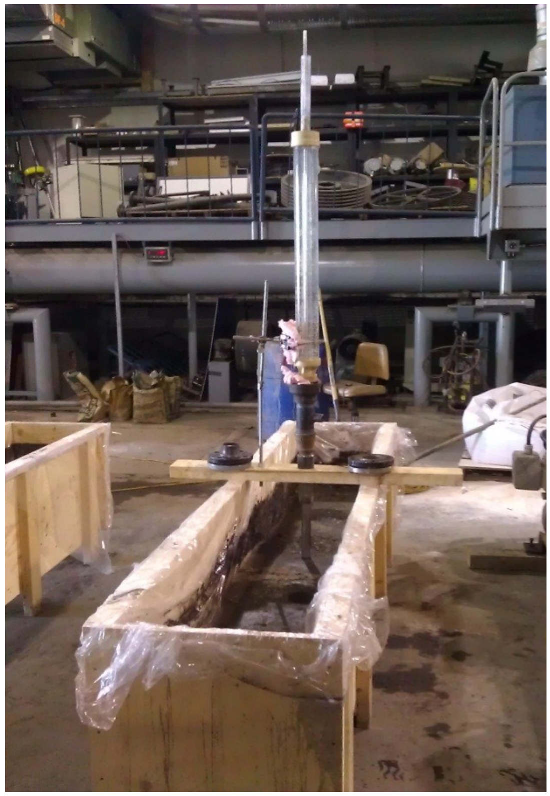

Figure III-7. Guelph permeameter test setup in Flume A13

### 3.2.3 Sampling Procedure

Frozen samples were retrieved from selected in-situ test areas once all in-situ tests were completed. An insulated box with an opened end was placed on the beach surface. The box was then filled with dry ice and sealed from the top to allow freezing of the underlying beach deposit. A combination of aluminum foil and fiberglass insulation was then used to further seal the box and insulate the area. Dry-ice filled trenches were often formed around the sampling area to shorten freezing time. Placement of the freezing box is illustrated in Figure 8 for flume A13. Depending on the thickness of the deposit, complete freezing of the area up to the target depth could be achieved within 5 - 6 hours for thinner deposits, or overnight within 16 hours. The resulting frozen blocks were then excavated, prepared for shipment in a freezer to the laboratory at the University of Alberta Geotechnical Centre.

Additionally, disturbed samples were collected from representative areas adjacent to test locations. Disturbed samples were also obtained from key areas selected in accordance with the variability of the beach slope profile and thickness of a given deposit in the test flumes. The disturbed samples were placed in air tight plastic freezer bags before being stored in coolers.

Figure III-8.  Freezing box setup; Placement of the box (Top) followed by filling with dry-ice pellets (Left) and sealing (Right) of the box. Fiberglass insulation and aluminum cover were added to promote the freezing process.

## 3.3 Laboratory Investigation

The laboratory-testing program was conducted at the University of Alberta Geotechnical Centre. The tests carried out included constant head k, particle size distribution, soil water characteristic curve, drying tests and direct shear. Undisturbed flume samples obtained from the frozen flume deposits and the disturbed flume samples described in Section 3.2 were used for the laboratory tests. Devon silt and coarse tailings beach sand samples were subjected to a number of similar laboratory tests for comparative purposes and to further characterize the behaviour of the beach samples. The tailing beach sand samples were the same as used by Kabwe et al. (2014). Large strain consolidation tests were also conducted on the undisturbed vertical core samples A3 and A5 which were used for constant head k measurements.

### 3.3.1 Preparation of Undisturbed Samples

A number of undisturbed frozen core samples were obtained from the frozen deposit blocks retrieved from the test flumes at SRC. Coring was carried out in directions normal and parallel to the beach deposit surface, i.e. in the vertical and horizontal directions respectively. Horizontal cores could not be retrieved from thinner frozen flume deposits. The frozen cores obtained were then trimmed using a soil lathe to a diameter of 10 cm for laboratory k measurements and consolidation tests. For the purpose of evaluating shear strength parameters, 6.3 cm diameter cores were prepared using the same procedure for direct shear tests. The frozen densities of the frozen cores were between 1.7 g/cm$^3$ and 1.9 g/cm$^3$. The undisturbed cores were allowed to thaw before testing was initiated. Dimensions of the trimmed frozen cores are provided in Appendix A.

### 3.3.2 Laboratory Hydraulic Conductivity (k) Measurement

Laboratory k measurements were carried out using large strain consolidation cells. The frozen cores were placed in the cells and allowed to thaw at room temperature for a period of 3 days. The cells were sealed during thawing to prevent any moisture loss. After thawing, the undisturbed samples were saturated with distilled water and later tested under a constant head flow condition following ASTM D2434. Both vertical and horizontal frozen flume samples were used for laboratory measurements of $k_v$ and $k_h$ respectively. This allowed for the comparison of laboratory data with the direct k measurements made in the flume beach deposits at SRC.

### 3.3.3 Particle Size Distribution (PSD)

Wet and dry sieving and hydrometer tests were conducted on the flume samples following ASTM D422-63. Wet sieving was carried out using warm water washing the sample over sieve #325 (0.044mm), until only a clear stream of water passed the mesh for a 500g flume deposit dry mass. The sieved sample was then oven dried for 24 hours, and the dry sample was brought to a mechanical sieve shaker for dry sieving in order to obtain the distribution of the coarser particles.

Separate samples were prepared for hydrometer tests with a 30g dry mass. Hydrometer tests were typically run for 32-36 hours to characterize the fines fraction of the beach deposits. Both dispersed, i.e. with the addition of 125ml of sodium metaphosphate (40g/l), and non-dispersed hydrometer tests were conducted. However, only non-dispersed hydrometer test results will be presented. Dispersed hydrometer test results are provided in Appendix B. After the laboratory k measurements were completed, both vertical and horizontal undisturbed core samples were also used for PSD tests. Additionally, the PSDs of Devon silt and tailings beach sand samples were determined for comparison with the flume deposits.

### 3.3.4 Soil Water Characteristic Curve Measurement

The soil water characteristic curve (SWCC) was measured for type I flume samples using an acrylic pressure plate device, i.e. Tempe cell, with 100 kPa (1 bar) ceramic high entry disc following standard methods (Fredlund and Rahardjo 1993). Air pressure is applied from the inlet located on top of the chamber. Once air is applied, an outlet located at the base plate underneath the high air entry disk allows the drainage of water from the specimen. The change in water content is measured by weighing the specimen and the cell after equilibrium is reached. The procedure is then repeated at progressively higher values of matric suctions. Once the highest pressure value is applied, the specimen is removed from the cell. The water content corresponding to the highest matric suction is measured by oven drying the specimen. This water content together with the previous changes in weight are used to back-calculate the water contents corresponding to the other suction values.

The matric suction is then plotted against corresponding water contents to give the SWCC. Disturbed bulk flume samples were used for SWCC measurements in Tempe cells. The SWCC of the coarse tailings beach sand sample was also determined. The mass of the empty Tempe cells was recorded before placement of the samples. After being placed in the cells, the samples were slowly saturated from the bottom by connecting the cell to a constant head source. The total mass, i.e. cell and saturated sample, was then measured and the aforementioned procedure was applied to yield the SWCC. The curve fit of experimental data was derived using SoilCover 2000 software.

### 3.3.5 Drying Tests

The evaporation tests were conducted in similar evaporation lysimeters (~180 mm in diameter) on flume deposit samples taken from the same batch as those used in the determination of the SWCC. Devon silt and coarse tailings beach sand samples were also included for comparative purposes. One lysimeter contained distilled water to determine the potential evaporation (PE), and the other lysimeters contained the deposit samples to determine the actual evaporation (AE). A controlled amount of water was added to each sample, and initial moisture contents were determined after mixing. Void ratio and moisture contents of the samples after mixing were presented in Table 1. The change in mass of each lysimeter was continually monitored to determine the rate of evaporation from the lysimeters. The temperature and relative humidity of the air above the evaporating surfaces were also monitored continuously. The test was completed when there was no change in mass. At the end of the test, samples were oven dried to determine the residual water content. The test setup is illustrated in Appendix C.

Table III-1. Characteristics of the lysimeters samples for drying tests

| Sample ID | Fines (%) | Clay (%) | Moisture content (%) | Solids content (%) | Void ratio |
|---|---|---|---|---|---|
| **A1** | 12.0 | 6.0 | 41.1 | 70.9 | 1.1 |
| **A3** | 9.0 | 5.5 | 40.8 | 71.0 | 1.1 |
| **A5** | 17.0 | 12.0 | 41.6 | 70.6 | 1.1 |
| **A13** | 11.5 | 8.0 | 42.8 | 70.0 | 1.1 |
| **Devon silt** | 100.0 | 30.0 | 47.3 | 67.9 | 1.2 |
| **Beach Sand** | 10.5 | / | 34.3 | 74.5 | 0.9 |

### 3.3.6 Direct Shear Tests

The frozen core samples trimmed to a diameter of 6.3 cm were used for direct shear tests. For each test, the frozen core was placed in the direct shear cell and allowed to thaw overnight with the housing reservoir filled with water. A strain rate of 0.003 in/min and a total travel distance of 10 mm were selected as test parameters. Normal stress magnitudes of 10, 25, 35 and 50 kPa were applied during direct shear testing. A normal stress magnitude of 75 kPa was used when necessary. The shear stress developed in the material was computed at regular time intervals, i.e. between 10 and 20 seconds. The change in height and horizontal displacement during shearing were also monitored. The peak and residual shear stresses were determined from the shear stress - horizontal displacement curves for each normal stress magnitude. The shear strength parameters were then obtained from the resulting failure envelopes in peak and residual conditions. Direct shear tests were also conducted on saturated tailings beach sand samples to determine the shear strength parameters in both peak and residual conditions with similar test parameters.

### 3.3.7 Large Strain Consolidation (LSC) Tests

The same undisturbed frozen cores acquired for the vertical k measurements, i.e. $k_h$, of A3 and A5 were used for LSC tests. The heights of the samples used were 6.6 cm and 5.7 cm for the flume deposits from A3 and A5 respectively. The diameter of the two cores was 10 cm. The frozen densities of the samples were between 1.6 $g/cm^3$ and 1.8 $g/cm^3$. The undisturbed cores were placed in the LSC cells and allowed to thaw for a period of 3 days before being saturated prior to the test. The magnitude of $k_h$ obtained from the procedure in Section 3.3.2 served as the initial k for the LSC test before the loading sequence was initiated. Additionally, constant head k measurements were made at the end of each loading step. This was to investigate both void ratio-effective stress and void ratio-k relationships as per the requirements of the LSC theory (Gibson et al.1967). LSC tests were conducted following the sequence of vertical stress application 0.4, 4.4, 10, 40, 80, 160, 280, 400 and 500 kPa.

# IV. CHAPTER 4. FIELD AND LABORATORY GEOTECHNICAL PROPERTIES OF OIL SANDS TAILINGS BEACH DEPOSITS IN FLUME TESTS

Paper accepted to the GeoRegina 2014 Conference in Regina, SK.

(The chapter suffix, i.e IV, was added to the numbering of Figures and Tables to match the organisation of the main body of the Thesis. The text however has not been amended and the conference paper formatting has been preserved)

# Field and laboratory geotechnical properties of oil sands tailings beach deposits in flume tests

William Anglow, G. Ward Wilson, Dave C. Sego & Louis K. Kabwe
*Department of Civil & Environmental Engineering – University of Alberta*
*Edmonton, Alberta, Canada*
Jianmin Kan
*TOTAL E&P Canada Ltd., Calgary, Alberta, Canada*

ABSTRACT
TOTAL E&P Canada Ltd. is performing beaching studies in test flumes using mature fine tailing (MFT) with different sand to fines ratio (SFR) at the Saskatchewan Research Council (SRC) facility in Saskatoon, SK. Results of measurements carried out on a test flume 0.25 m wide x 0.5 m height x 8.0 m length indicate that the fines content increases with increasing distance away from the discharge point (i.e., 11% fines at 2 m) to the toe of the beach slope (i.e., 15% fines at 7 m). Results also show that the hydraulic conductivity (k) measured at the same locations decreases with increasing fines content. A comparison of the in-situ data indicates that the k measured in the horizontal direction ($k_h$) was slightly lower (~2 times) than that measured in the vertical direction ($k_v$). A comparison of laboratory test data for undisturbed samples, however, does not show a significant difference between the measured $k_h$ and $k_v$. Results of the soil water characteristic curve (SWCC), drying test and direct shear measurements indicate that the beach deposits are characteristics of sand/silt materials with a slight difference in texture. Results of this study are of value for the oil sands industry for the disposal, management and modelling of hydraulically deposited oil sands tailings.

RÉSUMÉ
TOTAL E & P Canada Ltd. effectue des tests d'épandage en canaux inclinés pour les résidus fins d'extraction (MFT) avec différents rapports sable/fines (SFR) au Saskatchewan Research Council (SRC) à Saskatoon, SK. Les résultats des mesures effectuées sur un canal de 0,25 m de large x 0,5 m de haut x 8,0 m de long indiquent que la teneur en particules fines augmente avec la distance a partir du point d'alimentation de décharge (11% fines à 2 m) jusqu'au point de décharge du canal (15% fines à 7 m). Les résultats montrent également que la conductivité hydraulique (k), mesurée aux mêmes emplacements diminue avec l'augmentation de la teneur en particules fines. Une comparaison entre les données in-situ indique que k mesurée horizontalement ($k_h$) est légèrement 2 fois inférieure à celle mesurée verticalement ($k_v$). Cependant, une comparaison des données de laboratoire pour les échantillons non perturbés ne montre pas de différence significative entre $k_h$ et $k_v$. Les résultats de la courbe caractéristique de l'eau du sol (SWCC), des essais de séchage et de cisaillement direct indiquent que les dépôts d'épandage ont les caractéristiques similaires des matériaux sable/limon avec une légère différence dans leur texture. Les résultats de cette étude sont de valeur pour l'industrie des sables bitumineux pour l'entreposage, la gestion et la modélisation des résidus de sables bitumineux déchargés hydrauliquement.

## 1. INTRODUCTION

The disposal and reclamation of oil sands tailings have emerged in recent years as primary concerns governing the operations in the oil sands industry. Traditional disposal methods involved the discharge of total tailings in ponds and impoundments. Upon tailings deposition, the solids in the tailings stream segregate with the sand forming dykes and beaches, and about one-half of the fines and most of the water flowing into a tailings pond. Upon settling for two years these fluid fine tailings (FFT) reach a solids content of around 30% and are then termed mature fine tailings (MFT). The tailings are predominately medium-fine sand, but contain from 5% to 40% fine silt and clay and bitumen by mass. Concern about the growing volume of MFT resulted in the Energy Resources and Conservation Board (now Alberta Energy Regulator, AER) establishing new requirements for oil sands fine tailings (ERCB 2009). The objective was to reduce the amount of fluid tailings being produced by requiring 50% fines capture in dedicated disposal areas (DDAs). In light of this directive, the oil sands industry has been intensively researching possible improvements to tailings management practices, including the use of non-segregating composite and thickened tailings (TT) discharge (Matthews et al. 2002, Chalaturnyk et al. 2002) as well as heavy mineral recovery techniques from the tailings streams (Ciu et al. 2003). However, tailings are still mainly deposited as slurries, and the understanding of the depositional behaviour of the tailings slurry is of critical importance. Furthermore, the stability of the tailings beach formed upon deposition affects the integrity of the impoundment as a whole due to the susceptibility of the tailings sand to both static and cyclic liquefaction failures (Lade 1992, Pastor et al. 2002). Tailings beach studies have therefore become an integral part of the design and sustainable operation of tailings disposal sites.

Blight et al. (1985) showed that field conditions prevailing in the tailings beach could be adequately modelled to a smaller laboratory scale with the use of flume tests. The authors further highlighted the influence of the fines captured by the beach and their migration along the beach slope on the permeability of the deposit. Many authors have also reported a relationship between smaller particle sizes and the k based on Hazen's (1962) empirical formula (Mittal and Morgenstern 1975, Kenney 1984). Qiu and Sego (2006) emphasized the need to assess the permeability, in both saturated and unsaturated conditions, compressibility and unsaturated properties to model the geotechnical behaviour of deposited tailings in their evaluation of the sub-aerial deposition process.

The main objective of this paper is to examine the fines capture in TOTAL's beaching studies using MFT with different sand to fines ratio (SFR). The specific objectives are the determinations of field and laboratory geotechnical properties of the beach deposits.

## 2. FIELD PROGRAM

### 2.1 Plant Location

The flume tests were conducted at the Saskatchewan Research Council's (SRC) facilities in Saskatoon. Flume preparation details are provided in the next section.

### 2.2 Material and Methods

The materials deposited in the flume consisted of mixtures of MFT, fine sand and process water. Details of the feed materials used for deposition are given in Table 1. Two different flumes of rectangular cross sections were used, namely the type I wooden flumes (0.4 m wide x 0.5 m height x 2.4 m length) and type II pilot steel flume (0.25 m wide x 0.5 m height x 8.0 m length). The tailings mixtures were discharged from spigots located at one end of the flumes. The runoff was allowed to drain away from the opposite end, and the flumes were sealed afterwards. The newly formed beach deposits had both different slope angles (1% to 9% slope). The beach captured different proportions of fines and residual bitumen. The deposits were subsequently saturated before in-situ measurements were carried out directly in the flumes. A cross section of the type II flume deposit is shown in Figure 1. Because of its length, the type II flume was divided in three distinct tests zones which are referred to as zone 1, 2 and 3 as per the delineation shown in Figure 1.

Table IV-1. Composition of the tailings mixtures deposited into the test flumes

| Flume ID | Average Feed | | | Feed Fines | Feed Vol. |
|---|---|---|---|---|---|
| | Cw (w/w) | F/(F+W) (w/w) | SFR (w/w) | Captured (w/w) | Captured (v/v) |
| A1 (type I) | 0.6 | 0.1 | 9 | 0.7 | 0.6 |
| A3 (type I) | 0.6 | 0.1 | 6.5 | 0.5 | 0.6 |
| A5 (type I) | 0.5 | 0.2 | 5 | 0.2 | 0.2 |
| A13 (type I) | 0.5 | 0.1 | 9.5 | 0.6 | 0.6 |
| Pilot (type II) | 0.5 | 0.1 | 8 | 0.6 | 0.7 |

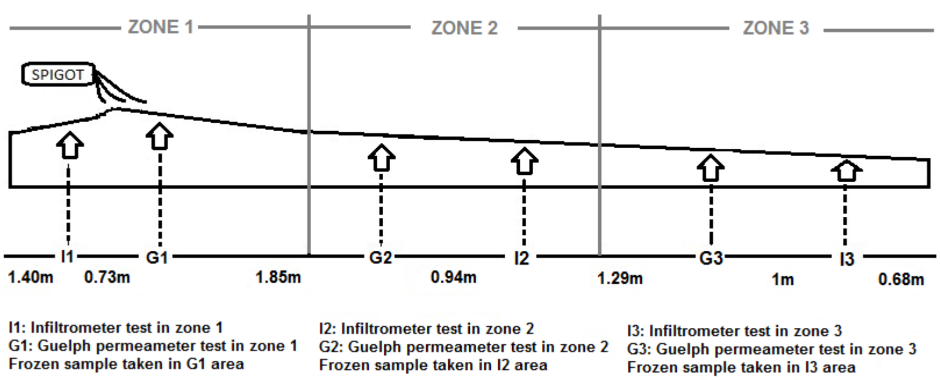


Figure IV-1. Testing locations in type II flume deposit

### 2.2.1 Double Ring Infiltrometer

The double ring infiltrometer was used to measure the in-situ $k_v$ of the deposited beach materials in the direction normal to the beach surface. Measurements were carried out according to ASTM D3385. A set of Mariotte bottles was used to supply water with flow at constant head for the duration of the test. Double ring infiltrometer tests were run for 4 to 5 hours until steady state was reached to determine $k_v$ at each test location

### 2.2.2 Guelph Permeameter

The Guelph permeameter (Model 2800K1) was used to measure the $k_h$ of the deposited beach materials in the direction parallel to the beach surface. The device was inserted directly through the saturated deposit without the preparation of a borehole. This direct contact with the deposit allowed horizontal flow to be measured during the test as water was discharged radially from the sealed permeameter tip. The method involved measuring the steady-state rate of water recharged horizontally into the deposit while a constant head of water was maintained

### 2.2.3 Sample Collection

Frozen samples were retrieved from selected in-situ test areas once all in-situ tests were completed. An insulated box with an opened end was placed on the beach surface. The box was then filled with dry ice and sealed from the top to allow freezing of the underlying beach deposit. The resulting frozen blocks were then excavated, prepared for shipment in a freezer to the laboratory at the University of Alberta Geotechnical Centre. Disturbed samples were also collected from representative areas adjacent to test locations along the slope of the beach profile. The disturbed samples were placed in air tight plastic bags before being stored in coolers. Figure 1 shows test and sampling locations for the type II flume.

## 3. LABORATORY PROGRAM

The laboratory-testing program was conducted at the University of Alberta Geotechnical Centre. The tests carried out included constant head hydraulic conductivity, particle size distribution, direct shear, soil water characteristic curve measurements and drying tests of the beach deposit using frozen and non-frozen samples.

### 3.1 Sample Preparation

A number of horizontal and vertical undisturbed core test specimens were obtained with a core barrel from the frozen blocks. The frozen cores were then trimmed to fit into both consolidation and direct shear cells that were used for k and shear measurements.

### 3.2 Hydraulic Conductivity Measurements

Laboratory k measurements were carried out using large strain consolidation cells. The frozen cores were first allowed to thaw in the cells at room temperature. The specimens were then tested under a constant head flow condition following ASTM D2434 to measure the $k_v$ and $k_h$ for comparison with the direct k measurements made in the flume beach deposits at SRC.

### 3.3 Particle Size Distribution (PSD)

After the k test was completed, the undisturbed samples were used to determine the PSD and fines content of the flume deposits. Wet and dry sieving and non-dispersed hydrometer tests were conducted on each sample following ASTM D422-63. PSD tests were also carried out on disturbed samples obtained adjacent to testing areas.

### 3.4 Direct Shear Measurement

Trimmed undisturbed core specimens were allowed to thaw overnight in the direct shear cell with the housing reservoir filled with water for each test. A strain rate of 0.003 in/min and a total travel distance of 10 mm were selected as test parameters. Normal stress magnitudes of 10, 25, 35 and 50 kPa were applied during direct shear testing to establish the failure envelopes of the saturated beach deposit samples.

### 3.5 Soil Water Characteristic Curve (SWCC) Measurement

SWCC was measured for type I flume samples using an acrylic pressure plate device with 100 kPa (1 bar) ceramic high entry disc following standard methods (Fredlund and Rahardjo 1993). Air pressure is applied from the inlet located on top of the chamber. Once air is applied, an outlet located at the base plate underneath the high air entry disk allows the drainage of water from the specimen. The change in water content is measured by weighing the specimen and the cell after equilibrium is reached. The procedure is then repeated at progressively higher values of matric suctions. Once the highest pressure value is applied, the specimen is removed from the cell. The water content corresponding to the highest matric suction is measured by oven drying the specimen. This water content together with the previous changes in weight are used to back-calculate the water contents corresponding to the other suction values. The matric suction is then plotted against corresponding water contents to give the SWCC. The curve fit of experimental data was derived using SoilCover 2000 software.

### 3.6 Drying Tests

The evaporation tests were conducted in similar evaporation lysimeters (180 mm in diameter) on flume deposit samples taken from the same batch as those used in the determination of the SWCC. One lysimeter contained distilled water to determine the potential evaporation (PE), and the other lysimeters contained the deposit samples to determine the actual evaporation (AE).

A controlled amount of water was added to each sample, and initial moisture contents were determined after mixing. The change in mass of each lysimeter was continually monitored to determine the rate of evaporation from the lysimeters. The temperature and relative humidity of the air above the evaporating surfaces were also monitored continuously. The test was completed when there was no change in mass. At the end of the test, samples were oven dried to determine the residual water content.

## 4. RESULTS AND DISCUSSION

### 4.1 Particle Size Distribution (PSD)

The particle size distribution curves of the flume deposits tested are shown in Figure 2. The corresponding amounts of fines and clay-size particles are summarized in Table 2. Average values are presented in Table 2 for the gradation of the type II flume locations. The amount of fines measured in the flume deposits range from 9% to 17%. Similarly the amount of clay-size particles range from 5.5% to 12%. With silt contents between 14% and 20%, the loose flume deposits qualify as liquefiable sands (Yamamuro and Covert 2001). Data in Table 2 indicate that the largest (17%) and lowest (9%) amounts of fines were captured in flumes A5 and A3, respectively.

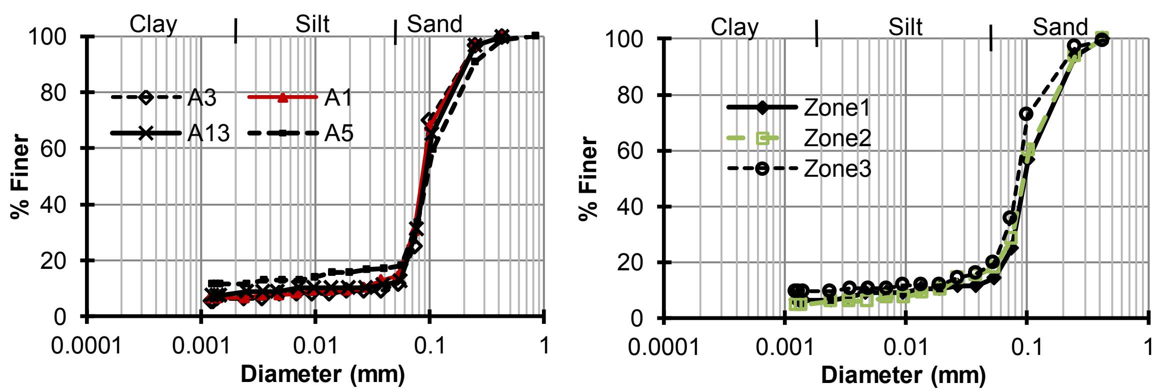


Figure IV-2. Particle size distribution of type I (left) and type II (right) flume deposits

### 4.2 Hydraulic Conductivity (k)

In-situ and laboratory k measurements are summarized in Table 3. The average $k_h$ and $k_v$ were measured in flume deposits A5 and A3 and were found to be $1.3x10^{-7}$ m/s and $2x10^{-6}$ m/s, respectively. The hydraulic conductivity of flume deposit A3 (9% fines) is higher than that of flume deposit A5 (17% fines) by one order of magnitude. Results indicate that k decreases with increasing fines content. It should be noted that the in-situ measurements of $k_h$ and $k_v$ were conducted using two different methods as described in Section 2.

The effect of the migration and capture of fines along the deposited beach of the type II flume is illustrated in Figure 4, which shows the variations of fines content and k as a function of distance (i.e., from the point of discharge to the toe of the beach slope in the flume). Results show that the fines content increases with increasing distance away from the discharge point. For example at 2 m and 7 m the captured fines have increased from 11.5% to 15%, respectively, and the hydraulic conductivities measured at the same locations have decreased from $1x10^{-6}$ m/s to $5x10^{-7}$ m/s, respectively. Results imply that the increase in fines is due to the migration and capture of fines in the direction parallel to the deposit surface.

Table IV-2. Summary of the gradation of tested flume deposits

| | TYPE I FLUME ID | | | | TYPE II FLUME | | |
|---|---|---|---|---|---|---|---|
| | A1 | A3 | A5 | A13 | Pilot zone1 | Pilot zone2 | Pilot zone3 |
| $D_{60}$ (μm) | 92 | 100 | 120 | 100 | 125 | 103 | 90 |
| $D_{50}$ (μm) | 88 | 90 | 95 | 90 | 95 | 95 | 82 |
| $D_{10}$ ( μm) | 25 | 35 | n/a | 55 | 9 | 19 | 2.5 |
| Cu | 3.7 | 2.2 | n/a | 1.8 | 13.9 | 5.4 | 36 |
| Fines (%) | 12 | 9 | 17 | 11.5 | 15 | 14 | 16 |
| Clay (%) | 6 | 5.5 | 12 | 8 | 6 | 5.5 | 10 |

Table IV-3. Summary of in-situ and laboratory $k_h$ and $k_v$ measurements of the flume deposits

| FLUME ID | IN-SITU K MEASUREMENTS | | LABORATORY K MEASUREMENTS |
|---|---|---|---|
| | Double Ring Infiltrometer (m/s) | Guelph Permeameter (m/s) | Constant Head Test - Consolidation Cell (undisturbed sample m/s) |
| A1 (12% fines, 6% clay) | $k_v = 8\times10^{-7}$ | $k_h = 8\times10^{-8}$ | $k_v = 8x10^{-7}$ $k_h = 5x10^{-7}$ |
| A3 (9% fines, 5.5% clay) | $k_v = 3\times10^{-6}$ | $k_h = 1\times10^{-6}$ | $k_v = 2x10^{-6}$ $k_h = 4x10^{-7}$ |
| A5 (17% fines, 12% clay) | $k_v = 2\times10^{-7}$ | $k_h = 6\times10^{-8}$ | $k_v = 3x10^{-7}$ ($k_h$ = n/a)[1] |
| A13 (11.5% fines, 8% clay) | $k_v = 3\times10^{-7}$ | $k_h = 1\times10^{-7}$ | $k_v = 2x10^{-6}$ $k_h = 1x10^{-6}$ |
| Pilot - zone 1 (15% fines, 6% clay) | $k_v = 4\times10^{-7}$ | $k_h = 2\times10^{-7}$ | $k_v = 1x10^{-6}$ $k_h = 2x10^{-6}$ |
| Pilot - zone 2 (14%fines, 5.5% clay) | $k_v = 2\times10^{-6}$ | $k_h = 1\times10^{-7}$ | $k_v = 1x10^{-6}$ $k_h = 1x10^{-6}$ |
| Pilot - zone 3 (16% fines, 10% clay) | $k_v = 3\times10^{-7}$ | $k_h = 1\times10^{-7}$ | $k_v = 5\times10^{-7}$ ($k_h$ = n/a)[1] |

[1] n/a = core could not be obtained due to the small thickness of the flume deposit or the limited size of the frozen block recovered from the flume

The comparison of in-situ and laboratory $k_h$ and $k_v$ are shown in Figures 3 and 5. It can be observed that all of the plots display a decreasing trend of k with increasing fines and clay-size contents. A comparison of the in-situ data in Figure 3 indicates that $k_h$ measured as a function of fines and clay-size contents was approximately 2 times lower than $k_v$. As mentioned earlier, it should be noted that the measurements in the horizontal and vertical directions were obtained using two different methods. The difference could also be attributed to the disturbance of the beach deposits structures during saturation of the flumes prior to the test. A comparison of laboratory data between $k_h$ and $k_v$ (Figure 5) indicates a steeper slope of the horizontal direction than that of the vertical direction. However, at low fines content there is no significant difference between the two hydraulic conductivities measured from the undisturbed flume samples. It is of importance to note that an undisturbed sample could not be obtained for $k_h$ measurements from flume deposit A5 (17% fines), which may have affected the observed slope in Figure 5.

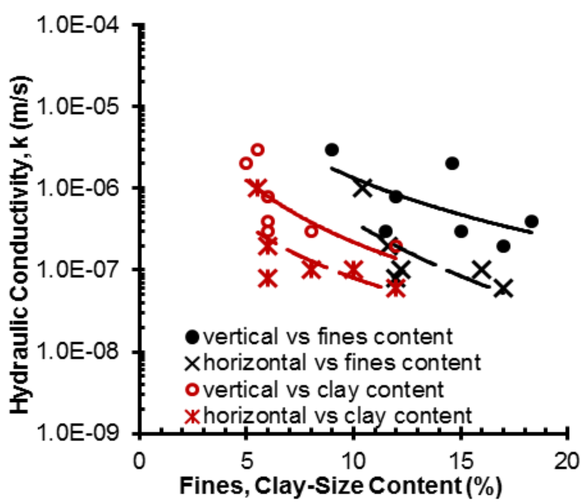


Figure IV-3. In-situ k vs. fines and clay-size content

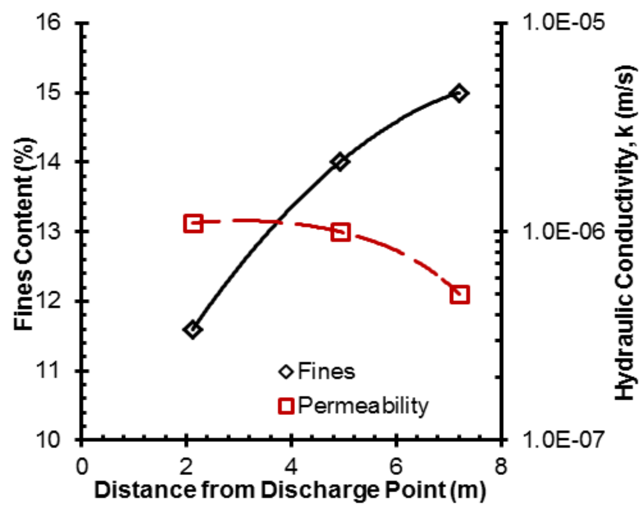


Figure IV-4. Fines content and k vs. distance in type II flume

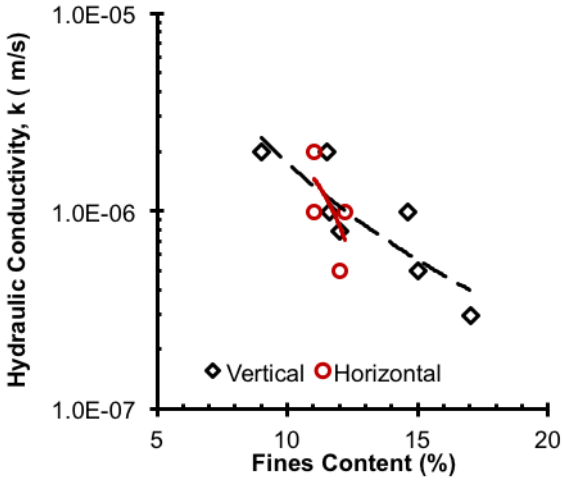


Figure IV-5. Laboratory k vs. fines content

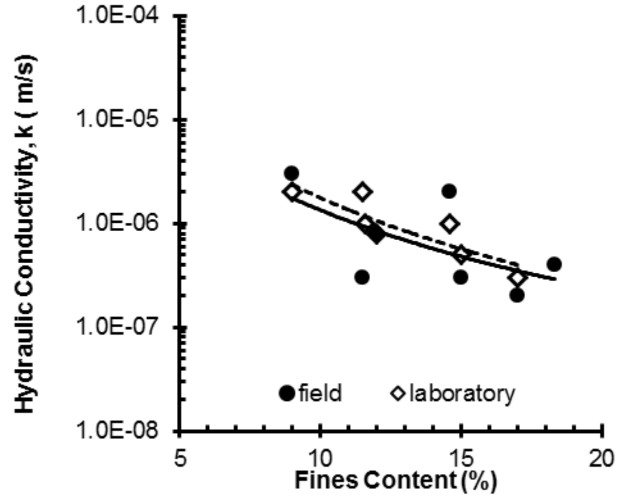


Figure IV-6. Laboratory and in-situ $k_v$ vs. fines content

Good agreement was generally observed between in-situ and laboratory data. To ascertain this observation, in-situ and laboratory data were compared in Figure 6. A comparison between in-situ and laboratory hydraulic conductivities both measured in the vertical direction, i.e. $k_v$, as a function of fines content indicates no significant difference between the two measured hydraulic conductivities in Figure 6.

In summary, results of in-situ and laboratory measured k obtained in this study indicated that k decreases with increasing fines content and the effect is more pronounced when a significant clay-size fraction is present. Results of the longer flume (type II) showed that the amount of fines increased with increasing distance along the slope of the beach profile towards the toe in the flume. This trend is due to the fact that small particles tend to migrate and occupy the void space between coarse particles in the soil matrix. Therefore, the flow of water through the soil becomes increasingly restricted, thereby reducing k. The surface properties and water retention ability of clay-size particles also have a significant effect on k (Mitchell and Madsen 1987). The in-situ test results show that $k_h$ was lower than $k_v$ in the depositional flumes used. The laboratory test results, however, showed no significant difference between $k_h$ and $k_v$ at low fines content. It should be noted that the comparison of in-situ k values was based on data obtained using different methods of measurements. The reliability and accuracy of the methods used were not evaluated due to the limited number of test results. Nonetheless, the trend in the variations of k with fines and clay-size contents should be preserved, as shown with the good agreement between laboratory and in-situ measurements illustrated in Figure 6.

### 4.3 Soil Water Characteristic Curve, Unsaturated Hydraulic Conductivity ($k_{sat}$) and Drying Curve

Figure 7 shows the SWCC plots of the beach deposit samples from flumes A1, A3 and A5. The solid symbols are measured data (from 0.1 kPa to 100 kPa suction), and the solid lines (0 kPa to 1 million kPa suction) represent the best fit curves generated using the SoilCover model (2000), which uses an equation developed by Fredlund and Xing (1994). The two important characteristics of the SWCC are the air entry value (AEV) and residual water content. The AEV corresponds to the suction at which the soil sample will begin to desaturate and, depending on the soil type, may or may not be well defined. Table 4 summarizes the SWCC characteristics for the deposit samples tested.

Table IV-4. Air entry values (AEV) and residual water contents of the soil water characteristic curves (SWCCs)

| Flume ID | Suction at AEV using SoilCover (kPa) | Residual Water content (tangent) (%) | Suction at residual water content (tangent) (kPa) | Suction at residual water content (calculated) (kPa) |
|---|---|---|---|---|
| A1 | 4.5 | 1.5 | 25 | 21 |
| A3 | 3.2 | 1 | 15 | 16 |
| A5 | 3.3 | 3 | 40 | n/a |

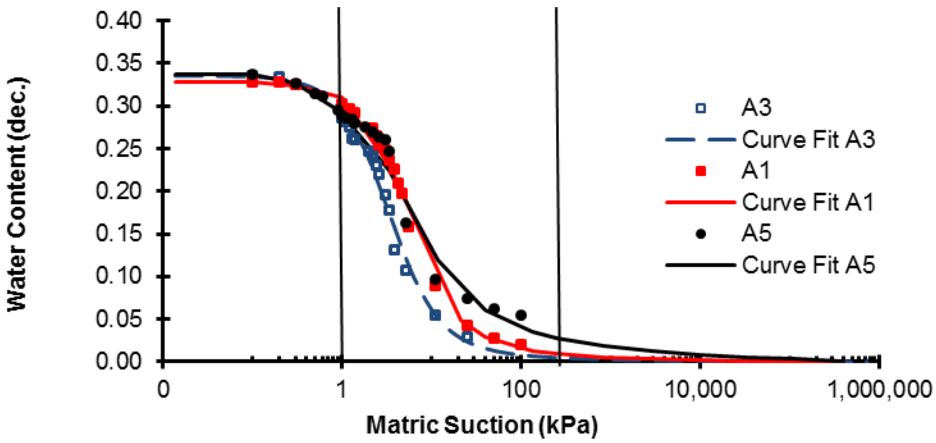


Figure IV-7. SWCCs of deposit samples A3, A1 and A5 with respective fines contents of 9%, 12% and 17%

SoilCover calculations yielded values of AEVs of 4.5 kPa, 3.2 kPa and 3.3 kPa for the deposit samples from flumes A1, A3 and A5, respectively. The AEVs are similar and well defined, characteristic of sand/silt material. The AEV is controlled primarily by the fines fraction. The small difference in the AEVs is due to slight variations in the fines/clay-size fractions of the beach deposit samples (i.e., 9%, 12% and 17% for flumes A3, A1 and A5, respectively). Kabwe et al. (2014) measured the SWCC of Syncrude beach sand and found an AEV of approximately 3 kPa. Yanful et al. (2003) measured the SWCC for fine sand and found an AEV of 3 kPa. Wilson et al. (1994) and Newman (1999) also measured the SWCCs for fine-grained materials (Beaver Creek sand), and both found an AEV of approximately 3 kPa.

The SWCCs show the samples start desaturating past the AEV and drain rapidly between values of matric suctions of 3 kPa and 10 kPa. For example, at 10 kPa suction, samples from flumes A3, A1 and A5 retained about 6%, 10% and 13% water content, respectively. The steep slopes and behaviour are characteristic of uniform sand and sand/silt materials and have also been described by others (Wilson et al. 1994, Barbour 1998). As the matric suction increases the samples reach their low residual values. The residual suctions ($\Psi_r$) (suction at residual water content) were determined using the tangent method applied to the SWCCs as described by Fredlund and Xing (1994) and were found to be approximately 15 kPa, 25 kPa and 40 kPa for samples from flumes A3, A1 and A5, respectively. Their corresponding residual water contents were 1%, 1.5% and 3% for flumes A3, A1 and A5, respectively. The calculated $\Psi_r$ in Table 4 was obtained using an expression found in Aubertin et al. (2003), which yielded values of 21 and 16 kPa for samples from flumes A1 and A3, respectively. These values are close to those determined graphically using the tangent method. It should be noted that the expression from Aubertin et al. (2003) is frequently impractical (or not applicable) for fine-grained soils because $D_{10}$ (particle size at which 10% is finer) and $C_u$ (coefficient of uniformity) are often unknown.

In summary, the SWCCs show that the beach deposit samples start to desaturate at a similar AEV between 3.5 kPa and 4.5 kPa due to slight variations in the texture of the materials. Results show that the residual water content is also controlled primarily by the fines content. For instance, sample A5 (17% fines content) reached its residual water when the matric suction approached 40 kPa. In contrast, samples A1 and A3, with respective fines content of about 9% and 12%, reached their residual water content when suction approached 15 kPa and 25 kPa, respectively.

## 4.4 Unsaturated Hydraulic Conductivity

A number of empirical relationships have been proposed to determine the unsaturated k as a function of volumetric water content, or suction $\psi$ (Richards 1931, Wind 1955, Gardner 1956, Davidson et al. 1969, Philip 1986, Ahuja et al. 1988, Fredlund and Xing 1994). However, the models proposed by Brooks and Corey (1964) and Mualem (1978) appear to be of wider applicability than other models. The Brooks and Corey (1964) relation to calculate k was used:

$$k(\psi) = k_{sat}\left[\frac{\Psi_{AEV}}{\Psi}\right]^{n}, \ \psi > \psi_{AEV} \qquad [1]$$

in which the measured $k_{sat}$ is defined as above at $\psi \leq \psi_{AEV}$, where $\psi_{AEV}$ is the suction corresponding to AEV and

$$n = 2 + 3 \qquad [2]$$

The relation between k and $\psi$ derived from the Brooks and Corey (1964) model for samples from flumes A1 and A3 are shown in Figure 8. The $k_{sat}$ used were determined in the laboratory using a constant head permeability test and were 2.0 x $10^{-6}$ m/s and 8.0 x $10^{-7}$ m/s for flumes A3 decreased rapidly with increasing $\psi$ beyond the AEVs, i.e. about 3 kPa and 4 kPa for samples A3 and A1, respectively. As suction was increased by two orders of magnitude, the k values are predicted to decrease by more than 10 orders of magnitude. At $\psi$ = 100 kPa, both k values decreased to < $10^{-14}$ m/s. It should be noted that the hydraulic conductivity is a measure of the ability of the soil to transmit water and depends upon both the properties of the soil and the fluid being transmitted (Klute and Dirksen 1986).and A1, respectively. The plots show the k values

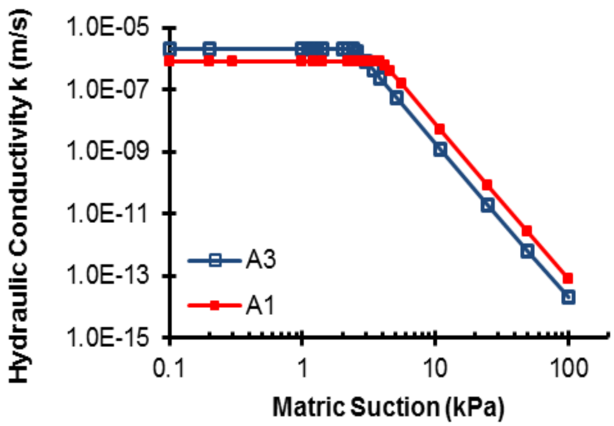


Figure IV-8. Hydraulic conductivity as a function of suction

4.5 Drying Curve

Figure 9 shows the drying curves of the beach deposit samples from flumes A1, A3, A5 and A13 obtained by evaporation at room temperature (21°C to 23°C). The drying curves display a similar desaturation pattern as the associated SWCCs.

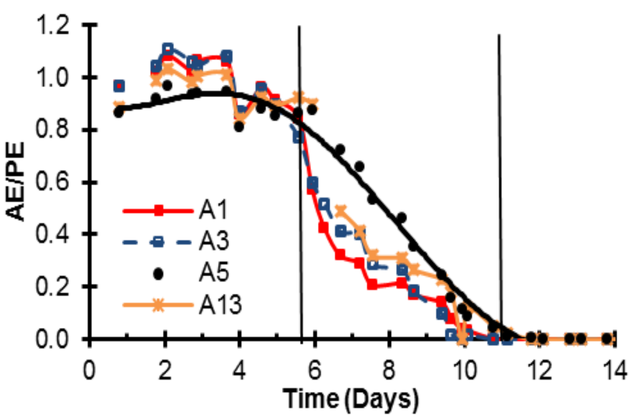


Figure IV-9. Drying curves for the deposit samples from flumes A1, A3, A5 and A13

During the initial five-day test period (Day 1 to Day 5), the actual evaporation to potential evaporation (AE/PE) ratios were close to unity (100%), and the surfaces of the lysimeters were saturated or close to saturation. During this stage, the evaporation rate is controlled by the atmospheric conditions (i.e., temperature, air humidity, wind, etc.). This early drying stage is similar to the initial part of the associated SWCC when suction is below the AEV (i.e., Figure 7). The increase in evaporation rate (i.e., when AE/PE > 1) was observed to occur immediately after cracks developed on the surfaces of the materials tested (A1, A3 and A13) and created more evaporating surfaces. The surface of sample A5, however, did not display any cracks, and the AE/PE was initially low (~0.85) but continued to gradually increase and remained constant just below 1. This behaviour occurs in most oil sands tailings containing residual bitumen. It should be noted that a thin layer of residual bitumen formed on the surface of sample A5 prior to the start of the test. The atmospheric drying process on oil sands tailings has been shown to slow significantly as the surface dries to a film and precludes further drying from deeper internal layers. Wilson et al. (1997) also attributed these deflections of AE/PE from unity to fluctuations in the aerodynamic resistance in the air spaces above the evaporating surfaces and their respective temperatures.

Between Day 5 and Day 11, the AE/PE ratios started decreasing more rapidly, but at a slower rate for sample A5. For example on Day 7 of the test period, the AE/PE ratios of samples A1, A3 and A13 were reduced to approximately 0.4; in contrast the AE/PE ratio for sample A5 was reduced to 0.7. This stage is called the soil profile-controlled stage, and the evaporation rate is dictated by the rate at which the gradually drying soil profile can deliver moisture toward the evaporation zone (Hillel 1980). In summary, the difference in the drying slopes of the deposit samples is due to slight variations in the sample textures (i.e., grain size, soil water characteristic curve and hydraulic conductivity function) and surface area conditions such as the presence of bitumen, which may lead to the formation of a surface film that reduces the evaporation rate.

Eventually, all of the samples reached a residual slow-rate drying stage (AE/PE = ~0) after Day 9, which may persist at a nearly steady rate for many days, weeks or even months. This stage apparently comes about after the surface zone has become so desiccated that further liquid water conduction through it effectively ceases. Water transmission through the desiccated layer thereafter occurs primarily by the slow process of vapor diffusion (Hillel 1980).

In summary, the drying process of the beach deposit samples has been observed to occur in three recognizable stages similar to those of the SWCC dewatering process: 1) the initial constant-rate stage controlled by the atmospheric conditions; 2) the intermediate falling-rate or soil profile-controlled stage which depends on the texture of the material and surface conditions; and 3) a residual slow-rate stage. Results show that the development of cracks on the surface of the deposited materials increases the evaporation rate and allows the materials to dry faster.

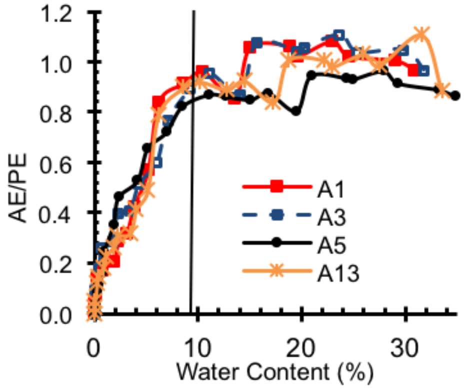


Figure IV-10. Evaporation rate vs. water content

Figure 10 shows a plot of AE/PE ratio versus water content for each deposit sample. It can be observed that the decline in evaporation rates occurred at approximately the same water content (i.e., 8%) for all four samples. This is attributed to the slight variation in texture of the deposit as discussed earlier.

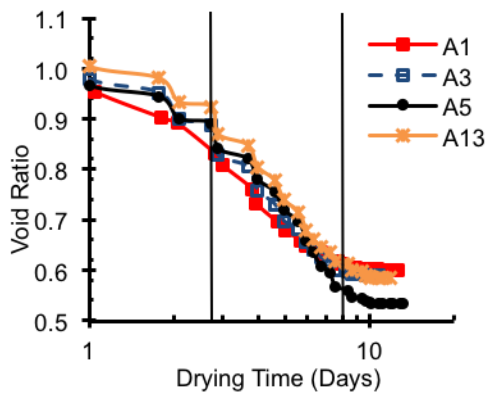


Figure IV-11. Change of void ratio with time

Figure 11 shows the change of void ratio with time for the deposit samples with similar initial void ratio of approximately 1. The curves are plotted on a logarithmic scale for a better visualization. Figure 11 shows that during the constant-rate stage (i.e., the initial four-day test period) while the surfaces are saturated, the void ratios change slowly from 1 to 0.8. The void ratios start decreasing rapidly after Day 3 to reach their lowest values of approximately 0.6 for samples A1, A3 and A13, and 0.55 for sample A5 after Day 8. During this stage (i.e., shrinkage phase), volume decrease is equal to the volume of water lost. On further drying after Day 8, the void ratios became almost constant, and this stage is called the shrinkage limit or the start of residual shrinkage (Tripathy et al. 2002). As the particles come in contact, the decrease in specimen volume is less than the volume of water lost. When all the particles come close together, no further shrinkage occurs while water is still being lost. This stage has been identified as the no-shrinkage stage by Stirk (1954).

### 4.6 Direct Shear

Direct shear tests were conducted to determine the failure envelopes of undisturbed beach deposit samples. The shear strength parameters and failure envelopes obtained are presented in Table 5. The samples showed dilatant behaviour under the applied normal stresses, though the volume change was relatively small. Values of the peak friction angles of the beach samples from Table 5 were found to be close to each other in the range of 37° to 40° with low cohesion, i.e. between 5 kPa and 6 kPa, which is typical of silty sand materials (Jewell 1989, Cerato and Lutenegger 2006). The peak failure envelope expressions in Table 5 indicated that a similar behaviour could be expected from all the beach deposits tested in terms of their normal stress response and shear stress development as the expressions are close to each other.

Variations of the measured peak and residual friction angles with fines and clay-size content are shown in Figures 12 and 13. The peak friction angle was found to increase slightly with both fines and clay-size content in a linear fashion. Salgado et al. (2000) also reported an increase in peak friction angle with fines content on Ottawa sand specimens with fines content in the range of 5% to 20%. As shearing progresses, fines tend to reach more stable arrangements in spaces between coarser particles, which increases interlocking, dilatancy and shear strength. However, the scatter of residual data in Figures 12 and 13 may imply that residual behaviour is more difficult to determine in terms of either fines or clay-size content of the beach deposits alone.

It is interesting to note that samples with a high proportion of clay-size in the fines fraction such as deposit A13 (8% clay-size for a fines fraction of about 11%) showed the largest drop in friction angle from peak to residual conditions. Lower residual friction angles have commonly been reported for clayey soils post failure in geotechnical investigations and failure analysis (Crooks 1986, Skempton and Vaughan 1993, Mesri and Shahien 2003). This observation could imply that large clay-size contents may be detrimental to the preservation of the sandy beach material shear strength in the residual state after failure. Prior to testing, soil contaminant levels and electrical resistivity at the site were measured and recorded to provide data for comparison. During the pilot test, power consumption, temperature distribution, water flow budget, MPE (multiphase extraction) and SVE (soil vapour extraction) operations and contaminant levels were monitored daily.

Results also imply that large shear stresses may develop in the tailings beach as subsequent lifts occur and more material is deposited, adding to the normal stresses acting on previous beach layers. This observation is of importance, considering the liquefiable nature of the beach deposit materials, which has been highlighted previously from the particle size distribution in Section 3.

Table IV-5. Shear strength parameters obtained from direct shear tests

| FLUME ID | Friction angle ϕ (°) | | Cohesion (kPa) | | Failure envelope | |
|---|---|---|---|---|---|---|
| | Peak | Residual | Peak | Residual | Peak | Residual |
| A1 (12% fines, 6% clay) | 37.4 | 36 | 5 | 2 | $\tau = 5 + \sigma \tan 37.4$ | $\tau = 2 + \sigma \tan 36$ |
| A3 (9% fines, 5.5% clay) | 36 | 33.2 | 6 | 3.5 | $\tau = 6 + \sigma \tan 36$ | $\tau = 3.5 + \sigma \tan 33.2$ |
| A5 (17% fines, 12% clay) | 38 | 34 | 5 | 2.2 | $\tau = 5 + \sigma \tan 38$ | $\tau = 2.2 + \sigma \tan 34$ |
| A13 (11.5% fines, 8% clay) | 40 | 27.4 | 6 | 5.2 | $\tau = 6 + \sigma \tan 40$ | $\tau = 5.2 + \sigma \tan 27.4$ |

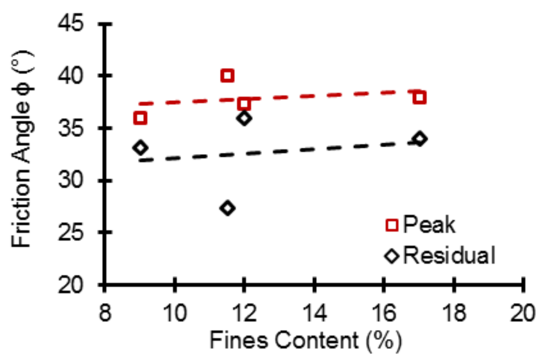


Figure IV-12. Variation of friction angle with fines

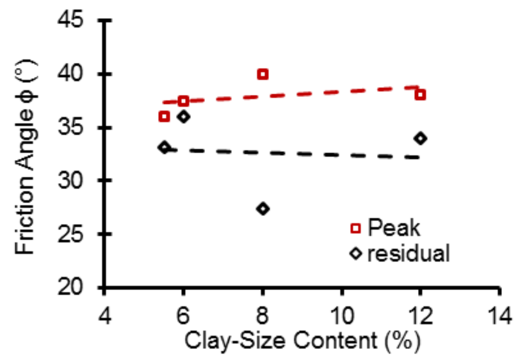


Figure IV-13. Change in friction angle with clay-size content

## 6. OBSERVATION AND CONCLUSION

Results of measurements carried out on flume beach deposits indicate that the fines content increases with increasing distance away from the point of discharge to the toe of the flume. This is attributed to the migration and capture of fines along the slope of the deposited beach. The amounts of fines captured in the flumes deposits range from 9% to 17%, and from 5.5% to 12% for fines content and clay-size, respectively. Results also show that the hydraulic conductivity (k) decreases with increasing fines content. The average hydraulic conductivities (i.e., in the horizontal and vertical directions) measured in the flumes range from $1.3 \times 10^{-7}$ m/s to $2 \times 10^{-6}$ m/s, characteristic of sand/silt materials. A comparison of the in-situ data indicates that the k measured in the horizontal direction ($k_h$) was slightly lower (~2 times) than that measured in the vertical direction ($k_v$). This may be attributed to the disturbances of the beach deposits during the saturation process prior to the test and, to a lesser degree, to the accuracy between the two methods of measurements used. A comparison of the laboratory data, however, does not show a significant difference between the measured $k_h$ and $k_v$. SoilCover calculations yielded similar AEVs of 4.5 kPa, 3.2 kPa and 3.3 kPa for the deposit samples from flumes A1, A3 and A5, respectively. The AEVs are characteristic of sand/silt material. The small difference in the AEVs is due to slight variations in the fines/clay-size fractions from the beach deposit samples (i.e., 9%, 12% and 17% for flumes A3, A1 and A5, respectively). The measured drying curves of the deposits display a similar desaturation pattern. The difference in the drying slopes of the deposits samples is due to slight variations in the sample textures. It was observed that the development of cracks on the surface of the deposited materials increased the evaporation rate and allowed the material to dry faster. It was also observed that the formation of a film on the surface of the deposit has reduced the evaporation rate. The direct shear peak friction angles of the beach deposits were found to increase slightly with increasing fines content. It was noted that residual behaviour was more difficult to determine with respect to changes in fines/clay content of the beach materials.

## ACKNOWLEDGEMENTS

Funding or this project was provided by Total E&P Canada Ltd. The authors would like to acknowledge the SRC and its staff for allowing the use of their facilities and their continued assistance with in-situ testing.

REFERENCES


Ahuja, L.R., Ross, J.D., Bruce, R.R., and Cassel, D.K. 1988. Determining unsaturated Hydraulic conductivity from tensiometric data alone, *Soil Science Society of America Journal*, 52: 27 - 34.

Aubertin, M., Mbonimpa, M., and Chapuis, R.P. 2003. A model to predict the water retention curve from basic geotechnical properties, *Canadian Geotechnical Journal*, 40: 1104 - 1122.

Barbour, S.L. 1998. Nineteenth Canadian Geotechnical Colloquium: The soil-water characteristic curve: a historical perspective, *Canadian Geotechnical Journal*, 35(5): 873 - 894.

Blight, G.E., Thomson, R.R. and Vorster, K. 1985. Profiles of hydraulic-fill tailings beaches, and seepage through hydraulically sorted tailings, *Journal of the South African Institute of Mining and Metallurgy*, 85(5): 157 - 161.

Brooks, R.H. and Corey, A.T. 1964. Hydraulic properties of porous media, *Colorado State University*, Fort Collins, Colo. Hydrology Paper No. 3.

Cerato, A.B. and Lutenegger, A.J. 2006. Specimen size and scale effects of direct shear box tests of sands, *Geotechnical Testing Journal*, 29(6): 1 - 10 ASTM.

Chalaturnyk, R.J., Scott, J.D. and Özüm, B. 2002. Management of oil sands tailings, *Petroleum Science and Technology*, 20, (9 & 10): 1025 - 1046.

Ciu, Z., Liu, Q., Etsell, T.H., Oxenford, J. and Coward, J 2003. Heavy minerals in the Athabasca oil sands tailings-potential and recovery processes, *Canadian Metallurgical Quarterly*, 42 (4): 383 - 392.

Crooks, J.H.A., Been, K. and Mickleborough, B.W. 1986. An embankment failure on soft fissured clay, *Canadian Geotechnical Journal*, 23: 528 - 540.

Davidson, J.M., Stone, L.R., Nielsen, D.R., and Larue, M.E. 1969. Field measurement and use of soil-water properties. *Water Resources Research*, (5): 1312 - 1321.

Fredlund, D.G., and Rahardjo, H. 1993. *Soil mechanics for unsaturated soils*. John Wiler and Sons, New York, NY, USA.

Fredlund, D.G., Xing, A., and Huang, S. 1994. Predicting the permeability function for unsaturated soils using the soil water characteristic curve. *Canadian Geotechnical Journal*, 31: 533 - 546.

Fredlund, D.G., and Xing, A. 1994. Equations for the Soil-Water Characteristic Curve. *Canadian Geotechnical Journal*, 31: 521 - 532.

Gardner, W.R. 1956. Calculation of capillary conductivity from pressure plate outflow data. *Soil Science Society of America Journal*, 20(3): 317 - 320.

Granger, R.J. 1989. Evaporation from natural non-saturated surfaces. *Journal of Hydrology*, 111: 21 - 29.

Hazen, A. 1892. Some physical properties of sands and gravels, with special reference to their use in filtration. 24th Annual Rep., *Massachusetts State Board of Health*, Pub. Doc. 34: 539 - 556 (as referenced by Barbour 1998)

Hillel, D. 1980. *Applications of Soil Physics*, Academic Press, Inc., New York, NY, USA.

Jewell, R.A. 1989. Direct shear tests on sand. *Géotechnique*, 39:(2): 309 - 322.

Kabwe, L., Wilson, W., and Scott, D., 2014. Influence of an Underlying Sand Beach on Drainage and Desiccation of Fine Tailings. Paper accepted for presentation at the International Oil Sands Tailings Conference 2014, Louise Lake, Alberta.

Kenney, T. C., Lau, D., and Ofoegbu, G. I. 1984. Permeability of compacted granular materials. *Canadian Geotechnical Journal*, 21: 726 - 729.

Lade, P.V. 1992. Static instability and liquefaction of loose fine sandy slopes. *Journal of Geotechnical Engineering*, 118: 51 - 71.

Matthews, J.G., Shaw, W.H., MacKinnon, M.D. and Cuddy, R.G. 2002. Development of composite tailings technology at Syncrude. *International Journal of Surface Mining, Reclamation and Environment*, 16(1): 24 - 39.

Mesri, G. and Shahien, M. 2003. Residual shear strength mobilized in first-time slope failures. *Journal of Geotechnical and Geoenvironmental Engineering*, 129(1): 12 - 31.

Mitchell, J.K. and Madsen, F.T. 1987. Chemical effects on clay hydraulic conductivity. *Proceedings of Geotechnical Practice for Waste Disposal '87*, in Geotechnical Special Publication (GSP), ASCE, 13: 87 - 116.

Mittal, H. K. and Morgenstern, N. R. 1975. Parameters for the design of tailings dams. *Canadian Geotechnical Journal*, 12: 235 - 261.

Mualem, Y. 1978. Hydraulic conductivity of unsaturated porous media: generalized macroscopic approach. *Water Resources Research*, 14: 325 - 334.

Pastor, M., Quecedo, M., Fernández Merodo, J. A., Herrores, M. I., González, E. and Mira, P. 2002. Modelling mine waste dumps and tailings dams failures. *Géotechnique*, 52(8): 579 - 591.

Philip, J.R. 1986. Linearized unsteady multidimentional infiltration. *Water Resources Research*, 22: 1717 - 1727.

Qiu, Y. and Sego, D.C. 2001. Laboratory properties of mine tailings. *Canadian Geotechnical Journal*, 38: 183 - 190.

Richards, L.A. 1931. Capillary conduction of liquid through porous medium. *Journal of Physics*, 1: 318 - 333.

Salgado, R., Bandini, P. and Karim, A. 2000. Shear strength and stiffness of silty sand. *Journal of Geotechnical and Geoenvironmental Engineering*, 126: 451 - 462.

Skempton, A.W. and Vaughan, P.R. 1993. The failure of Carsington dam. *Géotechnique*, 43(1): 151 - 173.

Stirk, G.B. 1954. Some aspects of soil shrinkage and the effect of cracking upon water entry into the soil. *Australian Journal of Agricultural Research*, 5: 279 - 291.

Tripathy, S., Subba Rao, K.S., and Fredlund, D.G. 2002. Water content – void ratio swell-sink paths compacted expansive soils. *Canadian Geotechnical Journal*, 39: 938 - 959.

Wilson, G.W., Fredlund, D.G. and Barbour, S.L. 1994. Coupled soil-atmosphere modeling for soil evaporation. *Canadian Geotechnical Journal*, 31: 151 - 161.

Wilson, G.W., Fredlund, D.G. and Barbour, S.L. 1997. The effect of soil suction on evaporative fluxes from soil surfaces. *Canadian Geotechnical Journal*, 34: 145 - 155.

Wind, G.P. 1955. Field experiment concerning capillary rise of moisture in heavy clay soil. *Netherlands Journal of Agricultural Science*, 3: 60 - 69.

Yammamuro, A.J. and Covert, M.K. 2001. Monotonic and cyclic liquefaction of very loose sands with high silt content. *Journal of Geotechnical and Geoenvironmental Engineering*, 127: 314 - 324.

Yanful, E.K. and Mousavi, S.M. 2003. Estimating falling rate of evaporation from finite soil columns. *The Science of the total Environment*, 313: 151 - 15.

# V. CHAPTER 5. CHARACTERISATION OF THE BEHAVIOUR OF TAILINGS BEACH DEPOSITS IN FLUME TESTS


## SUMMARY

The test program complements the oil sands tailings beach studies presented in Chapter 4, which were carried out in test flumes using mature fine tailing (MFT) with different sand to fines ratio (SFR). Results showed that the amount of fines captured was function of the slope of the beach deposit in the flumes. The flume deposit with lower slope (i.e., 0.5%) captured 17% of fines as compared to 9% for the deposit with higher slope (i.e., 8%). A difference of 3% in fines content was noted between samples obtained 5cm and 20 cm below the surface of the deposits. A comparison of results from particle size distribution (PSD), soil water characteristic curves (SWCC) and associated drying curves indicated that the behaviour of the flume deposits was within the envelope of the Devon silt (upper boundary) and typical tailings beach sand (lower boundary) samples. The mean peak and residual friction angles of the flume deposits were determined to be 38° and 33° respectively as compared to 41° and 37° for the beach sand. Large strain consolidation tests yielded low compressibility values, i.e. about 1% change in void ratio, and little change was observed in the hydraulic conductivity, k (i.e. between 1x $10^{-7}$ m/s and 5x$10^{-7}$ m/s). Results of this study are of value for the oil sands industry for the understanding and modelling of the geotechnical behaviour of oil sands tailings beach deposits with respect to the proportion of fines captured by the newly formed beach material.


## 1. INTRODUCTION

In northern Alberta, Canada, the exploitation of oil sands deposit has produced considerably large volumes of tailings over the years. Such tailings are still predominantly deposited as slurries and the various processes associated with tailings slurry discharge have been well documented (Camp 1977, Dusseault and Scott 1983, Fergusson et al. 2009, Penner and Foght 2010). However, the large

inventory of mature fine tailings (MFT) resulting from conventional tailings disposal methods is a major concern as new regulations by the Alberta Energy Regulator (AER) impose stringent requirements on oil sands tailings management and land reclamation. The current practice has therefore shifted towards the production of non-segregating tailings (NST), including composite and thickened tailings (Caughill et al. 1993, Matthews et al. 2002, Chalaturnyk et al. 2002), as well as heavy mineral recovery techniques from the tailings streams (Ciu et al. 2003). It is also crucial to measure the consolidation properties of deposited oil sand tailings to assess the build-up of strength in the material and to mitigate potential instability issues related to increases in pore pressures. The compressibility of oil sands tailings is often described in terms of the large strain consolidation theory (Gibson et al. 1967), which requires both the void ratio - stress and void ratio - hydraulic conductivity relationships to be determined.
Mathews et al. (2002) notably reported that NST could be obtained from mixtures of sand and fine tailings streams, referred to as composite tailings (CT), which could also include the current MFT inventory. Qiu and Sego (2001) compared the geotechnical behaviour of various mine tailings and CT. Wong (2008) studied the compressibility of NST mixtures consisting of both fine and coarse tailings, and proposed a mechanistic model to describe their consolidation behaviour on the basis of three stages in their response. The reliability and usefulness of flume tests to model and understand the deposition behaviour of oil sands tailings has been widely documented in the literature (Blight et al. 1985, Küpper 1992, Miller et al. 2009).

The experimentations discussed herein follow the oil sands tailings beach studies in test flumes described in Chapter 4. The Beach materials were formed upon the deposition of different mixtures of fine sand and MFT into test flumes. The main objective of this study was to investigate the characteristic behaviour of the resulting tailings beach materials. The specific objectives were the determination of the particle size distribution, soil water characteristic curve, drying properties and shear strength parameters of the flume deposits, which were compared to similar tests performed on Devon silt and coarse tailings beach sand samples. Large strain consolidation tests were also conducted on undisturbed flume samples obtained using an in-situ freezing technique.

## 2. FIELD PROGRAM

### 2.1 Flume Deposition

The flume tests were conducted at the Saskatchewan Research Council's (SRC) facilities in Saskatoon. The mixtures of MFT and fine sand used as well as the flume deposition process were as described in Chapter 4. The beach deposits had slope angles between 0.5% and 8% in the flumes. The tailings beach deposits captured different proportions of fines and residual bitumen, which were previously discussed in Chapter 4. Details of the sampling procedure of the tailings beach deposits for laboratory testing are provided in the next section.

### 2.2 Samples Collection

The sampling procedure and the undisturbed frozen samples obtained from the flumes were the same as described Chapter 4. Disturbed samples were also obtained at representative areas selected in accordance with the variability of the slope and thickness of a given deposit throughout its length. The disturbed samples were placed in air tight plastic freezer bags before being stored in coolers.

## 3. LABORATORY PROGRAM

Particle size distribution tests were carried out for disturbed flume samples. Tailings beach sand and Devon silt samples were subjected to a number of laboratory tests described in Chapter 4 for comparative purposes and to further characterize the behaviour of the beach samples. The tailing beach sand samples were the same as used by Kabwe et al. (2014). Large strain consolidation tests were also conducted on the undisturbed beach deposit samples A3 and A5 which were used for the laboratory k measurements in Chapter 4.

### 3.1 Particle Size Distribution (PSD)

PSD results of selected samples have already been reported in Chapter 4, and will only be discussed briefly in Section 4. New PSD tests conducted on disturbed samples obtained at various depths and locations throughout the flume deposits will be presented. Furthermore, the PSD was determined for the tailings beach sand and Devon silt samples for comparison, which will be discussed in Section 4.2. All PSD tests were conducted as per the procedures described in Chapter 4 and ASTM D422-63.

### 3.2 Comparative Studies

Devon silt and tailings beach sand samples were subjected to a number of experimentations described in Chapter 4 for the flume deposits. The tests selected are described below and subsequent tests results will be analysed in Sections 4.3 to 4.6.

#### 3.2.1 Soil Water Characteristic Curve (SWCC) Measurement

The SWCC was determined for the tailings beach sand sample using an acrylic pressure plate device with 100 kPa (1 bar) ceramic high entry disc following standard methods (Fredlund and Rahardjo 1993). The test procedure used was the same as that used for the flume samples in Chapter 4.

#### 3.2.2 Drying Tests

Evaporation tests were conducted on Devon silt and tailings beach sand samples in similar evaporation lysimeters (180 mm in diameter) used for the flume deposits and following the procedure described in Chapter 4. One lysimeter contained distilled water to determine the potential evaporation (PE), and the other lysimeters contained the deposit samples to determine the actual evaporation (AE). A controlled amount of water was added to each sample, and initial moisture contents were determined after mixing as presented in TableV-1. The test procedure was previously described in Chapter 4.

Table V-1. Initial characteristics of the lysimeters samples for drying tests

| Sample ID | Fines (%) | Clay (%) | Moisture content (%) | Solids content (%) | Void ratio |
|---|---|---|---|---|---|
| **A1** | 12.0 | 6.0 | 41.1 | 70.9 | 1.1 |
| **A3** | 9.0 | 5.5 | 40.8 | 71.0 | 1.1 |
| **A5** | 17.0 | 12.0 | 41.6 | 70.6 | 1.1 |
| **Devon silt** | 100.0 | 30.0 | 47.3 | 67.9 | 1.2 |
| **Beach Sand** | 10.5 | / | 34.3 | 74.5 | 0.9 |

### 3.2.3 Direct Shear

Direct shear tests were conducted on saturated tailings beach sand samples to determine the shear strength parameters in both peak and residual conditions. A strain rate of 0.003 in/min and a total travel distance of 10 mm were selected as test parameters, which were similar to those used for the flume deposits in Chapter 4. Normal stress magnitudes of 10, 25, 35 and 50 kPa were applied during direct shear tests to establish the peak and residual failure envelopes of the tailings beach sand.

### 3.2.4 Large Strain Consolidation (LSC) Tests

The same undisturbed frozen cores acquired for the vertical k measurements of A3 and A5 in chapter 4 were used for LSC tests. The heights of the samples used were 6.6 cm and 5.7 cm for the flume deposits from A3 and A5 respectively. The diameter of the two cores was 10 cm. The frozen densities of the samples were between 1.6 $g/cm^3$ and 1.8 $g/cm^3$. The undisturbed cores were allowed to thaw for a period of 3 days before testing was initiated. The thawed undisturbed samples were saturated in the LSC cell prior to the test. The initial k was then measured under a constant head flow condition following ASTM D2434 before the loading sequence was initiated. Additionally, constant head k measurements were made at the end of each loading step in order to investigate both void ratio-effective stress and void ratio-k relationships throughout the consolidation process. LSC tests were conducted following the sequence of vertical stress application 0.4, 4.4, 10, 40, 80, 160, 280, 400 and 500 kPa.

## 4. RESULTS AND DISCUSSION

### 4.1 Particle Size Distribution (PSD) of Disturbed Flume Samples

In Chapter 4, the amounts of fines captured by the beach were found to be 9%, 12% and 17% in flumes A3, A1 and A5 respectively. With an average silt content of 15%, the beach deposits were qualified as liquefiable sands (Salgado et al. 2000, Yamamuro and Covert 2001) which have been commonly identified in both oil sands and mine tailings sands.
Figures V-1 to V-2 show the changes in PSD with depth from disturbed samples obtained 5 cm, 15 cm and 22 cm below the surface of the beach deposits in Flumes A3 and A1. Because of its small thickness, the beach deposit in Flume A5 could not be sampled at various depths. From Figure V-1a, the fines content decreased from 11% at the surface to about 8% at a depth of 20 cm in Flume A3. Similarly from Figure V-2b, the fines content were 13% and 10% at depths of 5 cm and 20 cm respectively in Flume A1. Figures V-1 and V-2 implied that the tailings slurry compositions used in this testing program formed uniform beach deposits in the flumes, as the grain size curves obtained at different depths nearly overlap. The slightly larger fines content at shallow depths reflected both the effects of vertical sorting reported by Blight and Steffen (1979), and the capture of fines along the tailings beach surface which has been described by Blight et al. (1985).

Küpper et al. (1992) reported the formation of flatter beach slopes for slurry deposited at higher fines content in their review of the deposition of hydraulic fills in flume tests. The inclinations of the beach slopes in the flumes were 0.5%, 4% and 8% for respective fines captured of 17% (A5), 12% (A1) and 9% (A3). This highlighted a tendency for steeper beach slopes to form for MFT-fine sand slurries of larger sand-to-fines ratio (SFR) in this study.

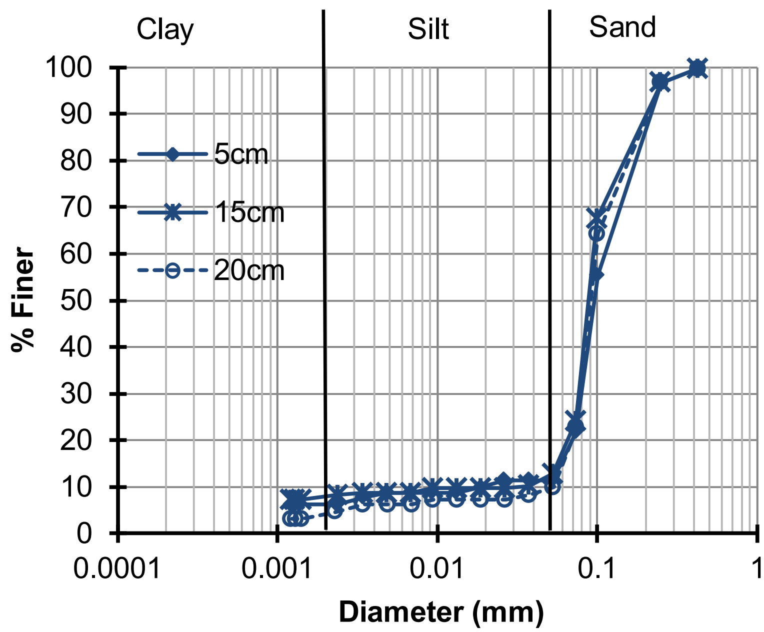


a)

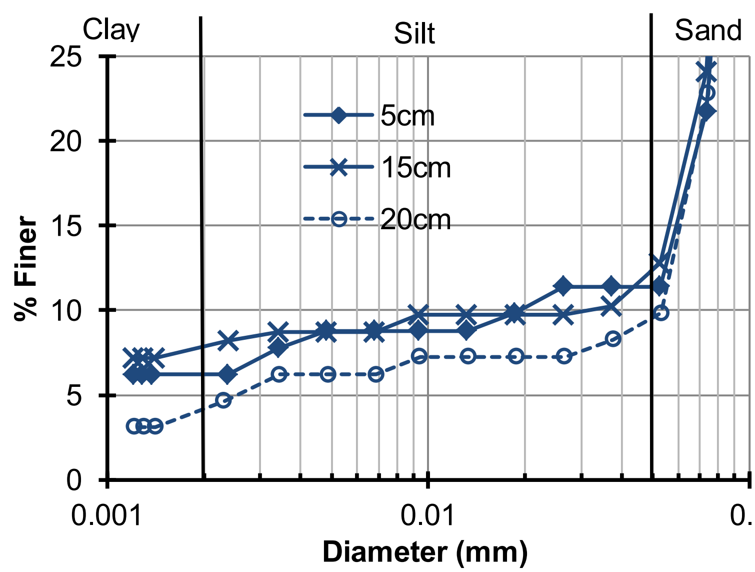


b)

Figure V-1. a) Entire range of variation of particle size distribution (PSD) with depth in flume A3; b) Variation of particle size distribution (PSD) of fines particles with depth in Flume A3

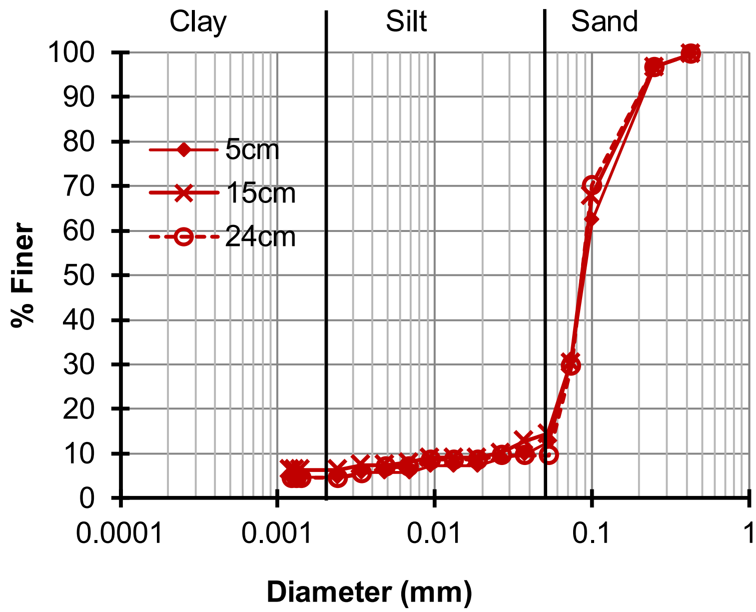


b)

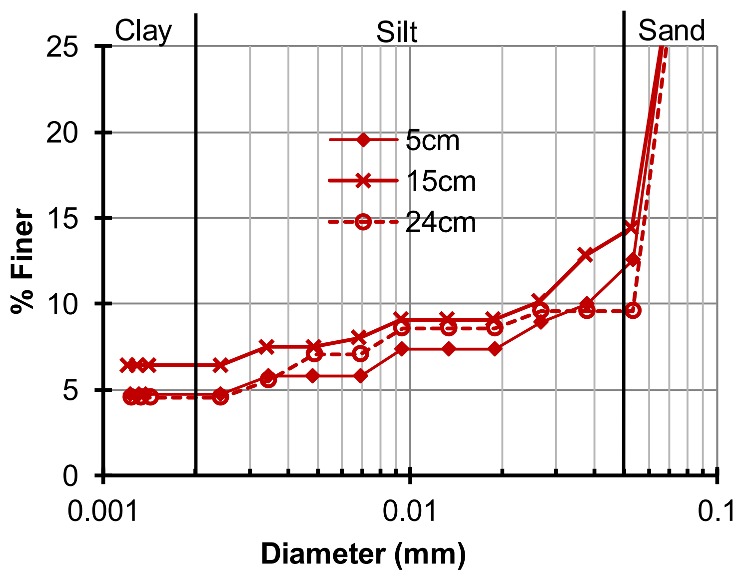


a)

Figure V-2. a) Entire range of variation of particle size distribution (PSD) with depth in Flume A1; b) Variation of particle size distribution (PSD) of fines particles with depth in Flume A1

Figure V-3 shows the PSD obtained at the crest and toe of the beach deposit slope in flume A5. As previously indicated, the slope was 0.5% for the deposit in Flume A5 which captured the largest amount of fines, i.e. 17%. It could be observed from Figure V-3 that the fines contents were similar at the crest and at the toe of flat beach deposit slope. However, the amount of clay-sized particles captured by the beach changed from 13% near the crest to 8% at the toe. It could be argued that the migration of fines along the beach was hindered by the low inclination of the slope, hence the large proportion of fine materials located in the vicinity of the point of deposition at the crest. Only a smaller fraction of the smallest particles, i.e. clay-sized, could then move towards the toe of the flat slope while the bulk of the fines fraction remained near the crest.

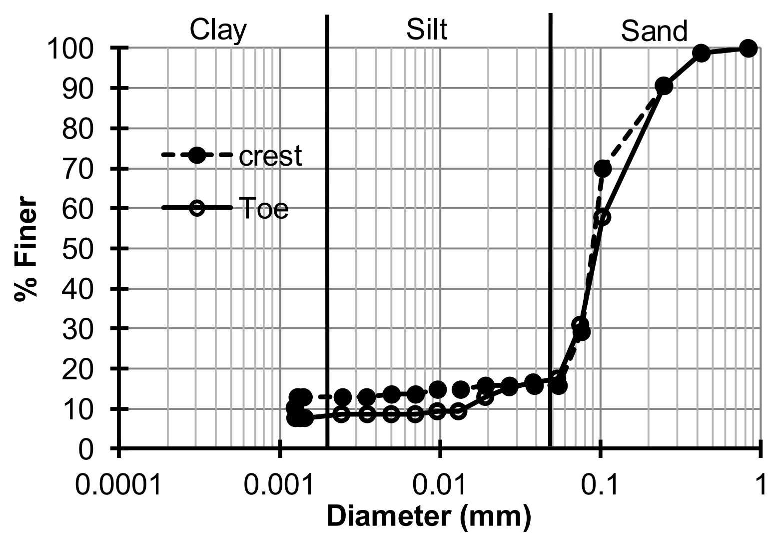


Figure V-3. Spatial variation of the particle size distribution (PSD) in Flume A5

In summary, the PSDs of the flume deposits showed that the tailings beach materials were predominantly liquefiable silty sands with a fines content ranging between 9% and 17%. Furthermore, the deposits were found to be essentially uniform. The higher fines content captured by the beach and the resulting flat slope of the deposit in flume A5 minimised the effects of the migration and capture of fines that typically occurs in such tailings. Slurry deposition parameters therefore play an important role in the capture of fines along the tailings beach material.

## 4.2 Comparison of Flume Deposits with Tailings Beach Sand and Devon Silt Samples

PSD tests conducted on tailings beach sand and Devon silt samples are presented in Figure V-4. The PSDs of the flume samples described in Chapter 4 were also included in Figure V-4 for comparison purposes. Results showed that the tailings beach sand sample captured around 10.5% fines and was coarser than the flume specimens. The mean grain size ($D_{50}$) for the beach sand was approximately 0.16 mm. In comparison, the average $D_{50}$ was approximately 0.09 mm for the flume deposits. The Devon silt specimen in Figure V-4 was found to be essentially a fine material with 100% of the particles having a diameter below 0.044mm, and 30% clay-size content. Furthermore, it is observed that the slope of the grain size curve of the Devon silt sample is flatter than that of the tailings beach sand.

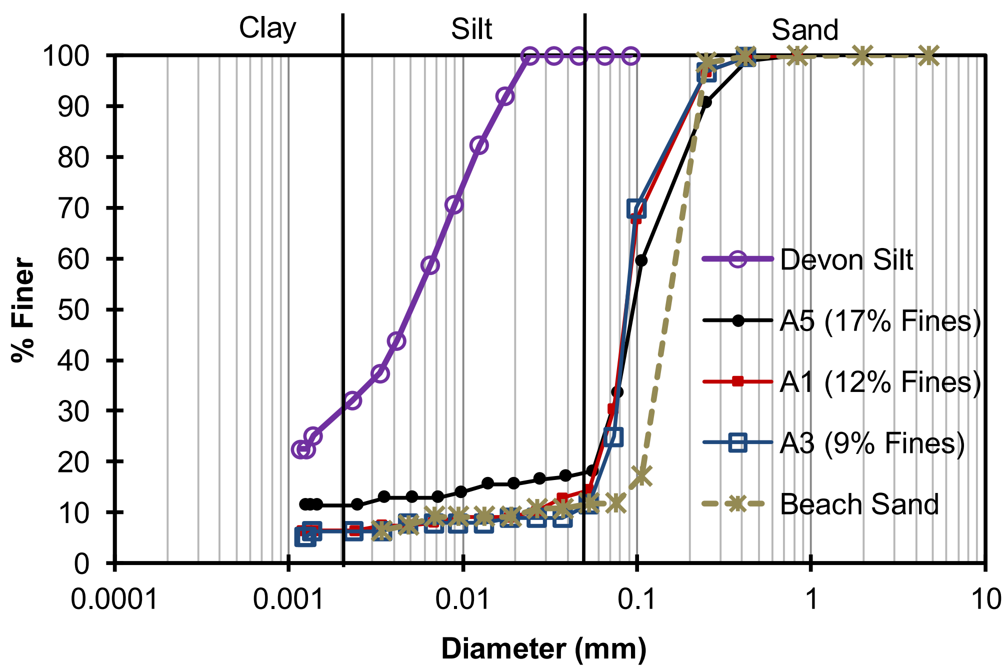


Figure V-4. Particles size distributions (PSDs) of the flume deposits, Devon silt and tailings sand samples

It can be seen from Figure V-4, that the grain size curves of the flume samples lie in between those obtained for the finer silt and coarser beach sand materials. An increase in the amount of fines captured by the beach appears to shift the grain size curve of the flume deposits towards that of silt as seen in Figure V-4. Moreover, this shift was accompanied by a flattening of the slope of the grain size curves for the flume deposits, which mirrored that of silt as observed with the fines-rich A5 in Figure V-4. However, the flume deposits remain predominantly sand. It is therefore expected that the behaviour of the flume deposits will be dominated by the sand fraction. Nonetheless, their behaviour should reflect characteristics of both fine and coarse materials.

The results from the PSD tests hinted towards the transitional nature of the behaviour of the MFT-sand tailings flume deposits which was dominated by the sand fraction. Furthermore, the behaviour of the flume deposits appears to vary within the boundaries of fine and coarse materials depending on the relative amounts of fines captured by the beach in the test flumes. This transitional behaviour will now be ascertained through complementary tests conducted using tailings beach sand and Devon silt samples. Results will be compared to the behaviour of the flume deposits observed upon the laboratory test program implemented in Chapter 1.

### 4.2.1 Soil Water Characteristic Curve (SWCC) Measurement

The SWCC was determined for the tailings beach sand specimen with the procedure described in Chapter 4. Figure V-5 shows the SWCC of the beach sand compared to the SWCCs of the flume deposits presented in Chapter 4. A description of the various stages and key features of the SWCC was also given in Chapter 4. The main characteristics of the SWCCs of the beach sand and flume deposits are summarized below in Table V-2. Calculations from SoilCover 2000 yielded values for the air entry values (AEV) between 3.2 kPa and 4.5 kPa for the flume deposits. The AEV was computed at 4.6 kPa for the tailings sand samples. Figure 5 shows that the AEVs are well defined and within the expected range for sandy materials (Wilson et al. 1994 and Yanful et al. 2003,). Also, the slope of the SWCC for tailings sand was steeper than that of SWCCs of the flume deposits, indicating a slower desaturation for the flume deposits. It is worth noting that the shape and slope of the SWCCs were dictated by the characteristics of the associated grain size curves discussed in Section 4.2. Fredlund et al. (2002) showed that the SWCC could be predicted directly from the associated PSD of the soil. Yang et al. (2004) highlighted the relationship between PSD and SWCC for sandy soils which is consistent with the observations made here. Nonetheless, the SWCCs in Figure V-5 remained close to each other until the onset of the residual phase.

Table V-2. Characteristics of the soil water characteristic curves (SWCCs)

| Flume ID | Suction at AEV using SoilCover (kPa) | Residual Water Content (tangent) (%) | Suction at Residual Water Content (tangent) (kPa) |
|---|---|---|---|
| A5 (17% Fines) | 3.3 | 3 | 40 |
| A1 (12% Fines) | 4.5 | 1.5 | 25 |
| A3 (9% Fines) | 3.2 | 1 | 15 |
| Tailings Sand | 4.6 | 1.2 | 10 |

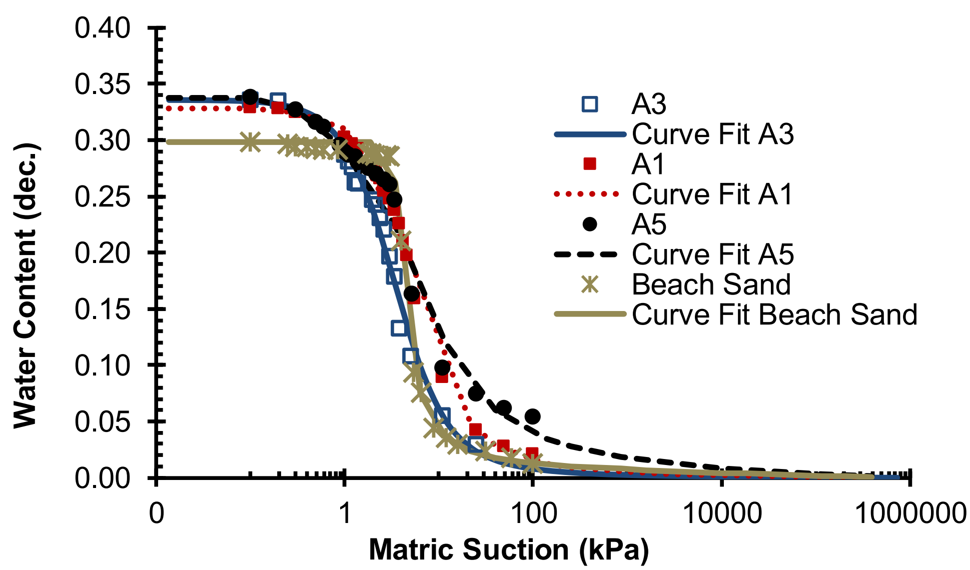


Figure V-5. Soil water characteristic curves (SWCC) of the flume deposits and tailings sand samples

The tangent method (Fredlund and Xing, 1994) was used to determine the residual characteristics of the samples from the SWCCs. The residual water contents were found to be 1.2%, 1%, 1.5% and 3% respectively for the beach sand, A3, A1 and A5. The corresponding values of suction at the residual water contents, $\Psi_r$, were 10%, 15%, 25% and 40% respectively for the beach sand, A3, A1 and A5. It can be seen that the fines capture process in the tailings beach during deposition strongly influenced residual behaviour, i.e. $\Psi_r$ and residual water content for both the flume samples and the tailings beach sand. The higher the amount of fines captured by the beach samples, the higher the magnitude of both $\Psi_r$ and residual water content. Yang et al. (2004) also reported that sandy soils with a small $D_{10}$, i.e. with finer particles, exhibited larger AEVs, $\Psi_r$ and residual water contents in comparison to coarser soils. However the amount of fines did not appear to have a strong influence on the AEVs in the fines content range studied in this test. An increase in the AEV should be expected at higher fines content in the beach materials.

In summary, the unsaturated behaviour of the flume deposits in this test was influenced by both the sand fraction and the fines captured by the beach. The sand fraction mainly dictated the overall desaturation behaviour as indicated by the similarities between the SWCCs of the flume deposits and the coarser tailings sand sample; whereas, the fines fraction mainly controlled the residual behavior, i.e. $\Psi_r$, and water retention in the beach, which affected the slope of the SWCC beyond the AEV for the beach deposits. The shape of the SWCC could also be related to that of the associated grain size curves.

### 4.2.2 Drying Tests

Evaporation tests were conducted on the tailings beach sand and Devon silt specimens. The resulting drying curves are presented in Figure V-6. As described in Chapter 4, the drying process comprised three stages: the initial constant rate stage, the soil profile-controlled stage, and the residual stage. The ratio of AE/PE remained close to 1 during the initial constant rate stage for the beach sand sample. Around Day 6 in Figure V-6, the AE/PE began to decline indicating the onset of the soil profile-controlled stage of the drying process for the material. The beach sand showed a sharp drop in AE/PE, i.e. a steep slope of the drying curve, which may be related to its coarser sand fraction. The beach sand then reached the residual stage between Day 9 and Day 10. It is worth mentioning that the steep slope of the AE/PE curve in the soil profile-controlled stage also reflected the steep slope observed for the associated SWCC during the second stage of the desaturation process.

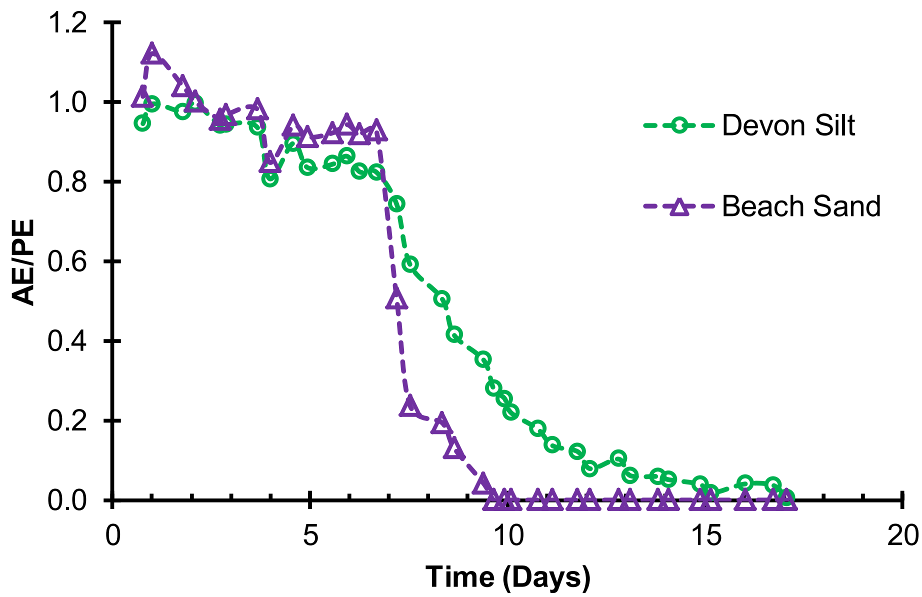


Figure V-6. Comparison between the drying curves of the tailings beach sand and Devon silt samples

In contrast, the drying curve of the Devon silt sample in Figure V-6 showed a slower and more gradual decrease in AE/PE during the initial constant rate stage until Day 6. The drying curve of the silt sample was then observed to decrease gradually with a gentle slope in the soil profile-controlled stage. This indicated a higher water retention ability which is characteristic of silt materials. The residual stage was then reached by the silt sample on Day 15, i.e. at a later time than the onset of the residual stage for the beach sand.

The aforementioned test results were compared to those obtained for the flume deposits A3, A1 and A5, where 9%, 12% and 17% fines were respectively captured by the beach. Drying test results for the flume deposits were previously discussed in Chapter 4. Figure V-7 shows that the drying curves of the flume deposits are at an intermediate stage between the beach sand and Devon silt samples The AE/PE curves of all flume deposits in Figure V-7 decreased with a gentler slope than that of the coarser beach sand in the soil profile-controlled stage. This indicated the influence of the fines captured by the beach on the evaporation rate which was slower than that of the coarser material. But, all flume deposits reached the residual stage at approximately the same time which was close to the behaviour of the beach sand in Figure V-7. Thus, the drying curves of the flume deposits emulated features from both coarser beach sand and finer silt drying curves, with the sand fraction dominating the overall behaviour of the material.

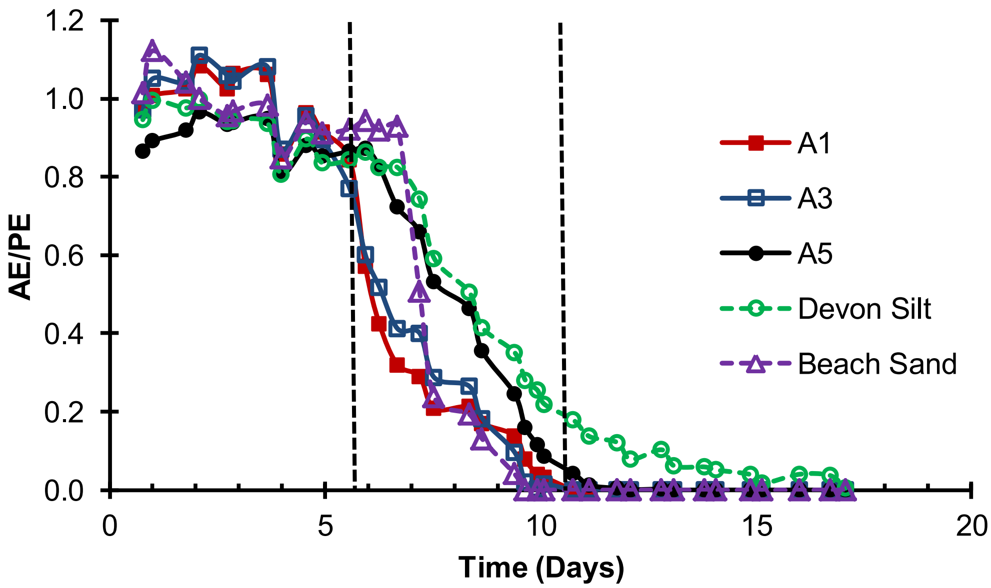


Figure V-7. Comparison between the drying curves of tailings sand, Devon silt and the flume deposits

For example in Figure V-7, changes in AE/PE with time for A3 which captured the least amount of fines (9%) closely reflected the changes observed for the coarser beach sand specimen during evaporation. In contrast, the variation in AE/PE for A5 which captured the largest amount of fines (17%) closely followed that of the finer silt sample throughout the test until the residual stage was reached for A5 between Day 10 and Day 11. Because of its larger water retention ability, the silt sample reached the residual stage at a later time on Day 15. These observations were consistent with those made in the previous section regarding the associated SWCCs, where the behaviour of the beach deposits portrayed the characteristics of both coarse and fine materials depending on the fines content.

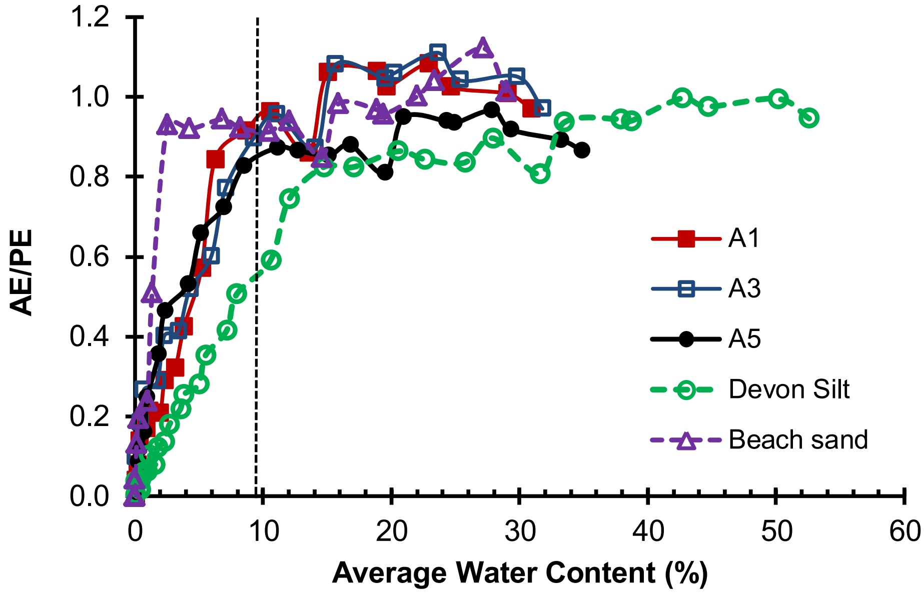


Figure V-8. Changes in AE/PE ratios of actual evaporation (AE) over potential evaporation (PE) with water content during evaporation tests

Figure V-8 provides the corresponding changes in AE/PE with the average water content during the evaporation tests. The AE/PE of the flume deposits was observed to decline rapidly below an average water content of 10%. A water content of 10% corresponds to the onset of the soil-profile controlled stage between Day 5 and Day 11 in Figure V-8. At this stage, the evaporation rate became predominantly controlled by the texture and inherent features of the materials. The rapid decline in AE/PE was observed to occur below water contents of 2% and 13% for the tailings beach sand and silt samples respectively. The rapid decline in AE/PE for the flume deposits was therefore observed to occur at intermediate water contents, i.e. in between that of the coarser and finer materials. The AE/PE of the coarser tailings sand material also decreased more abruptly with a sharper slope than the other samples. The

AE/PE curves of the flume deposits in Figure V-8 reflected more the behaviour of the silt sample with a gradual decrease in AE/PE in the soil profile-controlled stage. However, due to a lower water retention capability, the AE/PE curves of the flume deposits later converged with that of the tailings beach sand sample at water contents below 1%, i.e. in the residual stage.

Similar observations could be made for the changes in void ratio with time during evaporation presented in Figure V-9. The shrinkage limit described in Chapter 4 (where the void ratio becomes almost constant) was reached between Day 9 and Day 10 for the tailings beach sand, A3 and A1 which have fines contents of 7%, 9% and 12% respectively. The shrinkage limit was later attained on Day 12 for A5 (17% fines) and Day 15 for silt. This showed that the physical properties of the flume deposits such as the shrinkage limit were influenced by the relative proportions of fines captured by the beach. Furthermore, the shrinkage limits of the sand and silt samples were found to be lower and upper boundaries respectively for the onset of the shrinkage limit for the flume deposits during the evaporation tests.

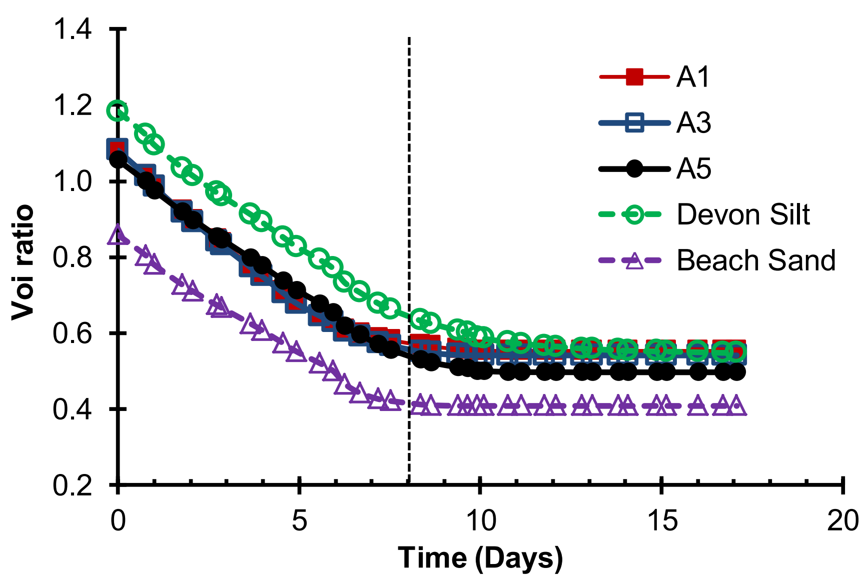


Figure V-9. Variations in void ratios with time during evaporation tests

In summary, an increase in the amount of fines captured by the beach in the flume deposits was translated into higher water retention ability which affected the drying characteristics of the materials. This could result in higher water contents being preserved in the tailings beach materials for longer periods of time. The extent of the fines capture by the oil sands tailings beach should therefore be carefully assessed for the safe operation of the tailings disposal facility.

### 4.2.3 Direct Shear Tests

Direct shear test were conducted on tailings sand specimens. The tailings beach sand sample was found to be cohesionless with a peak friction angle measured at 41°. The friction angle was found to be 37° in residual conditions. The cohesionless nature of the tailings beach sand sample emphasized the controlling effect of sand-to-sand contacts on the behaviour of the beach material as a result of its coarser sand fraction. Table V-3 compares the shear strength parameters of the tailings beach sand to those measured for the flume deposits in Chapter 4. It can be seen that the shear strength parameters of the flume deposits were close to those measured for the tailings sand. Indeed, the mean peak and residual friction angles of the flume deposits were determined to be 38° and 33° respectively. The small cohesion in the flume samples may be imparted by the larger amounts of fines captured by the beach in the flumes.

Table V-3. Comparison between the shear strength parameters of the samples

| FLUME ID | Friction angle ϕ (°) | | Cohesion (kPa) | | Failure Envelope | |
|---|---|---|---|---|---|---|
| | Peak | Residual | Peak | Residual | Peak | Residual |
| **A3 (9% fines)** | 36 | 33.2 | 6 | 3.5 | $\tau = 6 + \sigma\tan36$ | $\tau = 3.5 + \sigma\tan33.2$ |
| **A5 (17% fines)** | 38 | 34 | 5 | 2.2 | $\tau = 5 + \sigma\tan38$ | $\tau = 2.2 + \sigma\tan34$ |

| | | | | | | |
|---|---|---|---|---|---|---|
| **A1(12% fines)** | 37.4 | 36 | 5 | 2 | $\tau = 5 + \sigma\tan 37.4$ | $\tau = 2 + \sigma\tan 36$ |
| **Tailings Sand** | 41 | 37 | 0 | 0 | $\tau = \sigma\tan 41$ | $\tau = \sigma\tan 37$ |

The failure envelopes of the samples are presented in Figures V-10 and V-11 and further highlight the similarities in the normal stress response of the flume samples to that of sand. The failure envelopes of the flume deposits and tailings sand were found to be linear and close to one another. Thus, it could be implied that the strength of the flume deposits was controlled by the coarser sand particles, whereas the fines fraction imparted a small degree of cohesion in the flume materials. The development of cohesion, albeit small, indicated a departure of the tailings flume deposits from the behaviour of typical cohesionless tailings beach sand which is also coarser.

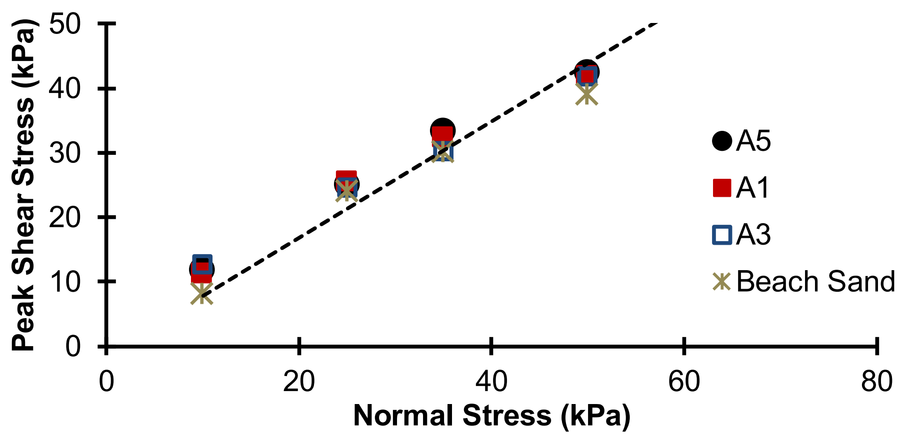


Figure V-10. Peak failure envelopes of the flume deposits samples and Beach sand in direct shear

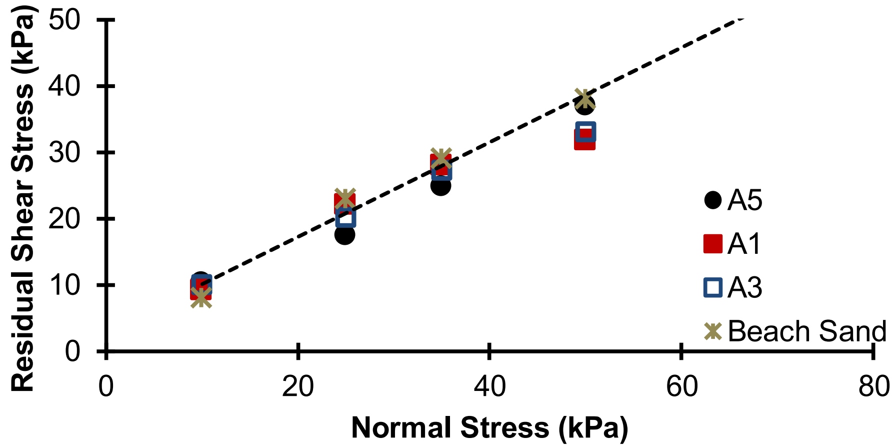


Figure V-11. Failure envelopes of the flume deposits samples and Beach sand in residual conditions

Figures V-12 and V-13 show the shear stress-displacement and volume change-displacement curves yielded from direct shear tests under a normal stress of 35 kPa for A3, A5 and the beach sand sample. Figure V-12 shows that the peak shear stress of the beach sand is not well defined in comparison to that of the flume deposits A3 and A5 at this stress level. Furthermore the peak shear strength appears to be mobilized at smaller displacements for the flume deposits.

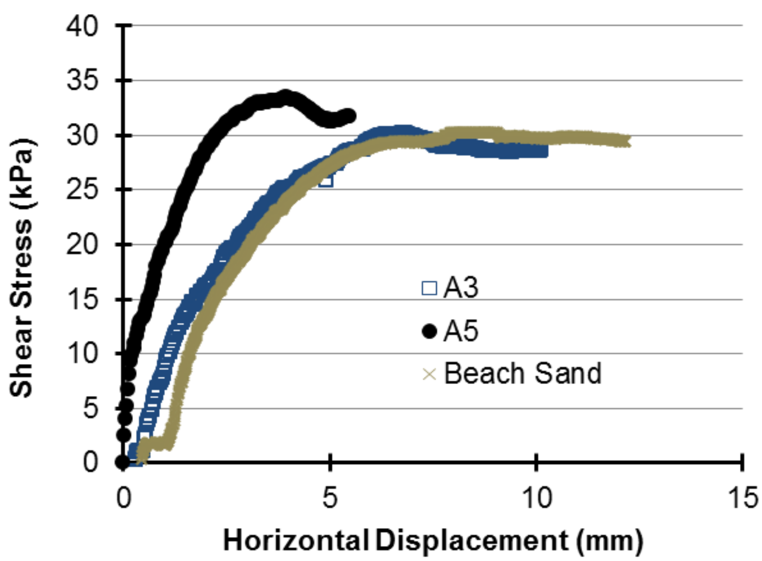


Figure V-12. Changes in shear stress with horizontal displacement during direct shear tests under 35 kPa normal stress

The corresponding changes in volume of the samples during shearing are presented in Figure V-13. The samples initially contracted and then began to dilate at horizontal displacements that corresponded to the onset of the peak shear stress in Figure V-12. This reversal of the volume change behaviour has also been reported by Yamamuro and Covert (2001) in their investigation of loose Nevada sand with various silt contents. The authors also related the occurrence of the contractile behaviour at low axial strains, to the liquefaction susceptibility of such loose materials under low applied stress levels. Yamamuro and Covert (2001) also noted that increasing silt contents extended the contractile behaviour to larger axial strains. However, due to the similarities and limited amount of samples tested in this program, the influence of the fines and silt contents on volume change properties could not be clearly determined.

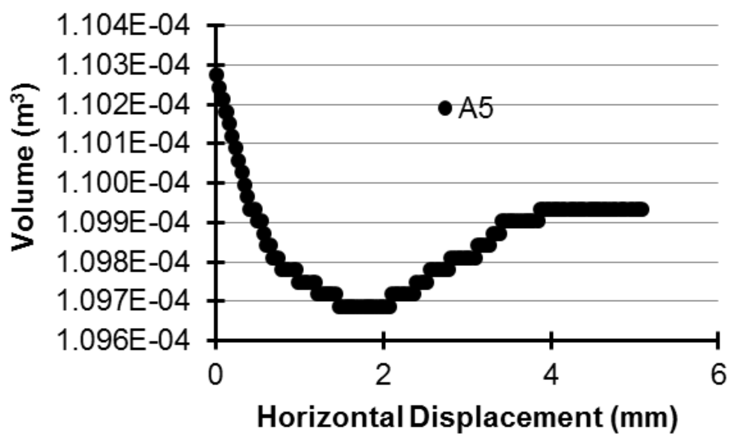


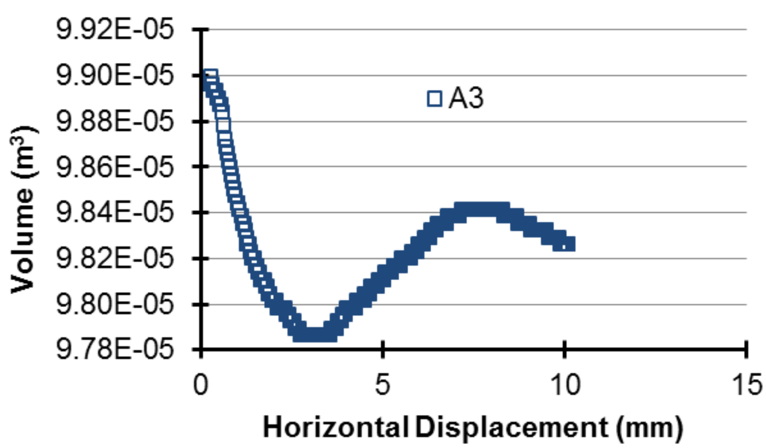

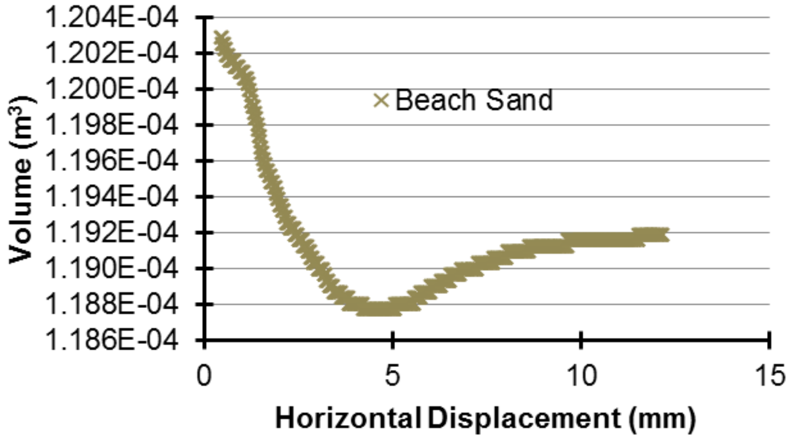


Figure V-13. Volume change as a function of horizontal displacement during direct shear tests under a normal stress of 35 kPa for A5 (Top), A3 (Middle) and the Beach Sand (Bottom)

4.3 Large Strain Consolidation (LSC) Test Results

LSC tests were conducted on undisturbed flume deposit samples in large strain consolidation cells from 0.4 kPa to a maximum applied stress of 500 kPa. The resulting void ratio - effective stress relationships are presented in Figures V-14. The changes in coefficient of volume compressibility ($m_v$), and void ratio (e) during consolidation are summarized in Table V-4.

Table V-4.Consolidation coefficients of the beach deposits ($M_v$ in $m^2/MN$)

| Stress (kPa) | **A3 (9% fines)** | | **A5 (17% fines)** | |
|---|---|---|---|---|
| | e | Mv | e | Mv |
| Initial | 0.83 | / | 0.68 | / |
| 0.4 | 0.83 | 4 | 0.68 | 4 |
| 4.4 | 0.83 | 3 | 0.68 | 3 |
| 10 | 0.83 | 5 | 0.68 | 6 |
| 40 | 0.83 | 21 | 0.67 | 24 |
| 80 | 0.83 | 43 | 0.67 | 47 |
| 510 | 0.82 | 280 | 0.67 | 310 |

The semi-logarithmic plot in Figure V-14 shows the relationship between e and the effective stress for the tailings beach deposits during consolidation. The undisturbed beach samples showed a similar response to the applied stress with a small overall change in void ratio of about 1%. For instance, the void ratio of the undisturbed sample in Flume A5 decreased from 0.68 initially, to 0.67 at the end of the test at 500 kPa in Figure V-14. This behaviour is characteristic of sand which has a low compressibility. From Table V-2, it could be observed that the values of $m_v$ for the beach deposits were also similar. The magnitude of $m_v$ gradually increased from 4 $m^2$/MN initially, to approximately 300 $m^2$/MN at the end of the consolidation tests for all beach deposits. A large range of variation of $m_v$ during consolidation was also reported by Qiu and Sego (2001), i.e. between 0.61 - 379 $m^2$/MN and 0.29 - 162 $m^2$/MN for CT and gold mine tailings respectively.

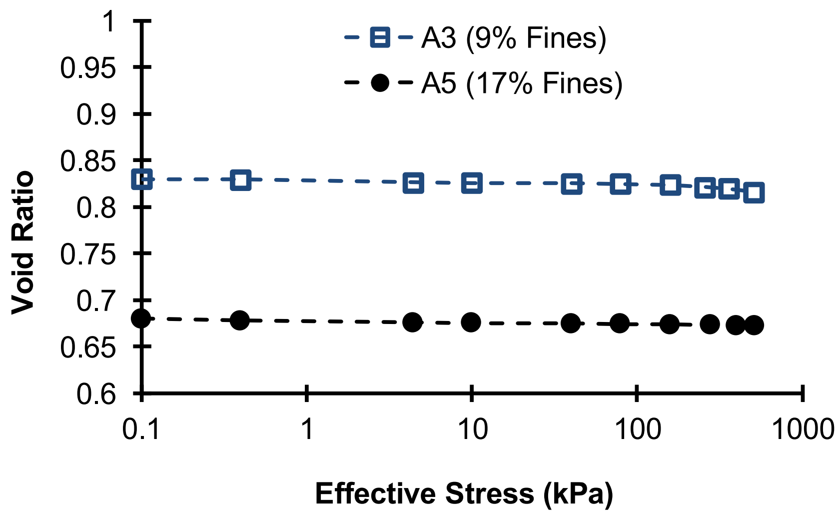


Figure V-14. Variations in void ratio (e) with applied stress for flumes A3 and A5

Wong et al. (2008) describes the consolidation behaviour of oil sands tailings mixtures comprising fine and coarse tailings (21% overall fines content) in 3 stages: 1) Stage I, where the compressibility of the tailings material is fines-controlled and follows the behaviour of fine tailings; 2) Stage II, which is the transition stage wherein the compressibility is dictated by both fines and sand fraction; and 3) Stage III, where the compressibility is sand-controlled and dominated by contacts between sand particles in the matrix. The beach materials tested in this program where formed from MFT-sand mixtures, and captured between 9% and 17% fines. The low compressibility of the beach appears to be strongly dominated by Stages II and III due to the relatively low amount of fines captured. Sand to sand contacts therefore predominantly controlled the consolidation behaviour. However, the influence of the proportion of fines captured by the beach on consolidation properties could not be fully assessed due to the limited number of test samples. Nonetheless, it could be suggested that a more significant contribution of the fines fraction to the consolidation behaviour, i.e. Stage I, would likely arise as the fines captured by the beach increases. An increase in the fines content of the beach would also be expected to cause changes in k as the fines particles would be reoriented and forced into void spaces under the applied stress (Suthaker and Scott 1996). Small changes in k were observed in this test as illustrated in Figures V-15 and V-16.

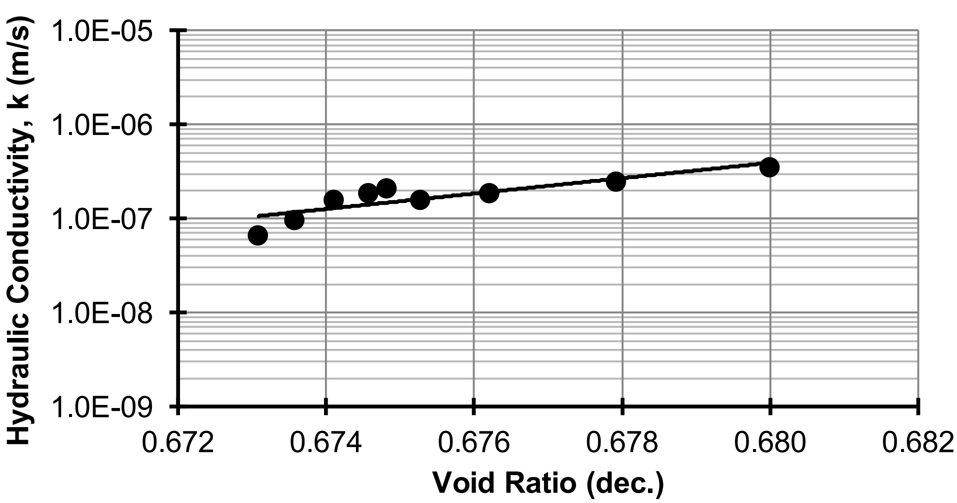


Figure V-15. Variations in hydraulic conductivity (k) with void ratio during consolidation in flume A5

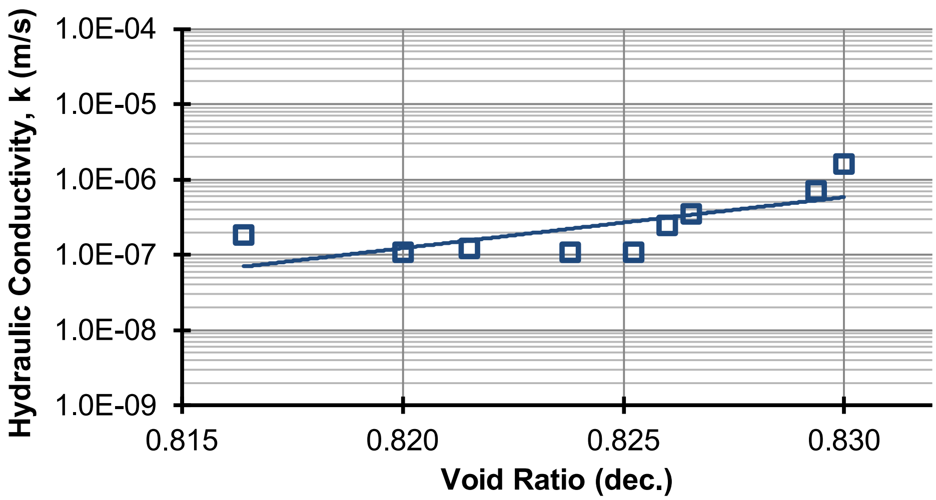


Figure V-16. Changes in hydraulic conductivity (k) with void ratio during consolidation in A3

The coefficient of consolidation, $C_v$, is related to the k, $m_v$ and the unit weight of water, $\gamma_w$, as follows (Head 1994):

$$C_v = \frac{k}{m_v \times \gamma_w} \qquad [1]$$

According to [1], $C_v$ would tend to decrease during consolidation of the beach samples. A wide range of variation is also expected for $C_v$ in light of the experimental data presented thus far. For example, using test data in Table V-2 and Figure V-13 (with $\gamma_w$ = 0.0098 MN/m$^3$), the magnitude of $C_v$ can be approximated to change from 207 m$^2$/year to 1 m$^2$/year between load steps 0.4 kPa and 500 kPa respectively for A5. This further confirms the predominance of sand to sand contacts at the later stages of consolidation where $C_v$ becomes very low.

In summary, the compressibility of the undisturbed beach deposit samples was dominated by inter-particle contacts between sand grains. This low compressibility renders the tailings beach prone to a build-up of pore pressures, which could lead to instability problems during the operation of the tailings disposal facility. The risk of instability is also expected to be magnified by a higher proportion of fines captured by the beach due in part to the lowering of k, and upon the loose deposition of the oil sands tailings material of this composition (Yamamuro and Covert, 2001).

## 5. OBSERVATIONS AND CONCLUSIONS

PSD test results showed that the tailings beach materials in the flumes captured between 9% and 17% fines, and were predominantly liquefiable silty sands (Salgado et al. 2000). Furthermore, the deposits were found to be essentially uniform. A larger proportion of fines captured by the beach in flume A5 resulted in a flat slope, which hindered the process of fines migration and capture that typically occurs in such tailings. Slurry deposition parameters therefore play an important role in the capture of fines along the beach profile of the tailings deposits.

The unsaturated behaviour of the flume deposits in this test was influenced by both the sand fraction and the fines captured by the beach. Similarities between the SWCCs of the flume deposits and the coarse tailings sand sample indicated that the sand fraction mainly dictated the overall desaturation behaviour; whereas, the fines fraction controlled the residual behaviour, which affected the slope of the SWCC beyond the AEV for the flume deposits. The shape of the SWCC was also related to that of the associated grain size curves. Additionally, an increase in the amount of fines captured by the beach in the flume deposits was translated into higher water retention ability which affected the drying characteristics of the materials. This could lead to higher water contents being preserved in the tailings beach deposits for extended periods of time.

The compressibility of the undisturbed beach deposit samples was dominated by inter-particle contacts between sand grains. This low compressibility renders the tailings beach prone to a build-up of pore pressures, which could lead to instability problems during the operation of the tailings disposal facility. The risk of instability is also expected to be magnified by a higher proportion of fines captured by the beach. Oil sands tailings are typically deposited in the loose state, which also increases the liquefaction susceptibility of beach materials of the composition studied in this program. The extent of the fines capture by the oil sands tailings beach should therefore be carefully assessed for the safe operation of the tailings disposal facility as the industry is shifting towards larger amounts of fines captured in disposal areas.

## REFERENCES


Blight, G. E. and Steffen, O. K. H. (1979). Geotechnics of gold mining waste disposal. *Current Geotechnical Practice in Mine Waste Disposal*, ASCE, 1 - 52.

Blight, G.E., Thomson, R.R. and Vorster, K. 1985. Profiles of hydraulic-fill tailings beaches, and seepage through hydraulically sorted tailings. *Journal of the South African Institute of Mining and Metallurgy*, 85(5): 157 - 161.

Camp, F.W. 1977. Processing Athabasca tar sands - tailings disposal. *The Canadian Journal of Chemical Engineering*, 55(5): 581 - 591.

Caughill, D.L., Morgenstern, N.R. and Scott J.D. 1993. Geotechnics of nonsegragating oil sand tailings. Canadian Geotechnical Journal, 30: 801 - 811.

Chalaturnyk, R.J., Scott, J.D. and Özüm, B. 2002. Management of oil sands tailings. *Petroleum Science and Technology*, 20, (9 & 10): 1025 - 1046.

Ciu, Z., Liu, Q., Etsell, T.H., Oxenford, J. and Coward, J 2003. Heavy minerals in the Athabasca oil sands tailings-potential and recovery processes. *Canadian Metallurgical Quarterly*, 42 (4): 383 - 392.

Dusseault, M.D., Scott J.D. 1983. Tailings pond behaviour and characterization of oil sand tailings sludge. *Particulate Science and Technology*, 1: 295 - 309.

Ferguson, G.P., Rudolph, D.L., Barker, J.F. 2009. Hydrodynamics of a large oil sand tailings impoundment and related environmental implications. *Canadian Geotechnical Journal*, 46: 1446 - 1460.

Fredlund, D.G., Xing, A., and Huang, S. 1994. Predicting the permeability function for unsaturated soils using the soil water characteristic curve. *Canadian Geotechnical Journal*, 31: 533 - 546.

Fredlund, M.D., Wilson, G.W. and Fredlund, D.G. 2002. Use of the grain size distribution for estimation of the soil water characteristic curve. *Canadian Geotechnical Journal*, 39: 1103 - 1117.

Head K.H. 1994. *Manual of Soil Laboratory Testing - Volume II: Permeability, Shear Strength and Compressibility tests*, 2nd Edition, Pentech Press, London

Kabwe, L., Wilson, W., and Scott, D., 2014. Influence of an Underlying Sand Beach on Drainage and Desiccation of Fine Tailings. Paper accepted for presentation at the International Oil Sands Tailings Conference 2014, Lake Louise, Alberta.

Matthews, J.G., Shaw, W.H., MacKinnon, M.D. and Cuddy, R.G. 2002. Development of composite tailings technology at Syncrude. *International Journal of Surface Mining, Reclamation and Environment*, 16(1): 24 - 39.

Miller, W.G., Scott, J.D., and Sego, D.C. 2009. Flume deposition modeling of caustic and noncaustic oil sands tailings. *Canadian Geotechnical Journal*, 46: 679 - 693.

Mittal H. K. and Morgenstern N. R. 1975. Parameters for the design of tailings dams. *Canadian Geotechnical Journal*, 12: 235 - 261.

Penner, T.J. and Foght J.M. 2010. Mature fine tailings from oil sands processing harbour diverse methanogenic communities. *Canadian Journal of Microbiology*, 56: 459 - 470.

Qiu, Y. and Sego, D.C. 2001. Laboratory properties of mine tailings. *Canadian Geotechnical Journal*, 38: 183 - 190.

Salgado, R., Bandini, P. and Karim, A. 2000. Shear strength and stiffness of silty sand. *Journal of Geotechnical and Geoenvironmental Engineering*, 126(5): 451 - 462.

Suthaker, N.N., and Scott J.D. 1996. Measurement of hydraulic conductivity in oil sand tailings slurries. *Canadian Geotechnical Journal*, 33: 642 - 653.

Yanful, E.K. and Mousavi, S.M. 2003. Estimating falling rate of evaporation from finite soil columns. *The Science of the total Environment*, 313: 151 - 152.

Wilson, G.W., Fredlund, D.G. and Barbour, S.L. 1994. Coupled soil-atmosphere modeling for soil evaporation. *Canadian Geotechnical Journal*, 31: 151 - 161.

Wong, R. C. K., Mills, B. N., and Liu Y.B. 2008. Mechanistic model for one-dimensional consolidation behavior of non-segregating oil sands tailings. *Journal of Geotechnical and Geoenvironmental Engineering*, 134(2): 195 - 202.

Yamamuro, A.J. and Covert, M.K. 2001. Monotonic and cyclic liquefaction of very loose sands with high silt content. *Journal of Geotechnical and Geoenvironmental Engineering*, 127: 314 - 324.

Yang H., Rahardjo H., Leong E-C. and Fredlund D.G. 2004. Factors affecting drying and wetting soil water characteristic curves of sandy soils. *Canadian Geotechnical Journal*, 41: 908 - 920.

# VI. CHAPTER 6. GENERAL CONCLUSIONS AND SUGGESTIONS FOR FURTHER STUDIES

- GENERAL OBSERVATIONS AND CONCLUSIONS

Beaching studies were conducted by Total EP Canada Ltd. at SRC facilities in Saskatoon, SK. Mixtures of MFT and fine sand were discharged into test flumes to form beach deposits of slope inclinations ranging from 0.5% to 8%. PSD test results showed that the flume deposits were essentially silty sands with an average silt content of 15%. The beach materials captured between 9% and 17% fines. A distribution of fines both with depth and along the slope of the beach deposits was observed with a higher concentration of fines content generally located near the toe area of the beach deposits slopes. Vertical sorting of the flume deposits resulted in a 3% difference in fines content between the surface and bottom of the deposits. Additionally, the extent of the process of migration and capture of fines was found to be related to the inclination of the slope of the beach materials. The flume deposit with the flattest slope (i.e., 0.5%) captured the largest amount of fines (i.e., 17%) in this program. However, the flat resulted in a larger concentration of fines near the point of deposition in contrast with the observations made with the other flume deposits.

In-situ and laboratory measurements of k for the flume deposits yielded values in the range of $1{\times}10^{-6}$m/s - $1{\times}10^{-8}$ m/s. The magnitude of k was found to be related to the amount and distribution of fines captured by the beach materials. Measurements carried out in a 0.25 m wide x 0.5 m height x 8.0 m length flume highlighted a decrease in k with increasing fines content from the crest to the toe of the flume deposit slope. Laboratory measurements of k conducted on undisturbed flume deposit samples showed that the magnitudes of $k_v$ and $k_h$ remained close to each other in the fines content range of this program. In general, a good agreement was noted between in-situ and laboratory experimental data. However, the absence of drainage provisions in the flumes at the time of testing may have affected in-situ $k_h$ measurements.

The SWCCs of the flume deposits yielded similar AEVs in the range of 3 - 4 kPa. Values of $\Psi_r$ for the flume deposits samples were determined to be between 10 and 15 kPa. The magnitude of $\Psi_r$ was observed to be dependent upon the texture of the flume deposits, i.e. the proportion of fines captured by the beach. Changes in the AEVs were also attributed to differences in the texture of the beach materials. Similar characteristics were noted between the SWCCs and PSD curves of the flume deposits. Drying test results showed that the changes in the AE/PE ratio of the flume samples with time exhibited similar characteristics with the associated SWCCs and occurred in three stages. The onset and extent of each stage was controlled by the beach materials texture, i.e. the amount of fines captured by the beach materials.

Direct shear tests were conducted on undisturbed flume deposits samples and yielded linear failure envelopes. Measured peak friction angles were found to vary between 37° and 40°. Residual friction angles were in the range of 30° to 35°. The flume deposits showed evidence of both contractile and dilatant behaviour under the applied normal stress range of 10 kPa - 50 kPa. Furthermore, the friction angle was found to increase with the amount of fines captured by the beach materials. However, it was emphasized from direct shear test results that residual behaviour was difficult to determine on the basis of the fines content alone.

LSC tests highlighted the low compressibility of the flume deposits with a total void ratio change approximating 1%. The compressibility of the beach materials was found to be affected by the amount of sand fraction which is less compressible. However, increasing amounts of fines captured by the beach will affect the compressibility of the deposited tailings beach materials.

Comparative studies were conducted using Devon silt and coarse tailings beach sand samples. Test results showed that the geotechnical characteristics of the flume deposits were within the envelopes of silt (upper boundary) and the beach sand (lower boundary), and were influence by variations in the proportions of fines captured by the beach.

The controlling effect of the fines capture process to meet the objective (ERCB 2009) of the amount of FFT being produced through capturing 50% of fines in the tailings feed and DDAs was also demonstrated in this study. It is therefore crucial to assess the implications of increasing fines content on the compressibility, the magnitude of k, and the strength of the deposited tailings material to ensure the safe operation of the DDA.

- SUGGESTIONS FOR FURTHER STUDIES

Further studies aimed towards the assessment of the volume change properties and dilatancy angle of the MFT-sand tailings beach material are suggested. For instance, triaxial shear tests would enable the determination of the fines content - dilatancy angle relationship for this material and evaluate its liquefaction susceptibility. Experimentations on flume deposits with fines captured exceeding 20% are also recommended to confirm the trends in behaviour observed in this program. This would also allow for a better understanding of the compressibility of the deposit and evaluate potential increases in pore pressures as more fines are captured by the beach material. Mixing sand and MFT provides an interesting opportunity to reduce the MFT inventory of the oil sand industry. However, predictive models for the behaviour of such deposited tailings material need to be developed further.

## REFERENCES


Aubertin, M., Ricard, J.F. and Chapuis, R. P. 1998. A predictive model for the water retention curve: application to tailings from hard-rock mines. *Canadian Geotechnical Journal*, 35: 55 - 69.

Aubertin, M., Mbonimpa, M., Bussière, B. and Chapuis R. P. 2003. A model to predict the water retention curve from basic geotechnical properties. *Canadian Geotechnical Journal*, 40: 1104 - 1122.

Barbour, S. L. 1998. Nineteenth Canadian Geotechnical Colloquium: The soil-water characteristic curve: a historical perspective. *Canadian Geotechnical Journal*, 35: 873 - 894.

Bear, J. 1972. *Dynamics of fluids in porous media*, Dover Publications Inc., New York.

Been, K. and Jefferies, M. 2004. Stress-dilatancy in very loose sands. *Canadian Geotechnical Journal*, 41: 972 - 989.

Benson, C.H. and Trast, J.M. 1995. Hydraulic conductivity of thirteen compacted clays. *Clays and Clay Minerals*, 43(6): 669 - 681.

Blight, G.E. and Bentel, G.M. 1983. The behaviour of mine tailings during hydraulic deposition. *Journal of the South African Institute of Mining and Metallurgy*, 83(4): 73 - 86.

Blight, G. E. and Steffen, O. K. H. (1979). Geotechnics of gold mining waste disposal. *Current Geotechnical Practice in Mine Waste Disposal*, ASCE, 1 - 52.

Blight, G.E., Thomson, R.R. and Vorster, K. 1985. Profiles of hydraulic-fill tailings beaches, and seepage through hydraulically sorted tailings. *Journal of the South African Institute of Mining and Metallurgy*, 85(5): 157 - 161.

Bolton, M.D. (1986). The strength and dilatancy of sands. *Géotechnique*, 36(1): 65 - 78.

Buckingham, E. 1907. Studies on the movement of soil moisture. *U.S. Department of Agriculture*, Soils Bulletin 38.

Bumb, A. C., Murphy, C. L. and Everett, L. G. 1992. A comparison of three functional forms to representing soil moisture characteristics. *Ground Water*, 3: 177 - 185.

Butler, R.M., McNab, G.S. and Lo H.Y. 1981. Theoretical studies on the gravity drainage of heavy oil during in-situ steam heating. *Canadian Journal of Chemical Engineering*, 59: 455 - 460.

Camp, F.W. (1977). Processing Athabasca tar sands - Tailings disposal. *The Canadian Journal of Chemical Engineering*, 55: 581 - 591.

Carter, M. R. (1993), *Soil sampling and methods of analysis,* Lewis, Boca Raton, Fla.

Childs, E. C. 1940. The use of soil moisture characteristics in soil studies. *Journal of Soil Science*, 50: 239 - 252.

Dusseault, M.D., Scott J.D. 1983. Tailings pond behaviour and characterization of oil sand tailings sludge. *Particulate Science and Technology*, 1: 295 - 309.

ECRB 2009. Directive 074 - Tailings performance criteria and requirements for oil sands mining schemes. *Alberta Energy Regulator (AER)*, February 3, 2009.

Fredlund, D. G. and Rahardjo, H. 1993, *Soil mechanics for unsaturated soils*, John Wiley and Sons, Inc., New York.

Fredlund, D. G., Xing, A. and Huang, S. 1994. Predicting the permeability function for unsaturated soils using the soil-water characteristic curve. *Canadian Geotechnical Journal*, 31: 533 - 546.

Fredlund, D.G. 2000. The 1999 R.M. Hardy lecture: The implementation of unsaturated soil mechanics into geotechnical engineering. *Canadian Geotechnical Journal*, 37: 963 - 986.

Fredlund, M.D., Wilson G.W. and Fredlund, D.G. 2002. Use of the grain-size distribution for estimation of the soil water characteristic curve. *Canadian Geotechnical Journal*, 39: 1103 - 1117.

Fredlund, D.G. 2006. Unsaturated soil mechanics in engineering practice. *Journal of Geotechnical and Geoenvironmental Engineering*, 132(3): 286 - 321.

Gibson, R.E., England, G.L. and Hussey, M.J.L. 1967. The theory of one-dimensional consolidation for saturated clays: 1. Finite non-linear consolidation of thin homogenous layers. *Géotechnique*, 17: 261 - 273.

Granger, R.J. and Gray, D.M. 1989. Evaporation from natural nonsaturated soil surfaces. *Journal of Hydrology*, 111: 21 - 29.

Haines, W. B. 1927. Studies on the physical properties of soils. *Journal of Agricultural Science*, 17: 264 - 290.

Haines, W. B. (1930), "Studies in the physical properties of soil: The hysteresis effect in capillary properties, and the modes of moisture distribution associated therewith", *Journal of Agricultural Science*, 20: 97 - 116.

Hazen, A. 1892. Some physical properties of sands and gravels, with special reference to their use in filtration. $24^{th}$ Annual Rep., Massachusetts State Board of Health, Pub. Doc. No. 34, 539 - 556 (as referenced by Barbour 1998)

Juang C. H. and Holtz R. D. 1986a. Fabric, pore size distribution and permeability of sandy soils. *Journal of Geotechnical Engineering*, 112: 855 - 868.

Juang, C. H. and Holtz, R. D. 1986b. A Note on preparation of specimens on non-cohesive material for Mercury Intrusion Porosimetry. *Geotechnical Testing Journal*, ASTM, Vol. 9, No. 3.

Kenney T. C., Lau D., and Ofoegbu G. I. 1984. Permeability of compacted granular materials. *Canadian Geotechnical Journal*, 21: 726 - 729.

King F. H. (1899), "Principles and conditions of the movement of groundwater", U.S. Geological Survey 19th Annual Report, Part 2, pp. 59-294.

Kovács, G. (1981), "Seepage hydraulics", Elsevier Science Publishers, Amsterdam.

Kwak, M., James, D.F. and Klein, K.A. 2005. Flow behaviour of tailings paste for surface disposal. *International Journal of Mineral Processing*, 77: 139 - 153.

Marshall, T. J., Holmes, J. W. and Rose, C. W. 1996. *Soil physics*, 3rd Edition, Cambridge University Press, Cambridge, U.K.

Miller, W.G., Scott, J.D., and Sego, D.C. 2009. Flume deposition modeling of caustic and noncaustic oil sands tailings. *Canadian Geotechnical Journal*, 46: 679 - 693.

Mitchell, J. K. and Madsen, F. T. 1987. Chemical effects on clay hydraulic conductivity. *Proceedings of Geotechnical Practice for Waste Disposal'87*, ASCE, Geotechnical Special Publication 13: 87 - 116.

Mittal, H. K. and Morgenstern, N. R. 1975. Parameters for the design of tailings dams. *Canadian Geotechnical Journal*, 12: 235 - 261.

Poulos, S.J., Robinsky, E.I. and Keller, T.O. 1985. Liquefaction resistance of thickened tailings. *Journal of Geotechnical Engineering*, 111(12): 1380 - 1394.

Quirk, J. P. and Schofield, R.K. 1955. The effect of electrolyte concentration on soil permeability. *Journal of soil science*, 6(2): 163 - 178.

Qiu, J., and Sego, D.C. 1998. Design of sub-aerial tailings deposition in arid regions. *Proceedings of 51st Canadian Geotechnical Conference*, 615 - 622.

Qiu, J., and Sego, D.C. 2006. Optimum deposition for sub-aerial tailings disposal: concepts and theories. International Journal of Mining, Reclamation and Environment 20(4): 272 - 285

Robinsky, E.I. 1975. Thickened discharge - A new approach to tailings disposal. *CIM Bulletin*, December 1975, 47 - 59. (as referenced by Lighthall 1987).

Rowe, P.V. 1962. The stress-dilatancy relation for static equilibrium of an assembly of particles in contact. *Proceedings of the Royal Society of London*, Series A, 269: 500 - 527.

Schanz, T. and Vermeer, P.A. 1996. Angles of friction and dilatancy of sand. *Géotechnique*, 46(1): 145 - 151.

Shah, A., Fishwick, R., Wood, J., Leeke G., Rigby S., and Greaves M. 2010. A review of novel techniques for heavy oil and bitumen extraction and upgrading. *Energy and Environmental Science*, 3: 700 - 714.

Slichter C.S. 1897-1898. Theoretical investigations of the motion of ground water. *U.S. Geological Survey*, Water Supply Paper 140 (as referenced by Barbour 1998).

Suthaker, N.N., and Scott J.D. 1996. Measurement of hydraulic conductivity in oil sand tailings slurries. *Canadian Geotechnical Journal*, 33: 642-653

Taylor, D.W. (1948). *Fundamentals of soil mechanics*. Wiley, New York.

Van Genuchten, M. Th. 1980. A closed form equation for predicting the hydraulic conductivity of unsaturated soils. *Soil Science Society of America Journal*, 44: 892 - 898.

Wong, R. C. K., Mills, B. N., and Liu Y.B. 2008. Mechanistic model for one-dimensional consolidation behavior of non-segregating oil sands tailings. *Journal of Geotechnical and Geoenvironmental Engineering*, 134(2): 195 - 202.

Yamamuro, A.J. and Covert, M.K. 2001. Monotonic and cyclic liquefaction of very loose sands with high silt content. *Journal of Geotechnical and Geoenvironmental Engineering*, 127: 314 - 324.

## VII. **APPENDIX A** - FLUME DEPOSITS AND IN SITU TESTS

1. Pictures of the Flume deposits

Figure VII-1. Flume deposits A1 (left) and A3 (right)

Figure VII-2. Flume deposits A5 (left) and A13 (right)

Figure VII-3. Pictures of the Pilot flume (Top) and of the Pilot flume deposit (Bottom)

2. Saturation Procedure of the Flume deposits

Two methods were used to saturate the flume deposits before testing was initiated. In the first method, Open tubes of approximately 12cm diameter were partially inserted in the beach deposits at one end of the flumes as illustrated in Figure VII-4. The tubes were filled with water which slowly spread downwards and sideways, gradually saturating the flume deposits from the bottom. This procedure was carried out over five days or more depending on the progress of saturation in the flumes. The second method involved the saturation of the flume deposits from the top by pouring water over the surface of the flume deposits up to a certain height to partially flood deposit. After an elapsed period of time up to five days (or less), the excess water was removed from the flumes with the aid of a pump. It is acknowledged that this procedure often resulted in the oversaturation of the flume deposits, which may have affected some in-situ k measurements due to absence of drainage provisions in the flumes. Additionally, flume deposits saturated using this procedure were tested two or three days after removal of the overlaying water to allow drying and evaporation of the excess water prior to the beginning of in-situ measurements.

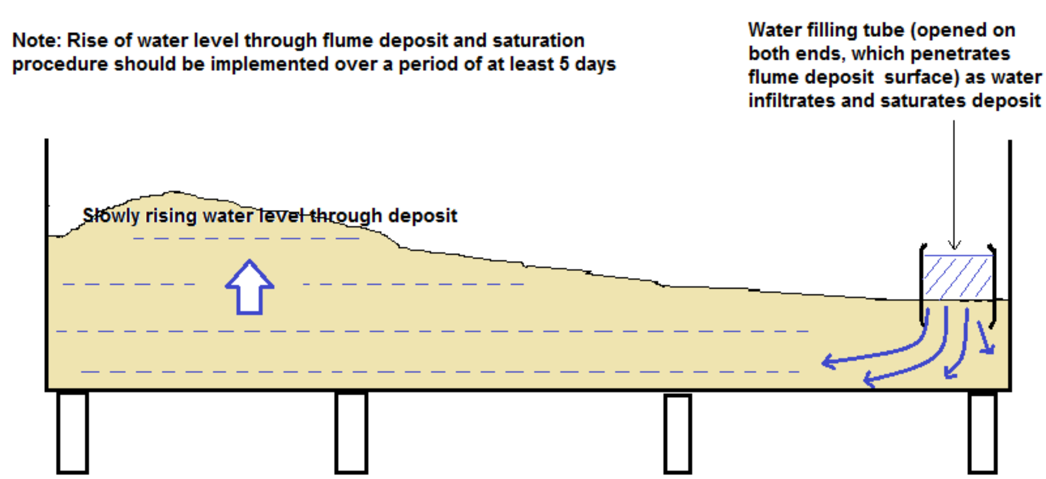


Figure VII-4. Flume deposit saturation procedure

3. Specific Gravity of the Flume deposits

The specific gravity (Gs) was determined from representative flume deposit bulk samples obtained directly from the flumes at SRC facilities. A water pycnometer test was conducted with a vacuum system to obtain Gs according to ASTM D854-10 whereby Gs is derived experimentally using:

$$Gs = \frac{M_S \times \rho_T}{(M_1 - M_2 + M_S) \times \rho_{20}} \quad [1]$$

Where $M_s$ is the dry mass of soil grains; $M_1$ is the mass of the pycnometer bottle and specified volume of water; $M_2$ is the mass of pycnometer bottle and specified volume of soil and water at temperature T; $\rho_T$ is the density of water at temperature T; and $\rho_{20}$ is the density of water at 20°C (i.e. 0.998203 g/cm$^3$).

Equation [1] yielded values of Gs between 2.53 and 2.65 at test temperatures ranging from 18.9 °C to 20.9 °C. Experimental data are summarised in table VII-1.

Table VII-1. Pycnometer test results for the flume deposit samples ($M_1$, $M_2$, $M_s$, T and $\rho_T$ are defined as per Equation [1])

| Flume ID | $M_1$ (g) | $M_2$ (g) | $M_s$ (g) | T(°C) | $\rho_T$ (g/cm$^3$) | Gs |
|---|---|---|---|---|---|---|
| A3 | 680.4 | 718.7 | 61.5 | 20.0 | 0.998203 | 2.65 |
| A1 | 680.4 | 719.0 | 62.1 | 20.9 | 0.998013 | 2.64 |
| A5 | 680.4 | 716.0 | 58.9 | 20.3 | 0.998141 | 2.53 |
| A13 | 680.4 | 718.9 | 63.1 | 18.9 | 0.998424 | 2.56 |
| Pilot | 678.6 | 715.8 | 60.5 | 20.6 | 0.998078 | 2.60 |

4. Frozen densities of the undisturbed flume deposit cores

Undisturbed frozen cores were obtained from the frozen beach deposits block samples acquired from the test flumes at SRC. The cores were trimmed to suitable dimensions using a soil lathe. The characteristics of the frozen cores are presented in Tables VII-2 to VII-4.

Table VII-2. Frozen densities of the trimmed vertical cores

| Sample ID | Diameter (cm) | Height (cm) | Mass (g) | Volume ($cm^3$) | Density ($g/cm^3$) |
|---|---|---|---|---|---|
| A1 - large strain | 10.0 | 8.7 | 1218.3 | 686.5 | 1.8 |
| A3 - large strain | 9.9 | 6.6 | 922.1 | 508.1 | 1.8 |
| A5 - large strain | 10.1 | 5.7 | 766.9 | 457.9 | 1.7 |
| G1 - large strain | 10.0 | 7.3 | 1011.4 | 578.1 | 1.7 |
| I2 - large strain | 10.1 | 9.0 | 1212.8 | 716.9 | 1.7 |
| I3 - large strain | 10.1 | 5.7 | 758.8 | 455.9 | 1.7 |
| A13 - large strain | 10.1 | 6.7 | 987.4 | 541.6 | 1.8 |

Table VII-3. Frozen densities of the trimmed direct shear cores

| Sample ID | Diameter (cm) | Height (cm) | Mass (g) | Volume ($cm^3$) | Density ($g/cm^3$) |
|---|---|---|---|---|---|
| A1 - 1 (10 kPa) | 6.3 | 3.5 | 194.1 | 107.5 | 1.8 |
| A1 - 2 (25 kPa) | 6.3 | 3.5 | 207.0 | 109.1 | 1.9 |
| A1 - 4 (50 kPa) | 6.3 | 3.8 | 200.3 | 118.1 | 1.7 |
| A1 - 5 (35 kPa) | 6.3 | 3.7 | 201.0 | 115.6 | 1.7 |
| A3 - 1 (10 kPa) | 6.2 | 3.7 | 206.9 | 113.0 | 1.8 |
| A3 - 2 (25 kPa) | 6.3 | 3.6 | 195.7 | 112.3 | 1.7 |
| A3 - 3 (35 kPa) | 6.2 | 3.5 | 183.1 | 106.8 | 1.7 |
| A3 - 4 (50 kPa) | 6.3 | 3.7 | 192.4 | 114.3 | 1.7 |
| A3 - 5 (70 kPa) | 6.2 | 3.7 | 190.7 | 111.9 | 1.7 |
| A5 - 1 (10 kPa) | 6.3 | 3.7 | 204.7 | 116.0 | 1.8 |
| A5 - 2 (25 kPa) | 6.2 | 3.6 | 197.9 | 111.7 | 1.8 |
| A5 - 3 (35 kPa) | 6.3 | 3.7 | 209.0 | 115.7 | 1.8 |
| A5 - 4 (50 kPa) | 6.3 | 3.5 | 197.4 | 110.2 | 1.8 |
| A5 - 5 (70 kPa) | 6.3 | 3.7 | 200.9 | 115.0 | 1.7 |
| A13 - 1 (10 kPa) | 6.3 | 3.5 | 193.8 | 108.6 | 1.8 |
| A13 - 2 (25 kPa) | 6.3 | 3.6 | 208.2 | 111.9 | 1.9 |
| A13 - 3 (35 kPa) | 6.3 | 3.6 | 209.7 | 112.5 | 1.9 |
| A13 - 5 (25 kPa) | 6.2 | 3.2 | 185.5 | 95.6 | 1.9 |

Table VII-4. Frozen densities of the trimmed horizontal cores

| Sample ID | Diameter (cm) | Height (cm) | Mass (g) | Volume ($cm^3$) | Density ($g/cm^3$) |
|---|---|---|---|---|---|
| A13 - large strain | 10.1 | 10.4 | 1473.9 | 834.8 | 1.8 |
| G1 - large strain | 10.1 | 11.8 | 1698.3 | 939.6 | 1.8 |
| I2 - large strain | 10.1 | 7.6 | 1029.6 | 608.1 | 1.7 |
| A3 - large strain | 10.3 | 8.8 | 1297.6 | 738.1 | 1.8 |
| A1 - large strain | 10.3 | 9.8 | 1452.7 | 828.3 | 1.8 |

## 5. In-Situ Measurements of Hydraulic Conductivity (k) in the Test Flumes

### 5.1 Guelph Permeameter

The operation of the Guelph permeameter requires the selection of a test method, head height ($H_1$) and the reservoir to be used. For the in-situ measurements conducted in this program, the single head method was used (only one head used for testing and calculations) with combined reservoirs. The permeameter reservoir was filled with water and the air inlet tip was filled. The head height was selected and adjusted dependent upon the nature of the flume deposits and the expected fines capture target. The initial water level in the reservoir was noted and measurements were initiated. Changes in water level were then recorded at regular time intervals until the steady rate of fall ($R_1$) was reached. The Guelph permeameter operating instructions manual provides the following expression to determine the measured k:

$$k = \frac{C_1 \times Q_1}{2\pi {H_1}^2 + \pi a^2 C_1 + 2\pi\left(\frac{H_1}{a^*}\right)} \qquad [2]$$

Where a is the radius of the borehole / permeameter tip; a* is the macroscopic capillary length parameter (0.04 $cm^{-1}$); $Q_1$ and $C_1$ are defined as follows:

$$C_1 = \left(\frac{{H_1}/{a}}{1.992 + 0.091\left({H_1}/{a}\right)}\right)^{0.683} \qquad [3]$$

$$Q_1 = R_1 \times 35.22 \qquad [4]$$

Details of the magnitude of the parameters used for the k calculations are given in Table VII-5. Guelph permeameter test data are provided in Tables VII-6 to VII-12. The values of k from Guelph permeameter measurements represented the in-situ horizontal hydraulic conductivity $k_h$ previously reported in Sections 4 and 5.

Table VII-5. Calculations of the hydraulic conductivity (k) from Guelph permeameter test data for the flume deposits (parameters are defined as above in equations [2] to [4])

| FLUME ID | $H_1$ (cm) | a (cm) | $R_1$ (cm/s) | $Q_1$ | $C_1$ | a* ($cm^{-1}$) | k (m/s) |
|---|---|---|---|---|---|---|---|
| A1 | 15.0 | 1.8 | 0.0004 | 0.01 | 2.13 | 0.04 | 7.9E-08 |
| A3 | 8.0 | 3.0 | 0.0050 | 0.18 | 1.13 | 0.04 | 1.2E-06 |
| A5 | 15.0 | 1.8 | 0.0003 | 0.01 | 2.13 | 0.04 | 5.9E-08 |
| A13 | 9.5 | 1.8 | 0.0005 | 0.02 | 1.68 | 0.04 | 1.4E-07 |
| Pilot - Zone 1 | 8.1 | 1.8 | 0.0006 | 0.02 | 1.54 | 0.04 | 1.9E-07 |
| Pilot - Zone 2 | 15.5 | 1.8 | 0.0006 | 0.02 | 2.17 | 0.04 | 1.2E-07 |
| Pilot - Zone 3 | 15.4 | 1.8 | 0.0008 | 0.03 | 2.16 | 0.04 | 1.5E-07 |

Table VII-6. Guelph permeameter measurements in flume A1

| Cumulative time (min) | Water level (cm) | level change (cm) | time interval (s) | rate of change (cm/s) |
|---|---|---|---|---|
| 0 | 19.5 | | | |
| 1 | 28.8 | 9.3 | 60 | 0.1550 |
| 6 | 29.1 | 0.3 | 300 | 0.0010 |
| 11 | 29.2 | 0.1 | 300 | 0.0003 |
| 21 | 29.3 | 0.1 | 600 | 0.0002 |
| 31 | 29.4 | 0.1 | 600 | 0.0002 |
| 52 | 29.7 | 0.3 | 1200 | 0.0003 |
| 81 | 30.4 | 0.7 | 1800 | 0.0004 |
| 142 | 31.9 | 1.5 | 3600 | 0.0004 |
| 202 | 33.3 | 1.4 | 3600 | 0.0004 |
| 262 | 34.9 | 1.6 | 3600 | 0.0004 |

Table VII-7. Guelph permeameter measurements in flume A3

| Cumulative time (min) | Water level (cm) | level change (cm) | time interval (s) | rate of change (cm/s) |
|---|---|---|---|---|
| 0 | 3 | | | |
| 1 | 4.8 | 1.8 | 60 | 0.030 |
| 2 | 6.1 | 1.3 | 60 | 0.022 |
| 4 | 8 | 1.9 | 120 | 0.016 |
| 6 | 9.5 | 1.5 | 120 | 0.013 |
| 8 | 10.6 | 1.1 | 120 | 0.009 |
| 10 | 11.7 | 1.1 | 120 | 0.009 |
| 12 | 12.9 | 1.2 | 120 | 0.010 |
| 14 | 13.9 | 1 | 120 | 0.008 |
| 16 | 15.1 | 1.2 | 120 | 0.010 |
| 18 | 16 | 0.9 | 120 | 0.008 |
| 20 | 17 | 1 | 120 | 0.008 |
| 22 | 18 | 1 | 120 | 0.008 |
| 24 | 18.9 | 0.9 | 120 | 0.007 |
| 26 | 19.9 | 1 | 120 | 0.008 |
| 28 | 20.7 | 0.8 | 120 | 0.007 |
| 30 | 21.7 | 1 | 120 | 0.008 |
| 32 | 22.5 | 0.8 | 120 | 0.007 |
| 37 | 24.5 | 2 | 300 | 0.007 |
| 43 | 26.6 | 2.1 | 300 | 0.007 |
| 48 | 28.5 | 1.9 | 300 | 0.006 |
| 53 | 30.5 | 2 | 300 | 0.007 |
| 62 | 34.2 | 3.7 | 600 | 0.006 |
| 72 | 37.5 | 3.3 | 600 | 0.006 |
| 82 | 41 | 3.5 | 600 | 0.006 |
| 113 | 50.8 | 9.8 | 1800 | 0.005 |
| 143 | 60.1 | 9.3 | 1800 | 0.005 |
| 203 | 77.1 | 17 | 3600 | 0.005 |

Table VII-8. Guelph permeameter measurements in flume A5

| Cumulative time (min) | Water level (cm) | level change (cm) | time interval (s) | rate of change (cm/s) |
|---|---|---|---|---|
| 0 | 24.9 | | | |
| 2 | 25 | 0.1 | 120 | 0.0008 |
| 4 | 25.1 | 0.1 | 120 | 0.0008 |
| 6 | 25.2 | 0.1 | 120 | 0.0008 |
| 11 | 25.3 | 0.1 | 300 | 0.0003 |
| 16 | 25.4 | 0.1 | 300 | 0.0003 |
| 21 | 25.5 | 0.1 | 300 | 0.0003 |
| 26 | 25.7 | 0.2 | 300 | 0.0007 |
| 31 | 25.8 | 0.1 | 300 | 0.0003 |
| 37 | 25.9 | 0.1 | 300 | 0.0003 |
| 42 | 26.1 | 0.2 | 300 | 0.0007 |
| 47 | 26.2 | 0.1 | 300 | 0.0003 |
| 52 | 26.3 | 0.1 | 300 | 0.0003 |
| 57 | 26.4 | 0.1 | 300 | 0.0003 |
| 63 | 26.5 | 0.1 | 300 | 0.0003 |
| 68 | 26.7 | 0.2 | 300 | 0.0007 |
| 78 | 26.9 | 0.2 | 600 | 0.0003 |
| 88 | 27.1 | 0.2 | 600 | 0.0003 |
| 98 | 27.4 | 0.3 | 600 | 0.0005 |
| 108 | 27.6 | 0.2 | 600 | 0.0003 |
| 118 | 27.8 | 0.2 | 600 | 0.0003 |
| 138 | 28.3 | 0.5 | 1200 | 0.0004 |
| 158 | 28.8 | 0.5 | 1200 | 0.0004 |
| 180 | 29.2 | 0.4 | 1200 | 0.0003 |
| 200 | 29.6 | 0.4 | 1200 | 0.0003 |
| 220 | 30 | 0.4 | 1200 | 0.0003 |
| 240 | 30.4 | 0.4 | 1200 | 0.0003 |

Table VII-9. Guelph permeameter measurements in flume A13

| Cumulative time (min) | Water level (cm) | level change (cm) | time interval (s) | rate of change (cm/s) |
|---|---|---|---|---|
| 0 | 11.2 | | | |
| 2 | 11.4 | 0.2 | 120 | 0.0017 |
| 4 | 11.5 | 0.1 | 120 | 0.0008 |
| 6 | 11.6 | 0.1 | 120 | 0.0008 |
| 8 | 11.7 | 0.1 | 120 | 0.0008 |
| 10 | 11.9 | 0.2 | 120 | 0.0017 |
| 12 | 12 | 0.1 | 120 | 0.0008 |
| 14 | 12.1 | 0.1 | 120 | 0.0008 |
| 16 | 12.3 | 0.2 | 120 | 0.0017 |
| 18 | 12.4 | 0.1 | 120 | 0.0008 |
| 20 | 12.5 | 0.1 | 120 | 0.0008 |
| 26 | 12.8 | 0.3 | 300 | 0.0010 |
| 31 | 13.1 | 0.3 | 300 | 0.0010 |
| 37 | 13.3 | 0.2 | 300 | 0.0007 |
| 41 | 13.5 | 0.2 | 300 | 0.0007 |
| 46 | 13.8 | 0.3 | 300 | 0.0010 |
| 51 | 14 | 0.2 | 300 | 0.0007 |
| 56 | 14.2 | 0.2 | 300 | 0.0007 |
| 61 | 14.4 | 0.2 | 300 | 0.0007 |
| 71 | 14.9 | 0.5 | 600 | 0.0008 |
| 82 | 15.3 | 0.4 | 600 | 0.0007 |
| 92 | 15.7 | 0.4 | 600 | 0.0007 |
| 102 | 16.2 | 0.5 | 600 | 0.0008 |
| 122 | 16.9 | 0.7 | 1200 | 0.0006 |
| 143 | 17.6 | 0.7 | 1200 | 0.0006 |
| 163 | 18.2 | 0.6 | 1200 | 0.0005 |
| 182 | 18.8 | 0.6 | 1200 | 0.0005 |
| 213 | 19.7 | 0.9 | 1800 | 0.0005 |
| 243 | 20.6 | 0.9 | 1800 | 0.0005 |

Table VII-10. Guelph permeameter measurements in Zone 1 for the Pilot flume

| Cumulative time (min) | Water level (cm) | level change (cm) | time interval (s) | rate of change (cm/s) |
|---|---|---|---|---|
| 0 | 12.7 | | | |
| 5 | 13.2 | 0.5 | 300 | 0.0017 |
| 10 | 13.6 | 0.4 | 300 | 0.0013 |
| 15 | 14 | 0.4 | 300 | 0.0013 |
| 20 | 14.4 | 0.4 | 300 | 0.0013 |
| 25 | 14.9 | 0.5 | 300 | 0.0017 |
| 30 | 15.3 | 0.4 | 300 | 0.0013 |
| 40 | 15.9 | 0.6 | 600 | 0.0010 |
| 50 | 16.5 | 0.6 | 600 | 0.0010 |
| 60 | 17 | 0.5 | 600 | 0.0008 |
| 70 | 17.6 | 0.6 | 600 | 0.0010 |
| 80 | 18.2 | 0.6 | 600 | 0.0010 |
| 90 | 18.7 | 0.5 | 600 | 0.0008 |
| 100 | 19.2 | 0.5 | 600 | 0.0008 |
| 110 | 19.8 | 0.6 | 600 | 0.0010 |
| 120 | 20.3 | 0.5 | 600 | 0.0008 |
| 130 | 20.7 | 0.4 | 600 | 0.0007 |
| 140 | 21.1 | 0.4 | 600 | 0.0007 |
| 150 | 21.5 | 0.4 | 600 | 0.0007 |
| 160 | 21.9 | 0.4 | 600 | 0.0007 |
| 170 | 22.3 | 0.4 | 600 | 0.0007 |
| 180 | 22.7 | 0.4 | 600 | 0.0007 |
| 200 | 23.4 | 0.7 | 1200 | 0.0006 |
| 220 | 24.1 | 0.7 | 1200 | 0.0006 |
| 240 | 24.8 | 0.7 | 1200 | 0.0006 |

Table VII-11. Guelph permeameter measurements in Zone 2 for the Pilot flume

| Cumulative time (min) | Water level (cm) | level change (cm) | time interval (s) | rate of change (cm/s) |
|---|---|---|---|---|
| 0 | 11.5 | | | |
| 5 | 11.8 | 0.3 | 300 | 0.0010 |
| 10 | 12.1 | 0.3 | 300 | 0.0010 |
| 15 | 12.3 | 0.2 | 300 | 0.0007 |
| 20 | 12.6 | 0.3 | 300 | 0.0010 |
| 25 | 12.8 | 0.2 | 300 | 0.0007 |
| 30 | 13 | 0.2 | 300 | 0.0007 |
| 35 | 13.3 | 0.3 | 300 | 0.0010 |
| 40 | 13.5 | 0.2 | 300 | 0.0007 |
| 45 | 13.7 | 0.2 | 300 | 0.0007 |
| 55 | 14 | 0.3 | 600 | 0.0005 |
| 65 | 14.4 | 0.4 | 600 | 0.0007 |
| 78 | 14.8 | 0.4 | 600 | 0.0007 |
| 85 | 15.2 | 0.4 | 600 | 0.0007 |
| 95 | 15.5 | 0.3 | 600 | 0.0005 |
| 105 | 16 | 0.5 | 600 | 0.0008 |
| 115 | 16.4 | 0.4 | 600 | 0.0007 |
| 125 | 16.6 | 0.2 | 600 | 0.0003 |
| 135 | 17 | 0.4 | 600 | 0.0007 |
| 145 | 17.4 | 0.4 | 600 | 0.0007 |
| 155 | 17.7 | 0.3 | 600 | 0.0005 |
| 165 | 18 | 0.3 | 600 | 0.0005 |
| 175 | 18.3 | 0.3 | 600 | 0.0005 |
| 185 | 18.7 | 0.4 | 600 | 0.0007 |
| 205 | 19.4 | 0.7 | 1200 | 0.0006 |
| 225 | 20.1 | 0.7 | 1200 | 0.0006 |
| 245 | 20.8 | 0.7 | 1200 | 0.0006 |
| 266 | 21.5 | 0.7 | 1200 | 0.0006 |
| 285 | 22.2 | 0.7 | 1200 | 0.0006 |

Table VII-12. Guelph permeameter measurements in Zone 3 for the Pilot flume

| Cumulative time (min) | Water level (cm) | level change (cm) | time interval (s) | rate of change (cm/s) |
|---|---|---|---|---|
| 0 | 6 | | | |
| 5 | 6.2 | 0.2 | 300 | 0.0007 |
| 10 | 6.5 | 0.3 | 300 | 0.0010 |
| 15 | 6.8 | 0.3 | 300 | 0.0010 |
| 20 | 7.2 | 0.4 | 300 | 0.0013 |
| 25 | 7.3 | 0.1 | 300 | 0.0003 |
| 30 | 7.6 | 0.3 | 300 | 0.0010 |
| 35 | 7.9 | 0.3 | 300 | 0.0010 |
| 40 | 8.2 | 0.3 | 300 | 0.0010 |
| 50 | 8.8 | 0.6 | 600 | 0.0010 |
| 60 | 9.3 | 0.5 | 600 | 0.0008 |
| 70 | 9.8 | 0.5 | 600 | 0.0008 |
| 80 | 10.3 | 0.5 | 600 | 0.0008 |
| 90 | 10.8 | 0.5 | 600 | 0.0008 |
| 100 | 11.2 | 0.4 | 600 | 0.0007 |
| 110 | 11.7 | 0.5 | 600 | 0.0008 |
| 120 | 12.2 | 0.5 | 600 | 0.0008 |

5.2 Double Ring Infiltrometer

Double ring infiltrometer test resluts are presented in this section. Only the inner ring data was used to yield the infiltration curve from which the maximum infiltration capacity, i.e. the saturated k, was determined for each flume deposit. The outer ring only provides a buffering effect to ensure the vertical infiltration of the water in section of the flume deposit tested.

Table VII-13. Double ring infiltrometer measurements in flume A1

| Water Level (cm) | Water Level change (m) | Time Interval (s) | Cumulative Time (s) | Infiltration Capacity (m/s) |
|---|---|---|---|---|
| 44.5 | - | - | - | - |
| 44.0 | 0.005 | 60 | 60 | 8.3E-05 |
| 41.5 | 0.025 | 120 | 180 | 2.1E-04 |
| 40.2 | 0.013 | 120 | 300 | 1.1E-04 |
| 38.2 | 0.020 | 120 | 420 | 1.7E-04 |
| 37.5 | 0.007 | 120 | 540 | 5.8E-05 |
| 36.8 | 0.007 | 120 | 660 | 5.8E-05 |
| 35.3 | 0.015 | 120 | 780 | 1.3E-04 |
| 34.8 | 0.005 | 120 | 900 | 4.2E-05 |
| 32.0 | 0.028 | 840 | 1740 | 3.3E-05 |
| 31.8 | 0.002 | 600 | 2340 | 3.3E-06 |
| 31.7 | 0.001 | 1200 | 3540 | 8.3E-07 |
| 31.6 | 0.001 | 1200 | 4740 | 8.3E-07 |

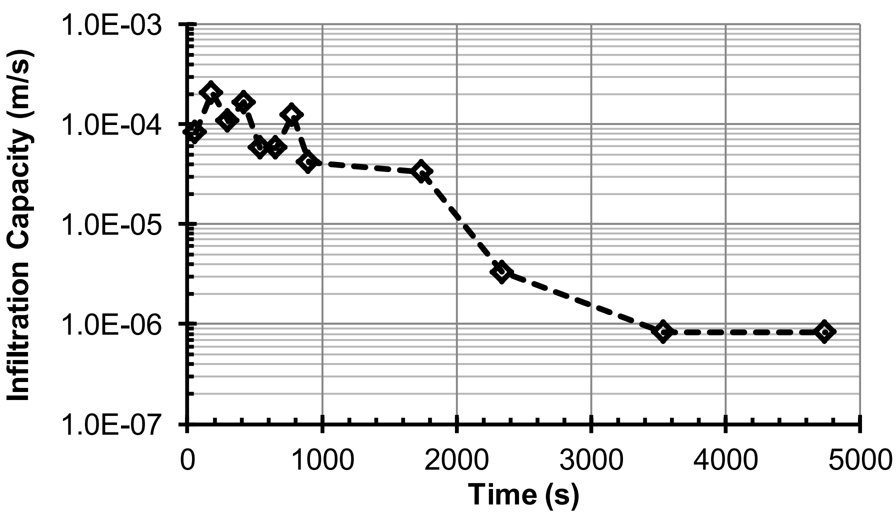


Figure VII-5. Changes in infiltration capacity with time for flume deposit A1

Table VII-14. Double ring infiltrometer measurements in flume A3

| Water Level (cm) | Water Level change (m) | Time Interval (s) | Cumulative Time (s) | Infiltration Capacity (m/s) |
|---|---|---|---|---|
| 41.5 | - | - | - | - |
| 39.2 | 0.023 | 120 | 120 | 1.9E-04 |
| 37.3 | 0.019 | 120 | 240 | 1.6E-04 |
| 36.2 | 0.011 | 120 | 360 | 9.2E-05 |
| 35.8 | 0.004 | 120 | 480 | 3.3E-05 |
| 35.7 | 0.001 | 120 | 600 | 8.3E-06 |
| 35.6 | 0.001 | 300 | 900 | 3.3E-06 |
| 34.3 | 0.013 | 5100 | 6000 | 2.5E-06 |
| 33.8 | 0.005 | 1800 | 7800 | 2.8E-06 |

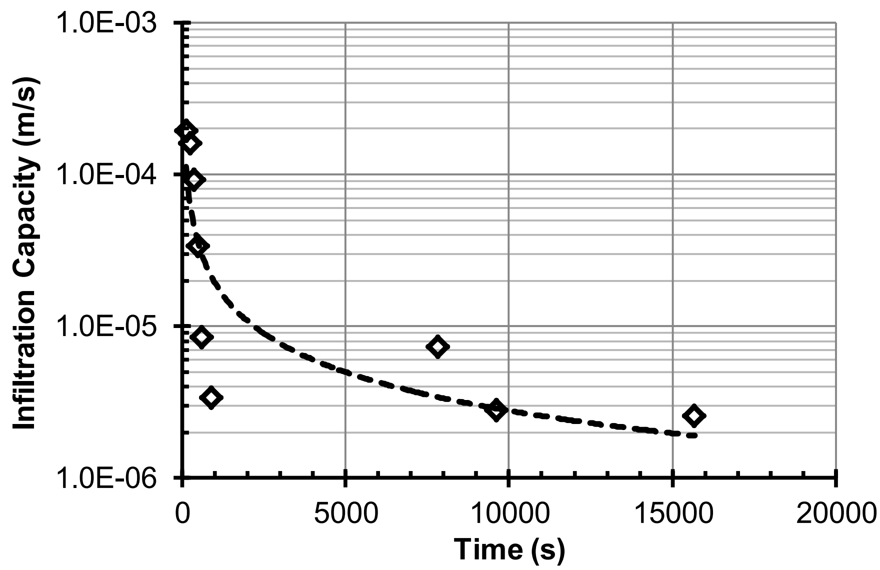


Figure VII-6. Changes in infiltration capacity with time for flume deposit A3

Table VII-15. Double ring infiltrometer measurements in flume A5

| Water Level (cm) | Water Level change (m) | Time Interval (s) | Cumulative Time (s) | Infiltration Capacity (m/s) |
|---|---|---|---|---|
| 38.0 | - | - | - | - |
| 37.3 | 0.007 | 120 | 120 | 5.8E-05 |
| 36.8 | 0.005 | 120 | 240 | 4.2E-05 |
| 36.1 | 0.007 | 120 | 360 | 5.8E-05 |
| 35.5 | 0.006 | 120 | 480 | 5.0E-05 |
| 35.0 | 0.005 | 120 | 600 | 4.2E-05 |
| 34.4 | 0.006 | 120 | 720 | 5.0E-05 |
| 34.2 | 0.002 | 120 | 840 | 1.7E-05 |
| 33.9 | 0.003 | 120 | 960 | 2.5E-05 |
| 33.6 | 0.003 | 120 | 1080 | 2.5E-05 |
| 33.3 | 0.003 | 120 | 1200 | 2.5E-05 |
| 33.1 | 0.002 | 120 | 1320 | 1.7E-05 |
| 32.9 | 0.002 | 120 | 1440 | 1.7E-05 |
| 32.7 | 0.002 | 120 | 1560 | 1.7E-05 |
| 32.5 | 0.002 | 120 | 1680 | 1.7E-05 |
| 32.3 | 0.002 | 120 | 1800 | 1.7E-05 |
| 32.2 | 0.001 | 120 | 1920 | 8.3E-06 |
| 32.1 | 0.001 | 120 | 2040 | 8.3E-06 |
| 32.0 | 0.001 | 120 | 2160 | 8.3E-06 |
| 31.9 | 0.001 | 120 | 2280 | 8.3E-06 |
| 31.8 | 0.001 | 120 | 2400 | 8.3E-06 |
| 31.7 | 0.001 | 120 | 2520 | 8.3E-06 |
| 31.6 | 0.001 | 120 | 2640 | 8.3E-06 |
| 31.5 | 0.001 | 120 | 2760 | 8.3E-06 |
| 31.4 | 0.001 | 300 | 3060 | 3.3E-06 |
| 31.3 | 0.001 | 600 | 3660 | 1.7E-06 |
| 31.2 | 0.001 | 900 | 4560 | 1.1E-06 |
| 31.1 | 0.001 | 3600 | 8160 | 2.8E-07 |
| 31.0 | 0.001 | 7200 | 15360 | 1.4E-07 |

Table VII-16. Double ring infiltrometer measurements in flume A13

| Water Level (cm) | Water Level change (m) | Time Interval (s) | Cumulative Time (s) | Infiltration Capacity (m/s) |
|---|---|---|---|---|
| 44.0 | - | - | - | - |
| 42.0 | 0.020 | 60 | 60 | 3.3E-04 |
| 41.3 | 0.007 | 60 | 120 | 1.2E-04 |
| 40.3 | 0.010 | 60 | 180 | 1.7E-04 |
| 39.3 | 0.010 | 60 | 240 | 1.7E-04 |
| 38.6 | 0.007 | 60 | 300 | 1.2E-04 |
| 37.3 | 0.013 | 120 | 420 | 1.1E-04 |
| 36.3 | 0.010 | 120 | 540 | 8.3E-05 |
| 35.5 | 0.008 | 120 | 660 | 6.7E-05 |
| 34.8 | 0.007 | 120 | 780 | 5.8E-05 |
| 34.3 | 0.005 | 120 | 900 | 4.2E-05 |
| 33.8 | 0.005 | 120 | 1020 | 4.2E-05 |
| 33.4 | 0.004 | 120 | 1140 | 3.3E-05 |
| 33.1 | 0.003 | 120 | 1260 | 2.5E-05 |
| 32.7 | 0.004 | 120 | 1380 | 3.3E-05 |
| 32.3 | 0.004 | 120 | 1500 | 3.3E-05 |
| 32.0 | 0.003 | 120 | 1620 | 2.5E-05 |
| 31.7 | 0.003 | 120 | 1740 | 2.5E-05 |
| 31.5 | 0.002 | 120 | 1860 | 1.7E-05 |
| 31.3 | 0.002 | 120 | 1980 | 1.7E-05 |
| 31.1 | 0.002 | 120 | 2100 | 1.7E-05 |
| 30.9 | 0.002 | 120 | 2220 | 1.7E-05 |
| 30.7 | 0.002 | 120 | 2340 | 1.7E-05 |
| 30.5 | 0.002 | 120 | 2460 | 1.7E-05 |
| 30.3 | 0.002 | 120 | 2580 | 1.7E-05 |
| 30.2 | 0.001 | 120 | 2700 | 8.3E-06 |
| 30.1 | 0.001 | 120 | 2820 | 8.3E-06 |
| 29.9 | 0.002 | 120 | 2940 | 1.7E-05 |
| 29.8 | 0.001 | 120 | 3060 | 8.3E-06 |
| 29.7 | 0.001 | 120 | 3180 | 8.3E-06 |
| 29.6 | 0.001 | 120 | 3300 | 8.3E-06 |
| 29.5 | 0.001 | 120 | 3420 | 8.3E-06 |
| 29.1 | 0.004 | 600 | 4020 | 6.7E-06 |
| 28.9 | 0.002 | 600 | 4620 | 3.3E-06 |
| 28.7 | 0.002 | 600 | 5220 | 3.3E-06 |
| 28.6 | 0.001 | 600 | 5820 | 1.7E-06 |
| 28.5 | 0.001 | 600 | 6420 | 1.7E-06 |
| 28.4 | 0.001 | 4200 | 10620 | 2.4E-07 |
| 28.3 | 0.001 | 3600 | 14220 | 2.8E-07 |
| 28.2 | 0.001 | 3600 | 17820 | 2.8E-07 |

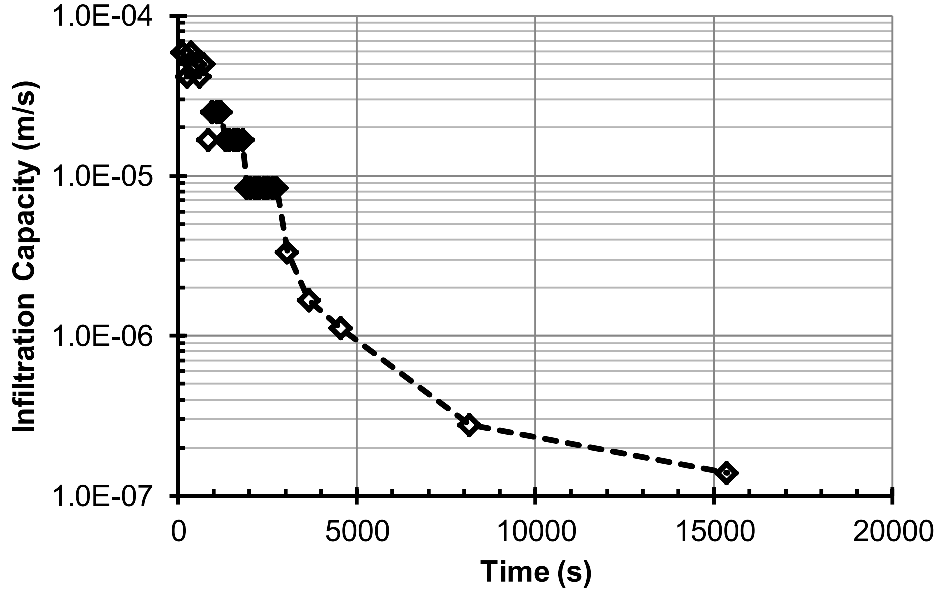


Figure VII-7. Changes in infiltration capacity with time for flume deposit A5

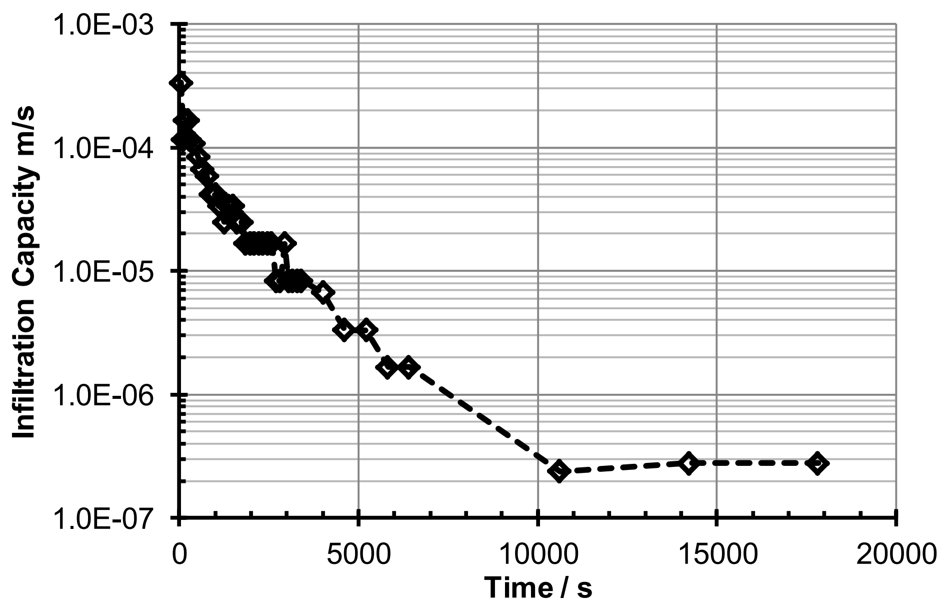


Figure VII-8. Changes in infiltration capacity with time for flume deposit A13

Table VII-17. Double ring infiltrometer measurements in Pilot flume Zone 1

| Water Level (cm) | Water Level change (m) | Time Interval (s) | Cumulative Time (s) | Infiltration Capacity (m/s) |
|---|---|---|---|---|
| 44.2 | - | - | - | - |
| 44.1 | 0.001 | 120 | 120 | 8.3E-06 |
| 44.0 | 0.001 | 120 | 240 | 8.3E-06 |
| 43.8 | 0.002 | 300 | 540 | 6.7E-06 |
| 43.5 | 0.003 | 300 | 840 | 1.0E-05 |
| 43.4 | 0.001 | 300 | 1140 | 3.3E-06 |
| 43.2 | 0.002 | 300 | 1440 | 6.7E-06 |
| 43.0 | 0.002 | 300 | 1740 | 6.7E-06 |
| 42.8 | 0.002 | 300 | 2040 | 6.7E-06 |
| 42.7 | 0.001 | 300 | 2340 | 3.3E-06 |
| 42.6 | 0.001 | 300 | 2640 | 3.3E-06 |
| 42.5 | 0.001 | 300 | 2940 | 3.3E-06 |
| 42.2 | 0.003 | 600 | 3540 | 5.0E-06 |
| 42 | 0.002 | 600 | 4140 | 3.3E-06 |
| 41.8 | 0.002 | 600 | 4800 | 3.3E-06 |
| 41.7 | 0.001 | 600 | 5400 | 1.7E-06 |
| 41.6 | 0.001 | 600 | 6000 | 1.7E-06 |
| 41.3 | 0.003 | 1200 | 7200 | 2.5E-06 |
| 41.1 | 0.002 | 1200 | 8400 | 1.7E-06 |
| 40.8 | 0.003 | 1200 | 9600 | 2.5E-06 |
| 40.7 | 0.001 | 1200 | 10800 | 8.3E-07 |
| 40.6 | 0.001 | 2400 | 13200 | 4.2E-07 |
| 40.5 | 0.001 | 2400 | 15600 | 4.2E-07 |
| 40.4 | 0.001 | 2400 | 18000 | 4.2E-07 |

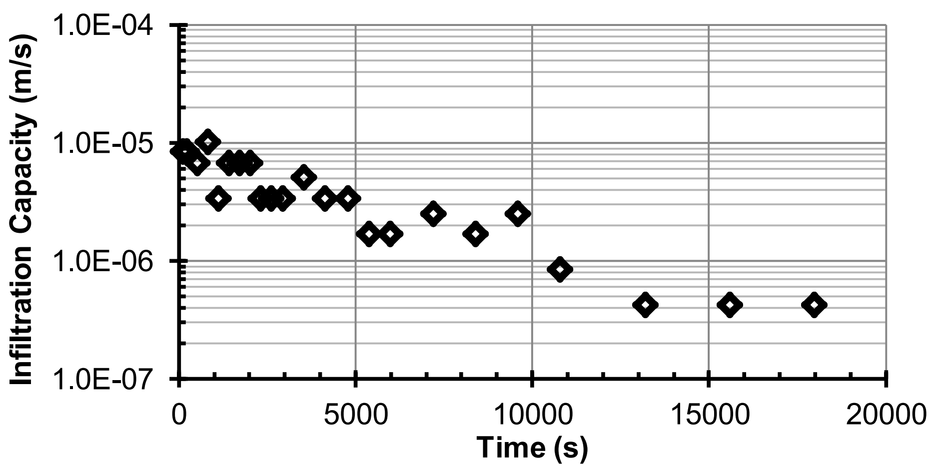

Figure VII-9. Changes in infiltration capacity with time in Zone 1 for the Pilot flume

Table VII-18. Double ring infiltrometer measurements in Pilot flume Zone 2

| Water Level (cm) | Water Level change (m) | Time Interval (s) | Cumulative Time (s) | Infiltration Capacity (m/s) |
|---|---|---|---|---|
| 36.2 | - | - | - | - |
| 36.0 | 0.002 | 180 | 180 | 1.1E-05 |
| 34.2 | 0.018 | 180 | 360 | 1.0E-04 |
| 33.4 | 0.008 | 180 | 540 | 4.4E-05 |
| 32.6 | 0.008 | 180 | 720 | 4.4E-05 |
| 32.0 | 0.006 | 180 | 900 | 3.3E-05 |
| 31.7 | 0.003 | 180 | 1080 | 1.7E-05 |
| 31.2 | 0.005 | 180 | 1260 | 2.8E-05 |
| 30.5 | 0.007 | 180 | 1440 | 3.9E-05 |
| 30.2 | 0.003 | 180 | 1620 | 1.7E-05 |
| 29.9 | 0.003 | 180 | 1800 | 1.7E-05 |
| 29.6 | 0.003 | 300 | 2100 | 1.0E-05 |
| 29 | 0.006 | 300 | 2400 | 2.0E-05 |
| 28.6 | 0.004 | 300 | 2700 | 1.3E-05 |
| 28.2 | 0.004 | 300 | 3000 | 1.3E-05 |
| 27.7 | 0.005 | 300 | 3360 | 1.7E-05 |
| 27.3 | 0.004 | 300 | 3660 | 1.3E-05 |
| 27 | 0.003 | 300 | 3960 | 1.0E-05 |
| 26.7 | 0.003 | 300 | 4260 | 1.0E-05 |
| 26.4 | 0.003 | 300 | 4560 | 1.0E-05 |
| 26 | 0.004 | 300 | 4860 | 1.3E-05 |
| 25.8 | 0.002 | 300 | 5160 | 6.7E-06 |
| 25.5 | 0.003 | 300 | 5460 | 1.0E-05 |
| 25.2 | 0.003 | 300 | 5760 | 1.0E-05 |
| 24.6 | 0.006 | 600 | 6540 | 1.0E-05 |
| 24.1 | 0.005 | 600 | 7200 | 8.3E-06 |
| 23.5 | 0.006 | 600 | 7800 | 1.0E-05 |
| 23.1 | 0.004 | 600 | 8400 | 6.7E-06 |
| 22.9 | 0.002 | 600 | 9000 | 3.3E-06 |
| 22.5 | 0.004 | 600 | 9600 | 6.7E-06 |
| 22.4 | 0.001 | 600 | 10200 | 1.7E-06 |
| 22.3 | 0.001 | 600 | 10800 | 1.7E-06 |
| 21.4 | 0.002 | 1200 | 14400 | 1.7E-06 |
| 21.2 | 0.002 | 1200 | 15600 | 1.7E-06 |

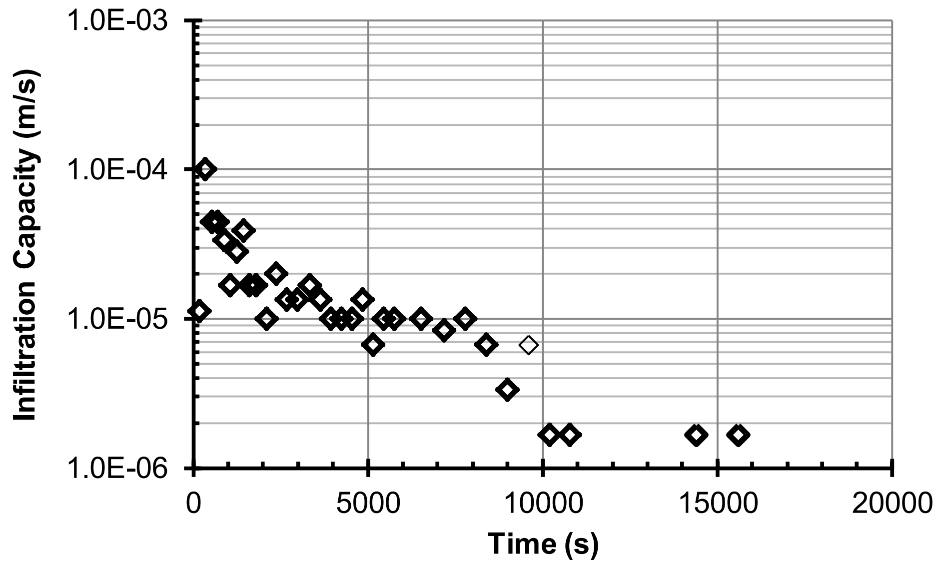


Figure VII-10. Changes in infiltration capacity with time in Zone 2 for the Pilot flume

Table VII-19. Double ring infiltrometer measurements in Pilot flume Zone 3

| Water Level (cm) | Water Level change (m) | Time Interval (s) | Cumulative Time (s) | Infiltration Capacity (m/s) |
|---|---|---|---|---|
| 40.8 | | | | |
| 40.6 | 0.002 | 300 | 300 | 6.7E-06 |
| 40.5 | 0.001 | 300 | 600 | 3.3E-06 |
| 40.4 | 0.001 | 300 | 900 | 3.3E-06 |
| 40.3 | 0.001 | 1200 | 2100 | 8.3E-07 |
| 40.2 | 0.001 | 1200 | 3300 | 8.3E-07 |
| 40.1 | 0.001 | 900 | 4200 | 1.1E-06 |
| 40.0 | 0.001 | 1200 | 5400 | 8.3E-07 |
| 39.9 | 0.001 | 1200 | 6600 | 8.3E-07 |
| 39.8 | 0.001 | 1200 | 7800 | 8.3E-07 |
| 39.7 | 0.001 | 1200 | 9000 | 8.3E-07 |
| 39.6 | 0.001 | 1200 | 10200 | 8.3E-07 |
| 39.5 | 0.001 | 2400 | 12600 | 4.2E-07 |
| 39.4 | 0.001 | 2400 | 15000 | 4.2E-07 |
| 39.3 | 0.001 | 4800 | 19800 | 2.1E-07 |

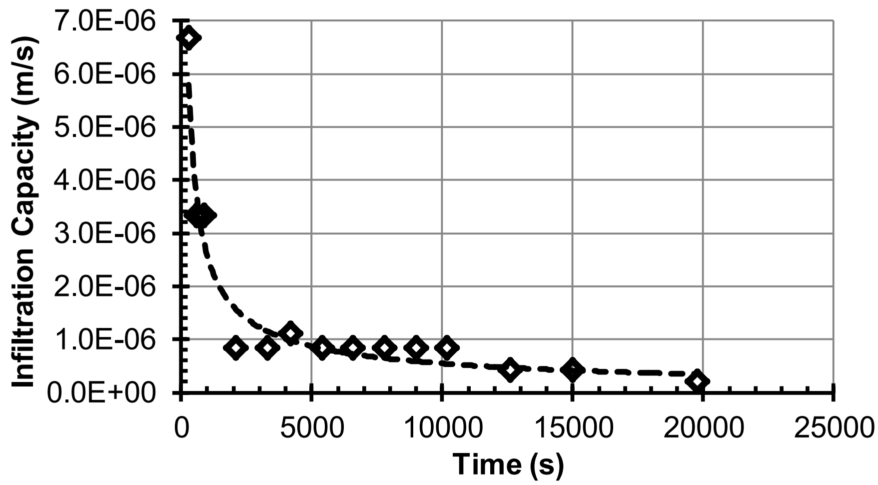


Figure VII-11. Changes in infiltration capacity with time in Zone 3 (Pilot flume)

## 5.3 Laboratory Measurements of the Hydraulic Conductivity (k)

The magnitude of k was determined for the undisturbed flume deposits using constant head tests (ASTM D2434) conducted in a large strain consolidation cells. Darcy's law (Head 1992) can be rearranged to calculate the k from the hydraulic gradient (i) and the measured flow rate (Q) as follows:

$$k = \frac{Q}{Ai} \qquad [5]$$

Where A is the cross sectional area of the sample (i.e. cross sectional area of the test cell). Test parameters are summarized in Table VII-20. Test results are presented in Tables VII-21 to VII-32 and Figures VII-12 to VII-23

Table VII-20. Test parameters for hydraulic conductivity (k) measurements

| | |
|---|---|
| Diameter of glass tube (m) | 4.0E-03 |
| Cross Sectional Area of Glass Tube ($m^2$) | 1.3E-05 |
| Large Strain Consolidation Cell diameter (m) | 1.0E-01 |
| Cross Sectional area of Large Strain Consolidation Cell ($m^2$) | 7.9E-03 |

### 5.3.1 Flume A1

Table VII-21. Constant head test results for the undisturbed vertical core A1 (Sample Height = 8.7 cm; i = 0.3)

| Distance (m) | Cumulative Distance (m) | Time (s) | Velocity (m/s) | Flow rate, Q ($m^3$/s) | k (= Q/Ai) (m/s) |
|---|---|---|---|---|---|
| 0.530 | 0 | 0 | 0 | 0 | 0 |
| 0.525 | 0.005 | 30 | 1.7E-04 | 2.1E-09 | 9.2E-07 |
| 0.520 | 0.010 | 64 | 1.6E-04 | 2.0E-09 | 8.6E-07 |
| 0.515 | 0.015 | 98 | 1.5E-04 | 1.9E-09 | 8.5E-07 |
| 0.510 | 0.020 | 135 | 1.5E-04 | 1.9E-09 | 8.2E-07 |
| 0.505 | 0.025 | 167 | 1.5E-04 | 1.9E-09 | 8.3E-07 |
| 0.500 | 0.030 | 207 | 1.4E-04 | 1.8E-09 | 8.0E-07 |
| 0.495 | 0.035 | 250 | 1.4E-04 | 1.8E-09 | 7.7E-07 |
| 0.490 | 0.040 | 289 | 1.4E-04 | 1.7E-09 | 7.6E-07 |
| 0.485 | 0.045 | 328 | 1.4E-04 | 1.7E-09 | 7.6E-07 |
| 0.480 | 0.050 | 365 | 1.4E-04 | 1.7E-09 | 7.6E-07 |
| 0.475 | 0.055 | 400 | 1.4E-04 | 1.7E-09 | 7.6E-07 |
| 0.470 | 0.060 | 434 | 1.4E-04 | 1.7E-09 | 7.6E-07 |
| 0.465 | 0.065 | 469 | 1.4E-04 | 1.7E-09 | 7.7E-07 |
| 0.460 | 0.070 | 497 | 1.4E-04 | 1.8E-09 | 7.8E-07 |
| 0.455 | 0.075 | 537 | 1.4E-04 | 1.8E-09 | 7.7E-07 |
| 0.450 | 0.080 | 576 | 1.4E-04 | 1.7E-09 | 7.7E-07 |
| 0.445 | 0.085 | 615 | 1.4E-04 | 1.7E-09 | 7.6E-07 |
| 0.440 | 0.090 | 651 | 1.4E-04 | 1.7E-09 | 7.6E-07 |
| 0.435 | 0.095 | 687 | 1.4E-04 | 1.7E-09 | 7.6E-07 |
| 0.430 | 0.100 | 723 | 1.4E-04 | 1.7E-09 | 7.6E-07 |
| 0.425 | 0.105 | 758 | 1.4E-04 | 1.7E-09 | 7.7E-07 |
| 0.420 | 0.110 | 790 | 1.4E-04 | 1.7E-09 | 7.7E-07 |
| 0.415 | 0.115 | 822 | 1.4E-04 | 1.8E-09 | 7.7E-07 |
| 0.410 | 0.120 | 858 | 1.4E-04 | 1.8E-09 | 7.7E-07 |
| 0.405 | 0.125 | 891 | 1.4E-04 | 1.8E-09 | 7.7E-07 |
| 0.400 | 0.130 | 928 | 1.4E-04 | 1.8E-09 | 7.7E-07 |
| 0.395 | 0.135 | 964 | 1.4E-04 | 1.8E-09 | 7.7E-07 |
| 0.390 | 0.140 | 1000 | 1.4E-04 | 1.8E-09 | 7.7E-07 |
| 0.385 | 0.145 | 1032 | 1.4E-04 | 1.8E-09 | 7.7E-07 |
| 0.380 | 0.150 | 1066 | 1.4E-04 | 1.8E-09 | 7.8E-07 |
| 0.370 | 0.160 | 1136 | 1.4E-04 | 1.8E-09 | 7.8E-07 |
| 0.360 | 0.170 | 1200 | 1.4E-04 | 1.8E-09 | 7.8E-07 |
| 0.350 | 0.180 | 1273 | 1.4E-04 | 1.8E-09 | 7.8E-07 |
| 0.340 | 0.190 | 1338 | 1.4E-04 | 1.8E-09 | 7.8E-07 |
| 0.330 | 0.200 | 1404 | 1.4E-04 | 1.8E-09 | 7.9E-07 |

Table VII-22. Constant head test results for the undisturbed horizontal core A1 (Sample Height = 9.8 cm; i = 0.3)

| Distance (m) | Cumulative Distance (m) | Time (s) | Velocity (m/s) | Flow rate, Q ($m^3$/s) | k (= Q/Ai) (m/s) |
|---|---|---|---|---|---|
| 0.700 | 0 | 0 | 0 | 0 | 0 |
| 0.695 | 0.005 | 40 | 1.3E-04 | 1.6E-09 | 6.8E-07 |
| 0.690 | 0.010 | 102 | 9.8E-05 | 1.2E-09 | 5.3E-07 |
| 0.685 | 0.015 | 145 | 1.0E-04 | 1.3E-09 | 5.6E-07 |
| 0.680 | 0.020 | 192 | 1.0E-04 | 1.3E-09 | 5.7E-07 |
| 0.675 | 0.025 | 245 | 1.0E-04 | 1.3E-09 | 5.5E-07 |
| 0.670 | 0.030 | 305 | 9.8E-05 | 1.2E-09 | 5.3E-07 |
| 0.665 | 0.035 | 360 | 9.7E-05 | 1.2E-09 | 5.3E-07 |
| 0.660 | 0.040 | 417 | 9.6E-05 | 1.2E-09 | 5.2E-07 |
| 0.655 | 0.045 | 466 | 9.7E-05 | 1.2E-09 | 5.2E-07 |
| 0.650 | 0.050 | 523 | 9.6E-05 | 1.2E-09 | 5.2E-07 |
| 0.640 | 0.060 | 628 | 9.6E-05 | 1.2E-09 | 5.2E-07 |
| 0.630 | 0.070 | 727 | 9.6E-05 | 1.2E-09 | 5.2E-07 |
| 0.620 | 0.080 | 837 | 9.6E-05 | 1.2E-09 | 5.2E-07 |
| 0.610 | 0.090 | 945 | 9.5E-05 | 1.2E-09 | 5.2E-07 |
| 0.600 | 0.100 | 1062 | 9.4E-05 | 1.2E-09 | 5.1E-07 |
| 0.590 | 0.110 | 1155 | 9.5E-05 | 1.2E-09 | 5.1E-07 |
| 0.507 | 0.193 | 1950 | 9.9E-05 | 1.2E-09 | 5.4E-07 |
| 0.477 | 0.223 | 2250 | 9.9E-05 | 1.2E-09 | 5.4E-07 |
| 0.450 | 0.250 | 2557 | 9.8E-05 | 1.2E-09 | 5.3E-07 |
| 0.428 | 0.272 | 2832 | 9.6E-05 | 1.2E-09 | 5.2E-07 |
| 0.388 | 0.312 | 3128 | 1.0E-04 | 1.3E-09 | 5.4E-07 |
| 0.358 | 0.342 | 3413 | 1.0E-04 | 1.3E-09 | 5.4E-07 |
| 0.328 | 0.372 | 3720 | 1.0E-04 | 1.3E-09 | 5.4E-07 |
| 0.298 | 0.402 | 4020 | 1.0E-04 | 1.3E-09 | 5.4E-07 |

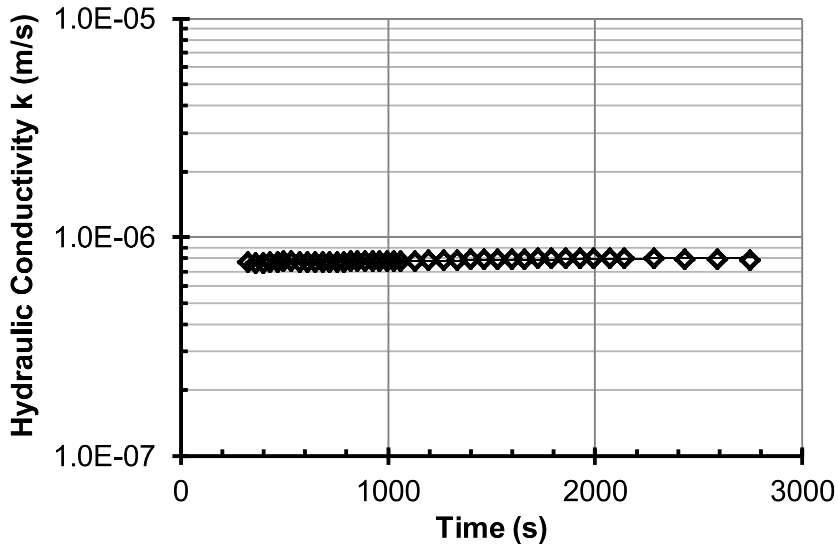


Figure VII-12. Changes in hydraulic conductivity (k) with time for the vertical core A1

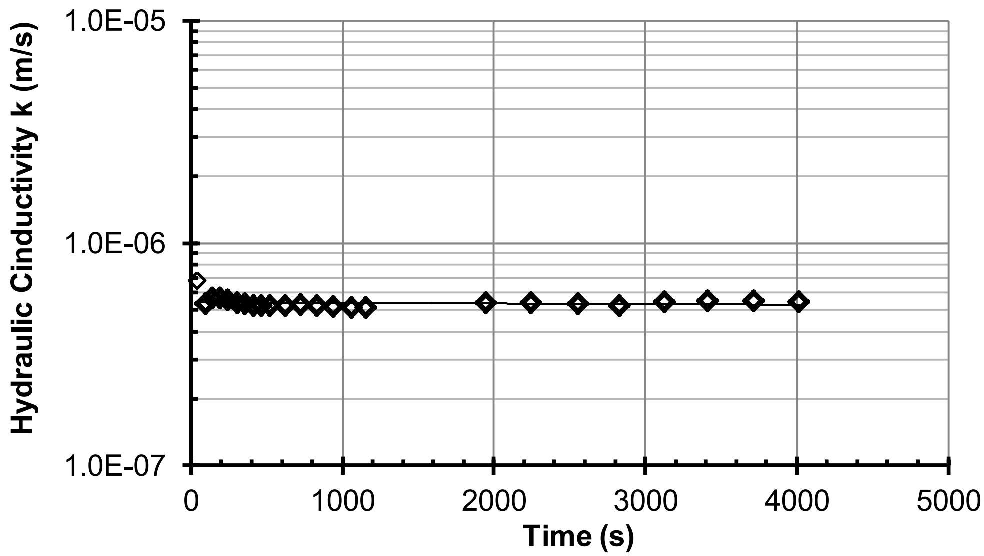


Figure VII-13. Changes in hydraulic conductivity (k) with time for the horizontal core A1

5.3.2 Flume A3

Table VII-23. Constant head test results for the undisturbed vertical core A3 (Sample Height = 6.6 cm; i = 0.3)

| Distance (m) | Cumulative Distance (m) | Time (s) | Velocity (m/s) | Flow rate, Q ($m^3/s$) | k (= Q/Ai) (m/s) |
|---|---|---|---|---|---|
| 0.53 | 0 | 0 | 0 | 0 | 0 |
| 0.52 | 0.01 | 28 | 3.6E-04 | 4.5E-09 | 1.8E-06 |
| 0.51 | 0.02 | 64 | 3.1E-04 | 3.9E-09 | 1.6E-06 |
| 0.50 | 0.03 | 95 | 3.2E-04 | 4.0E-09 | 1.6E-06 |
| 0.49 | 0.04 | 124 | 3.2E-04 | 4.1E-09 | 1.6E-06 |
| 0.48 | 0.05 | 156 | 3.2E-04 | 4.0E-09 | 1.6E-06 |
| 0.47 | 0.06 | 186 | 3.2E-04 | 4.1E-09 | 1.6E-06 |
| 0.46 | 0.07 | 219 | 3.2E-04 | 4.0E-09 | 1.6E-06 |
| 0.45 | 0.08 | 250 | 3.2E-04 | 4.0E-09 | 1.6E-06 |
| 0.44 | 0.09 | 284 | 3.2E-04 | 4.0E-09 | 1.6E-06 |
| 0.43 | 0.10 | 316 | 3.2E-04 | 4.0E-09 | 1.6E-06 |
| 0.42 | 0.11 | 346 | 3.2E-04 | 4.0E-09 | 1.6E-06 |
| 0.41 | 0.12 | 379 | 3.2E-04 | 4.0E-09 | 1.6E-06 |
| 0.40 | 0.13 | 410 | 3.2E-04 | 4.0E-09 | 1.6E-06 |
| 0.39 | 0.14 | 439 | 3.2E-04 | 4.0E-09 | 1.6E-06 |
| 0.38 | 0.15 | 473 | 3.2E-04 | 4.0E-09 | 1.6E-06 |
| 0.37 | 0.16 | 506 | 3.2E-04 | 4.0E-09 | 1.6E-06 |
| 0.36 | 0.17 | 537 | 3.2E-04 | 4.0E-09 | 1.6E-06 |
| 0.35 | 0.18 | 570 | 3.2E-04 | 4.0E-09 | 1.6E-06 |
| 0.34 | 0.19 | 602 | 3.2E-04 | 4.0E-09 | 1.6E-06 |
| 0.33 | 0.20 | 634 | 3.2E-04 | 4.0E-09 | 1.6E-06 |
| 0.32 | 0.21 | 666 | 3.2E-04 | 4.0E-09 | 1.6E-06 |
| 0.31 | 0.22 | 699 | 3.1E-04 | 4.0E-09 | 1.6E-06 |
| 0.30 | 0.23 | 731 | 3.1E-04 | 4.0E-09 | 1.6E-06 |
| 0.29 | 0.24 | 763 | 3.1E-04 | 4.0E-09 | 1.6E-06 |
| 0.28 | 0.25 | 792 | 3.2E-04 | 4.0E-09 | 1.6E-06 |
| 0.27 | 0.26 | 824 | 3.2E-04 | 4.0E-09 | 1.6E-06 |
| 0.26 | 0.27 | 857 | 3.2E-04 | 4.0E-09 | 1.6E-06 |

Table VII-24. Constant head test results for the undisturbed horizontal core A3 (Sample Height = 8.8 cm; i = 0.4)

| Distance (m) | Cumulative Distance (m) | Time (s) | Velocity (m/s) | Flow rate, Q ($m^3/s$) | k (= Q/Ai) (m/s) |
|---|---|---|---|---|---|
| 0.655 | 0 | 0 | 0 | 0 | 0 |
| 0.645 | 0.010 | 87 | 1.1E-04 | 1.4E-09 | 4.8E-07 |
| 0.635 | 0.020 | 180 | 1.1E-04 | 1.4E-09 | 4.6E-07 |
| 0.625 | 0.030 | 265 | 1.1E-04 | 1.4E-09 | 4.7E-07 |
| 0.615 | 0.040 | 359 | 1.1E-04 | 1.4E-09 | 4.6E-07 |
| 0.600 | 0.055 | 507 | 1.1E-04 | 1.4E-09 | 4.5E-07 |
| 0.590 | 0.065 | 599 | 1.1E-04 | 1.4E-09 | 4.5E-07 |
| 0.580 | 0.075 | 575 | 1.3E-04 | 1.6E-09 | 5.4E-07 |
| 0.570 | 0.085 | 779 | 1.1E-04 | 1.4E-09 | 4.5E-07 |
| 0.560 | 0.095 | 871 | 1.1E-04 | 1.4E-09 | 4.5E-07 |
| 0.550 | 0.105 | 961 | 1.1E-04 | 1.4E-09 | 4.5E-07 |
| 0.540 | 0.115 | 1051 | 1.1E-04 | 1.4E-09 | 4.5E-07 |
| 0.530 | 0.125 | 1142 | 1.1E-04 | 1.4E-09 | 4.5E-07 |
| 0.520 | 0.135 | 1229 | 1.1E-04 | 1.4E-09 | 4.6E-07 |
| 0.510 | 0.145 | 1320 | 1.1E-04 | 1.4E-09 | 4.6E-07 |
| 0.500 | 0.155 | 1403 | 1.1E-04 | 1.4E-09 | 4.6E-07 |
| 0.450 | 0.205 | 1841 | 1.1E-04 | 1.4E-09 | 4.6E-07 |
| 0.415 | 0.240 | 2148 | 1.1E-04 | 1.4E-09 | 4.6E-07 |
| 0.379 | 0.276 | 2460 | 1.1E-04 | 1.4E-09 | 4.7E-07 |
| 0.343 | 0.312 | 2770 | 1.1E-04 | 1.4E-09 | 4.7E-07 |
| 0.313 | 0.342 | 3048 | 1.1E-04 | 1.4E-09 | 4.7E-07 |
| 0.255 | 0.400 | 3600 | 1.1E-04 | 1.4E-09 | 4.6E-07 |

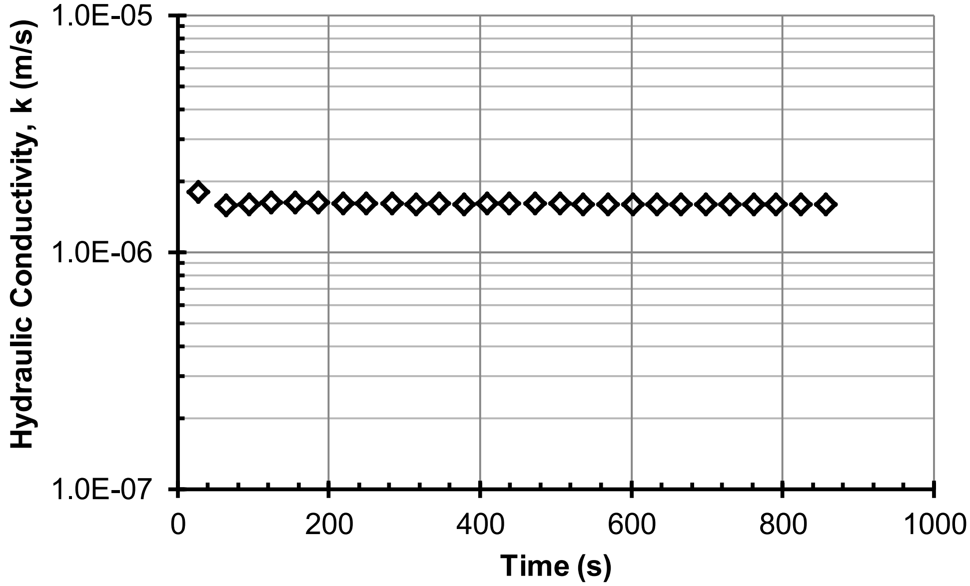


Figure VII-14. Constant head hydraulic conductivity (k) as a function of time for the vertical core A3

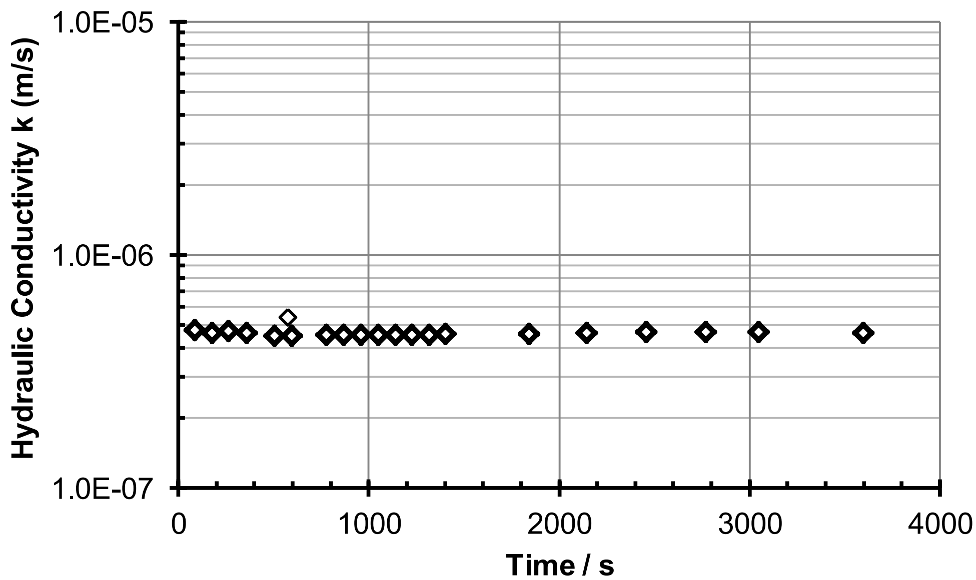


Figure VII-15. Constant head hydraulic conductivity (k) as a function of time for the horizontal core A3

5.3.3 Flume A5

Table VII-25. Constant head test results for the undisturbed vertical core A5 (Sample Height = 5.7 cm; i = 0.2)

| Distance (m) | Cumulative Distance (m) | Time (s) | Velocity (m/s) | Flow rate, Q ($m^3/s$) | k (= Q/Ai) (m/s) |
|---|---|---|---|---|---|
| 0.530 | 0 | 0 | 0 | 0 | 0 |
| 0.520 | 0.010 | 302 | 3.3E-05 | 4.2E-10 | 3.4E-07 |
| 0.510 | 0.020 | 602 | 3.3E-05 | 4.2E-10 | 3.4E-07 |
| 0.500 | 0.030 | 900 | 3.3E-05 | 4.2E-10 | 3.4E-07 |
| 0.489 | 0.041 | 1200 | 3.4E-05 | 4.3E-10 | 3.5E-07 |
| 0.478 | 0.052 | 1510 | 3.4E-05 | 4.3E-10 | 3.5E-07 |
| 0.468 | 0.062 | 1800 | 3.4E-05 | 4.3E-10 | 3.5E-07 |
| 0.457 | 0.073 | 2102 | 3.5E-05 | 4.4E-10 | 3.5E-07 |
| 0.445 | 0.085 | 2400 | 3.5E-05 | 4.5E-10 | 3.6E-07 |
| 0.435 | 0.095 | 2700 | 3.5E-05 | 4.4E-10 | 3.6E-07 |
| 0.420 | 0.110 | 3040 | 3.6E-05 | 4.5E-10 | 3.7E-07 |
| 0.410 | 0.120 | 3300 | 3.6E-05 | 4.6E-10 | 3.7E-07 |
| 0.398 | 0.132 | 3600 | 3.7E-05 | 4.6E-10 | 3.7E-07 |
| 0.374 | 0.156 | 4200 | 3.7E-05 | 4.7E-10 | 3.8E-07 |
| 0.350 | 0.180 | 4800 | 3.8E-05 | 4.7E-10 | 3.8E-07 |

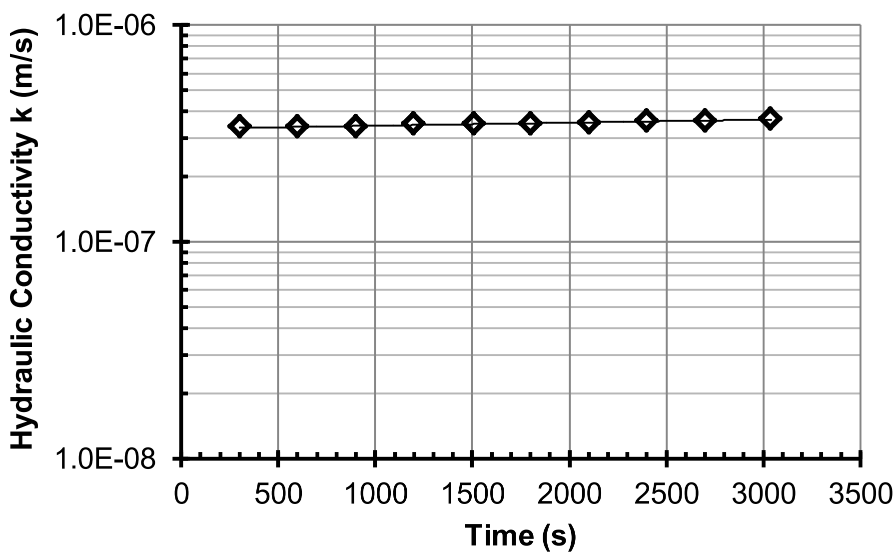


Figure VII-16. Changes in hydraulic conductivity (k) with time for the vertical core A5

5.3.4 Flume A13

Table VII-26. Constant head test results for the undisturbed vertical core A13 (Sample Height = 10.4 cm; i = 0.3)

| Distance (m) | Cumulative Distance (m) | Time (s) | Velocity (m/s) | Flow rate Q ($m^3$/s) | k (= Q/Ai) (m/s) |
|---|---|---|---|---|---|
| 0.67 | 0 | 0 | 0 | 0 | 0 |
| 0.66 | 0.01 | 32 | 3.1E-04 | 3.9E-09 | 1.9E-06 |
| 0.65 | 0.02 | 62 | 3.2E-04 | 4.1E-09 | 1.9E-06 |
| 0.64 | 0.03 | 91 | 3.3E-04 | 4.1E-09 | 2.0E-06 |
| 0.63 | 0.04 | 118 | 3.4E-04 | 4.3E-09 | 2.0E-06 |
| 0.62 | 0.05 | 147 | 3.4E-04 | 4.3E-09 | 2.0E-06 |
| 0.61 | 0.06 | 173 | 3.5E-04 | 4.4E-09 | 2.1E-06 |
| 0.60 | 0.07 | 202 | 3.5E-04 | 4.4E-09 | 2.1E-06 |
| 0.58 | 0.09 | 260 | 3.5E-04 | 4.3E-09 | 2.1E-06 |
| 0.56 | 0.11 | 315 | 3.5E-04 | 4.4E-09 | 2.1E-06 |
| 0.54 | 0.13 | 370 | 3.5E-04 | 4.4E-09 | 2.1E-06 |
| 0.52 | 0.15 | 426 | 3.5E-04 | 4.4E-09 | 2.1E-06 |
| 0.50 | 0.17 | 482 | 3.5E-04 | 4.4E-09 | 2.1E-06 |
| 0.48 | 0.19 | 535 | 3.6E-04 | 4.5E-09 | 2.1E-06 |
| 0.46 | 0.21 | 585 | 3.6E-04 | 4.5E-09 | 2.1E-06 |
| 0.44 | 0.23 | 638 | 3.6E-04 | 4.5E-09 | 2.1E-06 |
| 0.42 | 0.25 | 691 | 3.6E-04 | 4.5E-09 | 2.1E-06 |
| 0.40 | 0.27 | 741 | 3.6E-04 | 4.6E-09 | 2.2E-06 |
| 0.38 | 0.29 | 795 | 3.6E-04 | 4.6E-09 | 2.2E-06 |
| 0.36 | 0.31 | 846 | 3.7E-04 | 4.6E-09 | 2.2E-06 |
| 0.34 | 0.33 | 899 | 3.7E-04 | 4.6E-09 | 2.2E-06 |
| 0.32 | 0.35 | 953 | 3.7E-04 | 4.6E-09 | 2.2E-06 |
| 0.30 | 0.37 | 1003 | 3.7E-04 | 4.6E-09 | 2.2E-06 |
| 0.28 | 0.39 | 1055 | 3.7E-04 | 4.6E-09 | 2.2E-06 |
| 0.26 | 0.41 | 1109 | 3.7E-04 | 4.6E-09 | 2.2E-06 |
| 0.24 | 0.43 | 1164 | 3.7E-04 | 4.6E-09 | 2.2E-06 |
| 0.22 | 0.45 | 1218 | 3.7E-04 | 4.6E-09 | 2.2E-06 |
| 0.20 | 0.47 | 1272 | 3.7E-04 | 4.6E-09 | 2.2E-06 |

Table VII-27. Constant head test results for the undisturbed horizontal core A13 (Sample Height = 10.4 cm; i = 0.3)

| Distance (m) | Cumulative Distance (m) | Time (s) | Velocity (m/s) | Flow rate Q ($m^3$/s) | k (= Q/Ai) (m/s) |
|---|---|---|---|---|---|
| 0.66 | 0 | 0 | 0 | 0 | 0 |
| 0.65 | 0.01 | 39 | 2.6E-04 | 3.2E-09 | 1.4E-06 |
| 0.64 | 0.02 | 78 | 2.6E-04 | 3.2E-09 | 1.4E-06 |
| 0.63 | 0.03 | 120 | 2.5E-04 | 3.1E-09 | 1.3E-06 |
| 0.62 | 0.04 | 161 | 2.5E-04 | 3.1E-09 | 1.3E-06 |
| 0.61 | 0.05 | 201 | 2.5E-04 | 3.1E-09 | 1.3E-06 |
| 0.60 | 0.06 | 239 | 2.5E-04 | 3.2E-09 | 1.4E-06 |
| 0.59 | 0.07 | 280 | 2.5E-04 | 3.1E-09 | 1.3E-06 |
| 0.58 | 0.08 | 318 | 2.5E-04 | 3.2E-09 | 1.4E-06 |
| 0.57 | 0.09 | 359 | 2.5E-04 | 3.2E-09 | 1.4E-06 |
| 0.56 | 0.10 | 401 | 2.5E-04 | 3.1E-09 | 1.3E-06 |
| 0.55 | 0.11 | 439 | 2.5E-04 | 3.1E-09 | 1.3E-06 |
| 0.54 | 0.12 | 478 | 2.5E-04 | 3.2E-09 | 1.4E-06 |
| 0.53 | 0.13 | 515 | 2.5E-04 | 3.2E-09 | 1.4E-06 |
| 0.52 | 0.14 | 558 | 2.5E-04 | 3.2E-09 | 1.4E-06 |
| 0.51 | 0.15 | 597 | 2.5E-04 | 3.2E-09 | 1.4E-06 |
| 0.50 | 0.16 | 635 | 2.5E-04 | 3.2E-09 | 1.4E-06 |
| 0.48 | 0.18 | 712 | 2.5E-04 | 3.2E-09 | 1.4E-06 |
| 0.46 | 0.20 | 787 | 2.5E-04 | 3.2E-09 | 1.4E-06 |
| 0.44 | 0.22 | 860 | 2.6E-04 | 3.2E-09 | 1.4E-06 |
| 0.42 | 0.24 | 939 | 2.6E-04 | 3.2E-09 | 1.4E-06 |
| 0.40 | 0.26 | 1015 | 2.6E-04 | 3.2E-09 | 1.4E-06 |
| 0.38 | 0.28 | 1096 | 2.6E-04 | 3.2E-09 | 1.4E-06 |
| 0.36 | 0.30 | 1168 | 2.6E-04 | 3.2E-09 | 1.4E-06 |
| 0.34 | 0.32 | 1246 | 2.6E-04 | 3.2E-09 | 1.4E-06 |
| 0.32 | 0.34 | 1323 | 2.6E-04 | 3.2E-09 | 1.4E-06 |
| 0.30 | 0.36 | 1400 | 2.6E-04 | 3.2E-09 | 1.4E-06 |
| 0.28 | 0.38 | 1476 | 2.6E-04 | 3.2E-09 | 1.4E-06 |
| 0.26 | 0.41 | 1570 | 2.6E-04 | 3.2E-09 | 1.4E-06 |
| 0.24 | 0.42 | 1628 | 2.6E-04 | 3.2E-09 | 1.4E-06 |
| 0.22 | 0.44 | 1705 | 2.6E-04 | 3.2E-09 | 1.4E-06 |

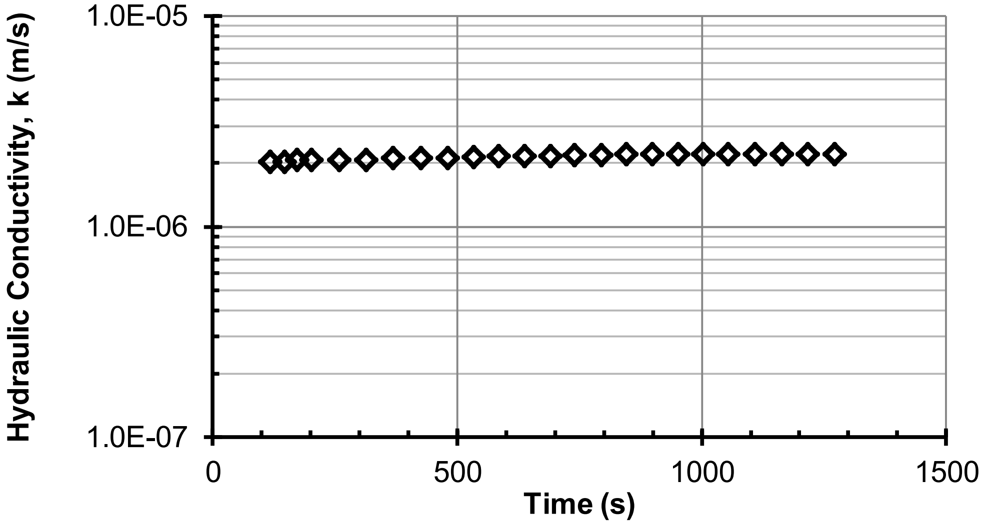


Figure VII-17. Constant head hydraulic conductivity (k) as a function of time for the vertical core A13

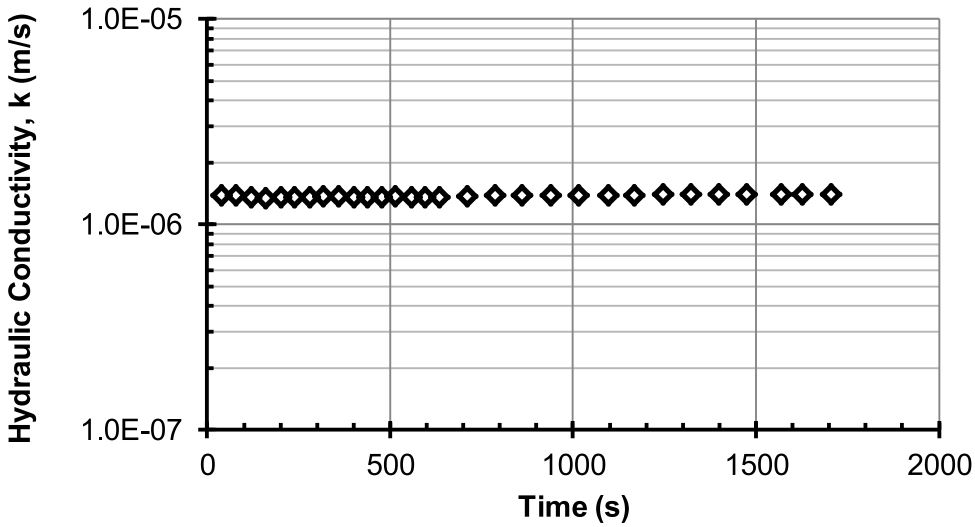


Figure VII-18. Constant head hydraulic conductivity (k) as a function of time for the horizontal core A13

5.3.5 Pilot Flume

5.3.5.a Pilot Zone 1

Table VII-28. Constant head test results for the undisturbed vertical core G1 (Sample Height = 7.3 cm; i = 0.2)

| Distance (m) | Cumulative Distance (m) | Time (s) | Velocity (m/s) | Flow rate, Q ($m^3$/s) | k (= Q/Ai) (m/s) |
|---|---|---|---|---|---|
| 0.680 | 0 | 0 | 0 | 0 | 0 |
| 0.670 | 0.010 | 77 | 1.3E-04 | 1.6E-09 | 9.5E-07 |
| 0.660 | 0.020 | 156 | 1.3E-04 | 1.6E-09 | 9.4E-07 |
| 0.650 | 0.030 | 229 | 1.3E-04 | 1.6E-09 | 9.6E-07 |
| 0.640 | 0.040 | 304 | 1.3E-04 | 1.7E-09 | 9.6E-07 |
| 0.630 | 0.050 | 372 | 1.3E-04 | 1.7E-09 | 9.8E-07 |
| 0.620 | 0.060 | 438 | 1.4E-04 | 1.7E-09 | 1.0E-06 |
| 0.610 | 0.070 | 509 | 1.4E-04 | 1.7E-09 | 1.0E-06 |
| 0.600 | 0.080 | 576 | 1.4E-04 | 1.7E-09 | 1.0E-06 |
| 0.590 | 0.090 | 641 | 1.4E-04 | 1.8E-09 | 1.0E-06 |
| 0.580 | 0.100 | 710 | 1.4E-04 | 1.8E-09 | 1.0E-06 |
| 0.570 | 0.110 | 774 | 1.4E-04 | 1.8E-09 | 1.0E-06 |
| 0.560 | 0.120 | 840 | 1.4E-04 | 1.8E-09 | 1.0E-06 |
| 0.550 | 0.130 | 903 | 1.4E-04 | 1.8E-09 | 1.1E-06 |
| 0.540 | 0.140 | 973 | 1.4E-04 | 1.8E-09 | 1.1E-06 |
| 0.530 | 0.150 | 1033 | 1.5E-04 | 1.8E-09 | 1.1E-06 |
| 0.520 | 0.160 | 1097 | 1.5E-04 | 1.8E-09 | 1.1E-06 |
| 0.510 | 0.170 | 1158 | 1.5E-04 | 1.8E-09 | 1.1E-06 |
| 0.500 | 0.180 | 1219 | 1.5E-04 | 1.9E-09 | 1.1E-06 |
| 0.451 | 0.229 | 1500 | 1.5E-04 | 1.9E-09 | 1.1E-06 |
| 0.400 | 0.280 | 1800 | 1.6E-04 | 2.0E-09 | 1.1E-06 |
| 0.344 | 0.336 | 2100 | 1.6E-04 | 2.0E-09 | 1.2E-06 |
| 0.290 | 0.390 | 2400 | 1.6E-04 | 2.0E-09 | 1.2E-06 |
| 0.236 | 0.444 | 2700 | 1.6E-04 | 2.1E-09 | 1.2E-06 |

Table VII-29. Constant head test results for the undisturbed horizontal core G1 (Sample Height = 11.8 cm; i = 0.3)

| Distance (m) | Cumulative Distance (m) | Time (s) | Velocity (m/s) | Flow rate Q, $m^3/s$ | k (= Q/Ai) (m/s) |
|---|---|---|---|---|---|
| 0.55 | 0 | 0 | 0 | 0 | 0 |
| 0.54 | 0.01 | 35 | 2.9E-04 | 3.6E-09 | 1.8E-06 |
| 0.53 | 0.02 | 71 | 2.8E-04 | 3.5E-09 | 1.8E-06 |
| 0.52 | 0.03 | 104 | 2.9E-04 | 3.6E-09 | 1.8E-06 |
| 0.51 | 0.04 | 137 | 2.9E-04 | 3.7E-09 | 1.8E-06 |
| 0.50 | 0.05 | 170 | 2.9E-04 | 3.7E-09 | 1.9E-06 |
| 0.49 | 0.06 | 203 | 3.0E-04 | 3.7E-09 | 1.9E-06 |
| 0.48 | 0.07 | 234 | 3.0E-04 | 3.8E-09 | 1.9E-06 |
| 0.47 | 0.08 | 268 | 3.0E-04 | 3.8E-09 | 1.9E-06 |
| 0.46 | 0.09 | 299 | 3.0E-04 | 3.8E-09 | 1.9E-06 |
| 0.45 | 0.10 | 330 | 3.0E-04 | 3.8E-09 | 1.9E-06 |
| 0.44 | 0.11 | 363 | 3.0E-04 | 3.8E-09 | 1.9E-06 |
| 0.43 | 0.12 | 393 | 3.1E-04 | 3.8E-09 | 1.9E-06 |
| 0.42 | 0.13 | 427 | 3.0E-04 | 3.8E-09 | 1.9E-06 |
| 0.41 | 0.14 | 460 | 3.0E-04 | 3.8E-09 | 1.9E-06 |
| 0.40 | 0.15 | 490 | 3.1E-04 | 3.8E-09 | 1.9E-06 |
| 0.39 | 0.16 | 522 | 3.1E-04 | 3.9E-09 | 1.9E-06 |
| 0.38 | 0.17 | 554 | 3.1E-04 | 3.9E-09 | 1.9E-06 |
| 0.37 | 0.18 | 584 | 3.1E-04 | 3.9E-09 | 1.9E-06 |
| 0.36 | 0.19 | 614 | 3.1E-04 | 3.9E-09 | 1.9E-06 |
| 0.35 | 0.20 | 646 | 3.1E-04 | 3.9E-09 | 1.9E-06 |
| 0.34 | 0.21 | 677 | 3.1E-04 | 3.9E-09 | 2.0E-06 |
| 0.33 | 0.22 | 706 | 3.1E-04 | 3.9E-09 | 2.0E-06 |
| 0.32 | 0.23 | 738 | 3.1E-04 | 3.9E-09 | 2.0E-06 |
| 0.31 | 0.24 | 773 | 3.1E-04 | 3.9E-09 | 2.0E-06 |
| 0.30 | 0.25 | 805 | 3.1E-04 | 3.9E-09 | 2.0E-06 |

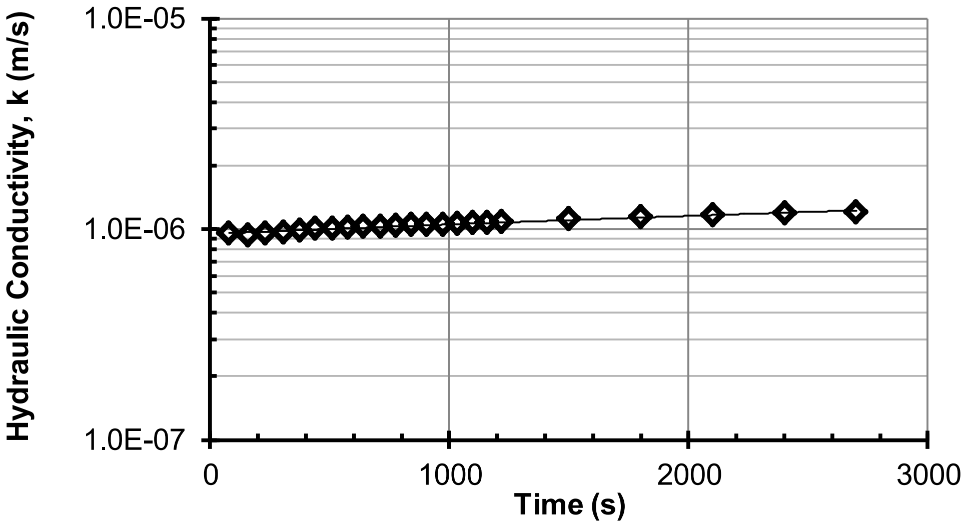


Figure VII-19. Constant head hydraulic conductivity (k) as a function of time for the vertical core G1

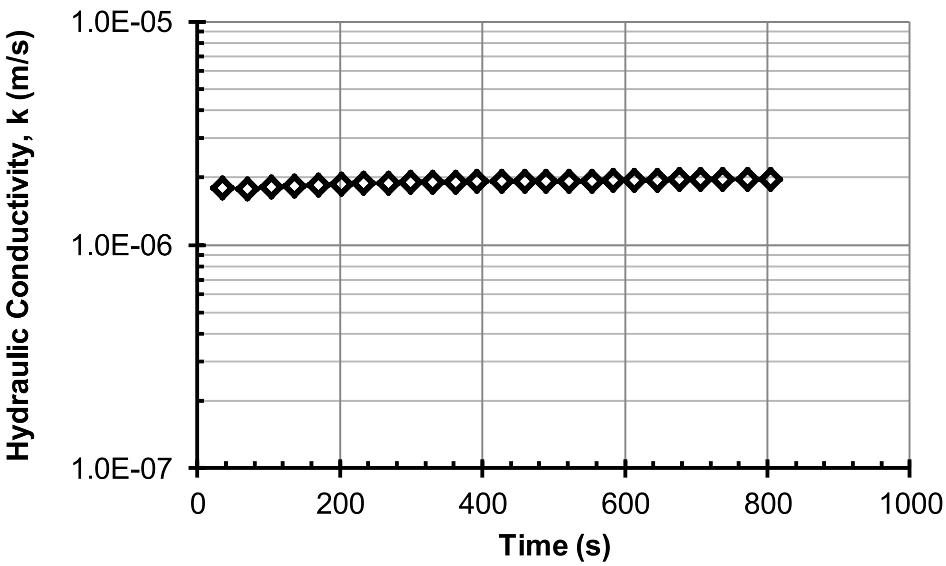


Figure VII-20. Constant head hydraulic conductivity (k) as a function of time for the horizontal core G1

5.3.5.b Pilot Zone 2

Table VII-30. Constant head test results for the undisturbed vertical core I2 (Sample Height = 9.0 cm; i = 0.2)

| Distance (m) | Cumulative Distance (m) | Time (s) | Velocity (m/s) | Flow rate Q ($m^3/s$) | k (= Q/Ai) (m/s) |
|---|---|---|---|---|---|
| 0.690 | 0 | 0 | 0 | 0 | 0 |
| 0.680 | 0.010 | 91 | 1.1E-04 | 1.4E-09 | 8.8E-07 |
| 0.670 | 0.020 | 185 | 1.1E-04 | 1.4E-09 | 8.7E-07 |
| 0.660 | 0.030 | 268 | 1.1E-04 | 1.4E-09 | 9.0E-07 |
| 0.650 | 0.040 | 344 | 1.2E-04 | 1.5E-09 | 9.3E-07 |
| 0.640 | 0.050 | 412 | 1.2E-04 | 1.5E-09 | 9.7E-07 |
| 0.630 | 0.060 | 486 | 1.2E-04 | 1.6E-09 | 9.9E-07 |
| 0.620 | 0.070 | 555 | 1.3E-04 | 1.6E-09 | 1.0E-06 |
| 0.610 | 0.080 | 621 | 1.3E-04 | 1.6E-09 | 1.0E-06 |
| 0.600 | 0.090 | 695 | 1.3E-04 | 1.6E-09 | 1.0E-06 |
| 0.590 | 0.100 | 764 | 1.3E-04 | 1.6E-09 | 1.0E-06 |
| 0.580 | 0.110 | 832 | 1.3E-04 | 1.7E-09 | 1.1E-06 |
| 0.570 | 0.120 | 905 | 1.3E-04 | 1.7E-09 | 1.1E-06 |
| 0.560 | 0.130 | 970 | 1.3E-04 | 1.7E-09 | 1.1E-06 |
| 0.550 | 0.140 | 1034 | 1.4E-04 | 1.7E-09 | 1.1E-06 |
| 0.540 | 0.150 | 1109 | 1.4E-04 | 1.7E-09 | 1.1E-06 |
| 0.530 | 0.160 | 1173 | 1.4E-04 | 1.7E-09 | 1.1E-06 |
| 0.520 | 0.170 | 1238 | 1.4E-04 | 1.7E-09 | 1.1E-06 |
| 0.510 | 0.180 | 1295 | 1.4E-04 | 1.7E-09 | 1.1E-06 |
| 0.500 | 0.190 | 1360 | 1.4E-04 | 1.8E-09 | 1.1E-06 |
| 0.451 | 0.239 | 1660 | 1.4E-04 | 1.8E-09 | 1.2E-06 |
| 0.403 | 0.287 | 1960 | 1.5E-04 | 1.8E-09 | 1.2E-06 |
| 0.355 | 0.335 | 2260 | 1.5E-04 | 1.9E-09 | 1.2E-06 |

Table VII-31. Constant head test results for the undisturbed horizontal core I2 (Sample Height = 7.6 cm; i = 0.2)

| Distance (m) | Cumulative Distance (m) | Time (s) | Velocity (m/s) | Flow rate Q ($m^3$/s) | k (= Q/Ai) (m/s) |
|---|---|---|---|---|---|
| 0.55 | 0 | 0 | 0 | 0 | 0 |
| 0.54 | 0.01 | 88 | 1.1E-04 | 1.4E-09 | 9.3E-07 |
| 0.53 | 0.02 | 175 | 1.1E-04 | 1.4E-09 | 9.3E-07 |
| 0.52 | 0.03 | 260 | 1.2E-04 | 1.4E-09 | 9.4E-07 |
| 0.51 | 0.04 | 343 | 1.2E-04 | 1.5E-09 | 9.5E-07 |
| 0.50 | 0.05 | 422 | 1.2E-04 | 1.5E-09 | 9.7E-07 |
| 0.49 | 0.06 | 506 | 1.2E-04 | 1.5E-09 | 9.7E-07 |
| 0.48 | 0.07 | 582 | 1.2E-04 | 1.5E-09 | 9.8E-07 |
| 0.47 | 0.08 | 667 | 1.2E-04 | 1.5E-09 | 9.8E-07 |
| 0.46 | 0.09 | 743 | 1.2E-04 | 1.5E-09 | 9.9E-07 |
| 0.45 | 0.10 | 823 | 1.2E-04 | 1.5E-09 | 9.9E-07 |
| 0.44 | 0.11 | 904 | 1.2E-04 | 1.5E-09 | 9.9E-07 |
| 0.43 | 0.12 | 988 | 1.2E-04 | 1.5E-09 | 9.9E-07 |
| 0.42 | 0.13 | 1068 | 1.2E-04 | 1.5E-09 | 9.9E-07 |
| 0.41 | 0.14 | 1148 | 1.2E-04 | 1.5E-09 | 9.9E-07 |
| 0.40 | 0.15 | 1222 | 1.2E-04 | 1.5E-09 | 1.0E-06 |
| 0.39 | 0.16 | 1304 | 1.2E-04 | 1.5E-09 | 1.0E-06 |
| 0.38 | 0.17 | 1378 | 1.2E-04 | 1.6E-09 | 1.0E-06 |
| 0.37 | 0.18 | 1456 | 1.2E-04 | 1.6E-09 | 1.0E-06 |
| 0.36 | 0.19 | 1532 | 1.2E-04 | 1.6E-09 | 1.0E-06 |
| 0.35 | 0.20 | 1608 | 1.2E-04 | 1.6E-09 | 1.0E-06 |
| 0.34 | 0.21 | 1682 | 1.2E-04 | 1.6E-09 | 1.0E-06 |
| 0.33 | 0.22 | 1760 | 1.3E-04 | 1.6E-09 | 1.0E-06 |
| 0.32 | 0.23 | 1832 | 1.3E-04 | 1.6E-09 | 1.0E-06 |
| 0.31 | 0.24 | 1912 | 1.3E-04 | 1.6E-09 | 1.0E-06 |
| 0.30 | 0.25 | 1990 | 1.3E-04 | 1.6E-09 | 1.0E-06 |
| 0.29 | 0.26 | 2062 | 1.3E-04 | 1.6E-09 | 1.0E-06 |
| 0.28 | 0.27 | 2140 | 1.3E-04 | 1.6E-09 | 1.0E-06 |

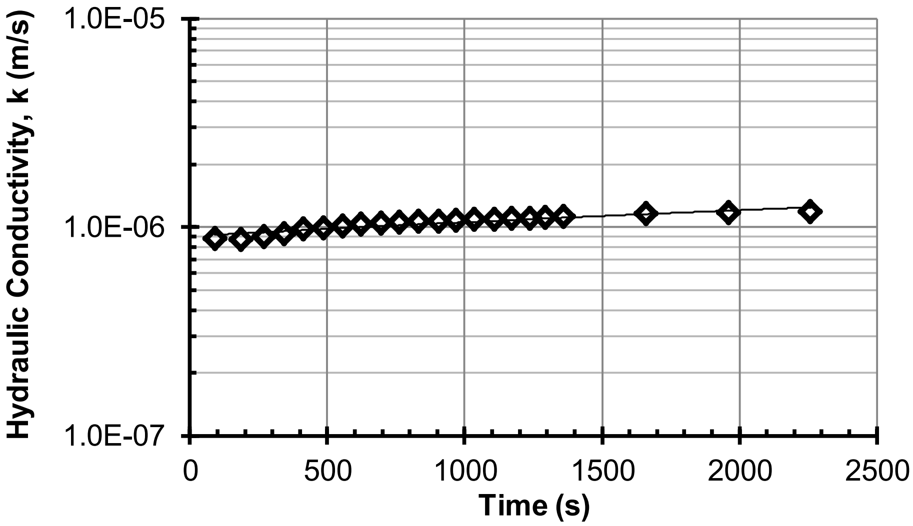


Figure VII-21. Constant head hydraulic conductivity (k) as a function of time for the vertical core I2

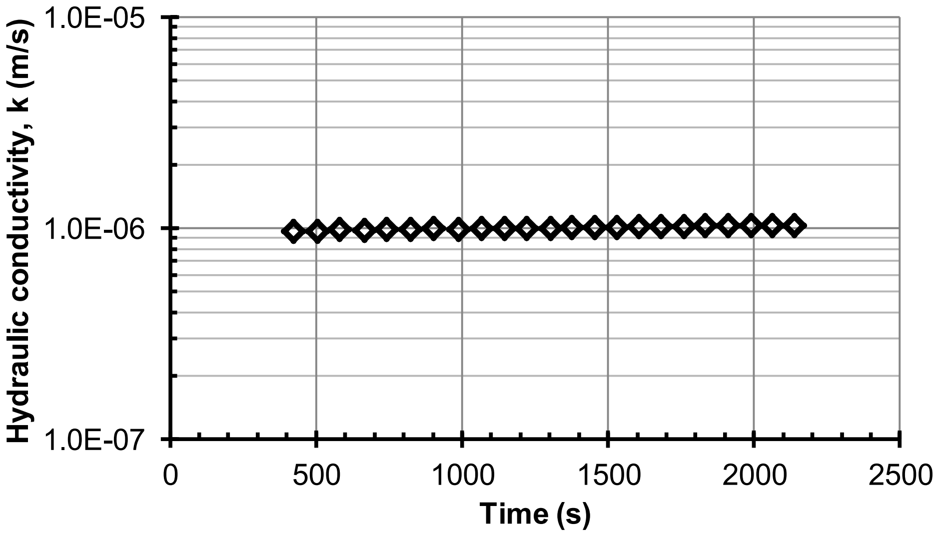


Figure VII-22. Constant head hydraulic conductivity (k) as a function of time for the horizontal core I2

5.3.5.c Pilot Zone 3

Table VII-32. Constant head test results for the undisturbed vertical core I3 (Sample Height = 5.7 cm; i = 0.2)

| Distance (m) | Cumulative Distance (m) | Time (s) | Velocity (m/s) | Flow rate, Q (m3/s) | k (= Q/Ai) (m/s) |
|---|---|---|---|---|---|
| 0.530 | 0 | 0 | 0 | 0 | 0 |
| 0.520 | 0.010 | 148 | 6.8E-05 | 8.5E-10 | 4.8E-07 |
| 0.510 | 0.020 | 288 | 6.9E-05 | 8.7E-10 | 4.9E-07 |
| 0.500 | 0.030 | 438 | 6.8E-05 | 8.6E-10 | 4.8E-07 |
| 0.490 | 0.040 | 566 | 7.1E-05 | 8.9E-10 | 5.0E-07 |
| 0.480 | 0.050 | 690 | 7.2E-05 | 9.1E-10 | 5.1E-07 |
| 0.469 | 0.061 | 845 | 7.2E-05 | 9.1E-10 | 5.1E-07 |
| 0.460 | 0.070 | 964 | 7.3E-05 | 9.1E-10 | 5.1E-07 |
| 0.450 | 0.080 | 1094 | 7.3E-05 | 9.2E-10 | 5.1E-07 |
| 0.440 | 0.090 | 1228 | 7.3E-05 | 9.2E-10 | 5.2E-07 |
| 0.430 | 0.100 | 1366 | 7.3E-05 | 9.2E-10 | 5.1E-07 |
| 0.420 | 0.110 | 1512 | 7.3E-05 | 9.1E-10 | 5.1E-07 |
| 0.410 | 0.120 | 1663 | 7.2E-05 | 9.1E-10 | 5.1E-07 |
| 0.400 | 0.130 | 1805 | 7.2E-05 | 9.1E-10 | 5.1E-07 |
| 0.390 | 0.140 | 1962 | 7.1E-05 | 9.0E-10 | 5.0E-07 |
| 0.380 | 0.150 | 2105 | 7.1E-05 | 9.0E-10 | 5.0E-07 |
| 0.370 | 0.160 | 2232 | 7.2E-05 | 9.0E-10 | 5.0E-07 |
| 0.360 | 0.170 | 2380 | 7.1E-05 | 9.0E-10 | 5.0E-07 |
| 0.340 | 0.190 | 2645 | 7.2E-05 | 9.0E-10 | 5.1E-07 |
| 0.330 | 0.200 | 2775 | 7.2E-05 | 9.1E-10 | 5.1E-07 |
| 0.320 | 0.210 | 2905 | 7.2E-05 | 9.1E-10 | 5.1E-07 |
| 0.308 | 0.222 | 3054 | 7.3E-05 | 9.1E-10 | 5.1E-07 |
| 0.300 | 0.230 | 3158 | 7.3E-05 | 9.2E-10 | 5.1E-07 |
| 0.290 | 0.240 | 3290 | 7.3E-05 | 9.2E-10 | 5.1E-07 |
| 0.280 | 0.250 | 3410 | 7.3E-05 | 9.2E-10 | 5.2E-07 |
| 0.268 | 0.262 | 3550 | 7.4E-05 | 9.3E-10 | 5.2E-07 |
| 0.260 | 0.270 | 3601 | 7.5E-05 | 9.4E-10 | 5.3E-07 |

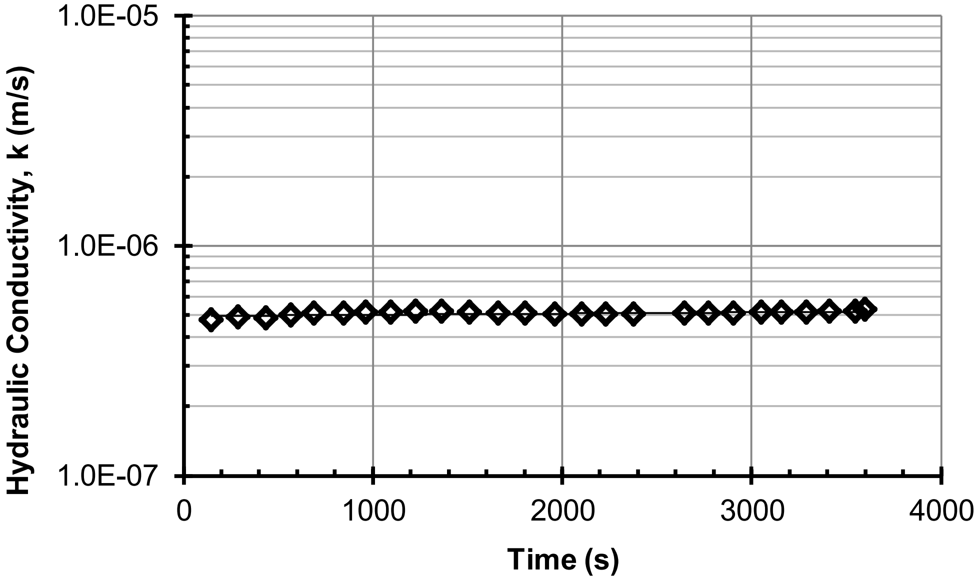


Figure VII-23. Constant head hydraulic conductivity (k) as a function of time for the vertical core I3

# VIII. **APPENDIX B** - PARTICLE SIZE DISTRIBUTION DATA

Particle Size Distribution (PSD) test data are presented in this section. Sieve analysis data used to determine the distribution of the coarse fraction are presented in Section 1. Dispersed and non-dispersed hydrometer test data are provided in Section 2. The same meniscus (+0.5) and zero correction (+5.5) were used for all hydrometer tests since the same precision hydrometer was utilised to run the experimentations following ASTM D422-63. Rc refers to the hydrometer readings after meniscus, zero and temperature (Ct) corrections were applied.

## 1 Sieve Analysis

Table VIII-1. Flume A1 mechanical sieve analysis results

| Sieve # | Diameter (mm) | Empty Sieve (g) | Sieve + Soil (g) | Soil Retained (g) | % Retained | % Passing |
|---|---|---|---|---|---|---|
| 4 | 4.750 | 471.4 | 471.4 | 0.0 | 0.0 | 100.0 |
| 10 | 2.000 | 431.8 | 431.8 | 0.0 | 0.0 | 100.0 |
| 20 | 0.840 | 378.7 | 379.1 | 0.4 | 0.1 | 99.9 |
| 40 | 0.425 | 338.5 | 341.3 | 2.8 | 0.6 | 99.3 |
| 60 | 0.250 | 315.2 | 332.2 | 17.0 | 3.6 | 95.8 |
| 140 | 0.106 | 300.9 | 571.4 | 270.5 | 56.8 | 39.0 |
| 200 | 0.075 | 352.0 | 501.4 | 149.4 | 31.3 | 7.7 |
| 325 | 0.044 | 320.0 | 355.9 | 35.9 | 7.5 | 0.1 |
| Pan | - | 375.7 | 376.6 | 0.9 | 0.2 | 0.0 |

Table VIII-2. Flume A3 mechanical sieve analysis results

| Sieve # | Diameter (mm) | Empty Sieve (g) | Sieve + Soil (g) | Soil Retained (g) | % Retained | % Passing |
|---|---|---|---|---|---|---|
| 4 | 4.750 | 471.4 | 471.4 | 0.0 | 0.0 | 100.0 |
| 10 | 2.000 | 431.8 | 431.8 | 0.0 | 0.0 | 100.0 |
| 20 | 0.840 | 378.7 | 378.7 | 0.0 | 0.0 | 100.0 |
| 40 | 0.425 | 338.5 | 340.1 | 1.6 | 0.3 | 99.7 |
| 60 | 0.250 | 315.2 | 329.5 | 14.3 | 2.9 | 96.8 |
| 140 | 0.106 | 300.8 | 583.5 | 282.7 | 57.7 | 39.1 |
| 200 | 0.075 | 351.9 | 496.2 | 144.3 | 29.4 | 9.7 |
| 325 | 0.044 | 320.0 | 367.1 | 47.1 | 9.6 | 0.1 |
| Pan | - | 375.7 | 376.1 | 0.4 | 0.1 | 0.0 |

Table VIII-3. Flume A5 mechanical sieve analysis results

| Sieve # | Diameter (mm) | Empty Sieve (g) | Sieve + Soil (g) | Soil Retained (g) | % Retained | % Passing |
|---|---|---|---|---|---|---|
| 4 | 4.750 | 530.8 | 530.8 | 0.0 | 0.0 | 100.0 |
| 10 | 2.000 | 431.8 | 431.8 | 0.0 | 0.0 | 100.0 |
| 20 | 0.840 | 378.7 | 379.0 | 0.3 | 0.0 | 100.0 |
| 40 | 0.425 | 338.5 | 345.7 | 7.1 | 1.2 | 98.8 |
| 60 | 0.250 | 315.3 | 365.1 | 49.8 | 8.1 | 90.7 |
| 140 | 0.106 | 306.2 | 713.3 | 407.1 | 66.3 | 24.4 |
| 200 | 0.075 | 335.5 | 459.0 | 123.6 | 20.1 | 4.3 |
| 325 | 0.044 | 319.7 | 354.3 | 34.7 | 5.6 | 0.0 |
| Pan | - | 375.7 | 376.5 | 0.8 | 0.1 | 0.0 |

Table VIII-4. Flume A13 mechanical sieve analysis results

| Sieve # | Diameter (mm) | Empty Sieve (g) | Sieve + Soil (g) | Soil Retained (g) | % Retained | % Passing |
|---|---|---|---|---|---|---|
| 4 | 4.750 | 530.7 | 530.7 | 0.0 | 0.0 | 100.0 |
| 10 | 2.000 | 431.8 | 431.8 | 0.0 | 0.0 | 100.0 |
| 20 | 0.840 | 378.7 | 378.8 | 0.1 | 0.0 | 100.0 |
| 40 | 0.425 | 338.5 | 339.0 | 0.5 | 0.1 | 99.9 |
| 60 | 0.250 | 315.3 | 335.8 | 20.6 | 3.3 | 96.6 |
| 140 | 0.106 | 306.3 | 743.7 | 437.4 | 69.7 | 26.9 |
| 200 | 0.075 | 335.4 | 466.2 | 130.8 | 20.9 | 6.1 |
| 325 | 0.044 | 319.6 | 356.1 | 36.5 | 5.8 | 0.2 |
| Pan | - | 375.7 | 377.4 | 1.7 | 0.3 | 0.0 |

Table VIII-5. Pilot flume Zone 1 mechanical sieve analysis results

| Sieve # | Diameter (mm) | Empty Sieve (g) | Sieve + Soil (g) | Soil Retained (g) | % Retained | % Passing |
|---|---|---|---|---|---|---|
| 4 | 4.750 | 471.4 | 471.4 | 0.0 | 0.0 | 100.0 |
| 10 | 2.000 | 432.5 | 432.5 | 0.0 | 0.0 | 100.0 |
| 20 | 0.840 | 386.3 | 386.5 | 0.2 | 0.0 | 100.0 |
| 40 | 0.425 | 338.5 | 341.9 | 3.4 | 0.6 | 99.4 |
| 60 | 0.250 | 315.7 | 351.4 | 35.7 | 5.9 | 93.5 |
| 140 | 0.106 | 306.3 | 723.8 | 417.6 | 69.5 | 24.0 |
| 200 | 0.075 | 379.0 | 512.4 | 133.4 | 22.2 | 1.8 |
| 325 | 0.044 | 444.2 | 454.4 | 10.2 | 1.7 | 0.1 |
| Pan | - | 375.4 | 375.9 | 0.5 | 0.1 | 0.0 |

Table VIII-6. Pilot flume Zone 2 mechanical sieve analysis results

| Sieve # | Diameter (mm) | Empty Sieve (g) | Sieve + Soil (g) | Soil Retained (g) | % Retained | % Passing |
|---|---|---|---|---|---|---|
| 4 | 4.750 | 471.3 | 471.3 | 0.0 | 0.0 | 100.0 |
| 10 | 2.000 | 432.5 | 432.5 | 0.0 | 0.0 | 100.0 |
| 20 | 0.840 | 386.3 | 386.3 | 0.0 | 0.0 | 100.0 |
| 40 | 0.425 | 338.4 | 339.0 | 0.6 | 0.1 | 99.9 |
| 60 | 0.250 | 315.8 | 353.6 | 37.8 | 6.0 | 93.9 |
| 140 | 0.106 | 306.3 | 777.8 | 471.6 | 74.5 | 19.5 |
| 200 | 0.075 | 378.9 | 492.1 | 113.2 | 17.9 | 1.6 |
| 325 | 0.044 | 444.2 | 454.2 | 9.9 | 1.6 | 0.0 |
| Pan | - | 375.4 | 375.8 | 0.4 | 0.1 | 0.0 |

Table VIII-7. Pilot flume Zone 3 mechanical sieve analysis results

| Sieve # | Diameter (mm) | Empty Sieve (g) | Sieve + Soil (g) | Soil Retained (g) | % Retained | % Passing |
|---|---|---|---|---|---|---|
| 4 | 4.750 | 471.4 | 471.4 | 0.0 | 0.0 | 100.0 |
| 10 | 2.000 | 432.5 | 432.5 | 0.0 | 0.0 | 100.0 |
| 20 | 0.840 | 386.3 | 386.7 | 0.3 | 0.1 | 99.9 |
| 40 | 0.425 | 338.5 | 341.6 | 3.1 | 0.5 | 99.4 |
| 60 | 0.250 | 315.8 | 328.5 | 12.7 | 2.3 | 97.1 |
| 140 | 0.106 | 306.3 | 654.5 | 348.2 | 61.7 | 35.4 |
| 200 | 0.075 | 379.0 | 577.1 | 198.1 | 35.1 | 0.3 |
| 325 | 0.044 | 444.2 | 451.2 | 6.9 | 1.2 | 0.0 |
| Pan | - | 375.4 | 375.7 | 0.3 | 0.1 | 0.0 |

Table VIII-8. Tailings beach sand mechanical sieve analysis results

| Sieve # | Diameter (mm) | Empty Sieve (g) | Sieve + Soil (g) | Soil Retained (g) | % Retained | % Passing |
|---|---|---|---|---|---|---|
| 4 | 4.750 | 470.7 | 470.7 | 0.0 | 0.0 | 100.0 |
| 10 | 2.000 | 503.6 | 503.7 | 0.1 | 0.0 | 100.0 |
| 20 | 0.840 | 378.8 | 379.2 | 0.4 | 0.1 | 99.9 |
| 40 | 0.425 | 338.5 | 339.4 | 0.9 | 0.2 | 99.7 |
| 60 | 0.250 | 315.7 | 322.4 | 6.7 | 1.2 | 98.5 |
| 140 | 0.106 | 306.3 | 797.7 | 491.4 | 89.3 | 9.3 |
| 200 | 0.075 | 335.2 | 377.7 | 42.5 | 7.7 | 1.5 |
| 325 | 0.044 | 319.6 | 326.7 | 7.1 | 1.3 | 0.3 |
| Pan | - | 268.9 | 269.2 | 0.3 | 0.1 | 0.2 |

## 2 Hydrometer tests

### 2.1 Flume A1

Table VIII-9. Flume A1 hydrometer at 5 cm depth (non-dispersed)

| T =22$^o$C, K = 0.01332, Ct =0.4 | | | | | | |
|---|---|---|---|---|---|---|
| Time (min) | Reading | Meniscus corrected | L | Diameter, D (mm) | Rc | % Finer |
| 0.25 | 11.0 | 11.5 | 14.4 | 0.1011 | 11.9 | 62.39 |
| 0.5 | 5.0 | 5.5 | 15.4 | 0.0739 | 5.9 | 30.93 |
| 1 | 1.5 | 2.0 | 16 | 0.0533 | 2.4 | 12.58 |
| 2 | 1.0 | 1.5 | 16.1 | 0.0377 | 1.9 | 9.96 |
| 4 | 0.8 | 1.3 | 16.1 | 0.0267 | 1.7 | 8.91 |
| 8 | 0.5 | 1.0 | 16.1 | 0.0189 | 1.4 | 7.34 |
| 16 | 0.5 | 1.0 | 16.1 | 0.0134 | 1.4 | 7.34 |
| 32 | 0.5 | 1.0 | 16.1 | 0.0094 | 1.4 | 7.34 |
| 60 | 0.2 | 0.7 | 16.2 | 0.0069 | 1.1 | 5.77 |
| 124 | 0.2 | 0.7 | 16.2 | 0.0048 | 1.1 | 5.77 |
| 240 | 0.2 | 0.7 | 16.2 | 0.0035 | 1.1 | 5.77 |
| 490 | 0.2 | 0.7 | 16.2 | 0.0024 | 1.1 | 5.77 |
| 1518 | 0.0 | 0.5 | 16.2 | 0.0014 | 0.9 | 4.72 |
| 1680 | 0.0 | 0.5 | 16.2 | 0.0013 | 0.9 | 4.72 |
| 1910 | 0.0 | 0.5 | 16.2 | 0.0012 | 0.9 | 4.72 |

Table VIII-10. Flume A1 hydrometer at 5 cm depth (dispersed)

| T =22$^o$C, K = 0.01332, Ct =0.4 | | | | | | |
|---|---|---|---|---|---|---|
| Time (min) | Reading | Meniscus corrected | L | Diameter, D (mm) | Rc | % Finer |
| 0.25 | 17.0 | 17.5 | 13.4 | 0.0975 | 12.4 | 55.26 |
| 0.5 | 11.5 | 12.0 | 14.3 | 0.0712 | 6.9 | 30.75 |
| 1 | 8.5 | 9.0 | 14.8 | 0.0512 | 3.9 | 17.38 |
| 2 | 8.0 | 8.5 | 14.9 | 0.0364 | 3.4 | 15.15 |
| 4 | 7.5 | 8.0 | 15 | 0.0258 | 2.9 | 12.92 |
| 8 | 7.0 | 7.5 | 15.1 | 0.0183 | 2.4 | 10.70 |
| 16 | 7.0 | 7.5 | 15.1 | 0.0129 | 2.4 | 10.70 |
| 32 | 7.0 | 7.5 | 15.1 | 0.0091 | 2.4 | 10.70 |
| 60 | 6.8 | 7.3 | 15.1 | 0.0067 | 2.2 | 9.80 |
| 122 | 6.5 | 7.0 | 15.2 | 0.0047 | 1.9 | 8.47 |
| 240 | 6.5 | 7.0 | 15.2 | 0.0034 | 1.9 | 8.47 |
| 480 | 6.5 | 7.0 | 15.2 | 0.0024 | 1.9 | 8.47 |
| 1508 | 6.5 | 7.0 | 15.2 | 0.0013 | 1.9 | 8.47 |
| 1670 | 6.2 | 6.7 | 15.1 | 0.0013 | 1.6 | 7.13 |
| 1900 | 6.0 | 6.5 | 15.1 | 0.0012 | 1.4 | 6.24 |

Table VIII-11. Flume A1 hydrometer at 15 cm depth (non-dispersed)

| T =23$^{o}$C, K = 0.01317, Ct =0.7 | | | | | | |
|---|---|---|---|---|---|---|
| Time (min) | Reading | Meniscus corrected | L | Diameter, D (mm) | Rc | % Finer |
| 0.25 | 11.5 | 12.0 | 14.3 | 0.0996 | 12.7 | 67.82 |
| 0.5 | 4.5 | 5.0 | 15.5 | 0.0733 | 5.7 | 30.44 |
| 1 | 1.5 | 2.0 | 16 | 0.0527 | 2.7 | 14.42 |
| 2 | 1.2 | 1.7 | 16.1 | 0.0373 | 2.4 | 12.82 |
| 4 | 0.7 | 1.2 | 16.1 | 0.0264 | 1.9 | 10.15 |
| 8 | 0.5 | 1.0 | 16.1 | 0.0187 | 1.7 | 9.08 |
| 16 | 0.5 | 1.0 | 16.1 | 0.0132 | 1.7 | 9.08 |
| 32 | 0.5 | 1.0 | 16.1 | 0.0093 | 1.7 | 9.08 |
| 60 | 0.3 | 0.8 | 16.1 | 0.0068 | 1.5 | 8.01 |
| 120 | 0.2 | 0.7 | 16.2 | 0.0048 | 1.4 | 7.48 |
| 240 | 0.2 | 0.7 | 16.2 | 0.0034 | 1.4 | 7.48 |
| 482 | 0.2 | 0.5 | 16.2 | 0.0024 | 1.2 | 7.48 |
| 1424 | 0.0 | 0.5 | 16.2 | 0.0014 | 1.2 | 6.41 |
| 1690 | 0.0 | 0.5 | 16.2 | 0.0013 | 1.2 | 6.41 |
| 1948 | 0.0 | 0.5 | 16.2 | 0.0012 | 1.2 | 6.41 |

Table VIII-12. Flume A1 hydrometer at 15 cm depth (dispersed)

| T =23$^{o}$C, K = 0.01317, Ct =0.7 | | | | | | |
|---|---|---|---|---|---|---|
| Time (min) | Reading | Meniscus corrected | L | Diameter, D (mm) | Rc | % Finer |
| 0.25 | 18.0 | 18.5 | 13.1 | 0.0953 | 13.7 | 62.94 |
| 0.5 | 9.5 | 10.0 | 14.7 | 0.0714 | 5.2 | 23.89 |
| 1 | 7.5 | 8.0 | 15 | 0.0510 | 3.2 | 14.70 |
| 2 | 7.0 | 7.5 | 15.1 | 0.0362 | 2.7 | 12.40 |
| 4 | 7.0 | 7.5 | 15.1 | 0.0256 | 2.7 | 12.40 |
| 8 | 7.0 | 7.5 | 15.1 | 0.0181 | 2.7 | 12.40 |
| 16 | 7.0 | 7.5 | 15.1 | 0.0128 | 2.7 | 12.40 |
| 32 | 7.0 | 7.5 | 15.1 | 0.0090 | 2.7 | 12.40 |
| 60 | 7.0 | 7.5 | 15.1 | 0.0066 | 2.7 | 12.40 |
| 120 | 7.0 | 7.5 | 15.1 | 0.0047 | 2.7 | 12.40 |
| 240 | 6.8 | 7.3 | 15.2 | 0.0033 | 2.5 | 11.48 |
| 482 | 6.8 | 7.3 | 15.2 | 0.0023 | 2.5 | 11.48 |
| 1415 | 6.8 | 7.3 | 15.2 | 0.0014 | 2.5 | 11.48 |
| 1681 | 6.8 | 7.3 | 15.2 | 0.0013 | 2.5 | 11.48 |
| 1939 | 6.5 | 7.0 | 15.2 | 0.0012 | 2.2 | 10.11 |

Table VIII-13. Flume A1 hydrometer at 20 cm depth (non-dispersed)

| T =22$^{o}$C, K = 0.01332, Ct =0.4 | | | | | | |
|---|---|---|---|---|---|---|
| Time (min) | Reading | Meniscus corrected | L | Diameter, D (mm) | Rc | % Finer |
| 0.25 | 13.0 | 13.5 | 14.1 | 0.1000 | 13.9 | 70.18 |
| 0.5 | 5.0 | 5.5 | 15.4 | 0.0739 | 5.9 | 29.79 |
| 1 | 1.0 | 1.5 | 16.1 | 0.0534 | 1.9 | 9.59 |
| 2 | 1.0 | 1.5 | 16.1 | 0.0377 | 1.9 | 9.59 |
| 4 | 1.0 | 1.5 | 16.1 | 0.0267 | 1.9 | 9.59 |
| 8 | 0.8 | 1.3 | 16.1 | 0.0189 | 1.7 | 8.58 |
| 16 | 0.8 | 1.3 | 16.1 | 0.0134 | 1.7 | 8.58 |
| 32 | 0.8 | 1.3 | 16.1 | 0.0094 | 1.7 | 8.58 |
| 60 | 0.5 | 1.0 | 16.1 | 0.0069 | 1.4 | 7.07 |
| 120 | 0.5 | 1.0 | 16.1 | 0.0049 | 1.4 | 7.07 |
| 240 | 0.2 | 0.7 | 16.2 | 0.0035 | 1.1 | 5.55 |
| 490 | 0.2 | 0.7 | 16.2 | 0.0024 | 1.1 | 5.55 |
| 1408 | 0.0 | 0.5 | 16.2 | 0.0014 | 0.9 | 4.54 |
| 1638 | 0.0 | 0.5 | 16.2 | 0.0013 | 0.9 | 4.54 |
| 1874 | 0.0 | 0.5 | 16.2 | 0.0012 | 0.9 | 4.54 |

Table VIII-14. Flume A1 hydrometer at 20 cm depth (dispersed)

| T =22$^{o}$C, K = 0.01332, Ct =0.4 | | | | | | |
|---|---|---|---|---|---|---|
| Time (min) | Reading | Meniscus corrected | L | Diameter, D (mm) | Rc | % Finer |
| 0.25 | 18.5 | 19.0 | 13.2 | 0.0968 | 13.9 | 60.69 |
| 0.5 | 11.0 | 11.5 | 14.4 | 0.0715 | 6.4 | 27.94 |
| 1 | 8.0 | 8.5 | 14.9 | 0.0514 | 3.4 | 14.84 |
| 2 | 7.5 | 8.0 | 15.0 | 0.0365 | 2.9 | 12.66 |
| 4 | 7.5 | 8.0 | 15.0 | 0.0258 | 2.9 | 12.66 |
| 8 | 7.5 | 8.0 | 15.0 | 0.0182 | 2.9 | 12.66 |
| 16 | 7.2 | 7.7 | 15.1 | 0.0129 | 2.6 | 11.35 |
| 32 | 7.2 | 7.7 | 15.1 | 0.0091 | 2.6 | 11.35 |
| 60 | 7.2 | 7.7 | 15.1 | 0.0067 | 2.6 | 11.35 |
| 120 | 7.0 | 7.5 | 15.1 | 0.0047 | 2.4 | 10.48 |
| 240 | 7.0 | 7.5 | 15.1 | 0.0033 | 2.4 | 10.48 |
| 482 | 7.0 | 7.5 | 15.1 | 0.0024 | 2.4 | 10.48 |
| 1400 | 7.0 | 7.5 | 15.1 | 0.0014 | 2.4 | 10.48 |
| 1630 | 6.8 | 7.3 | 15.2 | 0.0013 | 2.2 | 9.61 |
| 1866 | 6.8 | 7.3 | 15.2 | 0.0012 | 2.2 | 9.61 |

Table VIII-15. Hydrometer A1 horizontal core (non-dispersed)

| T =23°C, K = 0.01317, Ct =0.7 | | | | | | |
|---|---|---|---|---|---|---|
| Time (min) | Reading | Meniscus corrected | L | Diameter, D (mm) | Rc | % Finer |
| 0.25 | 11.5 | 12.0 | 14.3 | 0.0996 | 12.7 | 68.87 |
| 0.5 | 3.5 | 4.0 | 15.6 | 0.0736 | 4.7 | 25.49 |
| 1 | 1.5 | 2.0 | 16.0 | 0.0527 | 2.7 | 14.64 |
| 2 | 1.0 | 1.5 | 16.1 | 0.0373 | 2.2 | 11.93 |
| 4 | 1.0 | 1.5 | 16.1 | 0.0264 | 2.2 | 11.93 |
| 8 | 0.8 | 1.3 | 16.1 | 0.0187 | 2.0 | 10.85 |
| 16 | 0.8 | 1.3 | 16.1 | 0.0132 | 2.0 | 10.85 |
| 32 | 0.8 | 1.3 | 16.1 | 0.0093 | 2.0 | 10.85 |
| 60 | 0.5 | 1.0 | 16.0 | 0.0068 | 1.7 | 9.22 |
| 138 | 0.2 | 0.7 | 16.2 | 0.0045 | 1.4 | 7.59 |
| 256 | 0.2 | 0.7 | 16.2 | 0.0033 | 1.4 | 7.59 |
| 550 | 0.2 | 0.7 | 16.2 | 0.0023 | 1.4 | 7.59 |
| 1466 | 0.0 | 0.5 | 16.2 | 0.0014 | 1.2 | 6.51 |
| 1720 | 0.0 | 0.5 | 16.2 | 0.0013 | 1.2 | 6.51 |
| 2020 | 0.0 | 0.5 | 16.2 | 0.0012 | 1.2 | 6.51 |

Table VIII-16. Hydrometer A1 horizontal core (dispersed)

| T =23°C, K = 0.01317, Ct =0.7 | | | | | | |
|---|---|---|---|---|---|---|
| Time (min) | Reading | Meniscus corrected | L | Diameter, D (mm) | Rc | % Finer |
| 0.25 | 18.0 | 18.5 | 13.3 | 0.0959 | 13.7 | 62.24 |
| 0.5 | 10.0 | 10.5 | 14.6 | 0.0712 | 5.7 | 25.90 |
| 1 | 8.0 | 8.5 | 14.9 | 0.0508 | 3.7 | 16.81 |
| 2 | 8.0 | 8.5 | 14.9 | 0.0359 | 3.7 | 16.81 |
| 4 | 8.0 | 8.5 | 14.9 | 0.0254 | 3.7 | 16.81 |
| 8 | 8.0 | 8.5 | 14.9 | 0.0180 | 3.7 | 16.81 |
| 16 | 8.0 | 8.5 | 14.9 | 0.0127 | 3.7 | 16.81 |
| 32 | 7.8 | 8.3 | 15.0 | 0.0090 | 3.5 | 15.90 |
| 60 | 7.5 | 8.0 | 15.0 | 0.0066 | 3.2 | 14.54 |
| 130 | 7.5 | 8.0 | 15.0 | 0.0045 | 3.2 | 14.54 |
| 248 | 7.5 | 8.0 | 15.0 | 0.0032 | 3.2 | 14.54 |
| 542 | 7.2 | 7.7 | 15.1 | 0.0022 | 2.9 | 13.18 |
| 1458 | 7.0 | 7.5 | 15.1 | 0.0013 | 2.7 | 12.27 |
| 1712 | 7.0 | 7.5 | 15.1 | 0.0012 | 2.7 | 12.27 |
| 2012 | 7.0 | 7.5 | 15.1 | 0.0011 | 2.7 | 12.27 |

2.2 Flume A3

Table VIII-17. A3 hydrometer at depth 5 cm (non-dispersed)

| T =23°C, K = 0.01317, Ct =0.7 | | | | | | |
|---|---|---|---|---|---|---|
| Time (min) | Reading | Meniscus corrected | L | Diameter, D (mm) | Rc | % Finer |
| 0.25 | 10.0 | 10.5 | 14.6 | 0.1006 | 11.2 | 58.02 |
| 0.5 | 3.5 | 4.0 | 15.6 | 0.0736 | 4.7 | 24.35 |
| 1 | 1.5 | 2.0 | 16.0 | 0.0527 | 2.7 | 13.99 |
| 2 | 1.5 | 2.0 | 16.0 | 0.0373 | 2.7 | 13.99 |
| 4 | 1.5 | 2.0 | 16.0 | 0.0263 | 2.7 | 13.99 |
| 8 | 1.2 | 1.7 | 16.1 | 0.0187 | 2.4 | 12.43 |
| 16 | 1.0 | 1.5 | 16.1 | 0.0132 | 2.2 | 11.40 |
| 32 | 1.0 | 1.5 | 16.1 | 0.0093 | 2.2 | 11.40 |
| 60 | 1.0 | 1.5 | 16.1 | 0.0068 | 2.2 | 11.40 |
| 120 | 1.0 | 1.5 | 16.1 | 0.0048 | 2.2 | 11.40 |
| 240 | 0.8 | 1.3 | 16.1 | 0.0034 | 2.0 | 10.36 |
| 495 | 0.5 | 1.0 | 16.1 | 0.0024 | 1.7 | 8.81 |
| 1477 | 0.5 | 1.0 | 16.1 | 0.0014 | 1.7 | 8.81 |
| 1697 | 0.5 | 1.0 | 16.1 | 0.0013 | 1.7 | 8.81 |
| 1917 | 0.5 | 1.0 | 16.1 | 0.0012 | 1.7 | 8.81 |

Table VIII-18. A3 hydrometer at depth 5 cm (dispersed)

| T =23°C, K = 0.01317, Ct =0.7 | | | | | | |
|---|---|---|---|---|---|---|
| Time (min) | Reading | Meniscus corrected | L | Diameter, D (mm) | Rc | % Finer |
| 0 | 16.0 | 16.5 | 13.6 | 0.0971 | 11.7 | 51.34 |
| 1 | 9.0 | 9.5 | 14.8 | 0.0715 | 4.7 | 20.62 |
| 1 | 8.5 | 9.0 | 14.8 | 0.0507 | 4.2 | 18.43 |
| 2 | 8.0 | 8.5 | 14.9 | 0.0359 | 3.7 | 16.24 |
| 4 | 8.0 | 8.5 | 14.9 | 0.0254 | 3.7 | 16.24 |
| 8 | 8.0 | 8.5 | 14.9 | 0.0180 | 3.7 | 16.24 |
| 16 | 8.0 | 8.5 | 14.9 | 0.0127 | 3.7 | 16.24 |
| 32 | 8.0 | 8.5 | 14.9 | 0.0090 | 3.7 | 16.24 |
| 60 | 8.0 | 8.5 | 14.9 | 0.0066 | 3.7 | 16.24 |
| 120 | 7.8 | 8.3 | 15.0 | 0.0047 | 3.5 | 15.36 |
| 240 | 7.8 | 8.3 | 15.0 | 0.0033 | 3.5 | 15.36 |
| 485 | 7.8 | 8.3 | 15.0 | 0.0023 | 3.5 | 15.36 |
| 1467 | 7.5 | 8.0 | 15.0 | 0.0013 | 3.2 | 14.04 |
| 1687 | 7.2 | 7.7 | 15.1 | 0.0012 | 2.9 | 12.73 |
| 1907 | 7.2 | 7.7 | 15.1 | 0.0012 | 2.9 | 12.73 |

Table VIII-19. A3 hydrometer at depth 10 cm (non-dispersed)

| T =23°C, K = 0.01317, Ct =0.7 | | | | | | |
|---|---|---|---|---|---|---|
| Time (min) | Reading | Meniscus corrected | L | Diameter, D (mm) | Rc | % Finer |
| 0 | 12.5 | 13 | 14.2 | 0.0993 | 13.2 | 69.91 |
| 1 | 4.0 | 4.5 | 15.6 | 0.0734 | 4.7 | 24.89 |
| 1 | 1.5 | 2 | 16.0 | 0.0527 | 2.2 | 11.65 |
| 2 | 1.0 | 1.5 | 16.1 | 0.0373 | 1.7 | 9.00 |
| 4 | 1.0 | 1.5 | 16.1 | 0.0264 | 1.7 | 9.00 |
| 8 | 1.0 | 1.5 | 16.1 | 0.0187 | 1.7 | 9.00 |
| 16 | 0.8 | 1.3 | 16.1 | 0.0132 | 1.5 | 7.94 |
| 32 | 0.8 | 1.3 | 16.1 | 0.0093 | 1.5 | 7.94 |
| 60 | 0.8 | 1.3 | 16.1 | 0.0068 | 1.5 | 7.94 |
| 120 | 0.8 | 1.3 | 16.1 | 0.0048 | 1.5 | 7.94 |
| 240 | 0.5 | 1.0 | 16.1 | 0.0034 | 1.2 | 6.36 |
| 505 | 0.5 | 1.0 | 16.1 | 0.0024 | 1.2 | 6.36 |
| 1497 | 0.5 | 1.0 | 16.1 | 0.0014 | 1.2 | 6.36 |
| 1773 | 0.3 | 0.8 | 16.2 | 0.0013 | 1.0 | 5.30 |
| 1889 | 0.3 | 0.8 | 16.2 | 0.0012 | 1.0 | 5.30 |

Table VIII-20. A3 hydrometer at depth 10 cm (dispersed)

| T =23°C, K = 0.01317, Ct =0.7 | | | | | | |
|---|---|---|---|---|---|---|
| Time (min) | Reading | Meniscus corrected | L | Diameter, D (mm) | Rc | % Finer |
| 0 | 18.0 | 18.5 | 13.3 | 0.0959 | 13.2 | 59.97 |
| 1 | 8.0 | 8.5 | 14.9 | 0.0719 | 3.2 | 14.54 |
| 1 | 7.5 | 8.0 | 15.0 | 0.0510 | 2.7 | 12.27 |
| 2 | 7.5 | 8.0 | 15.0 | 0.0361 | 2.7 | 12.27 |
| 4 | 7.2 | 7.7 | 15.1 | 0.0256 | 2.4 | 10.90 |
| 8 | 7.2 | 7.7 | 15.1 | 0.0181 | 2.4 | 10.90 |
| 16 | 7.2 | 7.7 | 15.1 | 0.0128 | 2.4 | 10.90 |
| 32 | 7.2 | 7.7 | 15.1 | 0.0090 | 2.4 | 10.90 |
| 60 | 7.0 | 7.5 | 15.1 | 0.0066 | 2.2 | 10.00 |
| 120 | 7.0 | 7.5 | 15.1 | 0.0047 | 2.2 | 10.00 |
| 240 | 7.0 | 7.5 | 15.1 | 0.0033 | 2.2 | 10.00 |
| 495 | 6.8 | 7.3 | 15.2 | 0.0023 | 2.0 | 9.09 |
| 1487 | 6.5 | 7.0 | 15.2 | 0.0013 | 1.7 | 7.72 |
| 1763 | 6.5 | 7.0 | 15.2 | 0.0012 | 1.7 | 7.72 |
| 1881 | 6.5 | 7.0 | 15.2 | 0.0012 | 1.7 | 7.72 |

Table VIII-21. A3 hydrometer at depth 15 cm (non-dispersed)

| T =23°C, K = 0.01317, Ct =0.7 | | | | | | |
|---|---|---|---|---|---|---|
| Time (min) | Reading | Meniscus corrected | L | Diameter, D (mm) | Rc | % Finer |
| 0 | 12.0 | 12.5 | 14.3 | 0.0994 | 13.2 | 67.61 |
| 1 | 3.5 | 4.0 | 15.6 | 0.0736 | 4.7 | 24.07 |
| 1 | 1.3 | 1.8 | 16.0 | 0.0527 | 2.5 | 12.81 |
| 2 | 0.8 | 1.3 | 16.1 | 0.0373 | 2.0 | 10.24 |
| 4 | 0.7 | 1.2 | 16.1 | 0.0264 | 1.9 | 9.73 |
| 8 | 0.7 | 1.2 | 16.1 | 0.0187 | 1.9 | 9.73 |
| 16 | 0.7 | 1.2 | 16.1 | 0.0132 | 1.9 | 9.73 |
| 32 | 0.7 | 1.2 | 16.1 | 0.0093 | 1.9 | 9.73 |
| 60 | 0.5 | 1.0 | 16.1 | 0.0068 | 1.7 | 8.71 |
| 120 | 0.5 | 1.0 | 16.1 | 0.0048 | 1.7 | 8.71 |
| 240 | 0.5 | 1.0 | 16.1 | 0.0034 | 1.7 | 8.71 |
| 493 | 0.4 | 0.9 | 16.2 | 0.0024 | 1.6 | 8.20 |
| 1417 | 0.2 | 0.7 | 16.2 | 0.0014 | 1.4 | 7.17 |
| 1684 | 0.2 | 0.7 | 16.2 | 0.0013 | 1.4 | 7.17 |
| 1911 | 0.2 | 0.7 | 16.2 | 0.0012 | 1.4 | 7.17 |

Table VIII-22. A3 hydrometer at depth 15 cm (dispersed)

| T =23°C, K = 0.01317, Ct =0.7 | | | | | | |
|---|---|---|---|---|---|---|
| Time (min) | Reading | Meniscus corrected | L | Diameter, D (mm) | Rc | % Finer |
| 0 | 19.0 | 19.5 | 13.1 | 0.0953 | 14.7 | 64.37 |
| 1 | 11.0 | 11.5 | 14.4 | 0.0707 | 6.7 | 29.34 |
| 1 | 8.0 | 8.5 | 14.9 | 0.0508 | 3.7 | 16.20 |
| 2 | 7.8 | 8.3 | 15.0 | 0.0361 | 3.5 | 15.33 |
| 4 | 7.0 | 7.5 | 15.1 | 0.0256 | 2.7 | 11.82 |
| 8 | 7.0 | 7.5 | 15.1 | 0.0181 | 2.7 | 11.82 |
| 16 | 7.0 | 7.5 | 15.1 | 0.0128 | 2.7 | 11.82 |
| 32 | 7.0 | 7.5 | 15.1 | 0.0090 | 2.7 | 11.82 |
| 60 | 7.0 | 7.5 | 15.1 | 0.0066 | 2.7 | 11.82 |
| 120 | 7.0 | 7.5 | 15.1 | 0.0047 | 2.7 | 11.82 |
| 240 | 6.8 | 7.3 | 15.2 | 0.0033 | 2.5 | 10.95 |
| 484 | 6.5 | 7.0 | 15.2 | 0.0023 | 2.2 | 9.63 |
| 1408 | 6.2 | 6.7 | 15.3 | 0.0014 | 1.9 | 8.32 |
| 1675 | 6.2 | 6.7 | 15.3 | 0.0013 | 1.9 | 8.32 |
| 1902 | 6.2 | 6.7 | 15.3 | 0.0012 | 1.9 | 8.32 |

Table VIII-23. A3 hydrometer at depth 20 cm (non-dispersed)

| T =22°C, K = 0.01332, Ct =0.4 | | | | | | |
|---|---|---|---|---|---|---|
| Time (min) | Reading | Meniscus corrected | L | Diameter, D (mm) | Rc | % Finer |
| 0 | 12.0 | 12.5 | 14.1 | 0.1000 | 12.4 | 64.23 |
| 1 | 4.0 | 4.5 | 15.6 | 0.0743 | 4.4 | 22.79 |
| 1 | 1.5 | 2.0 | 16.0 | 0.0533 | 1.9 | 9.84 |
| 2 | 1.2 | 1.7 | 16.1 | 0.0377 | 1.6 | 8.29 |
| 4 | 1.0 | 1.5 | 16.1 | 0.0267 | 1.4 | 7.25 |
| 8 | 1.0 | 1.5 | 16.1 | 0.0189 | 1.4 | 7.25 |
| 16 | 1.0 | 1.5 | 16.1 | 0.0133 | 1.4 | 7.25 |
| 32 | 1.0 | 1.5 | 16.1 | 0.0094 | 1.4 | 7.25 |
| 60 | 0.8 | 1.3 | 16.1 | 0.0069 | 1.2 | 6.22 |
| 120 | 0.8 | 1.3 | 16.1 | 0.0049 | 1.2 | 6.22 |
| 240 | 0.8 | 1.3 | 16.1 | 0.0034 | 1.2 | 6.22 |
| 535 | 0.5 | 1.0 | 16.1 | 0.0023 | 0.9 | 4.66 |
| 1436 | 0.2 | 0.7 | 16.2 | 0.0014 | 0.6 | 3.11 |
| 1693 | 0.2 | 0.7 | 16.2 | 0.0013 | 0.6 | 3.11 |
| 1931 | 0.2 | 0.7 | 16.2 | 0.0012 | 0.6 | 3.11 |

Table VIII-24. A3 hydrometer at depth 20 cm (dispersed)

| T =22°C, K = 0.01332, Ct =0.4 | | | | | | |
|---|---|---|---|---|---|---|
| Time (min) | Reading | Meniscus corrected | L | Diameter, D (mm) | Rc | % Finer |
| 0 | 18.0 | 18.5 | 13.3 | 0.0970 | 12.9 | 60.29 |
| 1 | 9.0 | 9.5 | 14.8 | 0.0723 | 3.9 | 18.23 |
| 1 | 7.5 | 8 | 15.0 | 0.0516 | 2.4 | 11.22 |
| 2 | 7.5 | 8 | 15.0 | 0.0365 | 2.4 | 11.22 |
| 4 | 7.5 | 8 | 15.0 | 0.0258 | 2.4 | 11.22 |
| 8 | 7.2 | 7.7 | 15.1 | 0.0183 | 2.1 | 9.82 |
| 16 | 7.0 | 7.5 | 15.1 | 0.0129 | 1.9 | 8.88 |
| 32 | 7.0 | 7.5 | 15.1 | 0.0091 | 1.9 | 8.88 |
| 60 | 7.0 | 7.5 | 15.1 | 0.0067 | 1.9 | 8.88 |
| 120 | 6.8 | 7.3 | 15.2 | 0.0047 | 1.7 | 7.95 |
| 240 | 6.8 | 7.3 | 15.2 | 0.0034 | 1.7 | 7.95 |
| 525 | 6.5 | 7 | 15.2 | 0.0023 | 1.4 | 6.54 |
| 1426 | 6.2 | 6.7 | 15.3 | 0.0014 | 1.1 | 5.14 |
| 1683 | 6.2 | 6.7 | 15.3 | 0.0013 | 1.1 | 5.14 |
| 1921 | 6.2 | 6.7 | 15.3 | 0.0012 | 1.1 | 5.14 |

Table VIII-25. Hydrometer A3 horizontal core (non-dispersed)

| T =22oC, K = 0.01332, Ct =0.4 | | | | | | |
|---|---|---|---|---|---|---|
| Time (min) | Reading | Meniscus corrected | L | Diameter, D (mm) | Rc | % Finer |
| 0 | 12.5 | 13.0 | 14.2 | 0.1004 | 13.4 | 73.31 |
| 1 | 3.5 | 4.0 | 15.6 | 0.0744 | 4.4 | 24.07 |
| 1 | 1.2 | 1.7 | 16.1 | 0.0534 | 2.1 | 11.49 |
| 2 | 1.0 | 1.5 | 16.1 | 0.0377 | 1.9 | 10.39 |
| 4 | 1.0 | 1.5 | 16.1 | 0.0267 | 1.9 | 10.39 |
| 8 | 1.0 | 1.5 | 16.1 | 0.0189 | 1.9 | 10.39 |
| 16 | 1.0 | 1.5 | 16.1 | 0.0133 | 1.9 | 10.39 |
| 32 | 1.0 | 1.5 | 16.1 | 0.0094 | 1.9 | 10.39 |
| 60 | 1.0 | 1.5 | 16.1 | 0.0069 | 1.9 | 10.39 |
| 126 | 0.8 | 1.3 | 16.1 | 0.0048 | 1.7 | 9.30 |
| 250 | 0.5 | 1.0 | 16.1 | 0.0034 | 1.4 | 7.66 |
| 574 | 0.3 | 0.8 | 16.2 | 0.0022 | 1.2 | 6.56 |
| 1462 | 0.0 | 0.5 | 16.2 | 0.0014 | 0.9 | 4.92 |
| 1724 | 0.0 | 0.5 | 16.2 | 0.0013 | 0.9 | 4.92 |
| 1918 | 0.0 | 0.5 | 16.2 | 0.0012 | 0.9 | 4.92 |

Table VIII-26. Hydrometer A3 horizontal core (dispersed)

| T =22oC, K = 0.01332, Ct =0.4 | | | | | | |
|---|---|---|---|---|---|---|
| Time (min) | Reading | Meniscus corrected | L | Diameter, D (mm) | Rc | % Finer |
| 0 | 18.5 | 19.0 | 13.2 | 0.0968 | 13.9 | 62.43 |
| 1 | 11.0 | 11.5 | 14.4 | 0.0715 | 6.4 | 28.74 |
| 1 | 9.0 | 9.5 | 14.8 | 0.0512 | 4.4 | 19.76 |
| 2 | 8.5 | 9.0 | 14.8 | 0.0362 | 3.9 | 17.52 |
| 4 | 8.2 | 8.7 | 14.9 | 0.0257 | 3.6 | 16.17 |
| 8 | 8.2 | 8.7 | 14.9 | 0.0181 | 3.6 | 16.17 |
| 16 | 8.2 | 8.7 | 14.9 | 0.0128 | 3.6 | 16.17 |
| 32 | 8.2 | 8.7 | 14.9 | 0.0091 | 3.6 | 16.17 |
| 60 | 8.0 | 8.5 | 14.9 | 0.0066 | 3.4 | 15.27 |
| 120 | 8.0 | 8.5 | 14.9 | 0.0047 | 3.4 | 15.27 |
| 242 | 8.0 | 8.5 | 14.9 | 0.0033 | 3.4 | 15.27 |
| 566 | 7.8 | 8.3 | 15.0 | 0.0022 | 3.2 | 14.37 |
| 1454 | 7.5 | 8.0 | 15.0 | 0.0014 | 2.9 | 13.02 |
| 1716 | 7.5 | 8.0 | 15.0 | 0.0012 | 2.9 | 13.02 |
| 1910 | 7.2 | 7.7 | 15.2 | 0.0012 | 2.6 | 11.68 |

2.3 Flume A5

Table VIII-27. Hydrometer A5 vertical core (non-dispersed)

| T =23°C, K = 0.01358, Ct =0.7 | | | | | | |
|---|---|---|---|---|---|---|
| Time (min) | Reading | Meniscus corrected | L | Diameter, D (mm) | Rc | % Finer |
| 0.25 | 12.0 | 12.5 | 14.1 | 0.1020 | 13.2 | 71.55 |
| 0.5 | 5.0 | 5.5 | 15.4 | 0.0754 | 6.2 | 33.61 |
| 1 | 2.0 | 2.5 | 15.9 | 0.0541 | 3.2 | 17.35 |
| 2 | 2.0 | 2.5 | 15.9 | 0.0383 | 3.2 | 17.35 |
| 4 | 2.0 | 2.5 | 15.9 | 0.0271 | 3.2 | 17.35 |
| 8 | 2.0 | 2.5 | 15.9 | 0.0191 | 3.2 | 17.35 |
| 16 | 2.0 | 2.5 | 15.9 | 0.0135 | 3.2 | 17.35 |
| 32 | 2.0 | 2.5 | 15.9 | 0.0096 | 3.2 | 17.35 |
| 60 | 2.0 | 2.5 | 15.9 | 0.0070 | 3.2 | 17.35 |
| 120 | 1.8 | 2.3 | 16.0 | 0.0050 | 3.0 | 16.26 |
| 240 | 1.5 | 2.0 | 16.0 | 0.0035 | 2.7 | 14.64 |
| 518 | 1.5 | 2.0 | 16.0 | 0.0024 | 2.7 | 14.64 |
| 1430 | 1.2 | 1.7 | 16.1 | 0.0014 | 2.4 | 13.01 |
| 1691 | 1.2 | 1.7 | 16.1 | 0.0013 | 2.4 | 13.01 |
| 1884 | 1.2 | 1.7 | 16.1 | 0.0013 | 2.4 | 13.01 |

Table VIII-28. Hydrometer A5 vertical core (dispersed)

| T =23°C, K = 0.01358, Ct =0.7 | | | | | | |
|---|---|---|---|---|---|---|
| Time (min) | Reading | Meniscus corrected | L | Diameter, D (mm) | Rc | % Finer |
| 0.25 | 18.0 | 18.5 | 13.3 | 0.0991 | 13.7 | 62.80 |
| 0.5 | 11.0 | 11.5 | 14.4 | 0.0729 | 6.7 | 30.71 |
| 1 | 9.5 | 10.0 | 14.7 | 0.0521 | 5.2 | 23.84 |
| 2 | 9.0 | 9.5 | 14.6 | 0.0367 | 4.7 | 21.55 |
| 4 | 9.0 | 9.5 | 14.6 | 0.0259 | 4.7 | 21.55 |
| 8 | 9.0 | 9.5 | 14.6 | 0.0183 | 4.7 | 21.55 |
| 16 | 9.0 | 9.5 | 14.6 | 0.0130 | 4.7 | 21.55 |
| 32 | 9.0 | 9.5 | 14.6 | 0.0092 | 4.7 | 21.55 |
| 60 | 8.8 | 9.3 | 14.8 | 0.0067 | 4.5 | 20.63 |
| 120 | 8.5 | 9.0 | 14.8 | 0.0048 | 4.2 | 19.25 |
| 240 | 8.2 | 8.7 | 14.9 | 0.0034 | 3.9 | 17.88 |
| 508 | 8.0 | 8.5 | 14.9 | 0.0023 | 3.7 | 16.96 |
| 1420 | 8.0 | 8.5 | 14.9 | 0.0014 | 3.7 | 16.96 |
| 1681 | 8.0 | 8.5 | 14.9 | 0.0013 | 3.7 | 16.96 |
| 1874 | 8.0 | 8.5 | 14.9 | 0.0012 | 3.7 | 16.96 |

Table VIII-29. Hydrometer A5 vertical core at the crest (non-dispersed)

| T =22$^{o}$C, K = 0.01374, Ct =0.4 | | | | | | |
|---|---|---|---|---|---|---|
| Time (min) | Reading | Meniscus corrected | L | Diameter, D (mm) | Rc | % Finer |
| 0.25 | 12.0 | 12.5 | 14.3 | 0.1037 | 12.9 | 70.11 |
| 0.5 | 4.5 | 5.0 | 15.5 | 0.0765 | 5.4 | 29.35 |
| 1 | 2.0 | 2.5 | 15.9 | 0.0548 | 2.9 | 15.76 |
| 2 | 2.0 | 2.5 | 15.9 | 0.0387 | 2.9 | 15.76 |
| 4 | 2.0 | 2.5 | 15.9 | 0.0274 | 2.9 | 15.76 |
| 8 | 2.0 | 2.5 | 15.9 | 0.0194 | 2.9 | 15.76 |
| 16.5 | 2.0 | 2.5 | 15.9 | 0.0135 | 2.9 | 15.76 |
| 32 | 2.0 | 2.5 | 15.9 | 0.0097 | 2.9 | 15.76 |
| 60 | 2.0 | 2.5 | 15.9 | 0.0071 | 2.9 | 15.76 |
| 120 | 2.0 | 2.5 | 15.9 | 0.0050 | 2.9 | 15.76 |
| 242 | 1.5 | 2.0 | 16.0 | 0.0035 | 2.4 | 13.04 |
| 486 | 1.5 | 2.0 | 16.0 | 0.0025 | 2.4 | 13.04 |
| 1498 | 1.5 | 2.0 | 16.0 | 0.0014 | 2.4 | 13.04 |
| 1730 | 1.5 | 2.0 | 16.0 | 0.0013 | 2.4 | 13.04 |
| 1950 | 1.0 | 1.5 | 16.1 | 0.0012 | 1.9 | 10.33 |

Table VIII-30. Hydrometer A5 vertical core at the crest (dispersed)

| T =22$^{o}$C, K = 0.01374, Ct =0.4 | | | | | | |
|---|---|---|---|---|---|---|
| Time (min) | Reading | Meniscus corrected | L | Diameter, D (mm) | Rc | % Finer |
| 0.25 | 18.0 | 18.5 | 13.3 | 0.1000 | 13.4 | 64.51 |
| 0.5 | 10.5 | 11.0 | 14.5 | 0.0740 | 5.9 | 28.40 |
| 1 | 8.5 | 9.0 | 14.8 | 0.0529 | 3.9 | 18.77 |
| 2 | 8.5 | 9.0 | 14.8 | 0.0374 | 3.9 | 18.77 |
| 4 | 8.5 | 9.0 | 14.8 | 0.0264 | 3.9 | 18.77 |
| 8 | 8.5 | 9.0 | 14.8 | 0.0187 | 3.9 | 18.77 |
| 16 | 8.5 | 9.0 | 14.8 | 0.0132 | 3.9 | 18.77 |
| 32 | 8.0 | 8.5 | 14.9 | 0.0094 | 3.4 | 16.37 |
| 60 | 8.0 | 8.5 | 14.9 | 0.0068 | 3.4 | 16.37 |
| 120 | 8.0 | 8.5 | 14.9 | 0.0048 | 3.4 | 16.37 |
| 240 | 8.0 | 8.5 | 14.9 | 0.0034 | 3.4 | 16.37 |
| 480 | 8.0 | 8.5 | 14.9 | 0.0024 | 3.4 | 16.37 |
| 1489 | 7.5 | 8.0 | 15.0 | 0.0014 | 3.2 | 15.40 |
| 1721 | 7.5 | 8.0 | 15.0 | 0.0013 | 2.9 | 13.96 |
| 1941 | 7.5 | 8.0 | 15.0 | 0.0012 | 2.9 | 13.96 |

Table VIII-31. Hydrometer A5 vertical core at the toe (non-dispersed)

| T =22$^o$C, K = 0.01374, Ct =0.4 | | | | | | |
|---|---|---|---|---|---|---|
| Time (min) | Reading | Meniscus corrected | L | Diameter, D (mm) | Rc | % Finer |
| 0.25 | 12.0 | 12.5 | 14.3 | 0.1037 | 12.9 | 57.79 |
| 0.5 | 6.0 | 6.5 | 15.3 | 0.0759 | 6.9 | 30.91 |
| 1 | 3.0 | 3.5 | 15.7 | 0.0544 | 3.9 | 17.47 |
| 2 | 2.8 | 3.3 | 15.7 | 0.0385 | 3.7 | 16.58 |
| 4 | 2.5 | 3.0 | 15.8 | 0.0273 | 3.4 | 15.23 |
| 8 | 2.0 | 2.5 | 15.8 | 0.0193 | 2.9 | 12.99 |
| 17.5 | 1.2 | 1.7 | 15.9 | 0.0131 | 2.1 | 9.41 |
| 32 | 1.2 | 1.7 | 16 | 0.0097 | 2.1 | 9.41 |
| 60 | 1.0 | 1.5 | 16.1 | 0.0071 | 1.9 | 8.51 |
| 120 | 1.0 | 1.5 | 16.1 | 0.0050 | 1.9 | 8.51 |
| 240 | 1.0 | 1.5 | 16.1 | 0.0036 | 1.9 | 8.51 |
| 510 | 1.0 | 1.5 | 16.1 | 0.0024 | 1.9 | 8.51 |
| 1480 | 1.0 | 1.5 | 16.1 | 0.0014 | 1.7 | 7.62 |
| 1684 | 1.0 | 1.5 | 16.1 | 0.0014 | 1.7 | 7.62 |
| 1946 | 1.0 | 1.5 | 16.1 | 0.0013 | 1.7 | 7.62 |

Table VIII-32.Hydrometer A5 vertical core at the toe (dispersed)

| T =22$^o$C, K = 0.01374, Ct =0.4 | | | | | | |
|---|---|---|---|---|---|---|
| Time (min) | Reading | Meniscus corrected | L | Diameter, D (mm) | Rc | % Finer |
| 0.25 | 18.0 | 18.5 | 13.3 | 0.1000 | 13.4 | 61.69 |
| 0.75 | 10.5 | 11.0 | 14.5 | 0.0604 | 5.9 | 27.16 |
| 1 | 9.5 | 10.0 | 14.7 | 0.0527 | 4.9 | 22.56 |
| 2 | 9.0 | 9.5 | 14.8 | 0.0373 | 4.4 | 20.25 |
| 4 | 9.0 | 9.5 | 14.8 | 0.0264 | 4.4 | 20.25 |
| 8 | 9.0 | 9.5 | 14.8 | 0.0187 | 4.4 | 20.25 |
| 16 | 8.5 | 9.0 | 14.8 | 0.0132 | 3.9 | 17.95 |
| 32 | 8.0 | 8.5 | 14.9 | 0.0094 | 3.4 | 15.65 |
| 60 | 8.0 | 8.5 | 14.9 | 0.0068 | 3.4 | 15.65 |
| 120 | 8.0 | 8.5 | 14.9 | 0.0048 | 3.4 | 15.65 |
| 240 | 8.0 | 8.5 | 14.9 | 0.0034 | 3.4 | 15.65 |
| 500 | 8.0 | 8.5 | 14.9 | 0.0024 | 3.4 | 15.65 |
| 1470 | 8.0 | 8.5 | 14.9 | 0.0014 | 3.2 | 14.73 |
| 1674 | 8.0 | 8.5 | 14.9 | 0.0013 | 3.2 | 14.73 |
| 1936 | 8.0 | 8.5 | 14.9 | 0.0012 | 3.2 | 14.73 |

Table VIII-33. Hydrometer A5 bulk sample (non-dispersed)

| T =20°C, K = 0.01408, Ct =0 | | | | | | |
|---|---|---|---|---|---|---|
| Time (min) | Reading | Meniscus corrected | L | Diameter, D (mm) | Rc | % Finer |
| 0.25 | 11.0 | 11.5 | 14.4 | 0.1069 | 11.5 | 59.54 |
| 0.5 | 6.0 | 6.5 | 15.3 | 0.0778 | 6.5 | 33.65 |
| 1 | 3.0 | 3.5 | 15.7 | 0.0558 | 3.5 | 18.12 |
| 2 | 2.8 | 3.3 | 15.7 | 0.0394 | 3.3 | 17.09 |
| 4 | 2.7 | 3.2 | 15.8 | 0.0280 | 3.2 | 16.57 |
| 8 | 2.5 | 3.0 | 15.8 | 0.0198 | 3.0 | 15.53 |
| 16 | 2.5 | 3.0 | 15.8 | 0.0140 | 3.0 | 15.53 |
| 32 | 2.2 | 2.7 | 15.8 | 0.0099 | 2.7 | 13.98 |
| 60 | 2.0 | 2.5 | 15.9 | 0.0072 | 2.5 | 12.94 |
| 120 | 2.0 | 2.5 | 15.9 | 0.0051 | 2.5 | 12.94 |
| 248 | 2.0 | 2.5 | 15.9 | 0.0036 | 2.5 | 12.94 |
| 500 | 1.5 | 2.0 | 16.0 | 0.0025 | 2.2 | 11.39 |
| 1452 | 1.5 | 2.0 | 16.0 | 0.0015 | 2.2 | 11.39 |
| 1716 | 1.5 | 2.0 | 16.0 | 0.0013 | 2.2 | 11.39 |
| 1964 | 1.5 | 2.0 | 16.0 | 0.0013 | 2.2 | 11.39 |

Table VIII-34. Hydrometer A5 bulk sample (dispersed)

| T =20°C, K = 0.01408, Ct =0 | | | | | | |
|---|---|---|---|---|---|---|
| Time (min) | Reading | Meniscus corrected | L | Diameter, D (mm) | Rc | % Finer |
| 0.25 | 16.5 | 17.0 | 13.5 | 0.1035 | 11.5 | 52.21 |
| 0.5 | 12.0 | 12.5 | 14.3 | 0.0752 | 7.0 | 31.78 |
| 1 | 9.0 | 9.5 | 14.6 | 0.0538 | 4.0 | 18.16 |
| 2 | 9.0 | 9.5 | 14.6 | 0.0380 | 4.0 | 18.16 |
| 4 | 9.0 | 9.5 | 14.6 | 0.0269 | 4.0 | 18.16 |
| 8 | 9.0 | 9.5 | 14.6 | 0.0190 | 4.0 | 18.16 |
| 16 | 9.0 | 9.5 | 14.6 | 0.0134 | 4.0 | 18.16 |
| 32 | 9.0 | 9.5 | 14.6 | 0.0095 | 4.0 | 18.16 |
| 60 | 8.8 | 9.3 | 14.6 | 0.0069 | 3.8 | 17.25 |
| 120 | 8.5 | 9.0 | 14.9 | 0.0050 | 3.5 | 15.89 |
| 240 | 8.5 | 9.0 | 14.9 | 0.0035 | 3.5 | 15.89 |
| 500 | 8.0 | 8.5 | 14.9 | 0.0024 | 3.2 | 14.53 |
| 1443 | 8.0 | 8.5 | 14.9 | 0.0014 | 3.2 | 14.53 |
| 1707 | 8.0 | 8.5 | 14.9 | 0.0013 | 3.2 | 14.53 |
| 1955 | 8.0 | 8.5 | 14.9 | 0.0012 | 3.2 | 14.53 |

2.4 Flume A13

Table VIII-35. Hydrometer A13 at depth 5 cm (non-dispersed)

| T =22°C, K = 0.01374, Ct =0.4 | | | | | | |
|---|---|---|---|---|---|---|
| Time (min) | Reading | Meniscus corrected | L | Diameter, D (mm) | Rc | % Finer |
| 0.25 | 10.0 | 10.5 | 14.6 | 0.1050 | 10.9 | 58.97 |
| 0.5 | 4.5 | 5.0 | 15.5 | 0.0765 | 5.4 | 29.21 |
| 1 | 1.5 | 2.0 | 16.0 | 0.0550 | 2.4 | 12.98 |
| 2 | 1.5 | 2.0 | 16.0 | 0.0389 | 2.4 | 12.98 |
| 4 | 1.2 | 1.7 | 16.1 | 0.0275 | 2.1 | 11.36 |
| 8 | 1.0 | 1.5 | 16.1 | 0.0195 | 1.9 | 10.28 |
| 16 | 1.0 | 1.5 | 16.1 | 0.0138 | 1.9 | 10.28 |
| 32 | 1.0 | 1.5 | 16.1 | 0.0097 | 1.9 | 10.28 |
| 60 | 0.8 | 1.3 | 16.1 | 0.0071 | 1.7 | 9.20 |
| 128 | 0.8 | 1.3 | 16.1 | 0.0049 | 1.7 | 9.20 |
| 248 | 0.8 | 1.3 | 16.1 | 0.0035 | 1.7 | 9.20 |
| 502 | 0.5 | 1.0 | 16.1 | 0.0025 | 1.4 | 7.57 |
| 1432 | 0.2 | 0.7 | 16.2 | 0.0015 | 1.1 | 5.95 |
| 1876 | 0.2 | 0.7 | 16.2 | 0.0013 | 1.1 | 5.95 |
| 1942 | 0.2 | 0.7 | 16.2 | 0.0013 | 1.1 | 5.95 |

Table VIII-36. Hydrometer A13 at depth 5 cm (dispersed)

| T =22°C, K = 0.01374, Ct =0.4 | | | | | | |
|---|---|---|---|---|---|---|
| Time (min) | Reading | Meniscus corrected | L | Diameter, D (mm) | Rc | % Finer |
| 0.25 | 16.0 | 16.5 | 13.6 | 0.1013 | 11.4 | 50.88 |
| 0.5 | 10.0 | 10.5 | 14.6 | 0.0742 | 5.4 | 24.10 |
| 1 | 8.0 | 8.5 | 14.9 | 0.0530 | 3.4 | 15.17 |
| 2 | 8.0 | 8.5 | 14.9 | 0.0375 | 3.4 | 15.17 |
| 4 | 8.0 | 8.5 | 14.9 | 0.0265 | 3.4 | 15.17 |
| 8 | 8.0 | 8.5 | 14.9 | 0.0188 | 3.4 | 15.17 |
| 16 | 8.0 | 8.5 | 14.9 | 0.0133 | 3.4 | 15.17 |
| 32 | 7.8 | 8.3 | 15.0 | 0.0094 | 3.2 | 14.28 |
| 60 | 7.5 | 8.0 | 15.0 | 0.0069 | 2.9 | 12.94 |
| 120 | 7.5 | 8.0 | 15.0 | 0.0049 | 2.9 | 12.94 |
| 240 | 7.5 | 8.0 | 15.0 | 0.0034 | 2.9 | 12.94 |
| 494 | 7.2 | 7.7 | 15.1 | 0.0024 | 2.6 | 11.60 |
| 1424 | 7.0 | 7.5 | 15.1 | 0.0014 | 2.4 | 10.71 |
| 1868 | 7.0 | 7.5 | 15.1 | 0.0012 | 2.4 | 10.71 |
| 1934 | 7.0 | 7.5 | 15.1 | 0.0012 | 2.4 | 10.71 |

Table VIII-37. Hydrometer A13 at depth 10 cm (non-dispersed)

| T =22°C, K = 0.01374, Ct =0.4 | | | | | | |
|---|---|---|---|---|---|---|
| Time (min) | Reading | Meniscus corrected | L | Diameter, D (mm) | Rc | % Finer |
| 0.25 | 11.5 | 12.0 | 14.3 | 0.1039 | 12.4 | 65.21 |
| 0.5 | 5.0 | 5.5 | 15.4 | 0.0763 | 5.9 | 31.03 |
| 1 | 1.5 | 2.0 | 16.0 | 0.0550 | 2.4 | 12.62 |
| 2 | 1.2 | 1.7 | 16.1 | 0.0389 | 2.1 | 11.04 |
| 4 | 1.0 | 1.5 | 16.1 | 0.0275 | 1.9 | 9.99 |
| 8 | 1.0 | 1.5 | 16.1 | 0.0195 | 1.9 | 9.99 |
| 16 | 1.0 | 1.5 | 16.1 | 0.0138 | 1.9 | 9.99 |
| 32 | 1.0 | 1.5 | 16.1 | 0.0097 | 1.9 | 9.99 |
| 60 | 1.0 | 1.5 | 16.1 | 0.0071 | 1.9 | 9.99 |
| 142 | 0.8 | 1.3 | 16.1 | 0.0046 | 1.7 | 8.94 |
| 248 | 0.8 | 1.3 | 16.1 | 0.0035 | 1.7 | 8.94 |
| 496 | 0.8 | 1.3 | 16.1 | 0.0025 | 1.7 | 8.94 |
| 1444 | 0.5 | 1.0 | 16.1 | 0.0015 | 1.4 | 7.36 |
| 1644 | 0.5 | 1.0 | 16.1 | 0.0014 | 1.4 | 7.36 |
| 1962 | 0.5 | 1.0 | 16.1 | 0.0012 | 1.4 | 7.36 |

Table VIII-38. Hydrometer A13 at depth 10 cm (dispersed)

| T =22°C, K = 0.01374, Ct =0.4 | | | | | | |
|---|---|---|---|---|---|---|
| Time (min) | Reading | Meniscus corrected | L | Diameter, D (mm) | Rc | % Finer |
| 0.25 | 17.5 | 18.0 | 13.3 | 0.1002 | 12.9 | 59.75 |
| 0.5 | 11.0 | 11.5 | 14.4 | 0.0737 | 6.4 | 29.64 |
| 1 | 8.0 | 8.5 | 14.9 | 0.0530 | 3.4 | 15.75 |
| 2 | 7.2 | 7.7 | 15.1 | 0.0378 | 2.6 | 12.04 |
| 4 | 7.2 | 7.7 | 15.1 | 0.0267 | 2.6 | 12.04 |
| 8 | 7.2 | 7.7 | 15.1 | 0.0189 | 2.6 | 12.04 |
| 16 | 7.0 | 7.5 | 15.1 | 0.0133 | 2.4 | 11.12 |
| 32 | 7.0 | 7.5 | 15.1 | 0.0094 | 2.4 | 11.12 |
| 60 | 7.0 | 7.5 | 15.1 | 0.0069 | 2.4 | 11.12 |
| 134 | 6.8 | 7.3 | 15.2 | 0.0046 | 2.2 | 10.19 |
| 240 | 6.8 | 7.3 | 15.2 | 0.0035 | 2.2 | 10.19 |
| 488 | 6.8 | 7.3 | 15.2 | 0.0024 | 2.2 | 10.19 |
| 1436 | 6.5 | 7.0 | 15.2 | 0.0014 | 1.9 | 8.80 |
| 1636 | 6.2 | 6.7 | 15.3 | 0.0013 | 1.6 | 7.41 |
| 1954 | 6.2 | 6.7 | 15.3 | 0.0012 | 1.6 | 7.41 |

Table VIII-39. Hydrometer A13 at depth 20 cm (non-dispersed)

| T =22°C, K = 0.01374, Ct =0.4 | | | | | | |
|---|---|---|---|---|---|---|
| Time (min) | Reading | Meniscus corrected | L | Diameter, D (mm) | Rc | % Finer |
| 0.25 | 11.5 | 12.0 | 14.3 | 0.1039 | 12.4 | 67.24 |
| 0.5 | 5.0 | 5.5 | 15.4 | 0.0763 | 5.9 | 31.99 |
| 1 | 1.5 | 2.0 | 16.0 | 0.0550 | 2.4 | 13.01 |
| 2 | 1.5 | 2.0 | 16.0 | 0.0389 | 2.4 | 13.01 |
| 4 | 1.2 | 1.7 | 16.1 | 0.0275 | 2.1 | 11.39 |
| 8 | 1.0 | 1.5 | 16.1 | 0.0195 | 1.9 | 10.30 |
| 16 | 0.8 | 1.3 | 16.1 | 0.0138 | 1.7 | 9.22 |
| 32 | 0.8 | 1.3 | 16.1 | 0.0097 | 1.7 | 9.22 |
| 60 | 0.8 | 1.3 | 16.1 | 0.0071 | 1.7 | 9.22 |
| 130 | 0.8 | 1.3 | 16.1 | 0.0048 | 1.7 | 9.22 |
| 252 | 0.5 | 1.0 | 16.1 | 0.0035 | 1.4 | 7.59 |
| 480 | 0.5 | 1.0 | 16.1 | 0.0025 | 1.4 | 7.59 |
| 1408 | 0.5 | 1.0 | 16.1 | 0.0015 | 1.4 | 7.59 |
| 1738 | 0.2 | 0.7 | 16.2 | 0.0013 | 1.1 | 5.96 |
| 1938 | 0.2 | 0.7 | 16.2 | 0.0013 | 1.1 | 5.96 |

Table VIII-40. Hydrometer A13 at depth 20 cm (dispersed)

| T =22°C, K = 0.01374, Ct =0.4 | | | | | | |
|---|---|---|---|---|---|---|
| Time (min) | Reading | Meniscus corrected | L | Diameter, D (mm) | Rc | % Finer |
| 0.25 | 18.0 | 18.5 | 13.3 | 0.1000 | 13.4 | 60.45 |
| 0.5 | 12.0 | 12.5 | 14.1 | 0.0730 | 7.4 | 33.38 |
| 1 | 8.0 | 8.5 | 14.9 | 0.0530 | 3.4 | 15.34 |
| 2 | 7.5 | 8.0 | 15.0 | 0.0376 | 2.9 | 13.08 |
| 4 | 7.5 | 8.0 | 15.0 | 0.0266 | 2.9 | 13.08 |
| 8 | 7.5 | 8.0 | 15.0 | 0.0188 | 2.9 | 13.08 |
| 16 | 7.2 | 7.7 | 15.1 | 0.0133 | 2.6 | 11.73 |
| 32 | 7.0 | 7.5 | 15.1 | 0.0094 | 2.4 | 10.83 |
| 60 | 7.0 | 7.5 | 15.1 | 0.0069 | 2.4 | 10.83 |
| 122 | 7.0 | 7.5 | 15.1 | 0.0048 | 2.4 | 10.83 |
| 244 | 7.0 | 7.5 | 15.1 | 0.0034 | 2.4 | 10.83 |
| 480 | 6.8 | 7.3 | 15.2 | 0.0024 | 2.2 | 9.92 |
| 1400 | 6.5 | 7.0 | 15.2 | 0.0014 | 1.9 | 8.57 |
| 1730 | 6.5 | 7.0 | 15.2 | 0.0013 | 1.9 | 8.57 |
| 1930 | 6.5 | 7.0 | 15.2 | 0.0012 | 1.9 | 8.57 |

Table VIII-41. Hydrometer A13 at the toe (non-dispersed)

| T =22oC, K = 0.01374, Ct =0.4 | | | | | | |
|---|---|---|---|---|---|---|
| Time (min) | Reading | Meniscus corrected | L | Diameter, D (mm) | Rc | % Finer |
| 0.25 | 11.0 | 11.5 | 14.4 | 0.1056 | 11.7 | 63.09 |
| 0.5 | 4.5 | 5.0 | 15.5 | 0.0774 | 5.2 | 28.04 |
| 1 | 1.0 | 1.5 | 16.1 | 0.0557 | 1.7 | 9.17 |
| 2 | 0.8 | 1.3 | 16.1 | 0.0394 | 1.5 | 8.09 |
| 4 | 0.8 | 1.3 | 16.1 | 0.0279 | 1.5 | 8.09 |
| 8 | 0.8 | 1.3 | 16.1 | 0.0197 | 1.5 | 8.09 |
| 16 | 0.8 | 1.3 | 16.1 | 0.0139 | 1.5 | 8.09 |
| 32 | 0.8 | 1.3 | 16.1 | 0.0099 | 1.5 | 8.09 |
| 60 | 0.8 | 1.3 | 16.1 | 0.0072 | 1.5 | 8.09 |
| 120 | 0.5 | 1.0 | 16.1 | 0.0050 | 1.4 | 7.55 |
| 244 | 0.5 | 1.0 | 16.1 | 0.0035 | 1.4 | 7.55 |
| 480 | 0.5 | 1.0 | 16.1 | 0.0025 | 1.4 | 7.55 |
| 1475 | 0.3 | 0.8 | 16.1 | 0.0014 | 1.2 | 6.47 |
| 1693 | 0.3 | 0.8 | 16.1 | 0.0013 | 1.2 | 6.47 |
| 1981 | 0.3 | 0.8 | 16.1 | 0.0012 | 1.2 | 6.47 |

Table VIII-42. Hydrometer A13 at the toe (dispersed)

| T =22$^{o}$C, K = 0.01374, Ct =0.4 | | | | | | |
|---|---|---|---|---|---|---|
| Time (min) | Reading | Meniscus corrected | L | Diameter, D (mm) | Rc | % Finer |
| 0.25 | 19.0 | 19.5 | 13.1 | 0.1007 | 14.2 | 65.90 |
| 0.5 | 12.0 | 12.5 | 14.3 | 0.0743 | 7.2 | 33.42 |
| 1 | 7.0 | 7.5 | 15.1 | 0.0541 | 2.2 | 10.21 |
| 2 | 7.0 | 7.5 | 15.1 | 0.0382 | 2.2 | 10.21 |
| 4 | 7.0 | 7.5 | 15.1 | 0.0270 | 2.2 | 10.21 |
| 8 | 7.0 | 7.5 | 15.1 | 0.0191 | 2.2 | 10.21 |
| 16 | 7.0 | 7.5 | 15.1 | 0.0135 | 2.2 | 10.21 |
| 32 | 7.0 | 7.5 | 15.1 | 0.0096 | 2.2 | 10.21 |
| 60 | 7.0 | 7.5 | 15.1 | 0.0070 | 2.2 | 10.21 |
| 120 | 6.8 | 7.3 | 15.1 | 0.0049 | 2.2 | 10.21 |
| 244 | 6.7 | 7.2 | 15.2 | 0.0034 | 2.1 | 9.75 |
| 480 | 6.7 | 7.2 | 15.2 | 0.0024 | 2.1 | 9.75 |
| 1467 | 6.5 | 7.0 | 15.2 | 0.0014 | 1.9 | 8.82 |
| 1685 | 6.5 | 7.0 | 15.2 | 0.0013 | 1.9 | 8.82 |
| 1972 | 6.5 | 7.0 | 15.2 | 0.0012 | 1.9 | 8.82 |

Table VIII-43. Hydrometer A13 at the crest (non-dispersed)

| T =22°C, K = 0.01374, Ct =0.4 | | | | | | |
|---|---|---|---|---|---|---|
| Time (min) | Reading | Meniscus corrected | L | Diameter, D (mm) | Rc | % Finer |
| 0.25 | 10.0 | 10.5 | 14.6 | 0.1050 | 10.9 | 58.60 |
| 0.5 | 2.0 | 2.5 | 15.9 | 0.0775 | 2.9 | 15.59 |
| 1 | 1.0 | 1.5 | 16.1 | 0.0550 | 1.9 | 10.22 |
| 2 | 0.5 | 1.0 | 16.1 | 0.0390 | 1.4 | 7.53 |
| 4 | 0.5 | 1.0 | 16.1 | 0.0276 | 1.4 | 7.53 |
| 8 | 0.5 | 1.0 | 16.1 | 0.0195 | 1.4 | 7.53 |
| 16 | 0.5 | 1.0 | 16.1 | 0.0138 | 1.4 | 7.53 |
| 32 | 0.5 | 1.0 | 16.1 | 0.0097 | 1.4 | 7.53 |
| 60 | 0.5 | 1.0 | 16.1 | 0.0071 | 1.4 | 7.53 |
| 124 | 0.5 | 1.0 | 16.1 | 0.0050 | 1.4 | 7.53 |
| 244 | 0.3 | 0.8 | 16.1 | 0.0035 | 1.2 | 6.45 |
| 480 | 0.3 | 0.8 | 16.1 | 0.0025 | 1.2 | 6.45 |
| 1542 | 0.2 | 0.7 | 16.1 | 0.0014 | 1.1 | 5.91 |
| 1752 | 0.2 | 0.7 | 16.1 | 0.0013 | 1.1 | 5.91 |
| 1990 | 0.2 | 0.7 | 16.1 | 0.0012 | 1.1 | 5.91 |

Table VIII-44. Hydrometer A13 at the crest (dispersed)

| T =22°C, K = 0.01374, Ct =0.4 | | | | | | |
|---|---|---|---|---|---|---|
| Time (min) | Reading | Meniscus corrected | L | Diameter, D (mm) | Rc | % Finer |
| 0.25 | 18.0 | 18.5 | 13.8 | 0.1019 | 13.4 | 62.17 |
| 0.5 | 8.5 | 9.0 | 14.8 | 0.0748 | 3.9 | 18.10 |
| 1 | 7.5 | 8.0 | 15.1 | 0.0534 | 2.9 | 13.46 |
| 2 | 7.0 | 7.5 | 15.1 | 0.0378 | 2.4 | 11.14 |
| 4 | 7.0 | 7.5 | 15.1 | 0.0267 | 2.4 | 11.14 |
| 8 | 7.0 | 7.5 | 15.1 | 0.0189 | 2.4 | 11.14 |
| 16 | 7.0 | 7.5 | 15.1 | 0.0133 | 2.4 | 11.14 |
| 32 | 7.0 | 7.5 | 15.1 | 0.0094 | 2.4 | 11.14 |
| 60 | 7.0 | 7.5 | 15.1 | 0.0069 | 2.4 | 11.14 |
| 120 | 6.8 | 7.3 | 15.1 | 0.0049 | 2.2 | 10.21 |
| 240 | 6.5 | 7.0 | 15.2 | 0.0035 | 1.9 | 8.82 |
| 482 | 6.5 | 7.0 | 15.2 | 0.0024 | 1.9 | 8.82 |
| 1534 | 6.5 | 7.0 | 15.2 | 0.0014 | 1.9 | 8.82 |
| 1744 | 6.2 | 6.7 | 15.2 | 0.0013 | 1.6 | 7.42 |
| 1982 | 6.2 | 6.7 | 15.3 | 0.0012 | 1.6 | 7.42 |

Table VIII-45. Hydrometer A13 bulk sample (non-dispersed)

| T =22°C, K = 0.01374, Ct =0.4 | | | | | | |
|---|---|---|---|---|---|---|
| Time (min) | Reading | Meniscus corrected | L | Diameter, D (mm) | Rc | % Finer |
| 0.25 | 12.0 | 12.5 | 14.1 | 0.1032 | 12.9 | 67.67 |
| 0.5 | 4.5 | 5.0 | 15.5 | 0.0765 | 5.4 | 28.33 |
| 1 | 1.0 | 1.5 | 16.1 | 0.0550 | 1.9 | 9.97 |
| 2 | 0.8 | 1.3 | 16.1 | 0.0389 | 1.7 | 8.92 |
| 4 | 0.7 | 1.2 | 16.1 | 0.0276 | 1.6 | 8.39 |
| 8 | 0.7 | 1.2 | 16.1 | 0.0195 | 1.6 | 8.39 |
| 17.5 | 0.7 | 1.2 | 16.1 | 0.0132 | 1.6 | 8.39 |
| 32 | 0.7 | 1.2 | 16.1 | 0.0097 | 1.6 | 8.39 |
| 60 | 0.7 | 1.2 | 16.1 | 0.0071 | 1.6 | 8.39 |
| 120 | 0.7 | 1.2 | 16.1 | 0.0050 | 1.6 | 8.39 |
| 240 | 0.6 | 1.1 | 16.1 | 0.0036 | 1.5 | 7.87 |
| 480 | 0.5 | 1.0 | 16.1 | 0.0025 | 1.4 | 7.34 |
| 1452 | 0.5 | 1.0 | 16.1 | 0.0014 | 1.4 | 7.34 |
| 1677 | 0.3 | 0.8 | 16.1 | 0.0013 | 1.2 | 6.29 |
| 1942 | 0.3 | 0.8 | 16.1 | 0.0013 | 1.2 | 6.29 |

Table VIII-46. Hydrometer A13 bulk sample (dispersed)

| T =22°C, K = 0.01374, Ct =0.4 | | | | | | |
|---|---|---|---|---|---|---|
| Time (min) | Reading | Meniscus corrected | L | Diameter, D (mm) | Rc | % Finer |
| 0.25 | 20.0 | 20.5 | 13 | 0.0989 | 15.4 | 70.26 |
| 0.5 | 9.0 | 9.5 | 14.8 | 0.0746 | 4.4 | 20.07 |
| 1 | 7.0 | 7.5 | 15.1 | 0.0534 | 2.4 | 10.95 |
| 2 | 7.0 | 7.5 | 15.1 | 0.0378 | 2.4 | 10.95 |
| 4 | 6.9 | 7.5 | 15.1 | 0.0267 | 2.4 | 10.95 |
| 8 | 6.9 | 7.4 | 15.1 | 0.0189 | 2.3 | 10.49 |
| 16 | 6.9 | 7.4 | 15.1 | 0.0133 | 2.3 | 10.49 |
| 32 | 6.9 | 7.4 | 15.1 | 0.0094 | 2.3 | 10.49 |
| 60 | 6.9 | 7.4 | 15.1 | 0.0069 | 2.3 | 10.49 |
| 120 | 6.9 | 7.4 | 15.1 | 0.0049 | 2.3 | 10.49 |
| 240 | 6.8 | 7.3 | 15.2 | 0.0035 | 2.2 | 10.04 |
| 480 | 6.8 | 7.3 | 15.2 | 0.0024 | 2.2 | 10.04 |
| 1444 | 6.8 | 7.3 | 15.2 | 0.0014 | 2.2 | 10.04 |
| 1669 | 6.5 | 7.0 | 15.2 | 0.0013 | 1.9 | 8.67 |
| 1934 | 6.5 | 7.0 | 15.2 | 0.0012 | 1.9 | 8.67 |

Table VIII-47. Hydrometer A13 horizontal core (non-dispersed)

| T =23$^{o}$C, K = 0.01358, Ct =0.7 | | | | | | |
|---|---|---|---|---|---|---|
| Time (min) | Reading | Meniscus corrected | L | Diameter, D (mm) | Rc | % Finer |
| 0.25 | 9.5 | 10.0 | 14.7 | 0.1041 | 10.7 | 59.46 |
| 0.5 | 3.5 | 4.0 | 15.6 | 0.0759 | 4.7 | 26.12 |
| 1 | 1.5 | 2.0 | 16.0 | 0.0543 | 2.7 | 15.00 |
| 2 | 1.0 | 1.5 | 16.1 | 0.0385 | 2.2 | 12.23 |
| 4 | 0.8 | 1.3 | 16.1 | 0.0272 | 2.0 | 11.11 |
| 8 | 0.5 | 1.0 | 16.1 | 0.0193 | 1.7 | 9.45 |
| 16 | 0.5 | 1.0 | 16.1 | 0.0136 | 1.7 | 9.45 |
| 32 | 0.2 | 0.7 | 16.2 | 0.0096 | 1.4 | 7.78 |
| 60 | 0.2 | 0.7 | 16.2 | 0.0070 | 1.4 | 7.78 |
| 138 | 0.2 | 0.7 | 16.2 | 0.0046 | 1.4 | 7.78 |
| 250 | 0.2 | 0.7 | 16.2 | 0.0035 | 1.4 | 7.78 |
| 490 | 0.2 | 0.7 | 16.2 | 0.0025 | 1.4 | 7.78 |
| 1502 | 0.0 | 0.5 | 16.2 | 0.0014 | 1.2 | 6.67 |
| 1722 | 0.0 | 0.5 | 16.2 | 0.0013 | 1.2 | 6.67 |
| 1938 | 0.0 | 0.5 | 16.2 | 0.0012 | 1.2 | 6.67 |

Table VIII-48. Hydrometer A13 horizontal core (dispersed)

| T =23$^{o}$C, K = 0.01358, Ct =0.7 | | | | | | |
|---|---|---|---|---|---|---|
| Time (min) | Reading | Meniscus corrected | L | Diameter, D (mm) | Rc | % Finer |
| 0.25 | 16.5 | 17.0 | 13.5 | 0.0998 | 12.2 | 56.00 |
| 0.5 | 10.5 | 11.0 | 14.5 | 0.0731 | 6.2 | 28.46 |
| 1 | 8.0 | 8.5 | 14.9 | 0.0524 | 3.7 | 16.98 |
| 2 | 8.0 | 8.5 | 14.9 | 0.0371 | 3.7 | 16.98 |
| 4 | 8.0 | 8.5 | 14.9 | 0.0262 | 3.7 | 16.98 |
| 8 | 8.0 | 8.5 | 14.9 | 0.0185 | 3.7 | 16.98 |
| 16 | 8.0 | 8.5 | 14.9 | 0.0131 | 3.7 | 16.98 |
| 32 | 8.0 | 8.5 | 14.9 | 0.0093 | 3.7 | 16.98 |
| 60 | 7.8 | 8.3 | 15.0 | 0.0068 | 3.5 | 16.07 |
| 130 | 7.5 | 8.0 | 15.0 | 0.0046 | 3.2 | 14.69 |
| 240 | 7.5 | 8.0 | 15.0 | 0.0034 | 3.2 | 14.69 |
| 482 | 7.2 | 7.7 | 15.1 | 0.0024 | 2.9 | 13.31 |
| 1496 | 7.2 | 7.7 | 15.1 | 0.0014 | 2.9 | 13.31 |
| 1716 | 7.2 | 7.7 | 15.1 | 0.0013 | 2.9 | 13.31 |
| 1932 | 7.0 | 7.5 | 15.1 | 0.0012 | 2.7 | 12.39 |

## 2.5 Pilot Flume

### 2.5.a Pilot zone 1

Table VIII-49. Hydrometer Pilot zone 1 at depth 5 cm (non-dispersed)

| T =23°C, K = 0.01337, Ct =0.7 | | | | | | |
|---|---|---|---|---|---|---|
| Time (min) | Reading | Meniscus corrected | L | Diameter, D (mm) | Rc | % Finer |
| 0.25 | 11.5 | 12.0 | 14.3 | 0.1011 | 12.7 | 69.02 |
| 0.5 | 6.0 | 6.5 | 15.3 | 0.0738 | 7.2 | 39.13 |
| 1 | 3.2 | 3.7 | 15.7 | 0.0529 | 4.4 | 23.91 |
| 2 | 2.8 | 3.3 | 15.7 | 0.0375 | 4.0 | 21.74 |
| 4 | 2.2 | 2.7 | 15.8 | 0.0266 | 3.4 | 18.48 |
| 8 | 2.0 | 2.5 | 15.9 | 0.0188 | 3.2 | 17.39 |
| 16 | 2.0 | 2.5 | 15.9 | 0.0133 | 3.2 | 17.39 |
| 38 | 2.0 | 2.5 | 15.9 | 0.0086 | 3.2 | 17.39 |
| 60 | 1.8 | 2.3 | 16 | 0.0069 | 3.0 | 16.30 |
| 132 | 1.5 | 2.0 | 16 | 0.0047 | 2.7 | 14.67 |
| 240 | 1.3 | 1.8 | 16 | 0.0035 | 2.5 | 13.59 |
| 502 | 1.2 | 1.7 | 16 | 0.0024 | 2.4 | 13.04 |
| 1642 | 1.2 | 1.7 | 16 | 0.0013 | 2.4 | 13.04 |
| 1900 | 1.0 | 1.5 | 16.1 | 0.0012 | 2.2 | 11.96 |

Table VIII-50. Hydrometer Pilot zone 1 at depth 5 cm (dispersed)

| T =23°C, K = 0.01337, Ct =0.7 | | | | | | |
|---|---|---|---|---|---|---|
| Time (min) | Reading | Meniscus corrected | L | Diameter, D (mm) | Rc | % Finer |
| 0.25 | 20.5 | 21.0 | 12.9 | 0.0960 | 16.2 | 72.28 |
| 0.5 | 12.5 | 13.0 | 14.2 | 0.0713 | 8.2 | 36.59 |
| 1 | 10.2 | 10.7 | 14.6 | 0.0510 | 5.9 | 26.32 |
| 2 | 10.0 | 10.5 | 14.6 | 0.0361 | 5.7 | 25.43 |
| 4 | 9.8 | 10.3 | 14.7 | 0.0256 | 5.5 | 24.54 |
| 8 | 9.5 | 10.0 | 14.7 | 0.0181 | 5.2 | 23.20 |
| 16 | 9.5 | 10.0 | 14.7 | 0.0128 | 5.2 | 23.20 |
| 32 | 9.2 | 9.7 | 14.7 | 0.0091 | 4.9 | 21.86 |
| 60 | 8.8 | 9.3 | 14.8 | 0.0066 | 4.5 | 20.08 |
| 124 | 8.5 | 9.0 | 14.8 | 0.0046 | 4.2 | 18.74 |
| 240 | 8.0 | 8.5 | 14.9 | 0.0033 | 3.7 | 16.51 |
| 492 | 7.8 | 8.3 | 15.0 | 0.0023 | 3.5 | 15.62 |
| 1632 | 7.8 | 8.3 | 15.0 | 0.0013 | 3.5 | 15.62 |
| 1890 | 7.5 | 8.0 | 15.0 | 0.0012 | 3.2 | 14.28 |

Table VIII-51. Hydrometer Pilot zone 1 at depth 10 cm (non-dispersed)

| T =22$^{o}$C, K = 0.01353, Ct =0.4 | | | | | | |
|---|---|---|---|---|---|---|
| Time (min) | Reading | Meniscus corrected | L | Diameter, D (mm) | Rc | % Finer |
| 0.25 | 10.0 | 10.5 | 14.6 | 0.1034 | 10.9 | 58.57 |
| 0.5 | 5.0 | 5.5 | 15.4 | 0.0751 | 5.9 | 31.70 |
| 1 | 3.0 | 3.5 | 15.7 | 0.0536 | 3.9 | 20.96 |
| 2 | 2.5 | 3.0 | 15.8 | 0.0380 | 3.4 | 18.27 |
| 4 | 2.2 | 2.7 | 16.5 | 0.0275 | 3.1 | 16.66 |
| 8 | 1.0 | 1.5 | 16.1 | 0.0192 | 1.9 | 10.21 |
| 16 | 1.0 | 1.5 | 16.1 | 0.0136 | 1.9 | 10.21 |
| 32 | 0.8 | 1.3 | 16.1 | 0.0096 | 1.7 | 9.14 |
| 60 | 0.5 | 1.0 | 16.1 | 0.0070 | 1.4 | 7.52 |
| 120 | 0.5 | 1.0 | 16.1 | 0.0050 | 1.4 | 7.52 |
| 246 | 0.5 | 1.0 | 16.1 | 0.0035 | 1.4 | 7.52 |
| 516 | 0.2 | 0.7 | 16.2 | 0.0024 | 1.1 | 5.91 |
| 1428 | 0.2 | 0.7 | 16.2 | 0.0014 | 1.1 | 5.91 |
| 1750 | 0.0 | 0.5 | 16.2 | 0.0013 | 0.9 | 4.84 |
| 1932 | 0.0 | 0.5 | 16.2 | 0.0012 | 0.9 | 4.84 |

Table VIII-52. Hydrometer Pilot zone 1 at depth 10 cm (dispersed)

| T =22$^{o}$C, K = 0.01353, Ct =0.4 | | | | | | |
|---|---|---|---|---|---|---|
| Time (min) | Reading | Meniscus corrected | L | Diameter, D (mm) | Rc | % Finer |
| 0.25 | 20.0 | 20.5 | 13.0 | 0.0974 | 15.4 | 68.37 |
| 0.5 | 11.0 | 11.5 | 14.4 | 0.0726 | 6.4 | 28.42 |
| 1 | 9.0 | 9.5 | 14.8 | 0.0520 | 4.4 | 19.54 |
| 2 | 8.5 | 9.0 | 14.8 | 0.0368 | 3.9 | 17.32 |
| 4 | 8.2 | 8.7 | 14.9 | 0.0261 | 3.6 | 15.98 |
| 8 | 8.0 | 8.5 | 14.9 | 0.0185 | 3.4 | 15.10 |
| 16 | 7.5 | 8.0 | 15.0 | 0.0131 | 2.9 | 12.88 |
| 32 | 7.2 | 7.7 | 15.1 | 0.0093 | 2.6 | 11.54 |
| 60 | 7.0 | 7.5 | 15.1 | 0.0068 | 2.4 | 10.66 |
| 120 | 7.0 | 7.5 | 15.1 | 0.0048 | 2.4 | 10.66 |
| 240 | 7.0 | 7.5 | 15.1 | 0.0034 | 2.4 | 10.66 |
| 508 | 7.0 | 7.5 | 15.1 | 0.0023 | 2.4 | 10.66 |
| 1420 | 7.0 | 7.5 | 15.1 | 0.0014 | 2.4 | 10.66 |
| 1742 | 7.0 | 7.5 | 15.1 | 0.0013 | 2.4 | 10.66 |
| 1924 | 6.8 | 7.3 | 15.2 | 0.0012 | 2.2 | 9.77 |

Table VIII-53. Hydrometer Pilot zone 1 at depth 15 cm (non-dispersed)

| T =23°C, K = 0.01337, Ct =0.7 | | | | | | |
|---|---|---|---|---|---|---|
| Time (min) | Reading | Meniscus corrected | L | Diameter, D (mm) | Rc | % Finer |
| 0.25 | 10.0 | 10.5 | 14.6 | 0.1022 | 11.2 | 59.55 |
| 0.5 | 4.5 | 5.0 | 15.5 | 0.0744 | 5.7 | 30.31 |
| 1 | 2.5 | 3.0 | 15.8 | 0.0531 | 3.7 | 19.67 |
| 2 | 2.0 | 2.5 | 15.9 | 0.0377 | 3.2 | 17.02 |
| 4 | 1.5 | 2.0 | 16.0 | 0.0267 | 2.7 | 14.36 |
| 8 | 1.0 | 1.5 | 16.1 | 0.0189 | 2.2 | 11.70 |
| 16 | 1.0 | 1.5 | 16.1 | 0.0134 | 2.2 | 11.70 |
| 32 | 1.0 | 1.5 | 16.1 | 0.0095 | 2.2 | 11.70 |
| 60 | 0.8 | 1.3 | 16.1 | 0.0069 | 2.0 | 10.63 |
| 136 | 0.5 | 1.0 | 16.1 | 0.0046 | 1.7 | 9.04 |
| 254 | 0.2 | 0.7 | 16.2 | 0.0034 | 1.4 | 7.44 |
| 532 | 0.2 | 0.7 | 16.2 | 0.0023 | 1.4 | 7.44 |
| 1460 | 0.2 | 0.7 | 16.2 | 0.0014 | 1.4 | 7.44 |
| 1718 | 0.0 | 0.5 | 16.2 | 0.0013 | 1.2 | 6.38 |
| 1966 | 0.0 | 0.5 | 16.2 | 0.0012 | 1.2 | 6.38 |

Table VIII-54.Hydrometer Pilot zone 1 at depth 15 cm (dispersed)

| T =23oC, K = 0.01337, Ct =0.7 | | | | | | |
|---|---|---|---|---|---|---|
| Time (min) | Reading | Meniscus corrected | L | Diameter, D (mm) | Rc | % Finer |
| 0.25 | 18.0 | 18.5 | 13.3 | 0.0973 | 13.7 | 65.48 |
| 0.5 | 10.5 | 11.0 | 14.5 | 0.0720 | 6.2 | 29.63 |
| 1 | 9.0 | 9.5 | 14.8 | 0.0513 | 4.7 | 22.46 |
| 2 | 8.2 | 8.7 | 14.9 | 0.0364 | 3.9 | 18.64 |
| 4 | 8.0 | 8.5 | 14.9 | 0.0258 | 3.7 | 17.68 |
| 8 | 8.0 | 8.5 | 14.9 | 0.0182 | 3.7 | 17.68 |
| 16 | 7.5 | 8.0 | 15 | 0.0129 | 3.2 | 15.29 |
| 32 | 7.2 | 7.7 | 15.1 | 0.0092 | 2.9 | 13.86 |
| 60 | 7.0 | 7.5 | 15.1 | 0.0067 | 2.7 | 12.90 |
| 126 | 7.0 | 7.5 | 15.1 | 0.0046 | 2.7 | 12.90 |
| 244 | 7.0 | 7.5 | 15.1 | 0.0033 | 2.7 | 12.90 |
| 524 | 6.8 | 7.3 | 15.2 | 0.0023 | 2.5 | 11.95 |
| 1452 | 6.5 | 7.0 | 15.2 | 0.0014 | 2.2 | 10.51 |
| 1710 | 6.2 | 6.7 | 15.2 | 0.0013 | 1.9 | 9.08 |
| 1958 | 6.2 | 6.7 | 15.2 | 0.0012 | 1.9 | 9.08 |

Table VIII-55. Hydrometer G1 vertical core (non-dispersed)

| T =23°C, K = 0.01337, Ct =0.7 | | | | | | |
|---|---|---|---|---|---|---|
| Time (min) | Reading | Meniscus corrected | L | Diameter, D (mm) | Rc | % Finer |
| 0.25 | 9.5 | 10.0 | 14.7 | 0.1025 | 10.7 | 56.56 |
| 0.5 | 3.5 | 4.0 | 15.6 | 0.0747 | 4.7 | 24.85 |
| 1 | 1.5 | 2.0 | 16.0 | 0.0535 | 2.7 | 14.27 |
| 2 | 1.0 | 1.5 | 16.1 | 0.0379 | 2.2 | 11.63 |
| 4 | 1.0 | 1.5 | 16.1 | 0.0268 | 2.2 | 11.63 |
| 8 | 0.8 | 1.3 | 16.1 | 0.0190 | 2.0 | 10.57 |
| 16 | 0.8 | 1.3 | 16.1 | 0.0134 | 2.0 | 10.57 |
| 32 | 0.5 | 1.0 | 16.1 | 0.0095 | 1.7 | 8.99 |
| 60 | 0.5 | 1.0 | 16.1 | 0.0069 | 1.7 | 8.99 |
| 134 | 0.5 | 1.0 | 16.1 | 0.0046 | 1.7 | 8.99 |
| 260 | 0.2 | 0.7 | 16.2 | 0.0033 | 1.4 | 7.40 |
| 500 | 0.2 | 0.7 | 16.2 | 0.0024 | 1.4 | 7.40 |
| 1424 | 0.0 | 0.5 | 16.2 | 0.0014 | 1.2 | 6.34 |
| 1666 | 0.0 | 0.5 | 16.2 | 0.0013 | 1.2 | 6.34 |
| 1876 | 0.0 | 0.5 | 16.2 | 0.0012 | 1.2 | 6.34 |

Table VIII-56. Hydrometer G1 vertical core (dispersed)

| T =23°C, K = 0.01337, Ct =0.7 | | | | | | |
|---|---|---|---|---|---|---|
| Time (min) | Reading | Meniscus corrected | L | Diameter, D (mm) | Rc | % Finer |
| 0.25 | 16.5 | 17.0 | 13.5 | 0.0982 | 12.2 | 54.89 |
| 0.5 | 10.0 | 10.5 | 14.6 | 0.0722 | 5.7 | 25.64 |
| 1 | 8.0 | 8.5 | 14.9 | 0.0516 | 3.7 | 16.65 |
| 2 | 7.5 | 8.0 | 15.0 | 0.0366 | 3.2 | 14.40 |
| 4 | 7.5 | 8.0 | 15.0 | 0.0259 | 3.2 | 14.40 |
| 8 | 7.2 | 7.7 | 15.1 | 0.0183 | 2.9 | 13.05 |
| 16 | 7.0 | 7.5 | 15.1 | 0.0130 | 2.7 | 12.15 |
| 32 | 7.0 | 7.5 | 15.1 | 0.0092 | 2.7 | 12.15 |
| 60 | 7.0 | 7.5 | 15.1 | 0.0067 | 2.7 | 12.15 |
| 126 | 6.8 | 7.3 | 15.2 | 0.0046 | 2.5 | 11.25 |
| 252 | 6.5 | 7.0 | 15.2 | 0.0033 | 2.2 | 9.90 |
| 492 | 6.2 | 6.7 | 15.2 | 0.0024 | 1.9 | 8.55 |
| 1416 | 6.2 | 6.7 | 15.2 | 0.0014 | 1.9 | 8.55 |
| 1658 | 6.2 | 6.7 | 15.2 | 0.0013 | 1.9 | 8.55 |
| 1868 | 6.0 | 6.5 | 15.3 | 0.0012 | 1.7 | 7.65 |

Table VIII-57. Hydrometer G1 Horizontal core (non-dispersed)

| T =22°C, K = 0.01353, Ct =0.4 | | | | | | |
|---|---|---|---|---|---|---|
| Time (min) | Reading | Meniscus corrected | L | Diameter, D (mm) | Rc | % Finer |
| 0.25 | 10.0 | 10.5 | 14.6 | 0.1034 | 10.9 | 56.99 |
| 0.5 | 3.0 | 3.5 | 15.7 | 0.0758 | 3.9 | 20.39 |
| 1 | 1.5 | 2.0 | 16.0 | 0.0541 | 2.4 | 12.55 |
| 2 | 1.2 | 1.7 | 16.0 | 0.0383 | 2.1 | 10.98 |
| 4 | 1.0 | 1.5 | 16.1 | 0.0271 | 1.9 | 9.93 |
| 8 | 0.8 | 1.3 | 16.1 | 0.0192 | 1.7 | 8.89 |
| 16 | 0.8 | 1.3 | 16.1 | 0.0136 | 1.7 | 8.89 |
| 32 | 0.8 | 1.3 | 16.1 | 0.0096 | 1.7 | 8.89 |
| 60 | 0.8 | 1.3 | 16.1 | 0.0070 | 1.7 | 8.89 |
| 120 | 0.5 | 1.0 | 16.1 | 0.0050 | 1.4 | 7.32 |
| 258 | 0.2 | 0.7 | 16.2 | 0.0034 | 1.1 | 5.75 |
| 530 | 0.2 | 0.7 | 16.2 | 0.0024 | 1.1 | 5.75 |
| 1444 | 0.0 | 0.5 | 16.2 | 0.0014 | 0.9 | 4.71 |
| 1670 | 0.0 | 0.5 | 16.2 | 0.0013 | 0.9 | 4.71 |
| 1934 | 0.0 | 0.5 | 16.2 | 0.0012 | 0.9 | 4.71 |

Table VIII-58. Hydrometer G1 Horizontal core (dispersed)

| T =22°C, K = 0.01353, Ct =0.4 | | | | | | |
|---|---|---|---|---|---|---|
| Time (min) | Reading | Meniscus corrected | L | Diameter, D (mm) | Rc | % Finer |
| 0.25 | 17.5 | 18.0 | 13.3 | 0.0987 | 12.9 | 56.64 |
| 0.5 | 11.5 | 12.0 | 14.3 | 0.0724 | 6.9 | 30.30 |
| 1 | 9.0 | 9.5 | 14.8 | 0.0520 | 4.4 | 19.32 |
| 2 | 8.5 | 9.0 | 14.8 | 0.0368 | 3.9 | 17.12 |
| 4 | 8.5 | 9.0 | 14.8 | 0.0260 | 3.9 | 17.12 |
| 8 | 8.0 | 8.5 | 14.9 | 0.0185 | 3.4 | 14.93 |
| 16 | 8.0 | 8.5 | 14.9 | 0.0131 | 3.4 | 14.93 |
| 32 | 8.0 | 8.5 | 14.9 | 0.0092 | 3.4 | 14.93 |
| 60 | 7.8 | 8.3 | 15.0 | 0.0068 | 3.2 | 14.05 |
| 120 | 7.8 | 8.3 | 15.0 | 0.0048 | 3.2 | 14.05 |
| 250 | 7.2 | 7.7 | 15.1 | 0.0033 | 2.6 | 11.42 |
| 522 | 7.2 | 7.7 | 15.1 | 0.0023 | 2.6 | 11.42 |
| 1436 | 7.2 | 7.7 | 15.1 | 0.0014 | 2.6 | 11.42 |
| 1662 | 7.0 | 7.5 | 15.1 | 0.0013 | 2.4 | 10.54 |
| 1926 | 7.0 | 7.5 | 15.1 | 0.0012 | 2.4 | 10.54 |

2.5.b Pilot Zone 2

Table VIII-59. Hydrometer Pilot zone 2 at 5 cm depth (non-dispersed)

| T =22°C, K = 0.01353, Ct =0.4 | | | | | | |
|---|---|---|---|---|---|---|
| Time (min) | Reading | Meniscus corrected | L | Diameter, D (mm) | Rc | % Finer |
| 0.25 | 12.0 | 12.5 | 14.3 | 0.1021 | 12.9 | 69.34 |
| 0.5 | 4.0 | 4.5 | 15.6 | 0.0755 | 4.9 | 26.34 |
| 1 | 2.0 | 2.5 | 15.9 | 0.0540 | 2.9 | 15.59 |
| 2 | 1.2 | 1.7 | 16 | 0.0383 | 2.1 | 11.29 |
| 4 | 1.0 | 1.5 | 16.1 | 0.0271 | 1.9 | 10.21 |
| 8 | 1.0 | 1.5 | 16.1 | 0.0192 | 1.9 | 10.21 |
| 16 | 0.8 | 1.3 | 16.1 | 0.0136 | 1.7 | 9.14 |
| 32 | 0.5 | 1.0 | 16.1 | 0.0096 | 1.4 | 7.53 |
| 60 | 0.5 | 1.0 | 16.1 | 0.0070 | 1.4 | 7.53 |
| 120 | 0.2 | 0.7 | 16.2 | 0.0050 | 1.1 | 5.91 |
| 260 | 0.2 | 0.7 | 16.2 | 0.0034 | 1.1 | 5.91 |
| 495 | 0.2 | 0.7 | 16.2 | 0.0024 | 1.1 | 5.91 |
| 1432 | 0.2 | 0.7 | 16.2 | 0.0014 | 1.1 | 5.91 |
| 1684 | 0.0 | 0.5 | 16.2 | 0.0013 | 0.9 | 4.84 |
| 1914 | 0.0 | 0.5 | 16.2 | 0.0012 | 0.9 | 4.84 |

Table VIII-60. Hydrometer Pilot zone 2 at 5 cm depth (dispersed)

| T =22°C, K = 0.01353, Ct =0.4 | | | | | | |
|---|---|---|---|---|---|---|
| Time (min) | Reading | Meniscus corrected | L | Diameter, D (mm) | Rc | % Finer |
| 0.25 | 21.0 | 21.5 | 12.8 | 0.0968 | 16.4 | 74.67 |
| 0.5 | 10.0 | 10.5 | 14.6 | 0.0731 | 5.4 | 24.59 |
| 1 | 7.5 | 8.0 | 15 | 0.0524 | 2.9 | 13.20 |
| 2 | 7.5 | 8.0 | 15 | 0.0371 | 2.9 | 13.20 |
| 4 | 7.2 | 7.7 | 15.1 | 0.0262 | 2.6 | 11.84 |
| 8 | 7.0 | 7.5 | 15.1 | 0.0186 | 2.4 | 10.93 |
| 16 | 7.0 | 7.5 | 15.1 | 0.0131 | 2.4 | 10.93 |
| 32 | 6.8 | 7.3 | 15.2 | 0.0093 | 2.2 | 10.02 |
| 60 | 6.5 | 7.0 | 15.2 | 0.0068 | 1.9 | 8.65 |
| 120 | 6.2 | 6.7 | 15.2 | 0.0048 | 1.6 | 7.28 |
| 252 | 6.2 | 6.7 | 15.2 | 0.0033 | 1.6 | 7.28 |
| 490 | 6.0 | 6.5 | 15.3 | 0.0024 | 1.4 | 6.37 |
| 1424 | 6.0 | 6.5 | 15.3 | 0.0014 | 1.4 | 6.37 |
| 1676 | 6.0 | 6.5 | 15.3 | 0.0013 | 1.4 | 6.37 |
| 1906 | 6.0 | 6.5 | 15.3 | 0.0012 | 1.4 | 6.37 |

Table VIII-61. Hydrometer Pilot zone 2 at 15 cm depth (non-dispersed)

| T =22°C, K = 0.01353, Ct =0.4 | | | | | | |
|---|---|---|---|---|---|---|
| Time (min) | Reading | Meniscus corrected | L | Diameter, D (mm) | Rc | % Finer |
| 0.25 | 11.0 | 11.5 | 14.4 | 0.1027 | 11.9 | 64.03 |
| 0.5 | 3.5 | 4.0 | 15.6 | 0.0756 | 4.4 | 23.68 |
| 1 | 2.5 | 3.0 | 15.8 | 0.0538 | 3.4 | 18.29 |
| 2 | 2.0 | 2.5 | 15.9 | 0.0381 | 2.9 | 15.60 |
| 4 | 1.5 | 2.0 | 16.0 | 0.0271 | 2.4 | 12.91 |
| 8 | 1.5 | 2.0 | 16.0 | 0.0191 | 2.4 | 12.91 |
| 16 | 1.2 | 1.7 | 16.0 | 0.0135 | 2.1 | 11.30 |
| 32 | 1.2 | 1.7 | 16.0 | 0.0096 | 2.1 | 11.30 |
| 60 | 1.0 | 1.5 | 16.1 | 0.0070 | 1.9 | 10.22 |
| 120 | 1.0 | 1.5 | 16.1 | 0.0049 | 1.9 | 10.22 |
| 250 | 0.8 | 1.3 | 16.1 | 0.0034 | 1.7 | 9.15 |
| 488 | 0.8 | 1.3 | 16.1 | 0.0025 | 1.7 | 9.15 |
| 1716 | 0.5 | 1.0 | 16.1 | 0.0013 | 1.4 | 7.53 |
| 1974 | 0.2 | 0.7 | 16.2 | 0.0012 | 1.1 | 5.92 |

Table VIII-62. Hydrometer Pilot zone 2 at 15 cm depth (dispersed)

| T =22°C, K = 0.01353, Ct =0.4 | | | | | | |
|---|---|---|---|---|---|---|
| Time (min) | Reading | Meniscus corrected | L | Diameter, D (mm) | Rc | % Finer |
| 0.25 | 20.5 | 21.0 | 12.9 | 0.0972 | 15.9 | 73.76 |
| 0.5 | 10.0 | 10.5 | 14.6 | 0.0731 | 5.4 | 25.05 |
| 1 | 8.0 | 8.5 | 14.9 | 0.0522 | 3.4 | 15.77 |
| 2 | 7.5 | 8.0 | 15.0 | 0.0371 | 2.9 | 13.45 |
| 4 | 7.5 | 8.0 | 15.0 | 0.0262 | 2.9 | 13.45 |
| 8 | 7.5 | 8.0 | 15.0 | 0.0185 | 2.9 | 13.45 |
| 16 | 7.2 | 7.7 | 15.1 | 0.0131 | 2.6 | 12.06 |
| 32 | 7.2 | 7.7 | 15.1 | 0.0093 | 2.6 | 12.06 |
| 60 | 7.0 | 7.5 | 15.1 | 0.0068 | 2.4 | 11.13 |
| 120 | 7.0 | 7.5 | 15.1 | 0.0048 | 2.4 | 11.13 |
| 240 | 6.8 | 7.3 | 15.2 | 0.0034 | 2.2 | 10.21 |
| 482 | 6.5 | 7.0 | 15.2 | 0.0024 | 1.9 | 8.81 |
| 1708 | 6.5 | 7.0 | 15.2 | 0.0013 | 1.9 | 8.81 |
| 1966 | 6.2 | 6.7 | 15.2 | 0.0012 | 1.6 | 7.42 |

Table VIII-63. Hydrometer Pilot zone 2 at 20 cm depth (non-dispersed)

| T =23°C, K = 0.01337, Ct =0.7 | | | | | | |
|---|---|---|---|---|---|---|
| Time (min) | Reading | Meniscus corrected | L | Diameter, D (mm) | Rc | % Finer |
| 0.25 | 10.0 | 10.5 | 14.6 | 0.1022 | 11.2 | 61.42 |
| 0.5 | 4.0 | 4.5 | 15.6 | 0.0746 | 5.2 | 28.52 |
| 1 | 1.5 | 2.0 | 16.0 | 0.0535 | 2.7 | 14.81 |
| 2 | 1.5 | 2.0 | 16.0 | 0.0378 | 2.7 | 14.81 |
| 4 | 1.2 | 1.7 | 16.0 | 0.0268 | 2.4 | 13.16 |
| 8 | 1.0 | 1.5 | 16.1 | 0.0189 | 2.2 | 12.07 |
| 16 | 1.0 | 1.5 | 16.1 | 0.0134 | 2.2 | 12.07 |
| 32 | 1.0 | 1.5 | 16.1 | 0.0095 | 2.2 | 12.07 |
| 60 | 0.8 | 1.3 | 16.1 | 0.0069 | 2.0 | 10.97 |
| 128 | 0.8 | 1.3 | 16.1 | 0.0047 | 2.0 | 10.97 |
| 248 | 0.8 | 1.3 | 16.1 | 0.0034 | 2.0 | 10.97 |
| 490 | 0.8 | 1.3 | 16.1 | 0.0024 | 2.0 | 10.97 |
| 1425 | 0.5 | 1.0 | 16.1 | 0.0014 | 1.7 | 9.32 |
| 1679 | 0.5 | 1.0 | 16.1 | 0.0013 | 1.7 | 9.32 |
| 1913 | 0.5 | 1.0 | 16.1 | 0.0012 | 1.7 | 9.32 |

Table VIII-64. Hydrometer Pilot zone 2 at 20 cm depth (dispersed)

| T =23°C, K = 0.01337, Ct =0.7 | | | | | | |
|---|---|---|---|---|---|---|
| Time (min) | Reading | Meniscus corrected | L | Diameter, D (mm) | Rc | % Finer |
| 0.25 | 18.0 | 18.5 | 13.3 | 0.0973 | 13.7 | 65.88 |
| 0.5 | 10.5 | 11.0 | 14.5 | 0.0720 | 6.2 | 29.82 |
| 1 | 8.5 | 9.0 | 14.8 | 0.0514 | 4.2 | 20.20 |
| 2 | 8.0 | 8.5 | 14.9 | 0.0365 | 3.7 | 17.79 |
| 4 | 7.8 | 8.3 | 15.0 | 0.0258 | 3.5 | 16.83 |
| 8 | 7.5 | 8.0 | 15.0 | 0.0183 | 3.2 | 15.39 |
| 16 | 7.2 | 7.7 | 15.1 | 0.0130 | 2.9 | 13.95 |
| 32 | 7.0 | 7.5 | 15.1 | 0.0092 | 2.7 | 12.98 |
| 60 | 7.0 | 7.5 | 15.1 | 0.0067 | 2.7 | 12.98 |
| 120 | 7.0 | 7.5 | 15.1 | 0.0047 | 2.7 | 12.98 |
| 240 | 6.8 | 7.3 | 15.2 | 0.0034 | 2.5 | 12.02 |
| 482 | 6.5 | 7.0 | 15.2 | 0.0024 | 2.2 | 10.58 |
| 1417 | 6.5 | 7.0 | 15.2 | 0.0014 | 2.2 | 10.58 |
| 1671 | 6.5 | 7.0 | 15.2 | 0.0013 | 2.2 | 10.58 |
| 1905 | 6.5 | 7.0 | 15.2 | 0.0012 | 2.2 | 10.58 |

Table VIII-65. Hydrometer PI2 vertical core (non-dispersed)

| T =22°C, K = 0.01353, Ct =0.4 | | | | | | |
|---|---|---|---|---|---|---|
| Time (min) | Reading | Meniscus corrected | L | Diameter, D (mm) | Rc | % Finer |
| 0.25 | 10.5 | 11.0 | 14.5 | 0.1030 | 11.4 | 60.20 |
| 0.5 | 4.5 | 5.0 | 15.5 | 0.0753 | 5.4 | 28.52 |
| 1 | 2.5 | 3.0 | 15.8 | 0.0538 | 3.4 | 17.96 |
| 2 | 2.0 | 2.5 | 15.9 | 0.0381 | 2.9 | 15.32 |
| 4 | 1.8 | 2.3 | 16.0 | 0.0270 | 2.7 | 14.26 |
| 8 | 1.0 | 1.5 | 16.1 | 0.0192 | 1.9 | 10.03 |
| 16 | 0.8 | 1.3 | 16.1 | 0.0136 | 1.7 | 8.98 |
| 32 | 0.5 | 1.0 | 16.1 | 0.0096 | 1.4 | 7.39 |
| 60 | 0.5 | 1.0 | 16.1 | 0.0070 | 1.4 | 7.39 |
| 128 | 0.2 | 0.7 | 16.2 | 0.0048 | 1.1 | 5.81 |
| 256 | 0.2 | 0.7 | 16.2 | 0.0034 | 1.1 | 5.81 |
| 512 | 0.2 | 0.7 | 16.2 | 0.0024 | 1.1 | 5.81 |
| 1600 | 0.0 | 0.5 | 16.2 | 0.0014 | 0.9 | 4.75 |
| 1916 | 0.0 | 0.5 | 16.2 | 0.0012 | 0.9 | 4.75 |

Table VIII-66. Hydrometer PI2 vertical core (dispersed)

| T =22°C, K = 0.01353, Ct =0.4 | | | | | | |
|---|---|---|---|---|---|---|
| Time (min) | Reading | Meniscus corrected | L | Diameter, D (mm) | Rc | % Finer |
| 0.25 | 16.0 | 16.5 | 13.6 | 0.0998 | 11.4 | 51.40 |
| 0.5 | 11.0 | 11.5 | 14.4 | 0.0726 | 6.4 | 28.86 |
| 1 | 8.0 | 8.5 | 14.9 | 0.0522 | 3.4 | 15.33 |
| 2 | 8.0 | 8.5 | 14.9 | 0.0369 | 3.4 | 15.33 |
| 4 | 8.0 | 8.5 | 14.9 | 0.0261 | 3.4 | 15.33 |
| 8 | 7.8 | 8.3 | 15.0 | 0.0185 | 3.2 | 14.43 |
| 16 | 7.8 | 8.3 | 15.0 | 0.0131 | 3.2 | 14.43 |
| 32 | 7.5 | 8.0 | 15.0 | 0.0093 | 2.9 | 13.08 |
| 60 | 7.2 | 7.7 | 15.1 | 0.0068 | 2.6 | 11.72 |
| 122 | 7.0 | 7.5 | 15.1 | 0.0048 | 2.4 | 10.82 |
| 248 | 6.8 | 7.3 | 15.2 | 0.0033 | 2.2 | 9.92 |
| 504 | 6.5 | 7.0 | 15.2 | 0.0023 | 1.9 | 8.57 |
| 1592 | 6.5 | 7.0 | 15.2 | 0.0013 | 1.9 | 8.57 |
| 1908 | 6.5 | 7.0 | 15.2 | 0.0012 | 1.9 | 8.57 |

Table VIII-67. Hydrometer I2 horizontal core (non-dispersed)

| T =22$^o$C, K = 0.01353, Ct =0.4 | | | | | | |
|---|---|---|---|---|---|---|
| Time (min) | Reading | Meniscus corrected | L | Diameter, D (mm) | Rc | % Finer |
| 0.25 | 10.5 | 11.0 | 14.5 | 0.1030 | 11.4 | 59.59 |
| 0.5 | 4.0 | 4.5 | 15.6 | 0.0755 | 4.9 | 25.61 |
| 1 | 1.5 | 2.0 | 16.0 | 0.0541 | 2.4 | 12.54 |
| 2 | 1.3 | 1.8 | 16.0 | 0.0383 | 2.2 | 11.50 |
| 4 | 1.2 | 1.7 | 16.0 | 0.0271 | 2.1 | 10.98 |
| 8 | 1.0 | 1.5 | 16.1 | 0.0192 | 1.9 | 9.93 |
| 16 | 1.0 | 1.5 | 16.1 | 0.0136 | 1.9 | 9.93 |
| 32 | 1.0 | 1.5 | 16.1 | 0.0096 | 1.9 | 9.93 |
| 60 | 0.8 | 1.3 | 16.1 | 0.0070 | 1.7 | 8.89 |
| 136 | 0.5 | 1.0 | 16.1 | 0.0047 | 1.4 | 7.32 |
| 248 | 0.2 | 0.7 | 16.2 | 0.0035 | 1.1 | 5.75 |
| 562 | 0.2 | 0.7 | 16.2 | 0.0023 | 1.1 | 5.75 |
| 1472 | 0.2 | 0.7 | 16.2 | 0.0014 | 1.1 | 5.75 |
| 1712 | 0.0 | 0.5 | 16.2 | 0.0013 | 0.9 | 4.70 |
| 1978 | 0.0 | 0.5 | 16.2 | 0.0012 | 0.9 | 4.70 |

Table VIII-68. Hydrometer I2 horizontal core (dispersed)

| T =22$^o$C, K = 0.01353, Ct =0.4 | | | | | | |
|---|---|---|---|---|---|---|
| Time (min) | Reading | Meniscus corrected | L | Diameter, D (mm) | Rc | % Finer |
| 0.25 | 16.5 | 17.0 | 13.5 | 0.0994 | 11.9 | 52.52 |
| 0.5 | 10.5 | 11.0 | 14.5 | 0.0729 | 5.9 | 26.04 |
| 1 | 8.5 | 9.0 | 14.8 | 0.0521 | 3.9 | 17.21 |
| 2 | 8.0 | 8.5 | 14.9 | 0.0369 | 3.4 | 15.01 |
| 4 | 8.0 | 8.5 | 14.9 | 0.0261 | 3.4 | 15.01 |
| 8 | 8.0 | 8.5 | 14.9 | 0.0185 | 3.4 | 15.01 |
| 16 | 8.0 | 8.5 | 14.9 | 0.0131 | 3.4 | 15.01 |
| 32 | 8.0 | 8.5 | 14.9 | 0.0092 | 3.4 | 15.01 |
| 60 | 7.8 | 8.3 | 15.0 | 0.0068 | 3.2 | 14.12 |
| 126 | 7.5 | 8.0 | 15.0 | 0.0047 | 2.9 | 12.80 |
| 240 | 7.2 | 7.7 | 15.1 | 0.0034 | 2.6 | 11.47 |
| 554 | 7.2 | 7.7 | 15.1 | 0.0022 | 2.6 | 11.47 |
| 1464 | 7.0 | 7.5 | 15.1 | 0.0014 | 2.4 | 10.59 |
| 1704 | 7.0 | 7.5 | 15.1 | 0.0013 | 2.4 | 10.59 |
| 1970 | 6.8 | 7.3 | 15.2 | 0.0012 | 2.2 | 9.71 |

2.5.c Pilot Zone 3

Table VIII-69. Hydrometer Pilot zone 3 at depth 10cm (non-dispersed)

| T =22°C, K = 0.01353, Ct =0.4 | | | | | | |
|---|---|---|---|---|---|---|
| Time (min) | Reading | Meniscus corrected | L | Diameter, D (mm) | Rc | % Finer |
| 0.25 | 12.0 | 12.5 | 14.3 | 0.1021 | 12.9 | 66.48 |
| 0.5 | 5.5 | 6.0 | 15.3 | 0.0748 | 6.4 | 32.98 |
| 1 | 2.0 | 2.5 | 15.9 | 0.0540 | 2.9 | 14.95 |
| 2 | 1.5 | 2.0 | 16.0 | 0.0383 | 2.4 | 12.37 |
| 4 | 1.2 | 1.7 | 16.0 | 0.0271 | 2.1 | 10.82 |
| 8 | 1.0 | 1.5 | 16.1 | 0.0192 | 1.9 | 9.79 |
| 16 | 1.0 | 1.5 | 16.1 | 0.0136 | 1.9 | 9.79 |
| 32 | 0.8 | 1.3 | 16.1 | 0.0096 | 1.7 | 8.76 |
| 60 | 0.5 | 1.0 | 16.1 | 0.0070 | 1.4 | 7.22 |
| 120 | 0.5 | 1.0 | 16.1 | 0.0050 | 1.4 | 7.22 |
| 242 | 0.5 | 1.0 | 16.1 | 0.0035 | 1.4 | 7.22 |
| 490 | 0.2 | 0.7 | 16.2 | 0.0025 | 1.1 | 5.67 |
| 1520 | 0.0 | 0.5 | 16.2 | 0.0014 | 0.9 | 4.64 |
| 1730 | 0.0 | 0.5 | 16.2 | 0.0013 | 0.9 | 4.64 |
| 1912 | 0.0 | 0.5 | 16.2 | 0.0012 | 0.9 | 4.64 |

Table VIII-70. Hydrometer Pilot zone 3 at depth 10cm (dispersed)

| T =22°C, K = 0.01353, Ct =0.4 | | | | | | |
|---|---|---|---|---|---|---|
| Time (min) | Reading | Meniscus corrected | L | Diameter, D (mm) | Rc | % Finer |
| 0.25 | 20.0 | 20.5 | 13.0 | 0.0974 | 15.4 | 67.38 |
| 0.5 | 12.0 | 12.5 | 14.3 | 0.0722 | 7.4 | 32.38 |
| 1 | 9.0 | 9.5 | 14.8 | 0.0520 | 4.4 | 19.25 |
| 2 | 8.8 | 9.3 | 14.8 | 0.0368 | 4.2 | 18.38 |
| 4 | 8.5 | 9.0 | 14.8 | 0.0260 | 3.9 | 17.06 |
| 8 | 8.0 | 8.5 | 14.9 | 0.0185 | 3.4 | 14.88 |
| 16 | 8.0 | 8.5 | 14.9 | 0.0131 | 3.4 | 14.88 |
| 32 | 8.0 | 8.5 | 14.9 | 0.0092 | 3.4 | 14.88 |
| 60 | 7.8 | 8.3 | 15.0 | 0.0068 | 3.2 | 14.00 |
| 120 | 7.5 | 8.0 | 15.0 | 0.0048 | 2.9 | 12.69 |
| 240 | 7.2 | 7.7 | 15.1 | 0.0034 | 2.6 | 11.38 |
| 482 | 7.2 | 7.7 | 15.1 | 0.0024 | 2.6 | 11.38 |
| 1512 | 7.0 | 7.5 | 15.1 | 0.0014 | 2.4 | 10.50 |
| 1722 | 7.0 | 7.5 | 15.1 | 0.0013 | 2.4 | 10.50 |
| 1904 | 7.0 | 7.5 | 15.1 | 0.0012 | 2.4 | 10.50 |

Table VIII-71. Hydrometer Pilot zone 3 at depth 16cm (non-dispersed)

| T =23°C, K = 0.01337, Ct =0.7 | | | | | | |
|---|---|---|---|---|---|---|
| Time (min) | Reading | Meniscus corrected | L | Diameter, D (mm) | Rc | % Finer |
| 0.25 | 12.5 | 13.0 | 14.2 | 0.1008 | 13.7 | 72.68 |
| 0.5 | 5.5 | 6.0 | 15.3 | 0.0740 | 6.7 | 35.55 |
| 1 | 2.5 | 3.0 | 15.8 | 0.0531 | 3.7 | 19.63 |
| 2 | 1.8 | 2.3 | 16.0 | 0.0378 | 3.0 | 15.92 |
| 4 | 1.5 | 2.0 | 16.0 | 0.0267 | 2.7 | 14.32 |
| 8 | 1.0 | 1.5 | 16.1 | 0.0189 | 2.2 | 11.67 |
| 16 | 1.0 | 1.5 | 16.1 | 0.0134 | 2.2 | 11.67 |
| 32 | 1.0 | 1.5 | 16.1 | 0.0095 | 2.2 | 11.67 |
| 60 | 0.8 | 1.3 | 16.1 | 0.0069 | 2.0 | 10.61 |
| 120 | 0.8 | 1.3 | 16.1 | 0.0049 | 2.0 | 10.61 |
| 240 | 0.8 | 1.3 | 16.1 | 0.0035 | 2.0 | 10.61 |
| 510 | 0.6 | 1.1 | 16.1 | 0.0024 | 1.8 | 9.55 |
| 1444 | 0.6 | 1.1 | 16.1 | 0.0014 | 1.8 | 9.55 |
| 1690 | 0.6 | 1.1 | 16.1 | 0.0013 | 1.8 | 9.55 |
| 1930 | 0.6 | 1.1 | 16.1 | 0.0012 | 1.8 | 9.55 |

Table VIII-72. Hydrometer Pilot zone 3 at depth 16cm (dispersed)

| T =23°C, K = 0.01337, Ct =0.7 | | | | | | |
|---|---|---|---|---|---|---|
| Time (min) | Reading | Meniscus corrected | L | Diameter, D (mm) | Rc | % Finer |
| 0.25 | 21.0 | 21.5 | 12.8 | 0.0957 | 16.7 | 79.61 |
| 0.5 | 11.5 | 12.0 | 14.3 | 0.0715 | 7.2 | 34.32 |
| 1 | 8.5 | 9.0 | 14.8 | 0.0514 | 4.2 | 20.02 |
| 2 | 8.2 | 8.7 | 14.9 | 0.0364 | 3.9 | 18.59 |
| 4 | 8.0 | 8.5 | 14.9 | 0.0258 | 3.7 | 17.64 |
| 8 | 7.8 | 8.3 | 15.0 | 0.0183 | 3.5 | 16.68 |
| 16 | 7.8 | 8.3 | 15.0 | 0.0129 | 3.5 | 16.68 |
| 32 | 7.5 | 8.0 | 15.0 | 0.0092 | 3.2 | 15.25 |
| 60 | 7.2 | 7.7 | 15.1 | 0.0067 | 2.9 | 13.82 |
| 120 | 7.2 | 7.7 | 15.1 | 0.0047 | 2.9 | 13.82 |
| 244 | 7.0 | 7.5 | 15.1 | 0.0033 | 2.7 | 12.87 |
| 502 | 6.8 | 7.3 | 15.2 | 0.0023 | 2.5 | 11.92 |
| 1436 | 6.5 | 7.0 | 15.2 | 0.0014 | 2.2 | 10.49 |
| 1682 | 6.2 | 6.7 | 15.2 | 0.0013 | 1.9 | 9.06 |
| 1922 | 6.2 | 6.7 | 15.2 | 0.0012 | 1.9 | 9.06 |

Table VIII-73. Hydrometer I3 vertical core (non-dispersed)

| T =23°C, K = 0.01337, Ct =0.7 | | | | | | |
|---|---|---|---|---|---|---|
| Time (min) | Reading | Meniscus corrected | L | Diameter, D (mm) | Rc | % Finer |
| 0.25 | 16.5 | 17.0 | 13.6 | 0.0986 | 17.7 | 94.83 |
| 0.5 | 12.5 | 13.0 | 14.2 | 0.0713 | 13.7 | 73.40 |
| 1 | 2.5 | 3.0 | 15.8 | 0.0531 | 3.7 | 19.82 |
| 2 | 1.0 | 1.5 | 16.1 | 0.0379 | 2.2 | 11.79 |
| 4 | 1.0 | 1.5 | 16.1 | 0.0268 | 2.2 | 11.79 |
| 8 | 1.0 | 1.5 | 16.1 | 0.0189 | 2.2 | 11.79 |
| 16 | 1.0 | 1.5 | 16.1 | 0.0134 | 2.2 | 11.79 |
| 32 | 1.0 | 1.5 | 16.1 | 0.0095 | 2.2 | 11.79 |
| 60 | 1.0 | 1.5 | 16.1 | 0.0069 | 2.2 | 11.79 |
| 138 | 0.8 | 1.3 | 16.1 | 0.0046 | 2.0 | 10.72 |
| 264 | 0.5 | 1.0 | 16.1 | 0.0033 | 1.7 | 9.11 |
| 512 | 0.2 | 0.7 | 16.2 | 0.0024 | 1.4 | 7.50 |
| 1444 | 0.2 | 0.7 | 16.2 | 0.0014 | 1.4 | 7.50 |
| 1698 | 0.0 | 0.5 | 16.2 | 0.0013 | 1.2 | 6.43 |
| 1940 | 0.0 | 0.5 | 16.2 | 0.0012 | 1.2 | 6.43 |

Table VIII-74. Hydrometer I3 vertical core (dispersed)

| T =23°C, K = 0.01337, Ct =0.7 | | | | | | |
|---|---|---|---|---|---|---|
| Time (min) | Reading | Meniscus corrected | L | Diameter, D (mm) | Rc | % Finer |
| 0.25 | 23.0 | 23.5 | 12.5 | 0.0944 | 18.7 | 85.19 |
| 0.3 | 13.5 | 14.0 | 14.0 | 0.0913 | 9.2 | 41.91 |
| 1 | 9.0 | 9.5 | 14.8 | 0.0513 | 4.7 | 21.41 |
| 2 | 8.0 | 8.5 | 14.9 | 0.0365 | 3.7 | 16.86 |
| 4 | 8.0 | 8.5 | 14.9 | 0.0258 | 3.7 | 16.86 |
| 8 | 8.0 | 8.5 | 14.9 | 0.0182 | 3.7 | 16.86 |
| 16 | 8.0 | 8.5 | 14.9 | 0.0129 | 3.7 | 16.86 |
| 32 | 8.0 | 8.5 | 14.9 | 0.0091 | 3.7 | 16.86 |
| 60 | 7.8 | 8.3 | 15.0 | 0.0067 | 3.5 | 15.94 |
| 132 | 7.0 | 7.5 | 15.1 | 0.0045 | 2.7 | 12.30 |
| 254 | 7.0 | 7.5 | 15.1 | 0.0033 | 2.7 | 12.30 |
| 506 | 7.0 | 7.5 | 15.1 | 0.0023 | 2.7 | 12.30 |
| 1438 | 6.8 | 7.3 | 15.2 | 0.0014 | 2.5 | 11.39 |
| 1692 | 6.8 | 7.3 | 15.2 | 0.0013 | 2.5 | 11.39 |
| 1934 | 6.8 | 7.3 | 15.2 | 0.0012 | 2.5 | 11.39 |

2.6 Devon Silt

Table VIII-75. Hydrometer Devon Silt sample (non-dispersed)

| T =23°C, K = 0.01337, Ct =0.7 | | | | | | |
|---|---|---|---|---|---|---|
| Time (min) | Reading | Meniscus corrected | L | Diameter, D (mm) | Rc | % Finer |
| 0.25 | 28.0 | 28.5 | 11.7 | 0.0915 | 29.2 | 100.00 |
| 0.5 | 25.5 | 26.0 | 12 | 0.0655 | 26.7 | 100.00 |
| 1 | 25.0 | 25.5 | 12.1 | 0.0465 | 26.2 | 100.00 |
| 2 | 22.5 | 23.0 | 12.5 | 0.0334 | 23.7 | 100.00 |
| 4 | 19.0 | 19.5 | 13.1 | 0.0242 | 20.2 | 100.00 |
| 8 | 16.0 | 16.5 | 13.6 | 0.0174 | 17.2 | 91.91 |
| 16 | 14.2 | 14.7 | 13.9 | 0.0124 | 15.4 | 82.29 |
| 32 | 12.0 | 12.5 | 14.3 | 0.0089 | 13.2 | 70.54 |
| 62 | 9.8 | 10.3 | 14.7 | 0.0065 | 11.0 | 58.78 |
| 156 | 7.0 | 7.5 | 15.1 | 0.0042 | 8.2 | 43.82 |
| 246 | 5.8 | 6.3 | 15.3 | 0.0033 | 7.0 | 37.41 |
| 524 | 4.8 | 5.3 | 15.5 | 0.0023 | 6.0 | 32.06 |
| 1466 | 3.5 | 4.0 | 15.6 | 0.0014 | 4.7 | 25.11 |
| 1766 | 3.0 | 3.5 | 15.7 | 0.0013 | 4.2 | 22.44 |
| 2042 | 3.0 | 3.5 | 15.7 | 0.0012 | 4.2 | 22.44 |

Table VIII-76. Hydrometer Devon Silt sample dispersed

| T =23°C, K = 0.01337, Ct =0.7 | | | | | | |
|---|---|---|---|---|---|---|
| Time (min) | Reading | Meniscus corrected | L | Diameter, D (mm) | Rc | % Finer |
| 0.25 | 34.0 | 34.5 | 10.7 | 0.0873 | 29.7 | 100.00 |
| 0.5 | 32.0 | 32.5 | 11.0 | 0.0627 | 27.7 | 100.00 |
| 1 | 31.0 | 31.5 | 11.2 | 0.0446 | 26.7 | 100.00 |
| 2 | 29.0 | 29.5 | 11.5 | 0.0320 | 24.7 | 100.00 |
| 4 | 26.5 | 27.0 | 11.9 | 0.0231 | 22.2 | 100.00 |
| 8 | 24.5 | 25.0 | 12.2 | 0.0165 | 20.2 | 94.09 |
| 16 | 22.0 | 22.5 | 12.6 | 0.0119 | 17.7 | 82.45 |
| 32 | 20.2 | 20.7 | 12.9 | 0.0085 | 15.9 | 74.06 |
| 60 | 19.0 | 19.5 | 13.1 | 0.0062 | 14.7 | 68.47 |
| 146 | 17.0 | 17.5 | 13.4 | 0.0041 | 12.7 | 59.16 |
| 240 | 16.0 | 16.5 | 13.6 | 0.0032 | 11.7 | 54.50 |
| 516 | 15.2 | 15.7 | 13.7 | 0.0022 | 10.9 | 50.77 |
| 1458 | 14.8 | 15.3 | 13.8 | 0.0013 | 10.5 | 48.91 |
| 1758 | 14.0 | 14.5 | 13.9 | 0.0012 | 9.7 | 45.18 |
| 2034 | 14.0 | 14.5 | 13.9 | 0.0011 | 9.7 | 45.18 |

2.7 Tailings Beach Sand

Table VIII-77. Hydrometer Beach sand sample (non-dispersed)

| T =23°C, K = 0.01337, Ct =0.7 | | | | | | |
|---|---|---|---|---|---|---|
| Time (min) | Reading | Meniscus corrected | L | Diameter, D (mm) | Rc | % Finer |
| 0.25 | 2.0 | 2.5 | 15.9 | 0.1066 | 3.2 | 17.16 |
| 0.5 | 1.0 | 1.5 | 16.1 | 0.0758 | 2.2 | 11.79 |
| 1 | 1.0 | 1.5 | 16.1 | 0.0536 | 2.2 | 11.79 |
| 2 | 0.8 | 1.3 | 16.1 | 0.0379 | 2.0 | 10.72 |
| 4 | 0.8 | 1.3 | 16.1 | 0.0268 | 2.0 | 10.72 |
| 8 | 0.5 | 1.0 | 16.1 | 0.0190 | 1.7 | 9.11 |
| 16 | 0.5 | 1.0 | 16.1 | 0.0134 | 1.7 | 9.11 |
| 32 | 0.5 | 1.0 | 16.1 | 0.0095 | 1.7 | 9.11 |
| 60 | 0.5 | 1.0 | 16.1 | 0.0069 | 1.7 | 9.11 |
| 120 | 0.2 | 0.7 | 16.2 | 0.0049 | 1.4 | 7.51 |
| 248 | 0.0 | 0.5 | 16.2 | 0.0034 | 1.2 | 6.43 |
| 494 | 0.0 | 0.5 | 16.2 | 0.0024 | 1.2 | 6.43 |
| 1504 | 0.0 | 0.5 | 16.2 | 0.0014 | 1.2 | 6.43 |

Table VIII-78.Hydrometer Beach sand sample (dispersed)

| T =23oC, K = 0.01337, Ct =0.7 | | | | | | |
|---|---|---|---|---|---|---|
| Time (min) | Reading | Meniscus corrected | L | Diameter, D (mm) | Rc | % Finer |
| 0.25 | 9.0 | 9.5 | 14.8 | 0.1027 | 4.7 | 23.04 |
| 0.5 | 8.0 | 8.5 | 14.9 | 0.0730 | 3.7 | 18.14 |
| 1 | 8.0 | 8.5 | 14.9 | 0.0516 | 3.7 | 18.14 |
| 2 | 7.5 | 8.0 | 15.0 | 0.0366 | 3.2 | 15.69 |
| 4 | 7.0 | 7.5 | 15.1 | 0.0260 | 2.7 | 13.24 |
| 8 | 6.0 | 6.5 | 15.3 | 0.0185 | 1.7 | 8.33 |
| 16 | 6.0 | 6.5 | 15.3 | 0.0131 | 1.7 | 8.33 |
| 32 | 6.0 | 6.5 | 15.3 | 0.0092 | 1.7 | 8.33 |
| 60 | 5.8 | 6.3 | 15.3 | 0.0067 | 1.5 | 7.35 |
| 120 | 5.8 | 6.3 | 15.3 | 0.0048 | 1.5 | 7.35 |
| 240 | 5.8 | 6.3 | 15.3 | 0.0034 | 1.5 | 7.35 |
| 484 | 5.8 | 6.3 | 15.3 | 0.0024 | 1.5 | 7.35 |
| 1494 | 5.8 | 6.3 | 15.3 | 0.0014 | 1.5 | 7.35 |

# IX. **APPENDIX C** - WATER RETENTION AND DRYING TESTS

## 1. Soil Water Characteristic Curve (SWCC)

### 1.1. Soil Water Characteristic Curve for Flume deposit A13

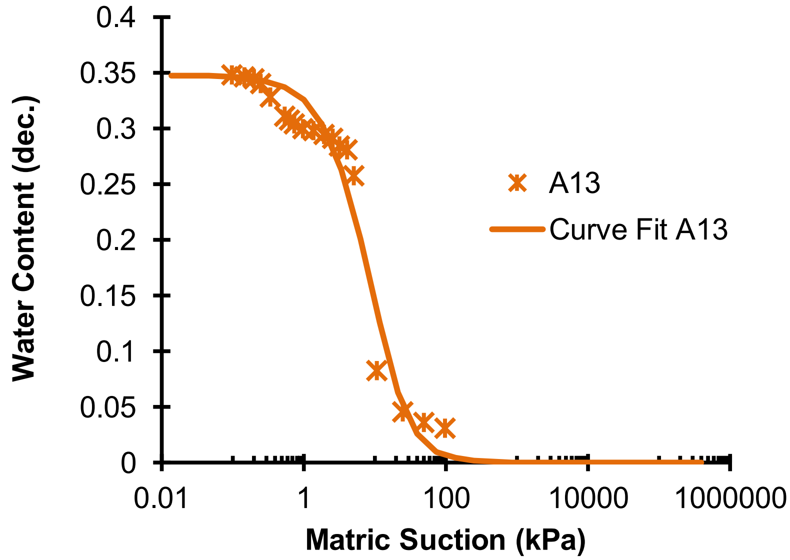


Figure IX-1. Soil water characteristic curve (SWCC) A13 - Soil cover AEV = 12.4 KPa (add residual suction and water content)

### 1.2 Experimental data for the flume deposits

Table IX-1. Change in height of samples upon measurement of the soil water characteristic curve (SWCC)

| Sample ID | A1 | A3 | A5 | A13 | Beach Sand |
|---|---|---|---|---|---|
| **Mass of empty cell (g)** | 1648.5 | 1617.3 | 1655.3 | 1626.3 | 1641.6 |
| **diameter (cm)** | 6.9 | 6.9 | 6.9 | 6.9 | 6.9 |
| **Initial Height (cm)** | 3.0 | 3.7 | 4.2 | 3.8 | 2.8 |
| **initial volume ($cm^3$)** | 112.2 | 138.4 | 157.0 | 142.1 | 104.7 |
| **Final Height (cm)** | 2.5 | 3.2 | 3.8 | 3.2 | 2.6 |
| **Final Volume ($cm^3$)** | 93.5 | 119.7 | 142.1 | 119.7 | 97.2 |

1.2.1 Flume A1 Measurememts

Table IX-2. Soil water characteristic curve (SWCC) measurement for flume deposit A1

| Suction (kPa) | Mass of cell with sample (g) | Gravimetric water content (dec.) | Saturation (%) |
|---|---|---|---|
| 0 | 1898.17 | 0.33 | 100.0 |
| 0.1 | 1898.17 | 0.33 | 100.0 |
| 0.2 | 1898.11 | 0.33 | 99.9 |
| 0.3 | 1897.49 | 0.32 | 98.8 |
| 1 | 1893.49 | 0.30 | 92.0 |
| 1.2 | 1892.50 | 0.30 | 90.3 |
| 1.4 | 1891.64 | 0.29 | 88.8 |
| 2.2 | 1888.62 | 0.27 | 83.7 |
| 2.4 | 1886.95 | 0.27 | 80.8 |
| 2.6 | 1885.00 | 0.25 | 77.5 |
| 3 | 1883.83 | 0.25 | 75.5 |
| 3.4 | 1881.90 | 0.24 | 72.2 |
| 3.8 | 1879.83 | 0.23 | 68.7 |
| 4.2 | 1877.04 | 0.21 | 63.9 |
| 4.6 | 1874.83 | 0.20 | 60.1 |
| 5.6 | 1867.91 | 0.16 | 48.3 |
| 11 | 1855.55 | 0.09 | 27.2 |
| 25 | 1847.15 | 0.04 | 12.8 |
| 50 | 1844.48 | 0.03 | 8.3 |
| 100 | 1843.33 | 0.02 | 6.3 |

### 1.2.2 Flume A3 Measurements

Table IX-3. Soil water characteristic curve (SWCC) measurement for flume deposit A3

| Suction (kPa) | Mass of cell with sample (g) | Gravimetric water content (dec.) | Saturation (%) |
|---|---|---|---|
| 0 | 1934.55 | 0.34 | 100.0 |
| 0.1 | 1934.26 | 0.34 | 99.6 |
| 0.2 | 1934.02 | 0.33 | 99.3 |
| 1 | 1924.01 | 0.29 | 85.0 |
| 1.1 | 1922.89 | 0.28 | 83.4 |
| 1.2 | 1921.71 | 0.28 | 81.7 |
| 1.3 | 1919.00 | 0.26 | 77.8 |
| 1.4 | 1918.79 | 0.26 | 77.5 |
| 2 | 1915.73 | 0.25 | 73.1 |
| 2.2 | 1914.94 | 0.24 | 72.0 |
| 2.4 | 1912.48 | 0.23 | 68.5 |
| 2.6 | 1910.30 | 0.22 | 65.4 |
| 3 | 1905.36 | 0.20 | 58.3 |
| 3.4 | 1901.58 | 0.18 | 52.9 |
| 3.8 | 1891.93 | 0.13 | 39.2 |
| 5.1 | 1886.92 | 0.11 | 32.0 |
| 11 | 1875.96 | 0.06 | 16.4 |
| 25 | 1870.65 | 0.03 | 8.8 |
| 50 | 1868.52 | 0.02 | 5.7 |
| 100 | 1866.26 | 0.01 | 2.5 |

1.2.3 Flume A5 Measurement

Table IX-4. Soil water characteristic curve (SWCC) measurement for flume deposit A5

| Suction (kPa) | Mass of cell with sample (g) | Gravimetric water content (dec.) | Saturation (%) |
|---|---|---|---|
| 0 | 1969.84 | 0.34 | 100.0 |
| 0.1 | 1969.84 | 0.34 | 100.0 |
| 0.3 | 1967.23 | 0.33 | 96.8 |
| 0.5 | 1964.49 | 0.32 | 93.3 |
| 0.6 | 1963.66 | 0.31 | 92.3 |
| 0.9 | 1959.64 | 0.29 | 87.3 |
| 1 | 1958.30 | 0.29 | 85.6 |
| 1.1 | 1957.62 | 0.29 | 84.8 |
| 1.3 | 1957.30 | 0.29 | 84.4 |
| 1.4 | 1956.09 | 0.28 | 82.9 |
| 1.8 | 1954.93 | 0.28 | 81.4 |
| 2.2 | 1953.68 | 0.27 | 79.9 |
| 2.6 | 1952.34 | 0.26 | 78.2 |
| 3 | 1951.40 | 0.26 | 77.0 |
| 3.4 | 1948.22 | 0.25 | 73.1 |
| 5.2 | 1928.22 | 0.16 | 48.2 |
| 11 | 1912.64 | 0.10 | 28.8 |
| 25 | 1907.23 | 0.07 | 22.0 |
| 50 | 1904.26 | 0.06 | 18.3 |
| 100 | 1902.38 | 0.05 | 16.0 |

### 1.2.4 Flume A13 Measurement

Table IX-5. Soil water characteristic curve (SWCC) measurement for flume deposit A13

| Suction (kPa) | Mass of cell with sample (g) | Gravimetric water content (dec.) | Saturation (%) |
|---|---|---|---|
| 0 | 1980.70 | 0.36 | 100.0 |
| 0.1 | 1977.70 | 0.35 | 96.1 |
| 0.15 | 1977.30 | 0.35 | 95.6 |
| 0.2 | 1976.98 | 0.34 | 95.2 |
| 0.25 | 1975.97 | 0.34 | 93.9 |
| 0.35 | 1973.48 | 0.33 | 90.7 |
| 0.55 | 1969.78 | 0.31 | 86.0 |
| 0.65 | 1968.98 | 0.31 | 84.9 |
| 0.75 | 1968.28 | 0.30 | 84.0 |
| 1 | 1967.40 | 0.30 | 82.9 |
| 1.4 | 1966.90 | 0.30 | 82.3 |
| 2 | 1966.29 | 0.29 | 81.5 |
| 2.6 | 1965.57 | 0.29 | 80.6 |
| 3.2 | 1964.09 | 0.28 | 78.7 |
| 4.2 | 1963.18 | 0.28 | 77.5 |
| 5.2 | 1958.18 | 0.26 | 71.1 |
| 11 | 1920.59 | 0.08 | 22.8 |
| 25 | 1912.71 | 0.05 | 12.6 |
| 50 | 1910.63 | 0.04 | 10.0 |
| 100 | 1909.57 | 0.03 | 8.6 |

### 1.2.5 Beach Sand Sample Measurements

Table IX-6. Soil water characteristic curve (SWCC) measurement for the beach sand sample

| Suction (kPa) | Mass of cell with sample (g) | Gravimetric water content (dec.) | Saturation (%) |
|---|---|---|---|
| 0 | 1933.53 | 0.30 | 92.7 |
| 0.1 | 1933.09 | 0.30 | 92.0 |
| 0.3 | 1932.67 | 0.29 | 91.3 |
| 0.4 | 1932.59 | 0.29 | 91.1 |
| 0.5 | 1932.36 | 0.29 | 90.8 |
| 0.6 | 1932.20 | 0.29 | 90.5 |
| 0.85 | 1932.14 | 0.29 | 90.4 |
| 1.75 | 1931.58 | 0.29 | 89.5 |
| 1.95 | 1931.56 | 0.29 | 89.5 |
| 2.15 | 1931.24 | 0.29 | 88.9 |
| 2.85 | 1931.12 | 0.29 | 88.7 |
| 4 | 1916.78 | 0.21 | 65.4 |
| 5.5 | 1894.50 | 0.09 | 29.0 |
| 6.5 | 1890.96 | 0.07 | 23.3 |
| 9 | 1884.93 | 0.04 | 13.4 |
| 12 | 1883.45 | 0.04 | 11.0 |
| 16 | 1882.20 | 0.03 | 9.0 |
| 32 | 1881.15 | 0.02 | 7.3 |
| 60 | 1879.89 | 0.02 | 5.2 |
| 100 | 1879.01 | 0.01 | 3.8 |

2. Drying Tests

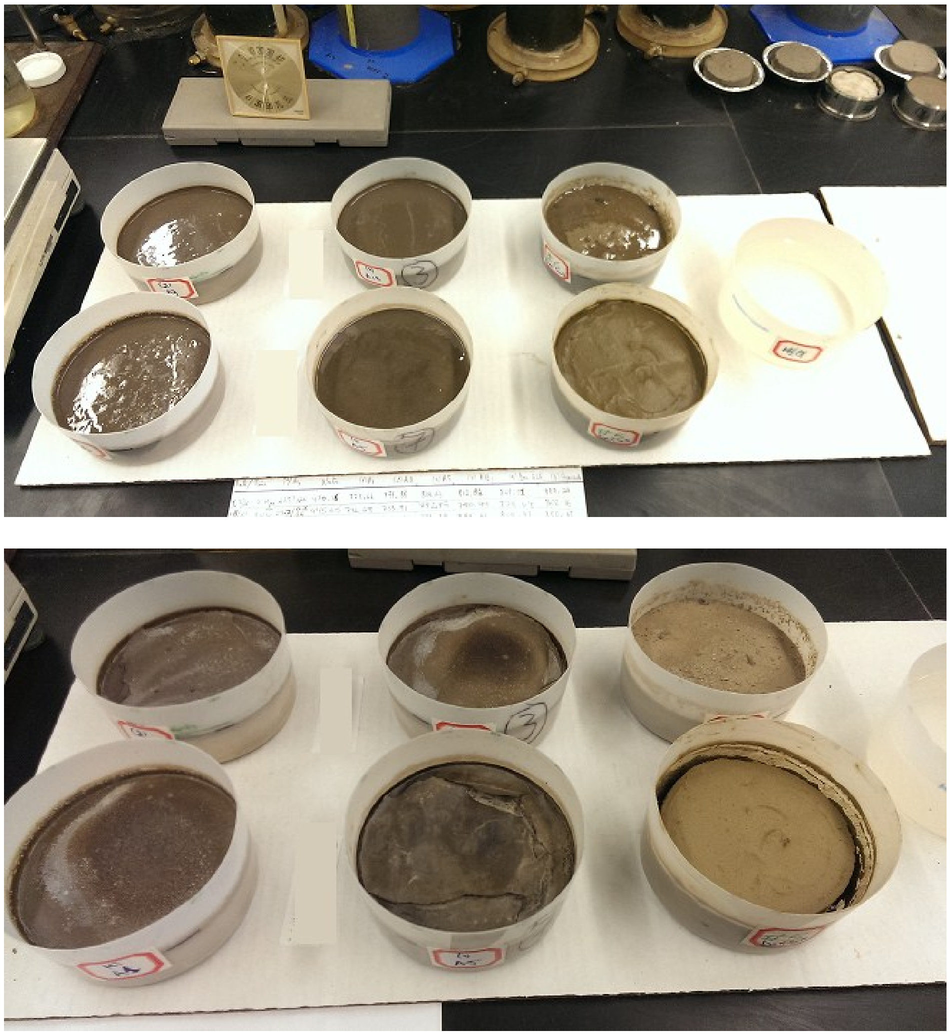

Figure IX-2. Test setup of for the evaporation tests

The change in state of the surface of the lysimeters at the beginning (Top) and at the end of the test (Bottom) can be observed with the appearance of surface cracks and minor evidence of shrinkage from the sides of the samples in Figure IX-2. The temperature (T) and relative humidity (RH) were monitored and recorded during the course of the drying tests.

2.1 Water lysimeter

Table IX-7. Measurement of the potential evaporation during drying tests

| Lysimeter mass (g) | Water lost (g) | Potential Evaporation, PE (mm/d) | T (K) | RH | Time (Days) |
|---|---|---|---|---|---|
| 470.36 | 0.00 | 0.00 | 296.5 | 36 | 0.0 |
| 445.65 | 24.71 | 1.81 | 296.7 | 38 | 0.8 |
| 435.39 | 10.26 | 2.50 | 296.8 | 38 | 1.0 |
| 411.94 | 23.45 | 1.71 | 297 | 40 | 1.8 |
| 403.43 | 8.51 | 1.56 | 296.2 | 40 | 2.1 |
| 385.90 | 17.53 | 1.54 | 296 | 40 | 2.7 |
| 382.14 | 3.76 | 1.46 | 296.2 | 40 | 2.9 |
| 362.47 | 19.67 | 1.41 | 296.2 | 40 | 3.7 |
| 352.77 | 9.70 | 1.76 | 296.6 | 42 | 4.0 |
| 435.63 | 17.19 | 1.64 | 296.6 | 44 | 4.6 |
| 424.51 | 11.12 | 1.74 | 296.9 | 48 | 4.9 |
| 409.00 | 15.51 | 1.37 | 296.2 | 43 | 5.6 |
| 398.94 | 10.06 | 1.58 | 296.6 | 44 | 5.9 |
| 381.40 | 17.54 | 3.04 | 296 | 40 | 6.3 |
| 369.47 | 11.93 | 1.62 | 296.7 | 40 | 6.7 |
| 354.38 | 15.09 | 1.66 | 296.1 | 43 | 7.2 |
| 444.22 | 10.16 | 1.69 | 296.7 | 45 | 7.5 |
| 422.16 | 22.06 | 1.54 | 295.3 | 44 | 8.3 |
| 414.35 | 7.81 | 1.46 | 295.8 | 38 | 8.6 |
| 394.50 | 19.85 | 1.50 | 295.7 | 40 | 9.4 |
| 387.19 | 7.31 | 1.66 | 295.8 | 40 | 9.6 |
| 367.84 | 19.35 | 3.90 | 295.9 | 41 | 9.9 |
| 362.63 | 5.21 | 1.77 | 296.5 | 42 | 10.1 |
| 342.22 | 20.41 | 1.73 | 296.6 | 43 | 10.8 |
| 430.95 | 11.77 | 1.78 | 296.7 | 42 | 11.1 |
| 412.76 | 18.19 | 1.60 | 296.2 | 44 | 11.8 |
| 403.10 | 9.66 | 1.73 | 296.1 | 42 | 12.1 |
| 383.36 | 19.74 | 1.55 | 296.2 | 45 | 12.8 |
| 374.58 | 8.78 | 1.70 | 296.6 | 49 | 13.1 |
| 354.27 | 20.31 | 1.64 | 296.4 | 49 | 13.8 |
| 346.82 | 7.45 | 1.52 | 296.6 | 48 | 14.1 |
| 328.84 | 17.98 | 1.29 | 295.9 | 44 | 14.9 |
| 322.37 | 6.47 | 1.35 | 295.8 | 49 | 15.1 |
| 303.05 | 19.32 | 1.27 | 295.6 | 46 | 16.0 |
| 286.89 | 16.16 | 1.29 | 295.5 | 48 | 16.7 |
| 378.13 | 8.76 | 1.40 | 296.2 | 50 | 17.1 |

2.2 Lysimeter A1

Table IX-8. Measurement of the normalised actual evaporation and void ratio change during evaporation for the flume deposit A1

| Lysimeter mass (g) | Water lost (g) | Water lost by Weight | Void ratio | Actual Evaporation, AE (mm/day) | (AE/PE) |
|---|---|---|---|---|---|
| 770.66 | 0 | 0 | 1.08 | 0 | 0 |
| 746.69 | 23.97 | 0.03 | 1.02 | 1.76 | 0.97 |
| 736.35 | 10.34 | 0.01 | 0.99 | 2.52 | 1.01 |
| 712.32 | 24.03 | 0.03 | 0.92 | 1.76 | 1.02 |
| 703.10 | 9.22 | 0.01 | 0.90 | 1.69 | 1.08 |
| 685.14 | 17.96 | 0.03 | 0.85 | 1.57 | 1.02 |
| 681.14 | 4.00 | 0.01 | 0.84 | 1.55 | 1.06 |
| 660.28 | 20.86 | 0.03 | 0.78 | 1.49 | 1.06 |
| 651.95 | 8.33 | 0.01 | 0.75 | 1.51 | 0.86 |
| 635.41 | 16.54 | 0.03 | 0.71 | 1.58 | 0.96 |
| 625.23 | 10.18 | 0.02 | 0.68 | 1.60 | 0.92 |
| 612.15 | 13.08 | 0.02 | 0.64 | 1.16 | 0.84 |
| 606.40 | 5.75 | 0.01 | 0.63 | 0.90 | 0.57 |
| 598.97 | 7.43 | 0.01 | 0.61 | 1.29 | 0.42 |
| 595.15 | 3.82 | 0.01 | 0.60 | 0.52 | 0.32 |
| 590.77 | 4.38 | 0.01 | 0.59 | 0.48 | 0.29 |
| 588.66 | 2.11 | 0.00 | 0.58 | 0.35 | 0.21 |
| 583.96 | 4.70 | 0.01 | 0.57 | 0.33 | 0.21 |
| 582.63 | 1.33 | 0.00 | 0.56 | 0.25 | 0.17 |
| 579.87 | 2.76 | 0.00 | 0.56 | 0.21 | 0.14 |
| 579.30 | 0.57 | 0.00 | 0.56 | 0.13 | 0.08 |
| 578.53 | 0.77 | 0.00 | 0.55 | 0.16 | 0.04 |
| 578.36 | 0.17 | 0.00 | 0.55 | 0.06 | 0.03 |
| 578.34 | 0.02 | 0.00 | 0.55 | 0.00 | 0.00 |
| 578.33 | 0.01 | 0.00 | 0.55 | 0.00 | 0.00 |
| 578.33 | 0.00 | 0.00 | 0.55 | 0.00 | 0.00 |
| 578.33 | 0.00 | 0.00 | 0.55 | 0.00 | 0.00 |

Table IX-9. Measurement of the change in gravimetric water content during evaporation for the flume deposit A1

| Time (day) | Lysemeter mass (g) | Gravimetric Water Content (%) |
|---|---|---|
| 0 | 770.66 | 35.29 |
| 0.8 | 746.69 | 30.90 |
| 1.0 | 736.35 | 29.00 |
| 1.8 | 712.32 | 24.60 |
| 2.1 | 703.10 | 22.91 |
| 2.7 | 685.14 | 19.62 |
| 2.9 | 681.14 | 18.89 |
| 3.7 | 660.28 | 15.07 |
| 4.0 | 651.95 | 13.54 |
| 4.6 | 635.41 | 10.52 |
| 4.9 | 625.23 | 8.65 |
| 5.6 | 612.15 | 6.25 |
| 5.9 | 606.40 | 5.20 |
| 6.3 | 598.97 | 3.84 |
| 6.7 | 595.15 | 3.14 |
| 7.2 | 590.77 | 2.34 |
| 7.5 | 588.66 | 1.95 |
| 8.3 | 583.96 | 1.09 |
| 8.6 | 582.63 | 0.85 |
| 9.4 | 579.87 | 0.34 |
| 9.6 | 579.30 | 0.24 |
| 9.9 | 578.53 | 0.10 |
| 10.1 | 578.36 | 0.07 |
| 10.8 | 578.34 | 0.06 |
| 11.1 | 578.33 | 0.06 |
| 11.8 | 578.33 | 0.06 |

2.3 Lysimeter A3

Table IX-10. Measurement of the normalised actual evaporation and void ratio change during evaporation for the flume deposit A3

| Lysimeter mass (g) | Water lost (g) | Water lost by Weight | Void ratio | Actual Evaporation, AE (mm/day) | (AE/PE) |
|---|---|---|---|---|---|
| 777.88 | 0 | 0 | 1.08 | 0 | 0 |
| 753.91 | 23.97 | 0.03 | 1.01 | 1.76 | 0.97 |
| 743.13 | 10.78 | 0.01 | 0.98 | 2.63 | 1.05 |
| 718.71 | 24.42 | 0.03 | 0.92 | 1.79 | 1.04 |
| 709.26 | 9.45 | 0.01 | 0.89 | 1.73 | 1.11 |
| 690.69 | 18.57 | 0.03 | 0.84 | 1.63 | 1.06 |
| 686.76 | 3.93 | 0.01 | 0.83 | 1.53 | 1.05 |
| 665.52 | 21.24 | 0.03 | 0.77 | 1.52 | 1.08 |
| 657.07 | 8.45 | 0.01 | 0.75 | 1.53 | 0.87 |
| 640.62 | 16.45 | 0.03 | 0.70 | 1.57 | 0.96 |
| 630.66 | 9.96 | 0.02 | 0.68 | 1.56 | 0.90 |
| 618.72 | 11.94 | 0.02 | 0.64 | 1.06 | 0.77 |
| 612.68 | 6.04 | 0.01 | 0.63 | 0.95 | 0.60 |
| 603.59 | 9.09 | 0.02 | 0.60 | 1.58 | 0.52 |
| 598.67 | 4.92 | 0.01 | 0.59 | 0.67 | 0.41 |
| 592.62 | 6.05 | 0.01 | 0.57 | 0.67 | 0.40 |
| 589.70 | 2.92 | 0.00 | 0.57 | 0.49 | 0.29 |
| 583.85 | 5.85 | 0.01 | 0.55 | 0.41 | 0.27 |
| 582.42 | 1.43 | 0.00 | 0.55 | 0.27 | 0.18 |
| 580.50 | 1.92 | 0.00 | 0.54 | 0.14 | 0.10 |
| 580.36 | 0.14 | 0.00 | 0.54 | 0.03 | 0.02 |
| 580.32 | 0.04 | 0.00 | 0.54 | 0.01 | 0.00 |
| 580.24 | 0.08 | 0.00 | 0.54 | 0.03 | 0.02 |
| 580.24 | 0.00 | 0.00 | 0.54 | 0.00 | 0.00 |
| 580.24 | 0.00 | 0.00 | 0.54 | 0.00 | 0.00 |
| 580.24 | 0.00 | 0.00 | 0.54 | 0.00 | 0.00 |

Table IX-11. Measurement of the change in gravimetric water content during evaporation for the flume deposit A3

| Time (day) | Lysemeter mass (g) | Gravimetric Water Content (%) |
|---|---|---|
| 0 | 777.88 | 36.16 |
| 0.8 | 753.91 | 31.78 |
| 1.0 | 743.13 | 29.81 |
| 1.8 | 718.71 | 25.34 |
| 2.1 | 709.26 | 23.62 |
| 2.7 | 690.69 | 20.22 |
| 2.9 | 686.76 | 19.50 |
| 3.7 | 665.52 | 15.62 |
| 4.0 | 657.07 | 14.07 |
| 4.6 | 640.62 | 11.07 |
| 4.9 | 630.66 | 9.25 |
| 5.6 | 618.72 | 7.06 |
| 5.9 | 612.68 | 5.96 |
| 6.3 | 603.59 | 4.30 |
| 6.7 | 598.67 | 3.40 |
| 7.2 | 592.62 | 2.29 |
| 7.5 | 589.70 | 1.76 |
| 8.3 | 583.85 | 0.69 |
| 8.6 | 582.52 | 0.44 |
| 9.4 | 580.50 | 0.07 |
| 9.6 | 580.36 | 0.05 |
| 9.9 | 580.32 | 0.04 |
| 10.1 | 580.24 | 0.03 |
| 10.8 | 580.24 | 0.03 |
| 10.8 | 580.24 | 0.03 |

2.4 Lysimeter A5

Table IX-12. Measurement of the normalised actual evaporation and void ratio change during evaporation for the flume deposit A5

| Lysimeter mass (g) | Water lost (g) | Water lost by Weight | Void ratio | Actual Evaporation, AE (mm/day) | (AE/PE) |
|---|---|---|---|---|---|
| 804.23 | 0 | 0 | 1.06 | 0 | 0 |
| 782.85 | 21.38 | 0.03 | 1.00 | 1.57 | 0.87 |
| 773.70 | 9.15 | 0.01 | 0.98 | 2.23 | 0.89 |
| 752.17 | 21.53 | 0.03 | 0.92 | 1.57 | 0.92 |
| 743.95 | 8.22 | 0.01 | 0.90 | 1.51 | 0.97 |
| 727.59 | 16.36 | 0.02 | 0.85 | 1.43 | 0.93 |
| 724.06 | 3.53 | 0.00 | 0.85 | 1.37 | 0.94 |
| 705.42 | 18.64 | 0.03 | 0.80 | 1.33 | 0.95 |
| 697.58 | 7.84 | 0.01 | 0.78 | 1.42 | 0.81 |
| 682.47 | 15.11 | 0.02 | 0.74 | 1.44 | 0.88 |
| 672.98 | 9.49 | 0.01 | 0.71 | 1.49 | 0.85 |
| 659.56 | 13.42 | 0.02 | 0.68 | 1.19 | 0.87 |
| 650.78 | 8.78 | 0.01 | 0.66 | 1.38 | 0.87 |
| 636.30 | 14.48 | 0.02 | 0.62 | 2.51 | 0.83 |
| 627.68 | 8.62 | 0.01 | 0.60 | 1.17 | 0.72 |
| 617.74 | 9.94 | 0.02 | 0.57 | 1.10 | 0.66 |
| 612.34 | 5.40 | 0.01 | 0.56 | 0.90 | 0.53 |
| 602.11 | 10.23 | 0.02 | 0.53 | 0.71 | 0.46 |
| 599.34 | 2.77 | 0.00 | 0.52 | 0.52 | 0.35 |
| 594.46 | 4.88 | 0.01 | 0.51 | 0.37 | 0.25 |
| 593.29 | 1.17 | 0.00 | 0.51 | 0.26 | 0.16 |
| 591.05 | 2.24 | 0.00 | 0.50 | 0.45 | 0.12 |
| 590.60 | 0.45 | 0.00 | 0.50 | 0.15 | 0.09 |
| 589.73 | 0.87 | 0.00 | 0.50 | 0.07 | 0.04 |
| 589.58 | 0.15 | 0.00 | 0.50 | 0.02 | 0.01 |
| 589.50 | 0.08 | 0.00 | 0.50 | 0.01 | 0.00 |
| 589.49 | 0.01 | 0.00 | 0.50 | 0.00 | 0.00 |
| 589.44 | 0.05 | 0.00 | 0.50 | 0.00 | 0.00 |
| 589.44 | 0.00 | 0.00 | 0.50 | 0.00 | 0.00 |
| 589.44 | 0.00 | 0.00 | 0.50 | 0.00 | 0.00 |
| 589.44 | 0.00 | 0.00 | 0.50 | 0.00 | 0.00 |

Table IX-13. Measurement of the change in gravimetric water content during evaporation for the flume deposit A5

| Time (day) | Lysemeter mass (g) | Gravimetric Water Content (%) |
|---|---|---|
| 0.0 | 804.23 | 38.71 |
| 0.8 | 782.85 | 34.86 |
| 1.0 | 773.70 | 33.22 |
| 1.8 | 752.17 | 29.34 |
| 2.1 | 743.95 | 27.87 |
| 2.7 | 727.59 | 24.92 |
| 2.9 | 724.06 | 24.29 |
| 3.7 | 705.42 | 20.94 |
| 4.0 | 697.58 | 19.53 |
| 4.6 | 682.47 | 16.81 |
| 4.9 | 672.98 | 15.10 |
| 5.6 | 659.56 | 12.69 |
| 5.9 | 650.78 | 11.11 |
| 6.3 | 636.30 | 8.50 |
| 6.7 | 627.68 | 6.95 |
| 7.2 | 617.74 | 5.17 |
| 7.5 | 612.34 | 4.20 |
| 8.3 | 602.11 | 2.36 |
| 8.6 | 599.34 | 1.86 |
| 9.4 | 594.46 | 0.98 |
| 9.6 | 593.29 | 0.77 |
| 9.9 | 591.05 | 0.37 |
| 10.1 | 590.60 | 0.29 |
| 10.8 | 589.73 | 0.13 |
| 11.1 | 589.58 | 0.10 |
| 11.8 | 589.50 | 0.09 |
| 12.1 | 589.49 | 0.09 |
| 12.8 | 589.44 | 0.08 |
| 13.1 | 589.44 | 0.08 |

2.5 Lysimeter A13

Table IX-14. Measurement of the normalised actual evaporation and void ratio change during evaporation for the flume deposit A13

| Lysimeter mass (g) | Water lost (g) | Water lost by Weight | Void ratio | Actual Evaporation, AE (mm/day) | (AE/PE) |
|---|---|---|---|---|---|
| 812.88 | 0 | 0 | 1.10 | 0 | 0 |
| 790.99 | 21.89 | 0.03 | 1.04 | 1.61 | 0.89 |
| 779.61 | 11.38 | 0.01 | 1.01 | 2.77 | 1.11 |
| 756.42 | 23.19 | 0.03 | 0.95 | 1.70 | 0.99 |
| 747.63 | 8.79 | 0.01 | 0.92 | 1.61 | 1.03 |
| 730.42 | 17.21 | 0.02 | 0.88 | 1.51 | 0.98 |
| 726.63 | 3.79 | 0.01 | 0.87 | 1.47 | 1.01 |
| 706.77 | 19.86 | 0.03 | 0.82 | 1.42 | 1.01 |
| 698.59 | 8.18 | 0.01 | 0.80 | 1.48 | 0.84 |
| 682.68 | 15.91 | 0.02 | 0.75 | 1.52 | 0.93 |
| 672.76 | 9.92 | 0.01 | 0.73 | 1.55 | 0.89 |
| 658.45 | 14.31 | 0.02 | 0.69 | 1.27 | 0.92 |
| 649.40 | 9.05 | 0.01 | 0.67 | 1.42 | 0.90 |
| 635.52 | 13.88 | 0.02 | 0.63 | 2.41 | 0.79 |
| 629.66 | 5.86 | 0.01 | 0.62 | 0.80 | 0.49 |
| 623.39 | 6.27 | 0.01 | 0.60 | 0.69 | 0.42 |
| 620.13 | 3.26 | 0.01 | 0.59 | 0.54 | 0.32 |
| 613.32 | 6.81 | 0.01 | 0.57 | 0.47 | 0.31 |
| 611.25 | 2.07 | 0.00 | 0.57 | 0.39 | 0.27 |
| 606.70 | 4.55 | 0.01 | 0.56 | 0.34 | 0.23 |
| 605.38 | 1.32 | 0.00 | 0.55 | 0.30 | 0.18 |
| 602.52 | 2.86 | 0.00 | 0.55 | 0.58 | 0.15 |
| 601.90 | 0.62 | 0.00 | 0.54 | 0.21 | 0.12 |
| 600.85 | 1.05 | 0.00 | 0.54 | 0.09 | 0.05 |
| 600.58 | 0.27 | 0.00 | 0.54 | 0.04 | 0.02 |
| 600.58 | 0.00 | 0.00 | 0.54 | 0.00 | 0.00 |
| 600.58 | 0.00 | 0.00 | 0.54 | 0.00 | 0.00 |
| 600.58 | 0.00 | 0.00 | 0.54 | 0.00 | 0.00 |

Table IX-15. Measurement of the change in gravimetric water content during evaporation for the flume deposit A13

| Time (day) | Lysemeter mass (g) | Gravimetric Water Content (%) |
|---|---|---|
| 0.0 | 812.88 | 37.43 |
| 0.8 | 790.99 | 33.58 |
| 1.0 | 779.61 | 31.58 |
| 1.8 | 756.42 | 27.49 |
| 2.1 | 747.63 | 25.94 |
| 2.7 | 730.42 | 22.91 |
| 2.9 | 726.63 | 22.25 |
| 3.7 | 706.77 | 18.75 |
| 4.0 | 698.59 | 17.31 |
| 4.6 | 682.68 | 14.51 |
| 4.9 | 672.76 | 12.76 |
| 5.6 | 658.45 | 10.24 |
| 5.9 | 649.40 | 8.65 |
| 6.3 | 635.52 | 6.20 |
| 6.7 | 629.66 | 5.17 |
| 7.2 | 623.39 | 4.07 |
| 7.5 | 620.13 | 3.49 |
| 8.3 | 613.32 | 2.29 |
| 8.6 | 611.25 | 1.93 |
| 9.4 | 606.70 | 1.13 |
| 9.6 | 605.38 | 0.90 |
| 9.9 | 602.52 | 0.39 |
| 10.1 | 601.90 | 0.28 |
| 10.8 | 600.85 | 0.10 |
| 11.1 | 600.58 | 0.05 |
| 11.8 | 600.58 | 0.05 |

2.6 Devon Silt lysimeter

Table IX-16. Measurement of the normalised actual evaporation and void ratio change during evaporation for the Devon silt sample

| Lysimeter mass (g) | Water lost (g) | Water lost by Weight | Void ratio | Actual Evaporation, AE (mm/day) | (AE/PE) |
|---|---|---|---|---|---|
| 849.01 | 0 | 0 | 1.18 | 0 | 0 |
| 825.64 | 23.37 | 0.03 | 1.12 | 1.72 | 0.95 |
| 815.43 | 10.21 | 0.01 | 1.09 | 2.49 | 1.00 |
| 792.55 | 22.88 | 0.03 | 1.03 | 1.67 | 0.98 |
| 784.07 | 8.48 | 0.01 | 1.01 | 1.55 | 1.00 |
| 767.59 | 16.48 | 0.02 | 0.97 | 1.44 | 0.94 |
| 764.04 | 3.55 | 0.00 | 0.96 | 1.38 | 0.94 |
| 745.63 | 18.41 | 0.02 | 0.91 | 1.32 | 0.94 |
| 737.80 | 7.83 | 0.01 | 0.89 | 1.42 | 0.81 |
| 722.39 | 15.41 | 0.02 | 0.85 | 1.47 | 0.90 |
| 713.10 | 9.29 | 0.01 | 0.83 | 1.46 | 0.84 |
| 700.01 | 13.09 | 0.02 | 0.79 | 1.16 | 0.84 |
| 691.32 | 8.69 | 0.01 | 0.77 | 1.36 | 0.86 |
| 676.86 | 14.46 | 0.02 | 0.73 | 2.51 | 0.82 |
| 667.03 | 9.83 | 0.01 | 0.71 | 1.34 | 0.82 |
| 655.81 | 11.22 | 0.02 | 0.68 | 1.24 | 0.74 |
| 649.80 | 6.01 | 0.01 | 0.66 | 1.00 | 0.59 |
| 638.65 | 11.15 | 0.02 | 0.63 | 0.78 | 0.51 |
| 635.41 | 3.24 | 0.01 | 0.62 | 0.61 | 0.41 |
| 628.43 | 6.98 | 0.01 | 0.61 | 0.53 | 0.35 |
| 626.38 | 2.05 | 0.00 | 0.60 | 0.46 | 0.28 |
| 621.45 | 4.93 | 0.01 | 0.59 | 0.99 | 0.25 |
| 620.31 | 1.14 | 0.00 | 0.59 | 0.39 | 0.22 |
| 616.66 | 3.65 | 0.01 | 0.58 | 0.31 | 0.18 |
| 615.05 | 1.61 | 0.00 | 0.57 | 0.24 | 0.14 |
| 612.84 | 2.21 | 0.00 | 0.57 | 0.19 | 0.12 |
| 612.08 | 0.76 | 0.00 | 0.56 | 0.14 | 0.08 |
| 610.05 | 2.03 | 0.00 | 0.56 | 0.16 | 0.10 |
| 609.51 | 0.54 | 0.00 | 0.56 | 0.10 | 0.06 |
| 608.31 | 1.20 | 0.00 | 0.55 | 0.10 | 0.06 |
| 607.93 | 0.38 | 0.00 | 0.55 | 0.08 | 0.05 |
| 607.22 | 0.71 | 0.00 | 0.55 | 0.05 | 0.04 |
| 607.11 | 0.11 | 0.00 | 0.55 | 0.02 | 0.02 |
| 606.33 | 0.78 | 0.00 | 0.55 | 0.05 | 0.04 |
| 605.73 | 0.60 | 0.00 | 0.55 | 0.05 | 0.04 |
| 605.69 | 0.04 | 0.00 | 0.55 | 0.01 | 0.00 |

Table IX-17. Measurement of the change in gravimetric water content during evaporation for the Devon silt sample

| Time (day) | Lysemeter mass (g) | Gravimetric Water Content (%) |
|---|---|---|
| 0 | 849.01 | 58.14 |
| 0.8 | 825.64 | 52.57 |
| 1.0 | 815.43 | 50.13 |
| 1.8 | 792.55 | 44.67 |
| 2.1 | 784.07 | 42.65 |
| 2.7 | 767.59 | 38.71 |
| 2.9 | 764.04 | 37.86 |
| 3.7 | 745.63 | 33.47 |
| 4.0 | 737.80 | 31.60 |
| 4.6 | 722.39 | 27.92 |
| 4.9 | 713.10 | 25.71 |
| 5.6 | 700.01 | 22.58 |
| 5.9 | 691.32 | 20.51 |
| 6.3 | 676.86 | 17.06 |
| 6.7 | 667.03 | 14.71 |
| 7.2 | 655.81 | 12.03 |
| 7.5 | 649.80 | 10.60 |
| 8.3 | 638.65 | 7.94 |
| 8.6 | 635.41 | 7.16 |
| 9.4 | 628.43 | 5.50 |
| 9.6 | 626.38 | 5.01 |
| 9.9 | 621.45 | 3.83 |
| 10.1 | 620.31 | 3.56 |
| 10.8 | 616.66 | 2.69 |
| 11.1 | 615.05 | 2.30 |
| 11.8 | 612.84 | 1.78 |
| 12.1 | 612.08 | 1.59 |
| 12.8 | 610.05 | 1.11 |
| 13.1 | 609.51 | 0.98 |
| 13.8 | 608.31 | 0.69 |
| 14.1 | 607.93 | 0.60 |
| 14.9 | 607.22 | 0.43 |
| 15.1 | 607.11 | 0.41 |
| 16.0 | 606.33 | 0.22 |
| 16.7 | 605.73 | 0.08 |
| 17.1 | 605.69 | 0.07 |

2.7 Beach Sand Lysimeter

Table IX-18. Measurement of the normalised actual evaporation and void ratio change during evaporation for the Beach sand sample

| Lysimeter mass (g) | Water lost (g) | Water lost by Weight | Void ratio | Actual Evaporation, AE (mm/day) | (AE/PE) |
|---|---|---|---|---|---|
| (g) | g | | | mm/d | |
| 887.22 | 0.00 | 0.00 | 0.86 | 0.00 | 0.00 |
| 862.16 | 25.06 | 0.03 | 0.80 | 1.84 | 1.01 |
| 850.65 | 11.51 | 0.01 | 0.78 | 2.80 | 1.12 |
| 826.24 | 24.41 | 0.03 | 0.73 | 1.79 | 1.04 |
| 817.72 | 8.52 | 0.01 | 0.71 | 1.56 | 1.00 |
| 800.97 | 16.75 | 0.02 | 0.67 | 1.47 | 0.96 |
| 797.33 | 3.64 | 0.00 | 0.67 | 1.41 | 0.97 |
| 778.02 | 19.31 | 0.02 | 0.62 | 1.38 | 0.98 |
| 769.79 | 8.23 | 0.01 | 0.61 | 1.49 | 0.85 |
| 753.63 | 16.16 | 0.02 | 0.57 | 1.54 | 0.94 |
| 743.49 | 10.14 | 0.01 | 0.55 | 1.59 | 0.91 |
| 729.18 | 14.31 | 0.02 | 0.52 | 1.27 | 0.92 |
| 719.69 | 9.49 | 0.01 | 0.50 | 1.49 | 0.94 |
| 703.57 | 16.12 | 0.02 | 0.47 | 2.80 | 0.92 |
| 692.49 | 11.08 | 0.02 | 0.44 | 1.51 | 0.93 |
| 684.83 | 7.66 | 0.01 | 0.43 | 0.84 | 0.51 |
| 682.42 | 2.41 | 0.00 | 0.42 | 0.40 | 0.24 |
| 678.14 | 4.28 | 0.01 | 0.41 | 0.30 | 0.19 |
| 677.12 | 1.02 | 0.00 | 0.41 | 0.19 | 0.13 |
| 676.30 | 0.82 | 0.00 | 0.41 | 0.06 | 0.04 |
| 676.30 | 0.00 | 0.00 | 0.41 | 0.00 | 0.00 |
| 676.30 | 0.00 | 0.00 | 0.41 | 0.00 | 0.00 |
| 676.30 | 0.00 | 0.00 | 0.41 | 0.00 | 0.00 |

Table IX-19. Measurement of the change in gravimetric water content during evaporation for the Beach sand sample

| Time (day) | Lysemeter mass (g) | Gravimetric Water Content (%) |
|---|---|---|
| 0 | 887.22 | 32.82 |
| 0.8 | 862.16 | 28.93 |
| 1.0 | 850.65 | 27.14 |
| 1.8 | 826.24 | 23.34 |
| 2.1 | 817.72 | 22.02 |
| 2.7 | 800.97 | 19.41 |
| 2.9 | 797.33 | 18.84 |
| 3.7 | 778.02 | 15.84 |
| 4.0 | 769.79 | 14.56 |
| 4.6 | 753.63 | 12.05 |
| 4.9 | 743.49 | 10.47 |
| 5.6 | 729.18 | 8.25 |
| 5.9 | 719.69 | 6.77 |
| 6.3 | 703.57 | 4.26 |
| 6.7 | 692.49 | 2.54 |
| 7.2 | 684.83 | 1.35 |
| 7.5 | 682.42 | 0.97 |
| 8.3 | 678.14 | 0.31 |
| 8.6 | 677.12 | 0.15 |
| 9.4 | 676.30 | 0.02 |
| 9.6 | 676.30 | 0.02 |
| 9.9 | 676.30 | 0.02 |
| 10.1 | 676.30 | 0.02 |
| 10.8 | 676.30 | 0.02 |

# X. **APPENDIX D** - DIRECT SHEAR

## 1. Direct Shear Failure Envelopes

Table X-1. Peak and residual shear stresses of the samples tested

| Sample ID | Normal Stress (kPa) | Peak Shear Stress (kPa) | Residual Stress (kPa) |
|---|---|---|---|
| A1 | 10 | 11.2 | 9.2 |
| | 25 | 25.4 | 22.1 |
| | 35 | 32.3 | 28.0 |
| | 50 | 41.8 | 31.7 |
| A3 | 10 | 12.7 | 10.0 |
| | 25 | 24.6 | 20.2 |
| | 35 | 30.2 | 27.3 |
| | 50 | 41.8 | 33.1 |
| A5 | 10 | 11.8 | 10.3 |
| | 25 | 24.9 | 17.4 |
| | 35 | 33.3 | 24.8 |
| | 50 | 42.5 | 36.9 |
| A13 | 10 | 12.6 | 10.6 |
| | 25 | 31.0 | 17.5 |
| | 35 | 32.6 | 23.6 |
| Beach Sand | 10 | 8.3 | 8.0 |
| | 25 | 24.0 | 23.0 |
| | 35 | 30.0 | 29.0 |
| | 50 | 39.0 | 38.0 |
| | 75 | 69.0 | 56.0 |

2. Direct Shear Test Data

2.1 Flume Deposit A1 Test Data

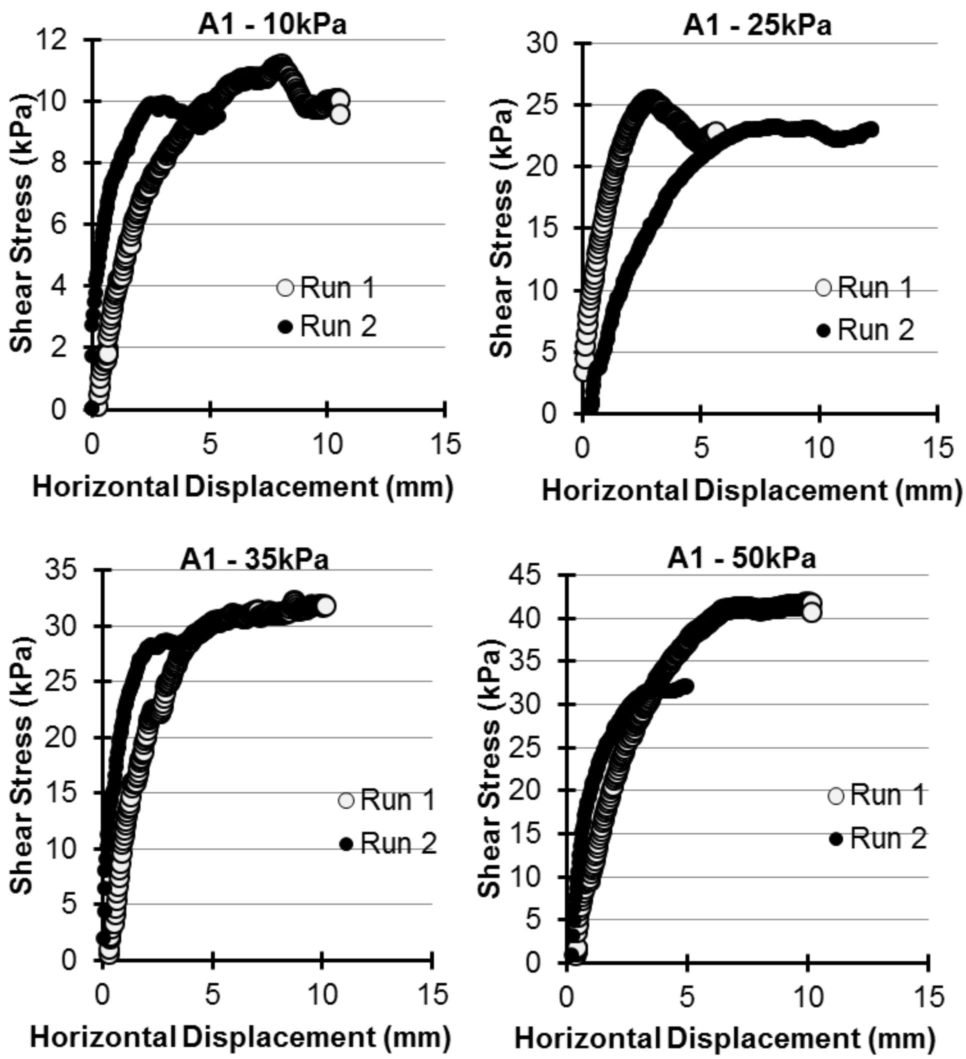


Figure X-1. Variations in Peak and residual shear stresses with horizontal displacement for A1

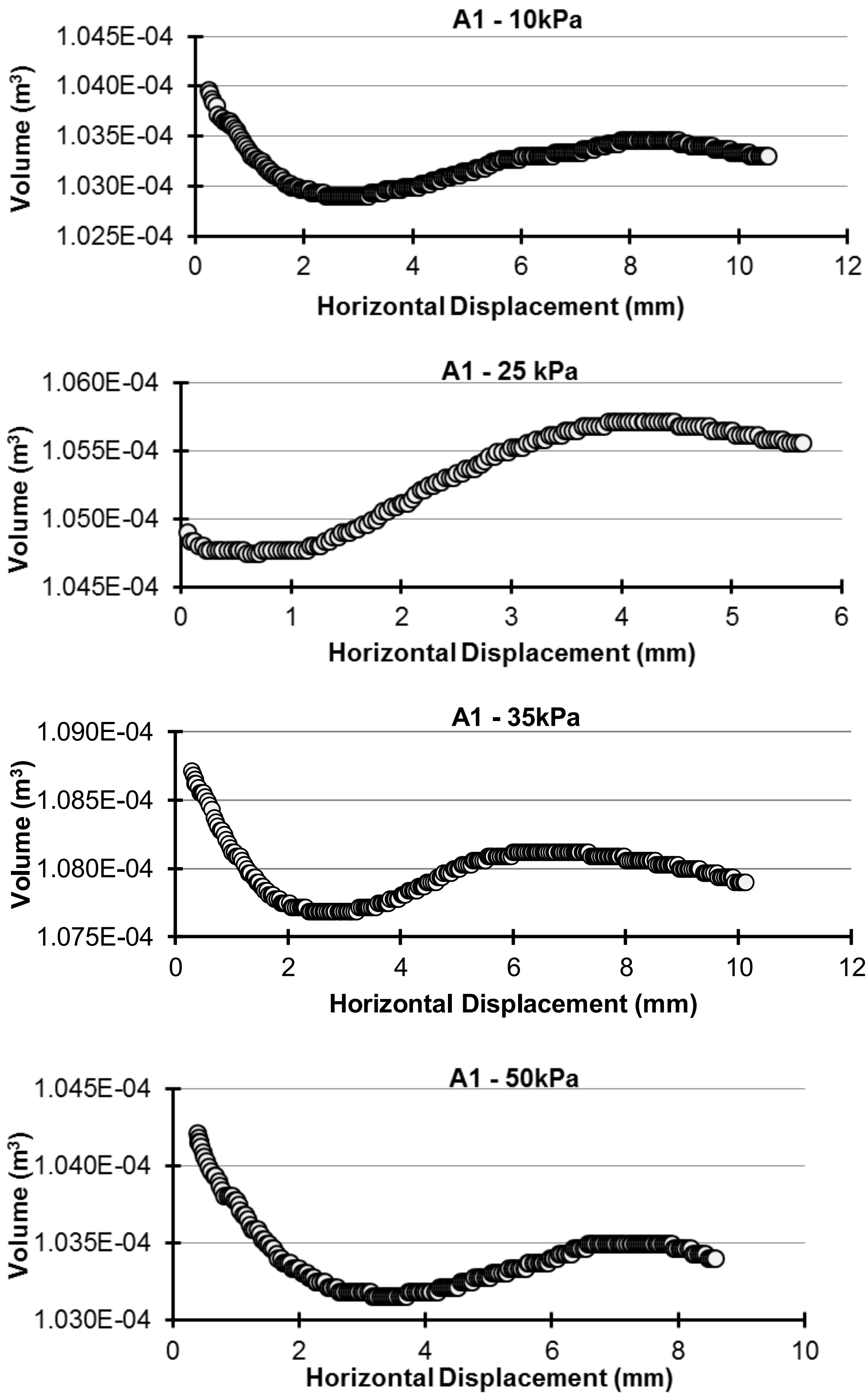


Figure X-2. Changes in volume as a function of displacement during direct shear tests for A1

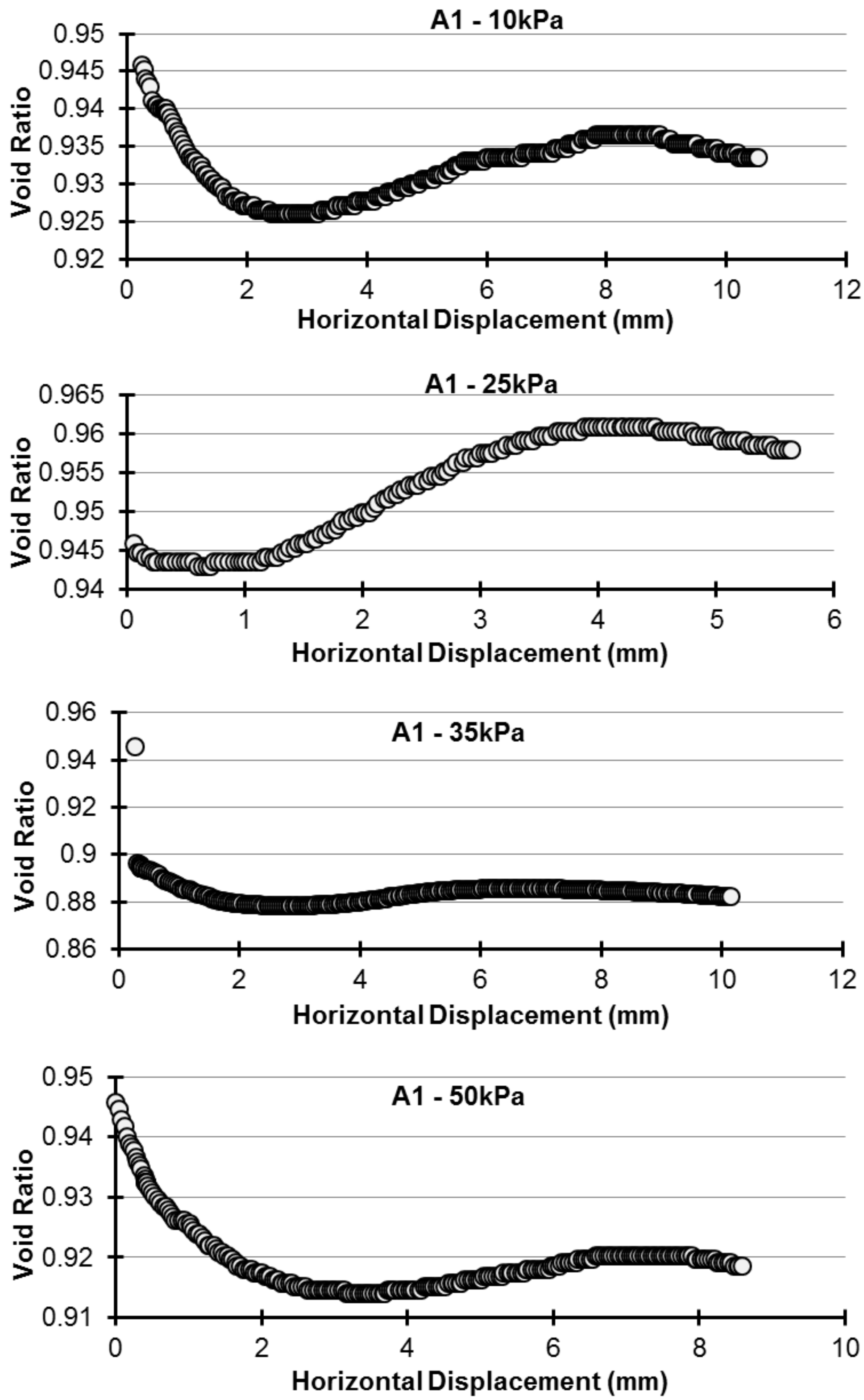


Figure X-3. Changes in void ratio with displacement during direct shear tests for A1

2.2 Flume Deposit A3 Test Data

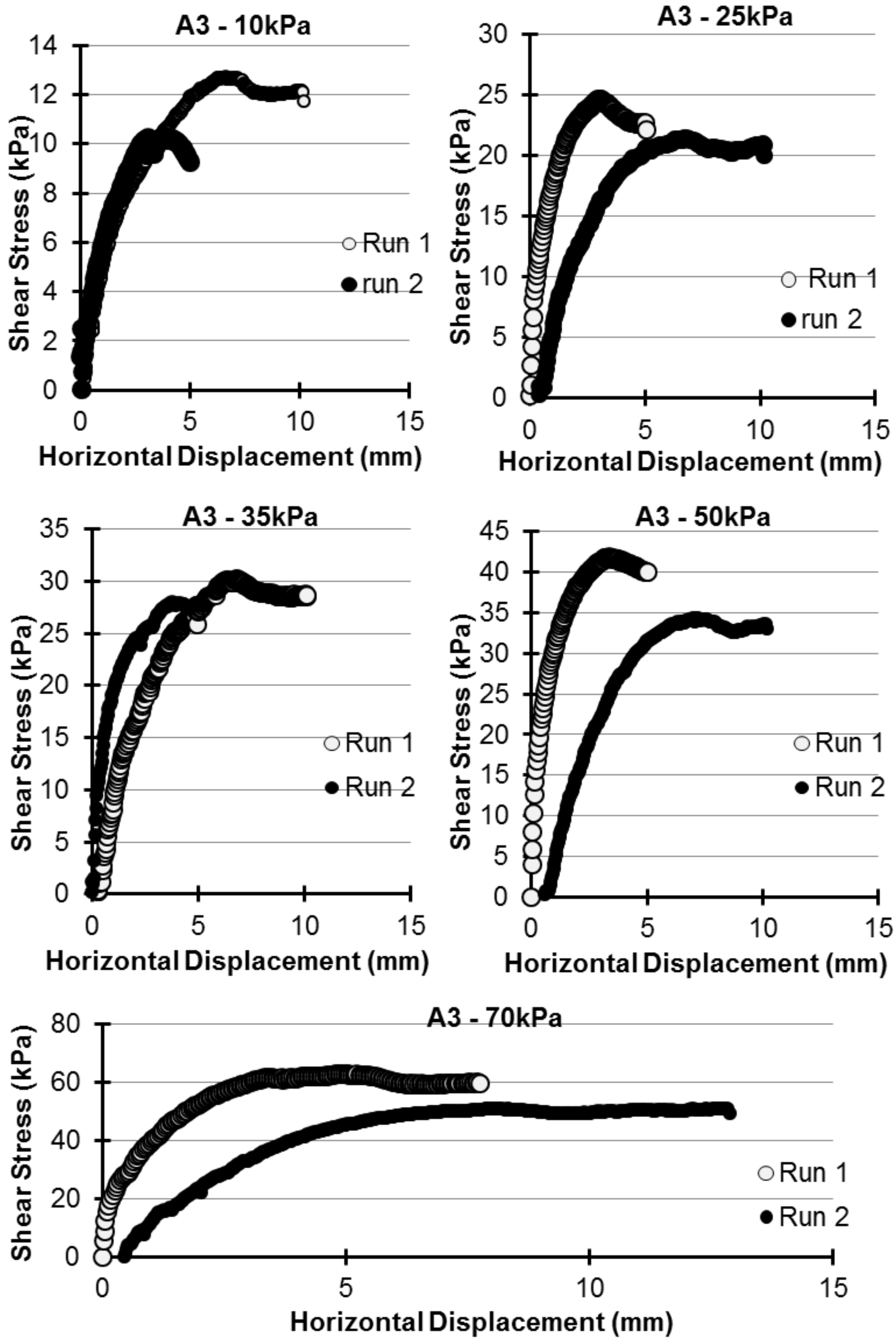


Figure X-4. Peak and residual shear stresses as a function of displacement during direct shear tests for A3

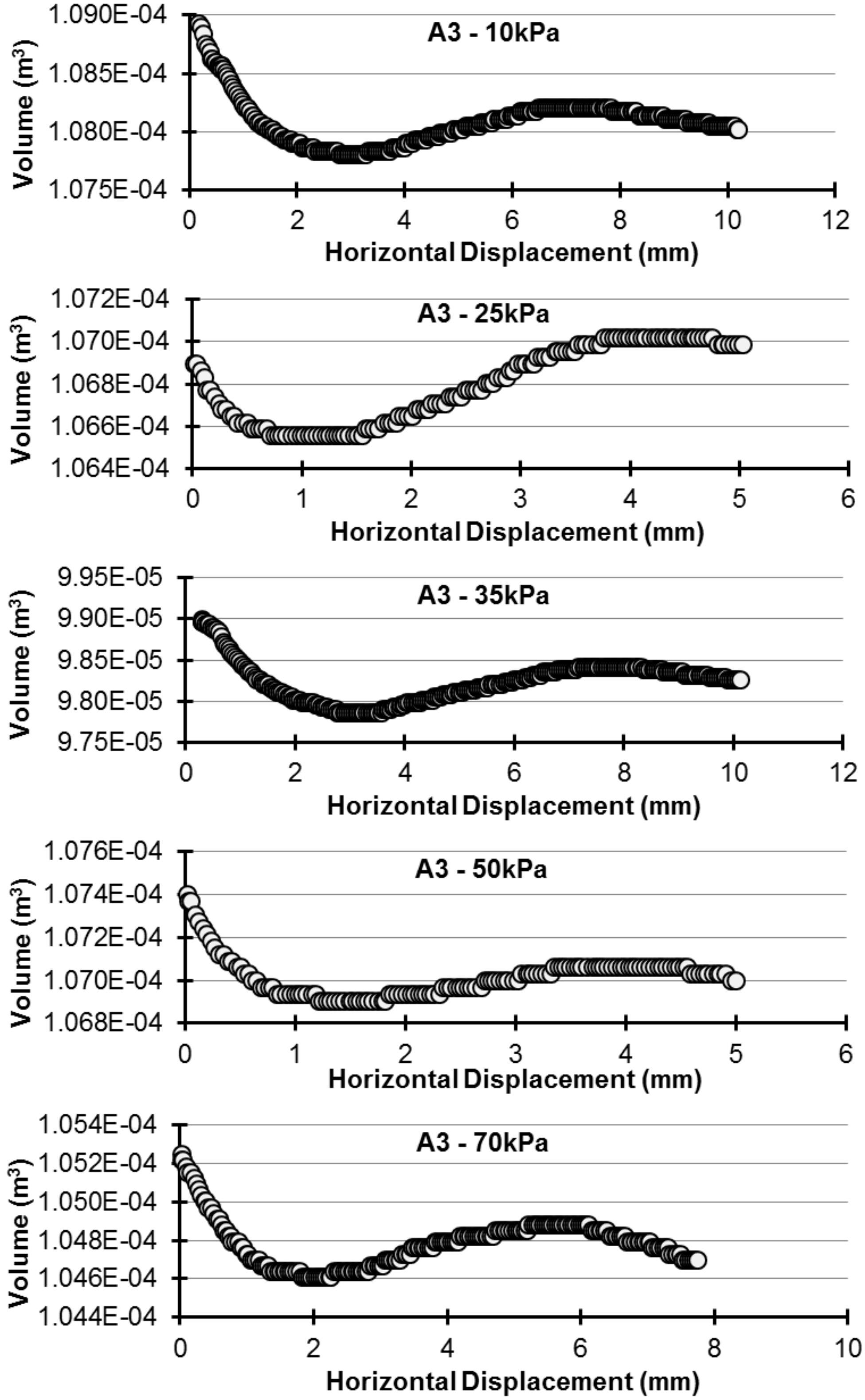


Figure X-5. Changes in volume with displacement during direct shear tests for A3

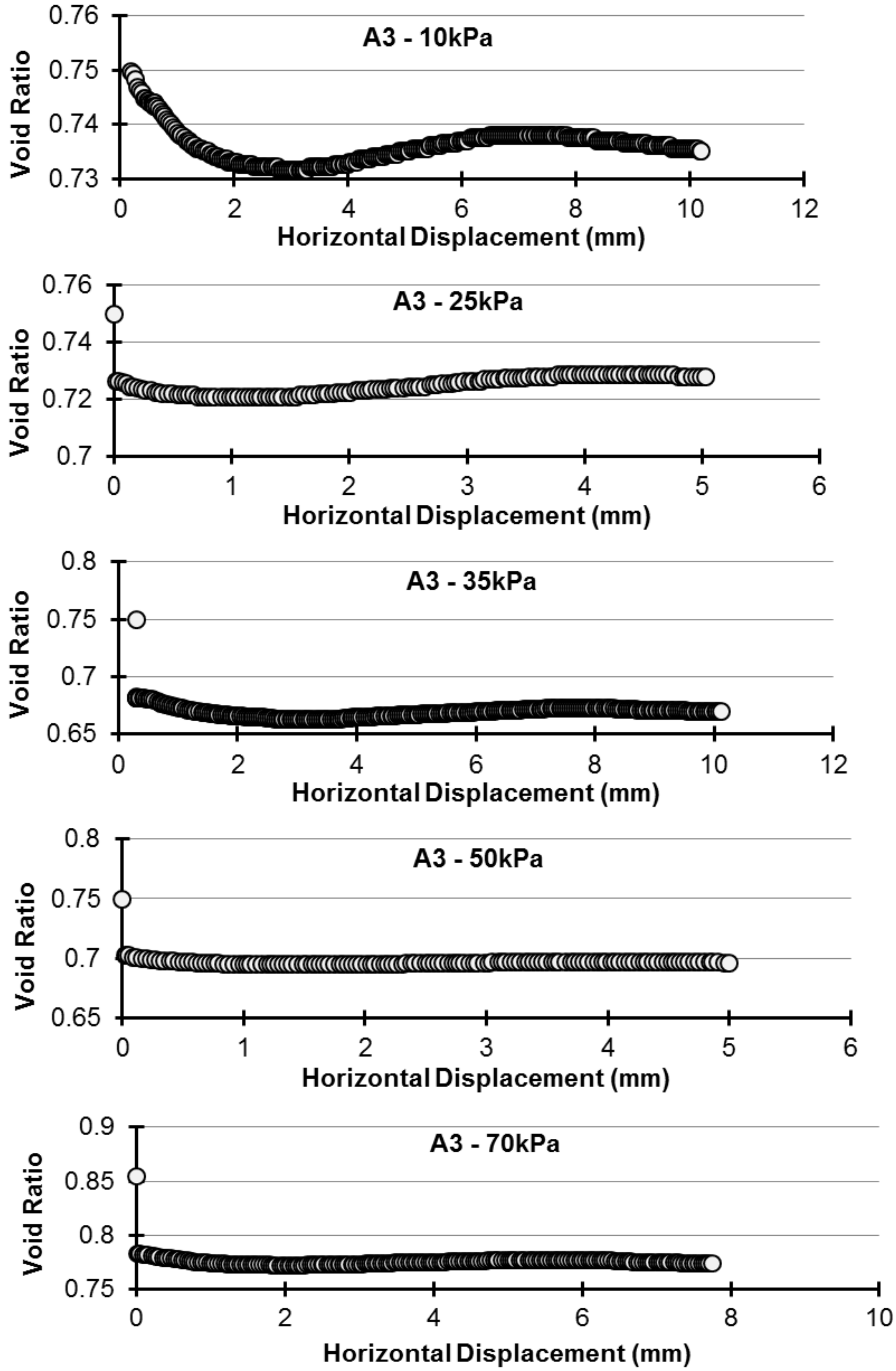


Figure X-6. Changes in void ratio with displacement during direct shear tests for A3

2.3 Flume Deposit A5 Test Data

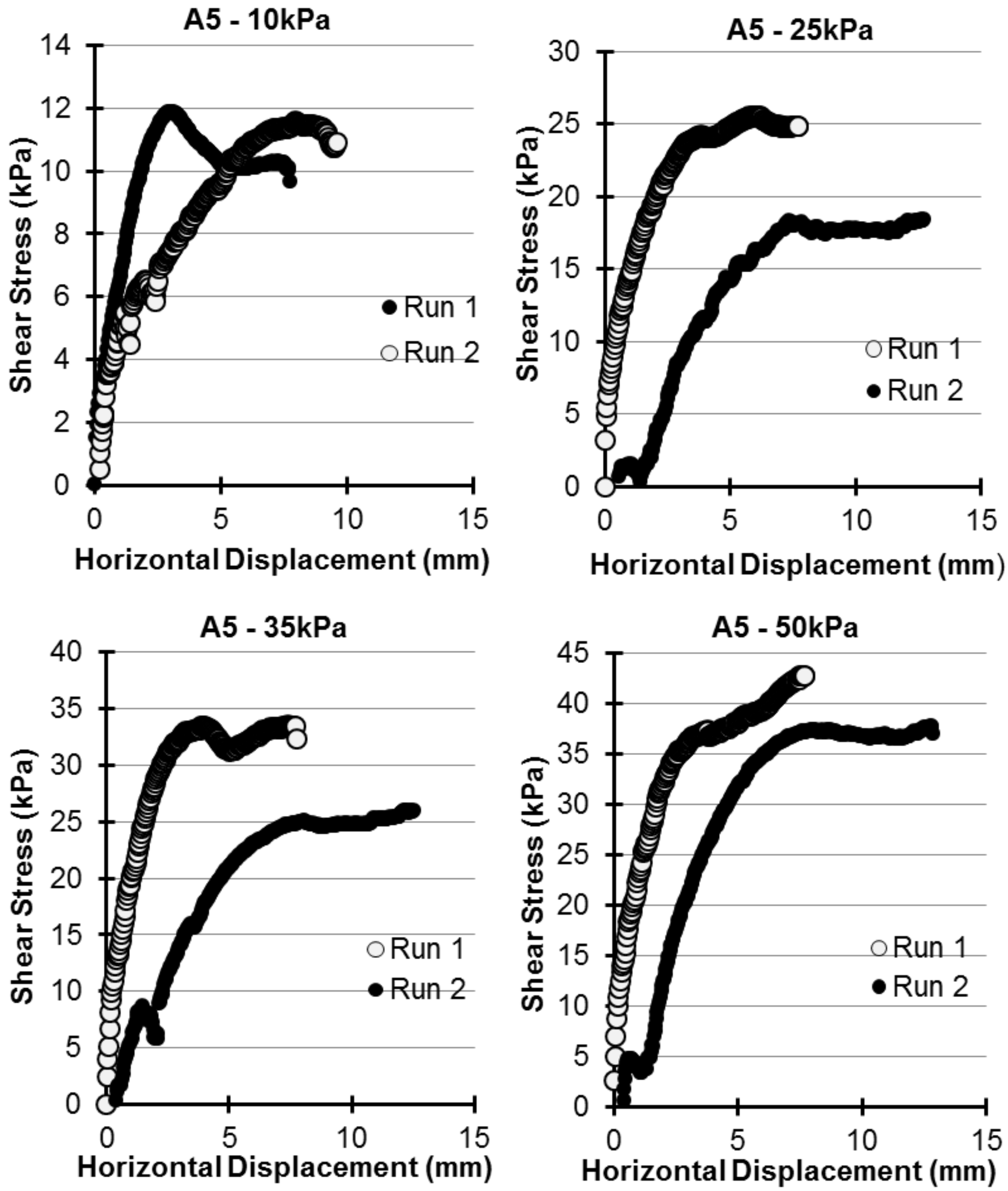


Figure X-7. Variations in peak and residual shear stresses with displacement during direct shear tests for A5

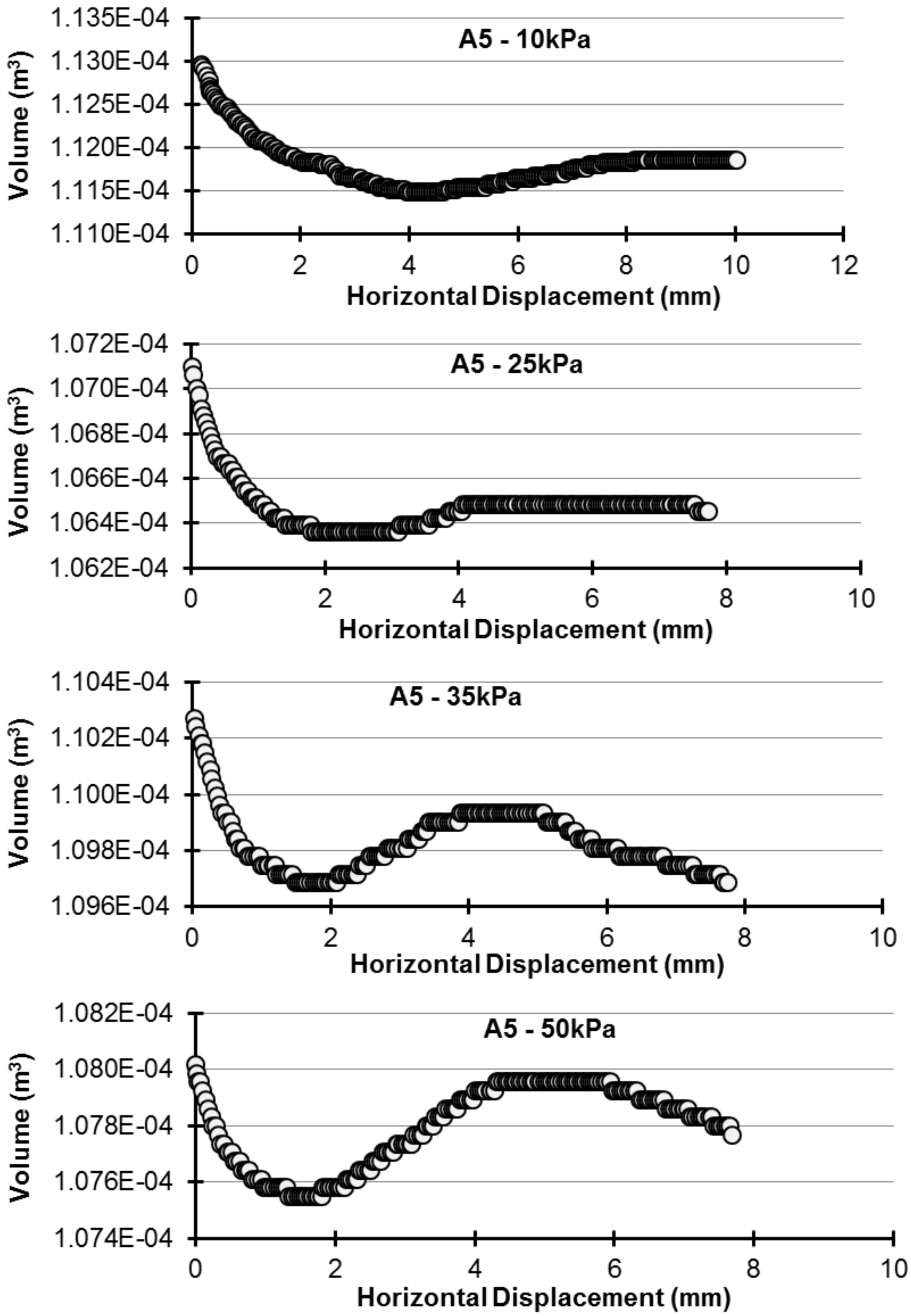


Figure X-8. Changes in volume with displacement during direct shear tests for A5

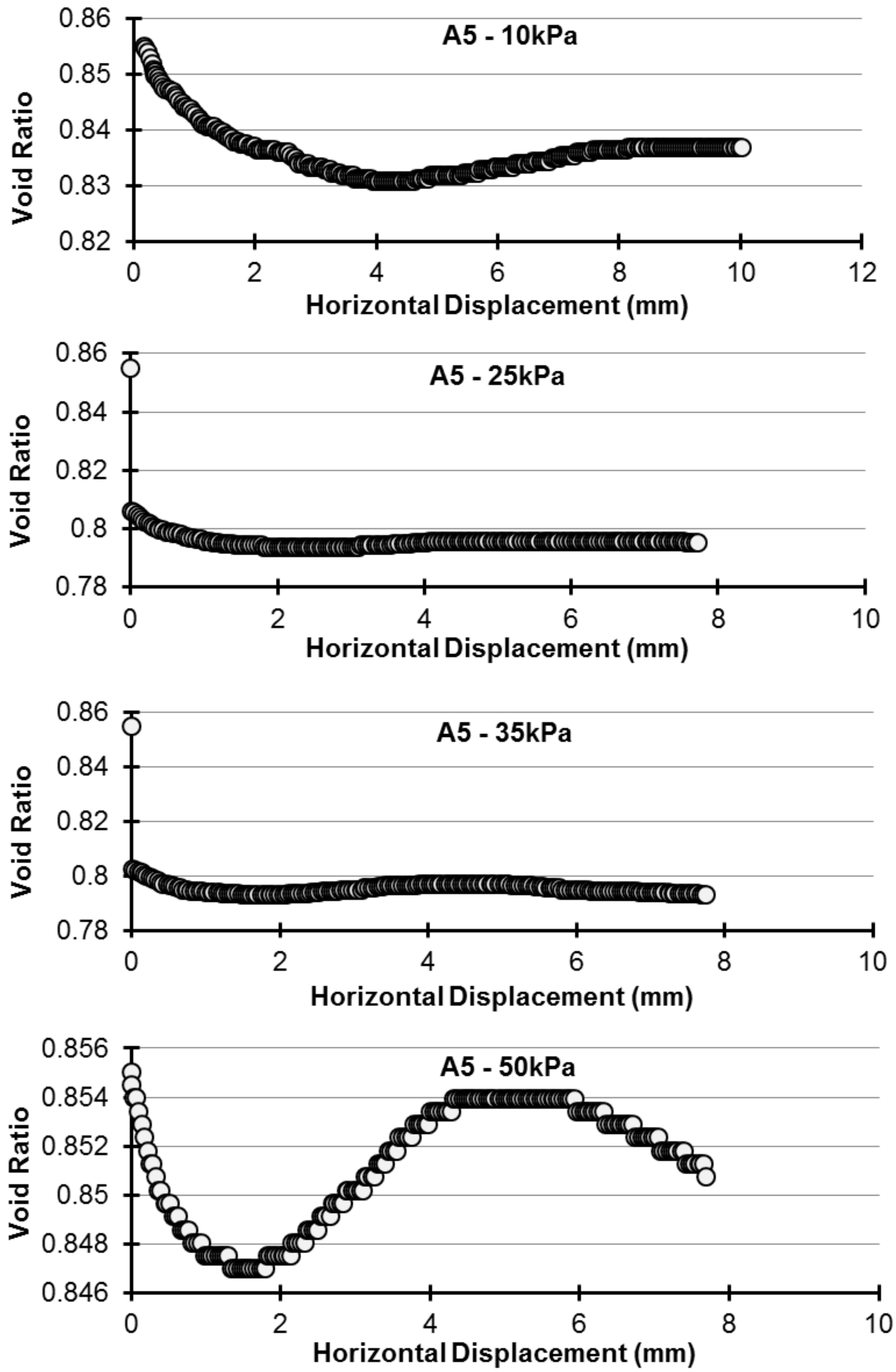


Figure X-9. Changes in void ratio with displacement during direct shear tests for A5

2.4 Flume Deposit A13 Test Data

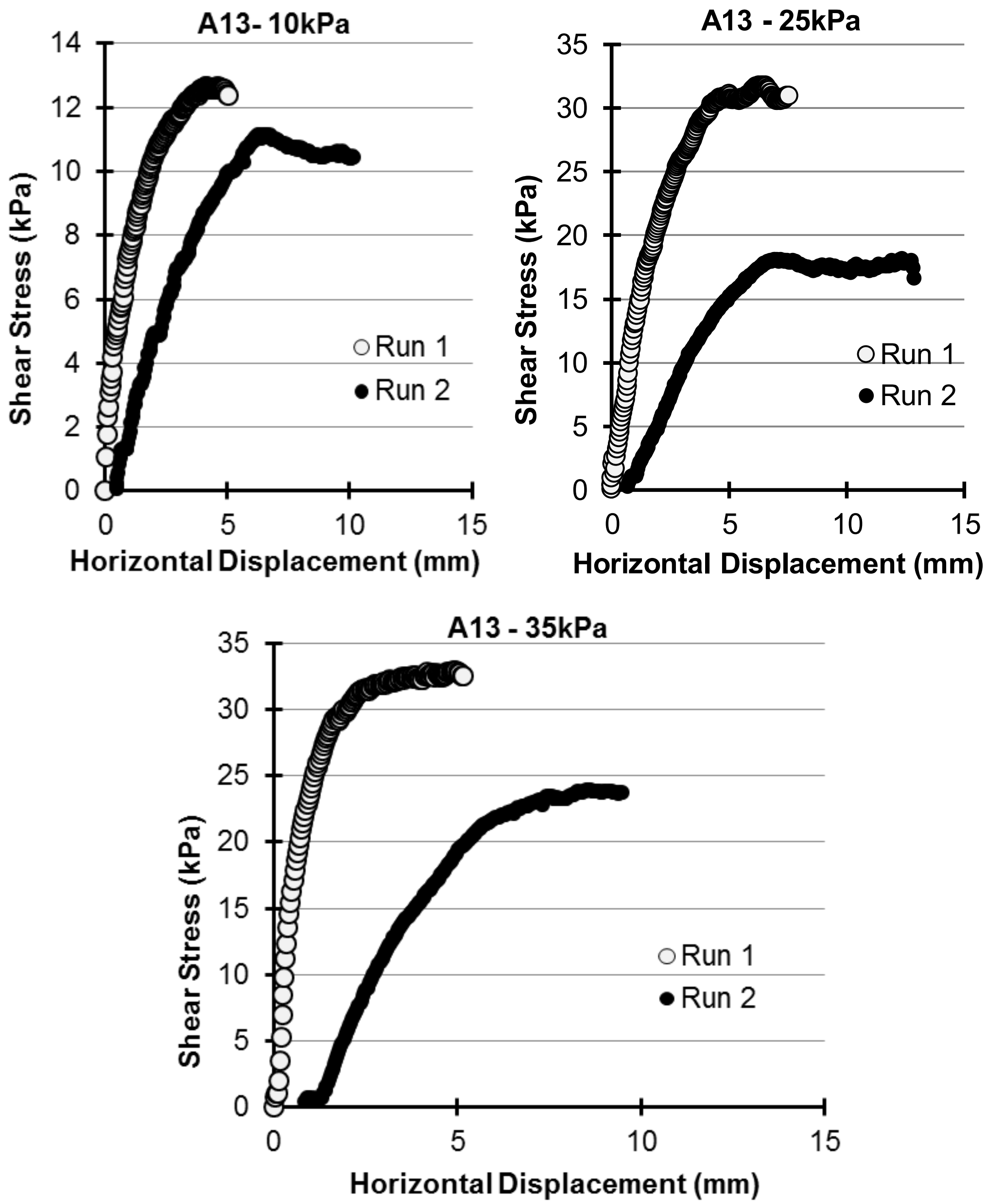


Figure X-10. Variations in peak and residual shear stresses with horizontal displacement during direct shear tests for A13

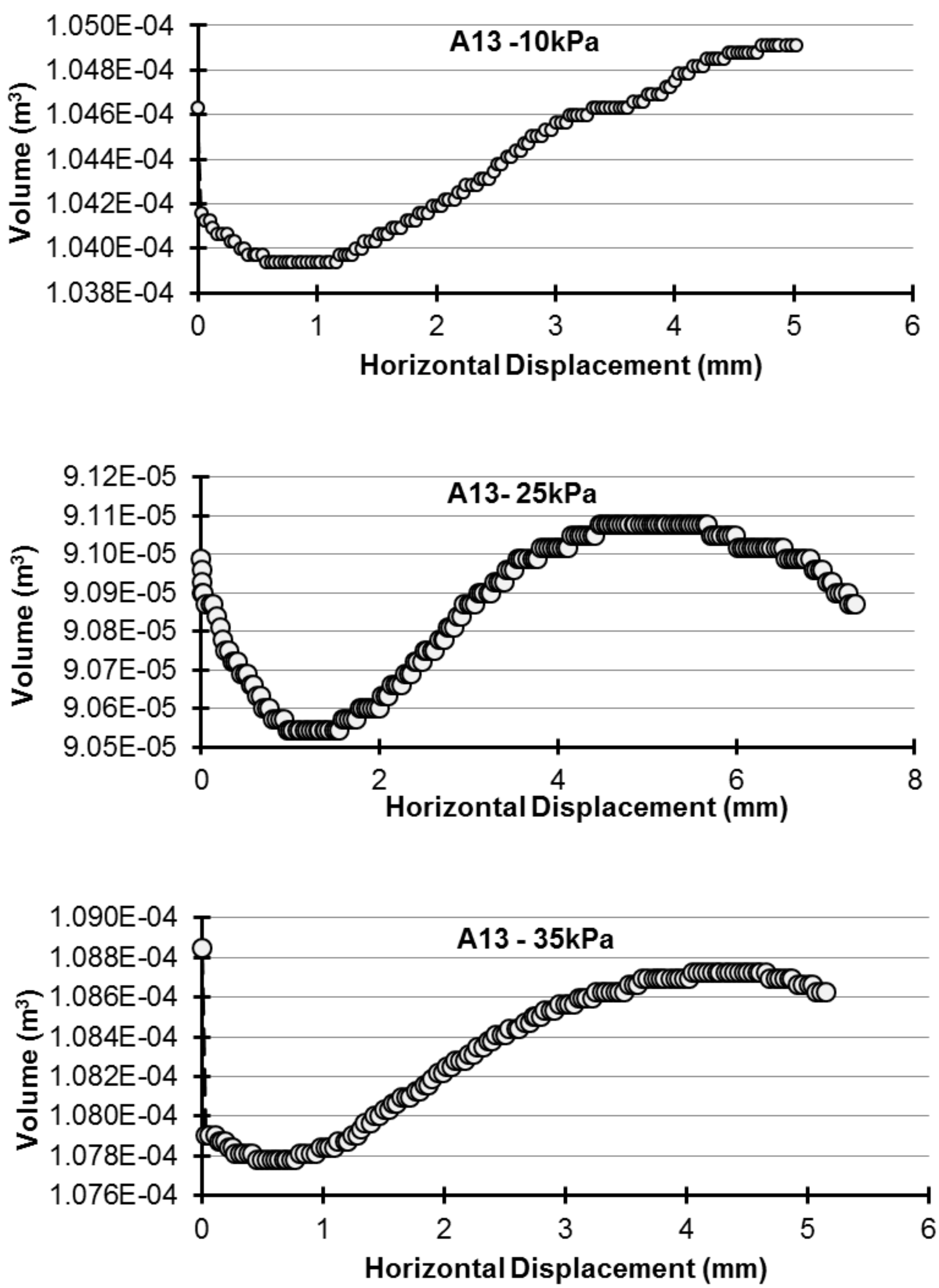


Figure X-11. Changes in volume with horizontal displacement during direct shear tests for A13

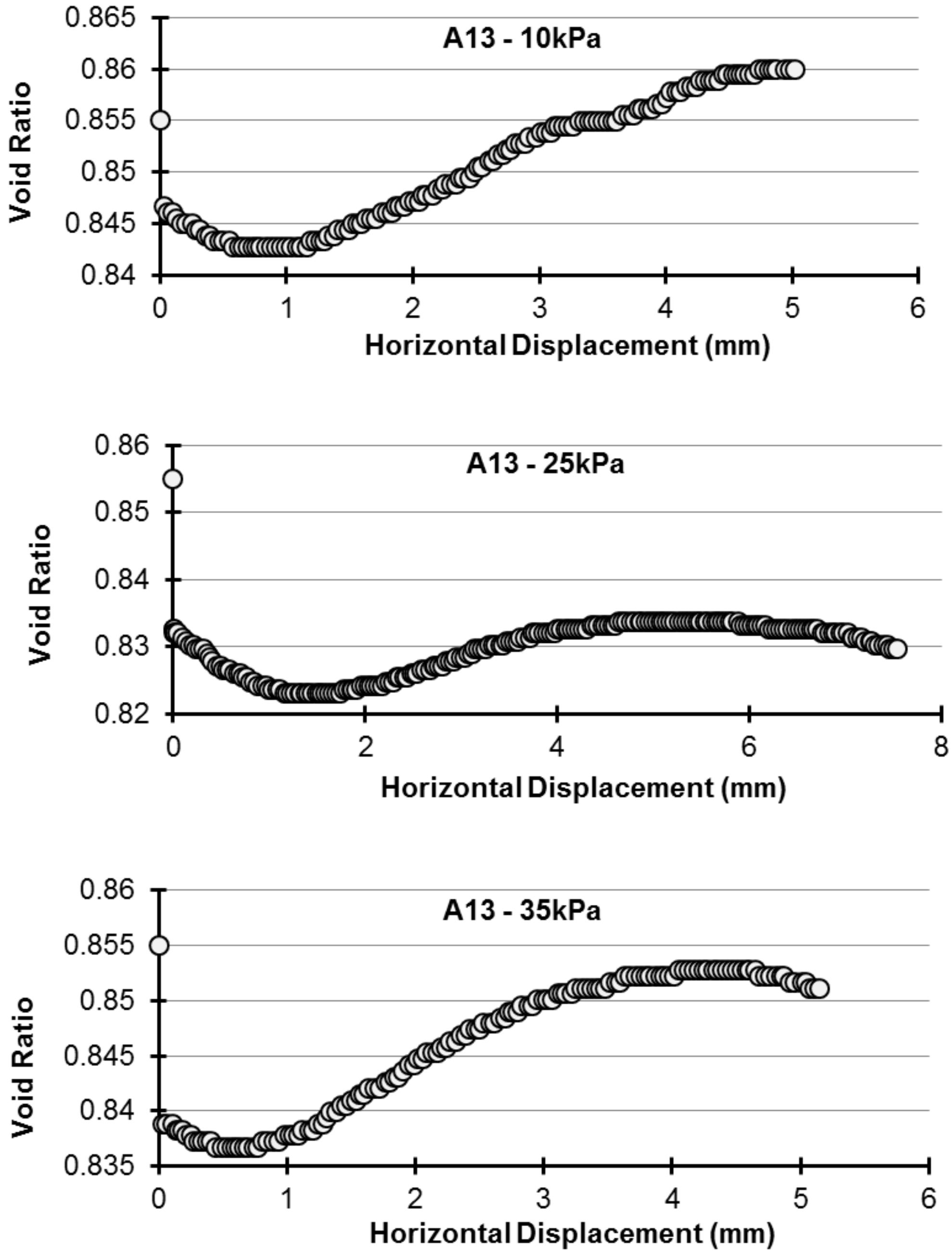


Figure X-12. Changes in void ratio as a function of horizontal displacement during direct shear tests for A13

## 2.5 Beach Sand Test Data

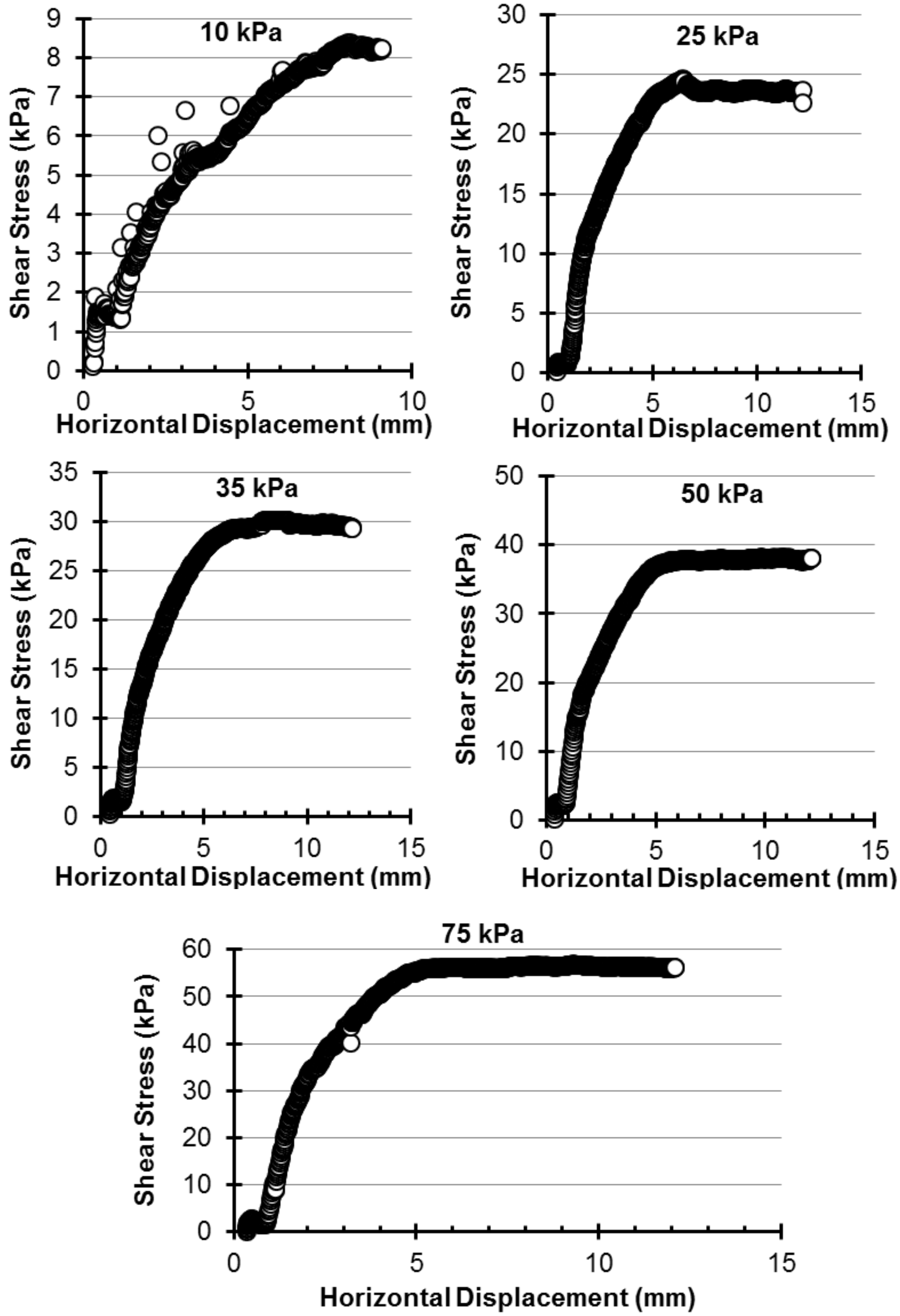


Figure X-13. Variations in peak and residual shear stresses with displacement during direct shear tests for the tailings beach sand sample

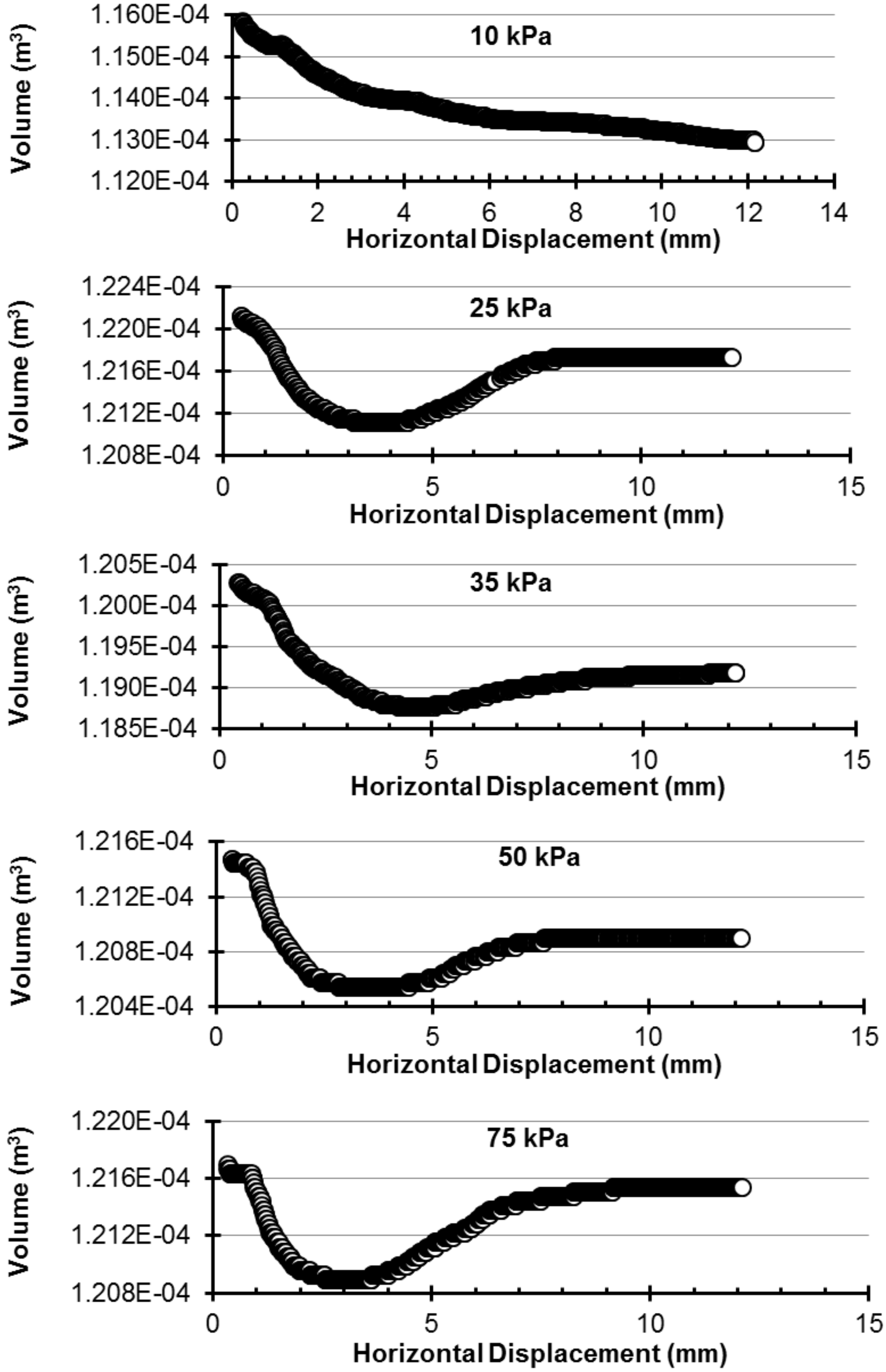


Figure X-14. Variations in volume with horizontal displacement during direct shear tests for the tailings beach sand sample

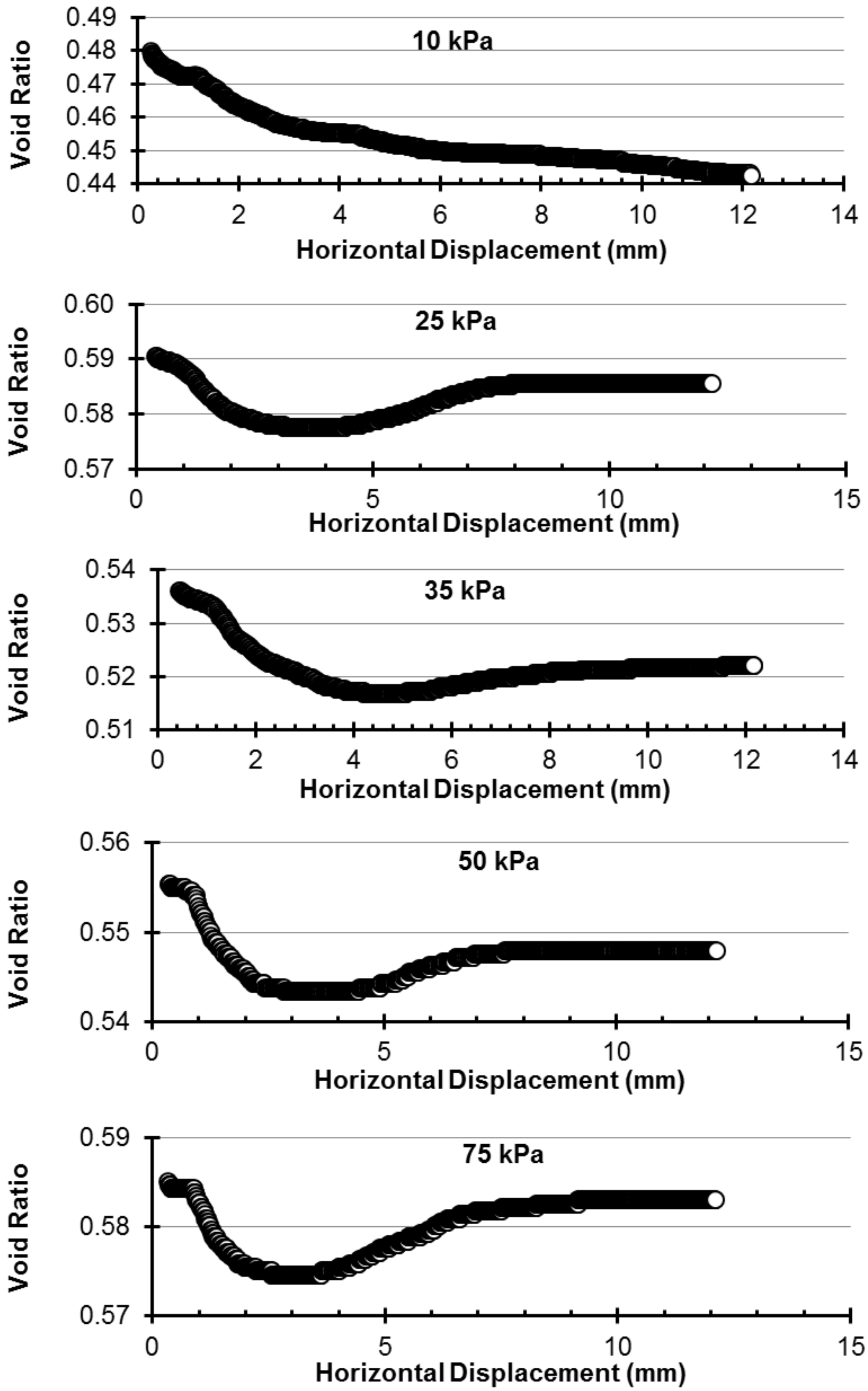


Figure X-15. Void ratio change with horizontal displacement during direct shear tests for the tailings beach sand sample

# XI. **APPENDIX E** - LARGE STRAIN CONSOLIDATION DATA

## 1. Large Strain Consolidation (LSC) Data Summary Tables

Table XI-1. Flume deposit A5 consolidation data

| Load step (kPa) | Height, H (mm) | Void Ratio, e | Mv ($m^2$/MN) | k (m/s) | Cv ($m^2$/year) |
|---|---|---|---|---|---|
| 0.1 | 57.36 | 0.68 | - | 3.5E-07 | - |
| 0.4 | 57.29 | 0.68 | 3.9 | 2.5E-07 | 207.7 |
| 4.4 | 57.23 | 0.68 | 3.2 | 1.9E-07 | 186.9 |
| 10 | 57.20 | 0.68 | 5.7 | 1.6E-07 | 89.5 |
| 40 | 57.18 | 0.67 | 23.5 | 2.1E-07 | 29.1 |
| 80 | 57.17 | 0.67 | 47.4 | 1.9E-07 | 12.8 |
| 160 | 57.16 | 0.67 | 95.1 | 1.6E-07 | 5.4 |
| 280 | 57.14 | 0.67 | 166.9 | 9.6E-08 | 1.9 |
| 380 | 57.12 | 0.67 | 238.6 | 6.7E-08 | 0.9 |
| 500 | 57.11 | 0.67 | 310.4 | 2.9E-08 | 0.3 |

Table XI-2. Flume deposit A3 consolidation data

| Load step (kPa) | Height, H (mm) | Void Ratio, e | Mv ($m^2$/MN) | k (m/s) | Cv ($m^2$/year) |
|---|---|---|---|---|---|
| 0.1 | 66.41 | 0.83 | - | 1.6E-06 | - |
| 0.4 | 66.39 | 0.83 | 4.3 | 7.1E-07 | 533.7 |
| 4.4 | 66.29 | 0.83 | 3.1 | 3.5E-07 | 363.6 |
| 10 | 66.26 | 0.83 | 5.1 | 2.4E-07 | 153.2 |
| 40 | 66.25 | 0.83 | 21.5 | 7.1E-08 | 10.7 |
| 80 | 66.24 | 0.83 | 43.4 | 1.1E-07 | 8.1 |
| 160 | 66.19 | 0.82 | 87.2 | - | - |
| 260 | 66.10 | 0.82 | 142.1 | 1.2E-07 | 2.7 |
| 360 | 66.05 | 0.82 | 197.2 | 1.1E-07 | 1.8 |
| 500 | 65.92 | 0.82 | 279.8 | 1.8E-07 | 2.1 |

2. Change in Height During Large Strain Consolidation

2.1 Flume A5

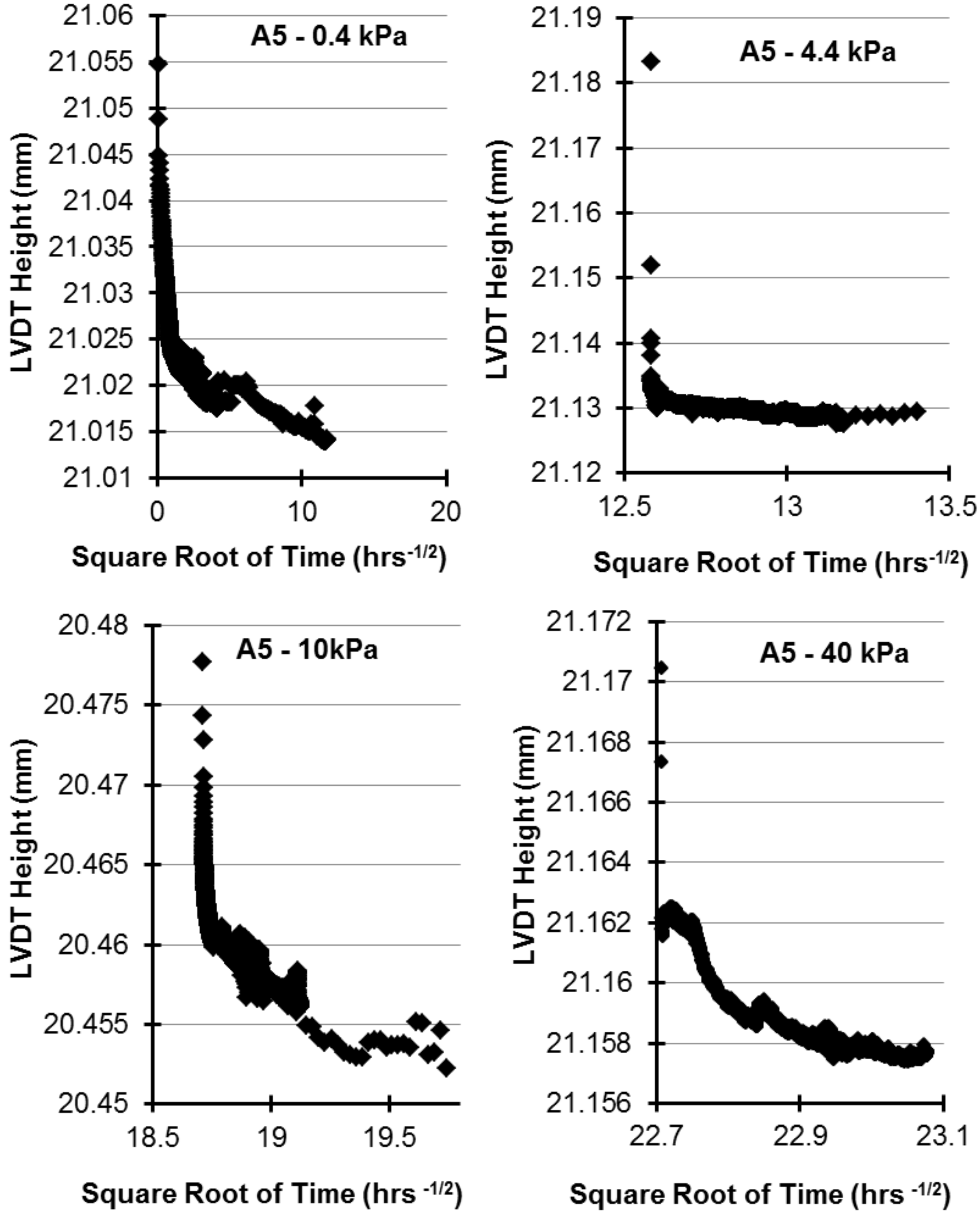


Figure XI-1. Recorded height as a function of the square root of time during consolidation for A5 between 0.4 kPa and 40 kPa applied stresses

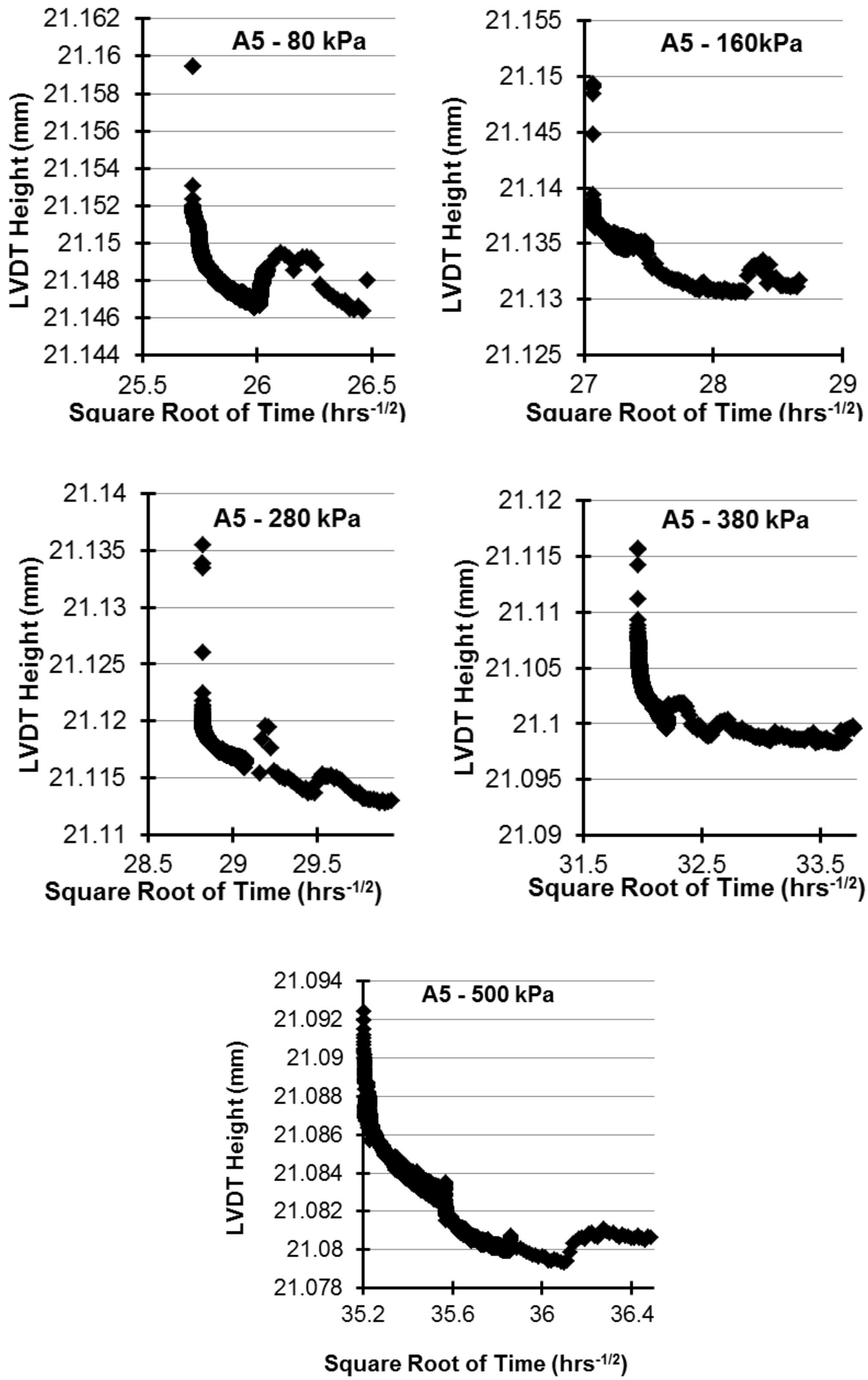


Figure XI-2. Recorded height as a function of the square root of time during consolidation for A5 between 80 kPa and 500 kPa applied stresses

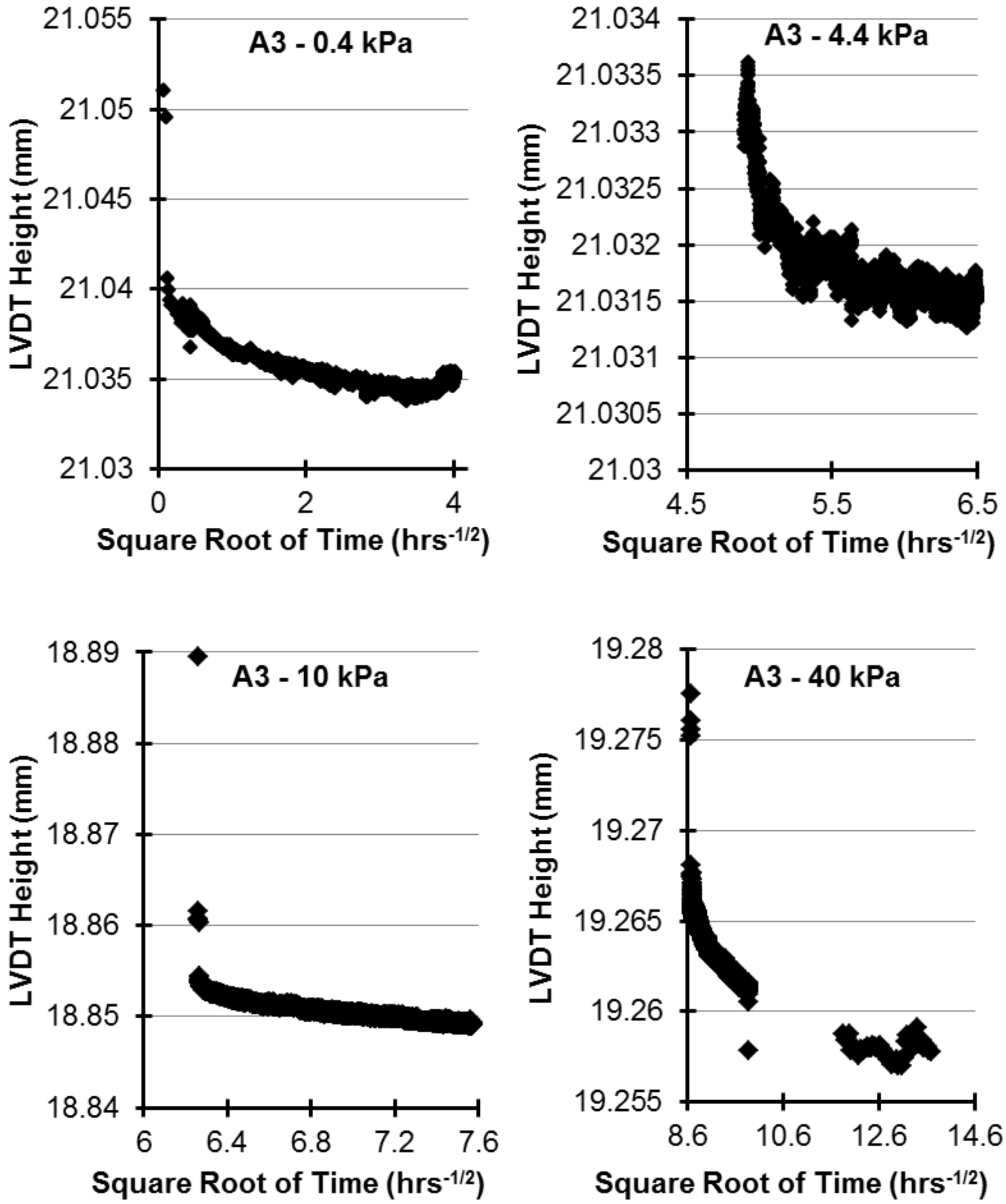


Figure XI-3. Recorded height as a function of the square root of time during consolidation for A3 between 0.4 kPa and 40 kPa applied stresses

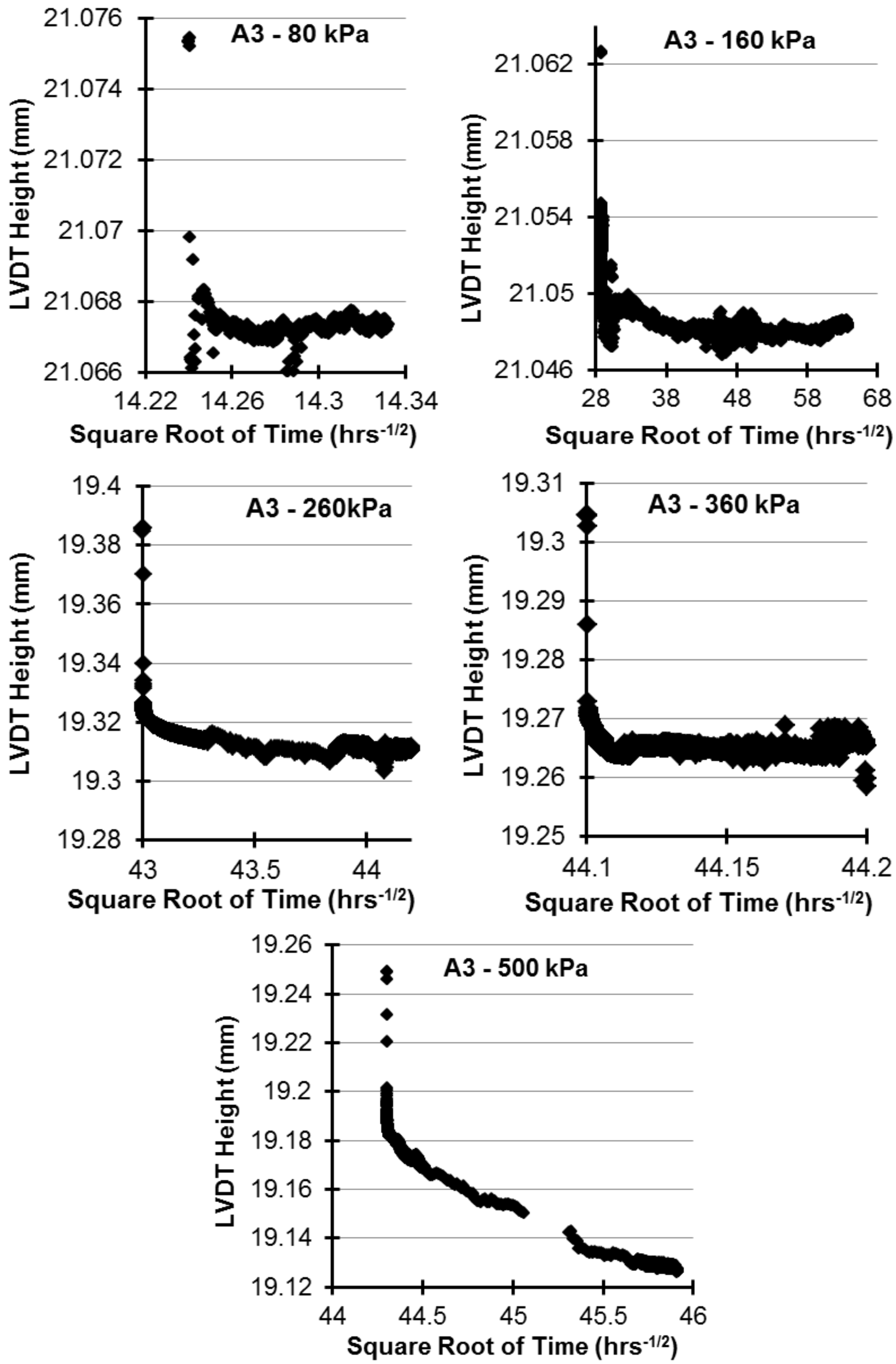


Figure XI-4. Recorded height as a function of the square root of time during consolidation for A3 between 80 kPa and 500 kPa applied stresses

## 3. Hydraulic Conductivity Measurements

### 3.1 Flume A5 Data

Table XI-3. Hydraulic conductivity (k) measurements at 0.4 kPa for A5

| Sample Height = 5.730 cm ; i = 0.3 | | | | | |
|---|---|---|---|---|---|
| Distance (m) | Cumulative Distance (m) | Time (s) | Velocity (m/s) | Flow rate, Q ($m^3$/s) | k (=Q/Ai) (m/s) |
| 0.540 | 0 | 0 | 0 | 0 | 0 |
| 0.530 | 0.010 | 270 | 3.7E-05 | 4.7E-10 | 2.3E-07 |
| 0.520 | 0.020 | 505 | 4.0E-05 | 5.0E-10 | 2.4E-07 |
| 0.510 | 0.030 | 760 | 3.9E-05 | 5.0E-10 | 2.4E-07 |
| 0.500 | 0.040 | 998 | 4.0E-05 | 5.0E-10 | 2.4E-07 |
| 0.490 | 0.050 | 1247 | 4.0E-05 | 5.0E-10 | 2.5E-07 |
| 0.480 | 0.060 | 1486 | 4.0E-05 | 5.1E-10 | 2.5E-07 |
| 0.470 | 0.070 | 1722 | 4.1E-05 | 5.1E-10 | 2.5E-07 |
| 0.460 | 0.080 | 1964 | 4.1E-05 | 5.1E-10 | 2.5E-07 |
| 0.450 | 0.090 | 2200 | 4.1E-05 | 5.1E-10 | 2.5E-07 |
| 0.408 | 0.132 | 3165 | 4.2E-05 | 5.2E-10 | 2.5E-07 |
| 0.369 | 0.171 | 4020 | 4.3E-05 | 5.3E-10 | 2.6E-07 |
| 0.331 | 0.209 | 4920 | 4.2E-05 | 5.3E-10 | 2.6E-07 |
| 0.298 | 0.242 | 5820 | 4.2E-05 | 5.2E-10 | 2.5E-07 |
| 0.263 | 0.277 | 6720 | 4.1E-05 | 5.2E-10 | 2.5E-07 |
| 0.230 | 0.310 | 7620 | 4.1E-05 | 5.1E-10 | 2.5E-07 |

Table XI-4. Hydraulic conductivity (k) measurements at 4.4 kPa for A5

| Sample Height = 5.723 cm ; i = 0.2 | | | | | |
|---|---|---|---|---|---|
| Distance (m) | Cumulative Distance (m) | Time (s) | Velocity (m/s) | Flow rate, Q ($m^3$/s) | k (=Q/Ai) (m/s) |
| 0.540 | 0 | 0 | 0 | 0 | 0 |
| 0.530 | 0.010 | 630 | 1.6E-05 | 2.0E-10 | 1.6E-07 |
| 0.520 | 0.020 | 1255 | 1.6E-05 | 2.0E-10 | 1.6E-07 |
| 0.510 | 0.030 | 1836 | 1.6E-05 | 2.1E-10 | 1.7E-07 |
| 0.500 | 0.040 | 2420 | 1.7E-05 | 2.1E-10 | 1.7E-07 |
| 0.490 | 0.050 | 2970 | 1.7E-05 | 2.1E-10 | 1.7E-07 |
| 0.476 | 0.064 | 3660 | 1.7E-05 | 2.2E-10 | 1.8E-07 |
| 0.457 | 0.083 | 4560 | 1.8E-05 | 2.3E-10 | 1.9E-07 |
| 0.441 | 0.099 | 5520 | 1.8E-05 | 2.3E-10 | 1.8E-07 |
| 0.405 | 0.135 | 7320 | 1.8E-05 | 2.3E-10 | 1.9E-07 |
| 0.370 | 0.170 | 9120 | 1.9E-05 | 2.3E-10 | 1.9E-07 |
| 0.297 | 0.243 | 12900 | 1.9E-05 | 2.4E-10 | 1.9E-07 |

Table XI-5. Hydraulic conductivity (k) measurements at 10 kPa for A5

| Sample Height = 5.720 cm ; i = 0.2 | | | | | |
|---|---|---|---|---|---|
| Distance (m) | Cumulative Distance (m) | Time (s) | Velocity (m/s) | Flow rate, Q ($m^3$/s) | k (=Q/Ai) (m/s) |
| 0.540 | 0 | 0 | 0 | 0 | 0 |
| 0.530 | 0.010 | 588 | 1.7E-05 | 2.1E-10 | 1.4E-07 |
| 0.520 | 0.020 | 1162 | 1.7E-05 | 2.2E-10 | 1.4E-07 |
| 0.510 | 0.030 | 1697 | 1.8E-05 | 2.2E-10 | 1.5E-07 |
| 0.500 | 0.040 | 2265 | 1.8E-05 | 2.2E-10 | 1.5E-07 |
| 0.490 | 0.050 | 2820 | 1.8E-05 | 2.2E-10 | 1.5E-07 |
| 0.480 | 0.060 | 3285 | 1.8E-05 | 2.3E-10 | 1.5E-07 |
| 0.470 | 0.070 | 3720 | 1.9E-05 | 2.4E-10 | 1.6E-07 |
| 0.460 | 0.080 | 4200 | 1.9E-05 | 2.4E-10 | 1.6E-07 |
| 0.450 | 0.090 | 4740 | 1.9E-05 | 2.4E-10 | 1.6E-07 |
| 0.440 | 0.100 | 5220 | 1.9E-05 | 2.4E-10 | 1.6E-07 |
| 0.413 | 0.127 | 6420 | 2.0E-05 | 2.5E-10 | 1.6E-07 |
| 0.386 | 0.154 | 7620 | 2.0E-05 | 2.5E-10 | 1.7E-07 |
| 0.345 | 0.195 | 9600 | 2.0E-05 | 2.6E-10 | 1.7E-07 |
| 0.308 | 0.232 | 11400 | 2.0E-05 | 2.6E-10 | 1.7E-07 |
| 0.277 | 0.263 | 12600 | 2.1E-05 | 2.6E-10 | 1.7E-07 |
| 0.248 | 0.292 | 15060 | 1.9E-05 | 2.4E-10 | 1.6E-07 |

Table XI-6. Hydraulic conductivity (k) measurements at 40 kPa for A5

| Sample Height = 5.718 cm ; i = 0.2 | | | | | |
|---|---|---|---|---|---|
| Distance (m) | Cumlative Distance (m) | Time (s) | Velocity (m/s) | Flow rate, Q ($m^3$/s) | k (=Q/Ai) (m/s) |
| 0.540 | 0 | 0 | 0 | 0 | 0 |
| 0.530 | 0.010 | 307 | 3.3E-05 | 4.1E-10 | 2.1E-07 |
| 0.520 | 0.020 | 614 | 3.3E-05 | 4.1E-10 | 2.1E-07 |
| 0.510 | 0.030 | 932 | 3.2E-05 | 4.0E-10 | 2.1E-07 |
| 0.500 | 0.040 | 1230 | 3.3E-05 | 4.1E-10 | 2.1E-07 |
| 0.490 | 0.050 | 1536 | 3.3E-05 | 4.1E-10 | 2.1E-07 |
| 0.480 | 0.060 | 1845 | 3.3E-05 | 4.1E-10 | 2.1E-07 |
| 0.444 | 0.096 | 2895 | 3.3E-05 | 4.2E-10 | 2.2E-07 |
| 0.414 | 0.126 | 3720 | 3.4E-05 | 4.3E-10 | 2.2E-07 |
| 0.380 | 0.160 | 4680 | 3.4E-05 | 4.3E-10 | 2.2E-07 |
| 0.351 | 0.189 | 5520 | 3.4E-05 | 4.3E-10 | 2.2E-07 |
| 0.288 | 0.252 | 7320 | 3.4E-05 | 4.3E-10 | 2.2E-07 |
| 0.231 | 0.309 | 9120 | 3.4E-05 | 4.3E-10 | 2.2E-07 |

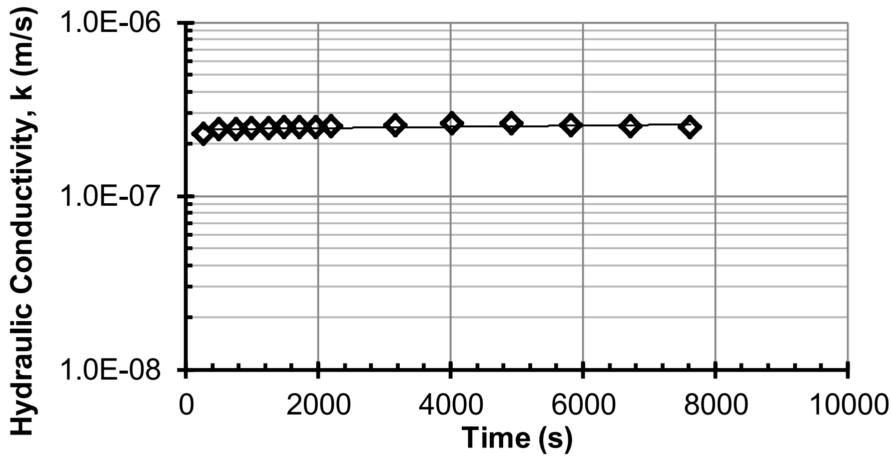


Figure XI-5. Constant head test results at 0.4 kPa for A5

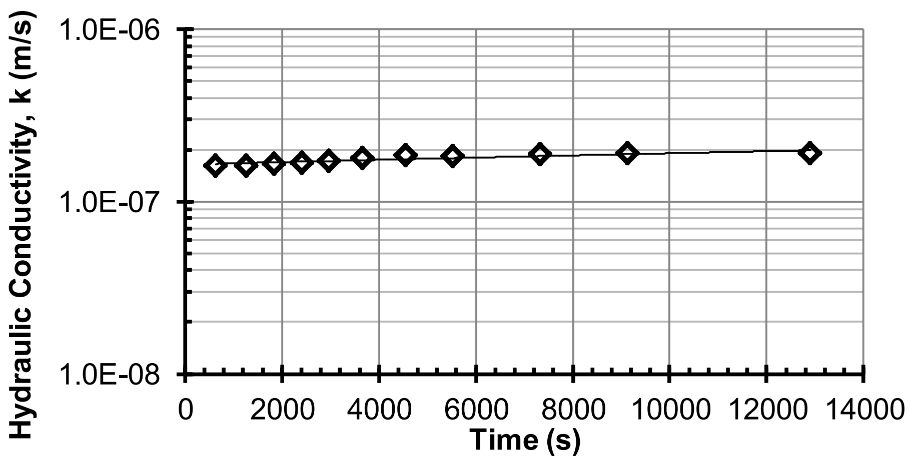


Figure XI-6. Constant head test results at 4.4 kPa for A5

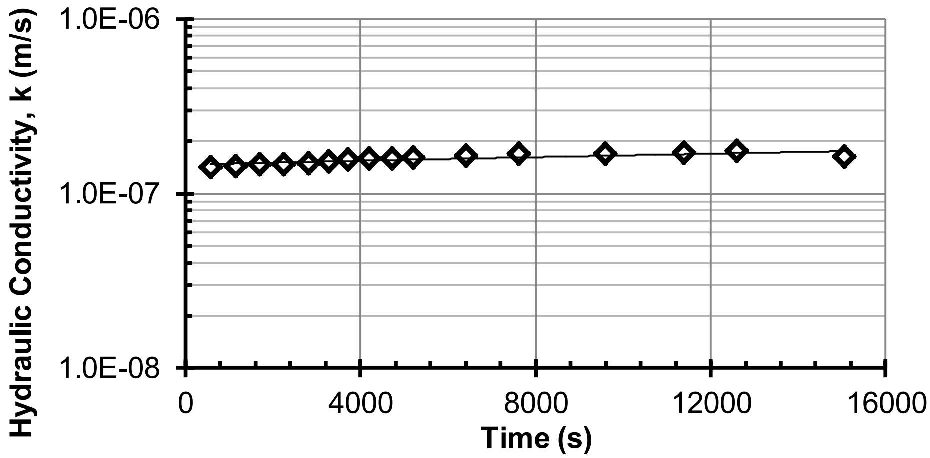


Figure XI-7. Constant head test results at 10 kPa for A5

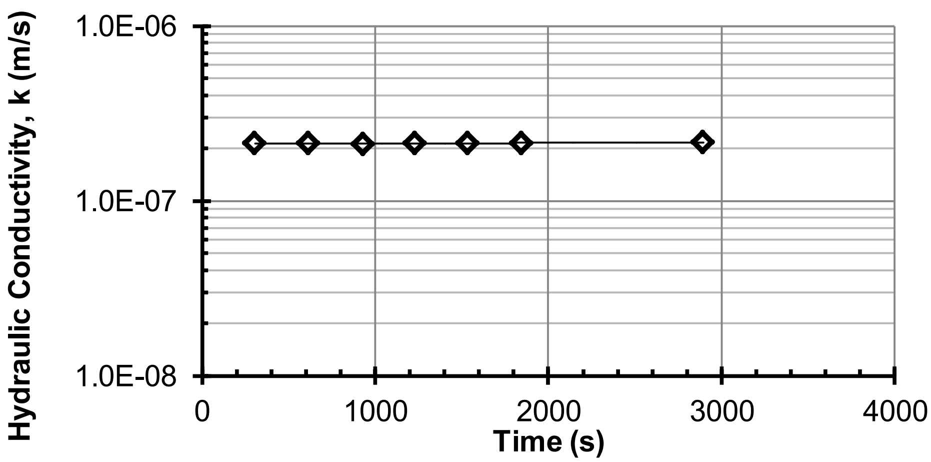


Figure XI-8. Constant head test results at 40 kPa for A5

Table XI-7. Hydraulic conductivity (k) measurements at 80 kPa for A5

| Sample Height = 5.717 cm ; i = 0.2 | | | | | |
|---|---|---|---|---|---|
| Distance (m) | Cumlative Distance (m) | Time (s) | Velocity (m/s) | Flow rate, Q ($m^3$/s) | k (=Q/Ai) (m/s) |
| 0.540 | 0 | 0 | 0 | 0 | 0 |
| 0.530 | 0.010 | 540 | 1.9E-05 | 2.3E-10 | 1.5E-07 |
| 0.520 | 0.020 | 990 | 2.0E-05 | 2.5E-10 | 1.7E-07 |
| 0.510 | 0.030 | 1465 | 2.0E-05 | 2.6E-10 | 1.7E-07 |
| 0.500 | 0.040 | 1942 | 2.1E-05 | 2.6E-10 | 1.7E-07 |
| 0.490 | 0.050 | 2400 | 2.1E-05 | 2.6E-10 | 1.7E-07 |
| 0.444 | 0.096 | 4440 | 2.2E-05 | 2.7E-10 | 1.8E-07 |
| 0.400 | 0.140 | 6120 | 2.3E-05 | 2.9E-10 | 1.9E-07 |
| 0.357 | 0.183 | 7980 | 2.3E-05 | 2.9E-10 | 1.9E-07 |
| 0.316 | 0.224 | 9720 | 2.3E-05 | 2.9E-10 | 1.9E-07 |
| 0.238 | 0.302 | 13320 | 2.3E-05 | 2.8E-10 | 1.9E-07 |

Table XI-8. Hydraulic Conductivity (k) measurements at 160 kPa for A5

| Sample Height = 5.716 cm ; i = 0.2 | | | | | |
|---|---|---|---|---|---|
| Distance (m) | Cumlative Distance (m) | Time (s) | Velocity (m/s) | Flow rate, Q ($m^3/s$) | k (=Q/Ai) (m/s) |
| 0.540 | 0 | 0 | 0 | 0 | 0 |
| 0.530 | 0.010 | 505 | 2.0E-05 | 2.5E-10 | 1.5E-07 |
| 0.520 | 0.020 | 990 | 2.0E-05 | 2.5E-10 | 1.5E-07 |
| 0.480 | 0.060 | 2854 | 2.1E-05 | 2.6E-10 | 1.6E-07 |
| 0.442 | 0.098 | 4620 | 2.1E-05 | 2.7E-10 | 1.6E-07 |
| 0.402 | 0.138 | 6420 | 2.1E-05 | 2.7E-10 | 1.6E-07 |
| 0.362 | 0.178 | 8220 | 2.2E-05 | 2.7E-10 | 1.7E-07 |
| 0.284 | 0.256 | 11820 | 2.2E-05 | 2.7E-10 | 1.7E-07 |

Table XI-9. Hydraulic conductivity (k) measurements at 280 kPa for A5

| Sample Height = 5.714 cm ; i = 0.2 | | | | | |
|---|---|---|---|---|---|
| Distance (m) | Cumlative Distance (m) | Time (s) | Velocity (m/s) | Flow rate, Q ($m^3/s$) | k (=Q/Ai) (m/s) |
| 0.540 | 0 | 0 | 0 | 0 | 0 |
| 0.530 | 0.010 | 1260 | 7.9E-06 | 1.0E-10 | 8.1E-08 |
| 0.520 | 0.020 | 2280 | 8.8E-06 | 1.1E-10 | 8.9E-08 |
| 0.510 | 0.030 | 3360 | 8.9E-06 | 1.1E-10 | 9.1E-08 |
| 0.500 | 0.040 | 4440 | 9.0E-06 | 1.1E-10 | 9.2E-08 |
| 0.481 | 0.059 | 6360 | 9.3E-06 | 1.2E-10 | 9.4E-08 |
| 0.460 | 0.080 | 8160 | 9.8E-06 | 1.2E-10 | 1.0E-07 |
| 0.421 | 0.119 | 11700 | 1.0E-05 | 1.3E-10 | 1.0E-07 |
| 0.381 | 0.159 | 15300 | 1.0E-05 | 1.3E-10 | 1.1E-07 |
| 0.342 | 0.198 | 18900 | 1.0E-05 | 1.3E-10 | 1.1E-07 |
| 0.311 | 0.229 | 22500 | 1.0E-05 | 1.3E-10 | 1.0E-07 |

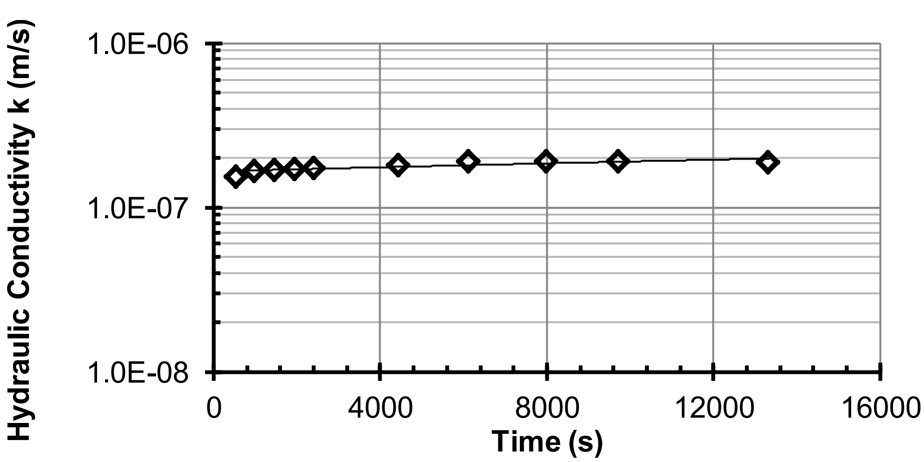


Figure XI-9. Constant head test results at 80 kPa for A5

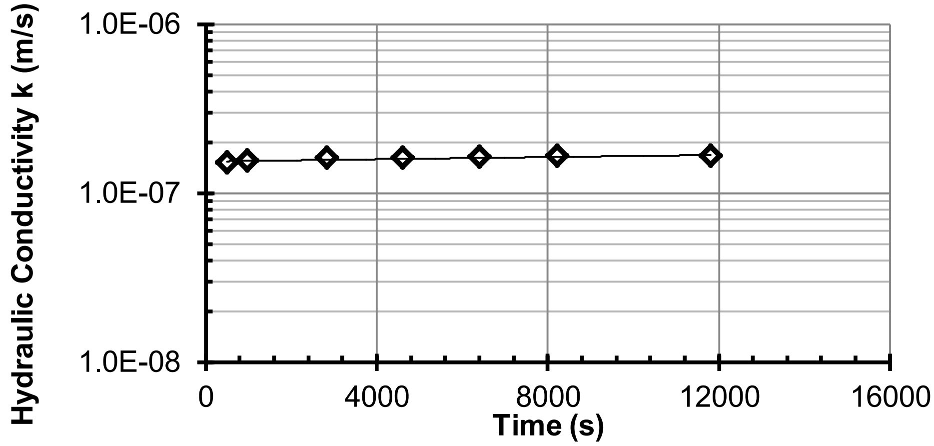


Figure XI-10. Constant head test results at 160 kPa for A5

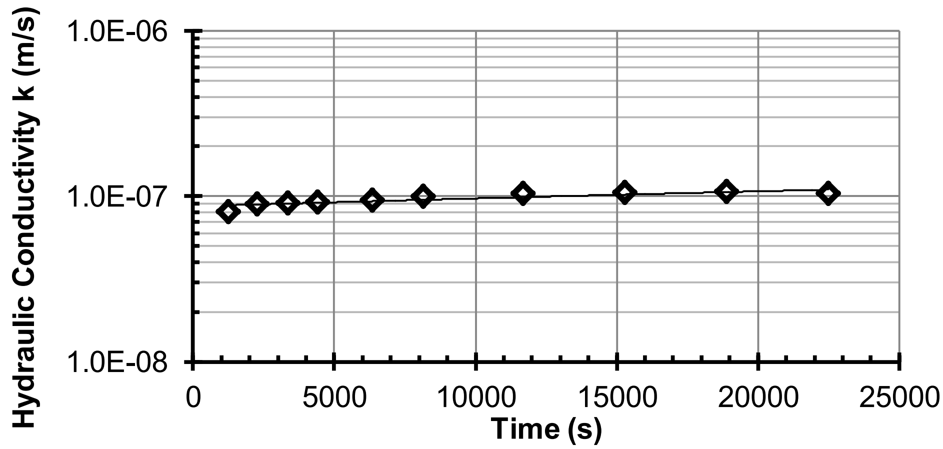


Figure XI-11. Constant head test results at 280 kPa for A5

Table XI-10. Hydraulic conductivity (k) measurements at 380 kPa for A5

| Sample Height = 5.712 cm ; i = 0.1 | | | | | |
|---|---|---|---|---|---|
| Distance (m) | Cumlative Distance (m) | Time (s) | Velocity (m/s) | Flow rate, Q ($m^3$/s) | k (=Q/Ai) (m/s) |
| 0.545 | 0 | 0 | 0 | 0 | 0 |
| 0.536 | 0.009 | 2100 | 4.3E-06 | 5.4E-11 | 5.6E-08 |
| 0.526 | 0.019 | 3900 | 4.9E-06 | 6.1E-11 | 6.4E-08 |
| 0.516 | 0.029 | 5700 | 5.1E-06 | 6.4E-11 | 6.6E-08 |
| 0.506 | 0.039 | 7500 | 5.2E-06 | 6.5E-11 | 6.8E-08 |
| 0.498 | 0.047 | 9300 | 5.1E-06 | 6.4E-11 | 6.6E-08 |
| 0.487 | 0.058 | 11100 | 5.2E-06 | 6.6E-11 | 6.8E-08 |
| 0.476 | 0.069 | 12960 | 5.3E-06 | 6.7E-11 | 7.0E-08 |
| 0.465 | 0.080 | 14820 | 5.4E-06 | 6.8E-11 | 7.0E-08 |

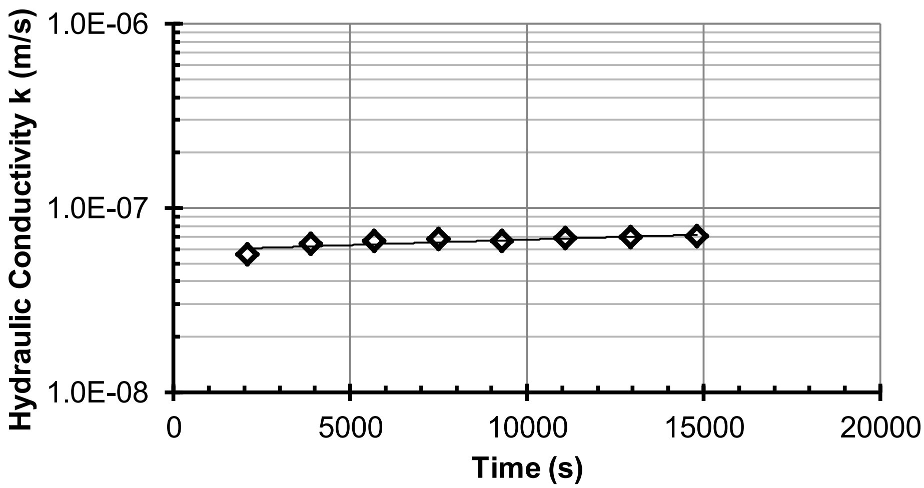


Figure XI-12. Constant head test results at 380 kPa for A5

Table XI-11. Hydraulic Conductivity (k) measurements at 500 kPa for A5

| Sample Height = 5.711 cm ; i = 0.1 | | | | | |
|---|---|---|---|---|---|
| Distance (m) | Cumlative Distance (m) | Time (s) | Velocity (m/s) | Flow rate, Q ($m^3$/s) | k (=Q/Ai) (m/s) |
| 0.550 | 0 | 0 | 0 | 0 | 0 |
| 0.546 | 0.004 | 1800 | 2.2E-06 | 2.8E-11 | 4.1E-08 |
| 0.543 | 0.007 | 3600 | 1.9E-06 | 2.4E-11 | 3.6E-08 |
| 0.538 | 0.012 | 7200 | 1.7E-06 | 2.1E-11 | 3.0E-08 |
| 0.533 | 0.017 | 10800 | 1.6E-06 | 2.0E-11 | 2.9E-08 |
| 0.529 | 0.021 | 14400 | 1.5E-06 | 1.8E-11 | 2.7E-08 |
| 0.523 | 0.027 | 18000 | 1.5E-06 | 1.9E-11 | 2.7E-08 |
| 0.515 | 0.035 | 21600 | 1.6E-06 | 2.0E-11 | 3.0E-08 |
| 0.504 | 0.046 | 28800 | 1.6E-06 | 2.0E-11 | 2.9E-08 |
| 0.496 | 0.054 | 32400 | 1.7E-06 | 2.1E-11 | 3.0E-08 |
| 0.385 | 0.165 | 82800 | 2.0E-06 | 2.5E-11 | 3.6E-08 |
| 0.378 | 0.172 | 86400 | 2.0E-06 | 2.5E-11 | 3.6E-08 |

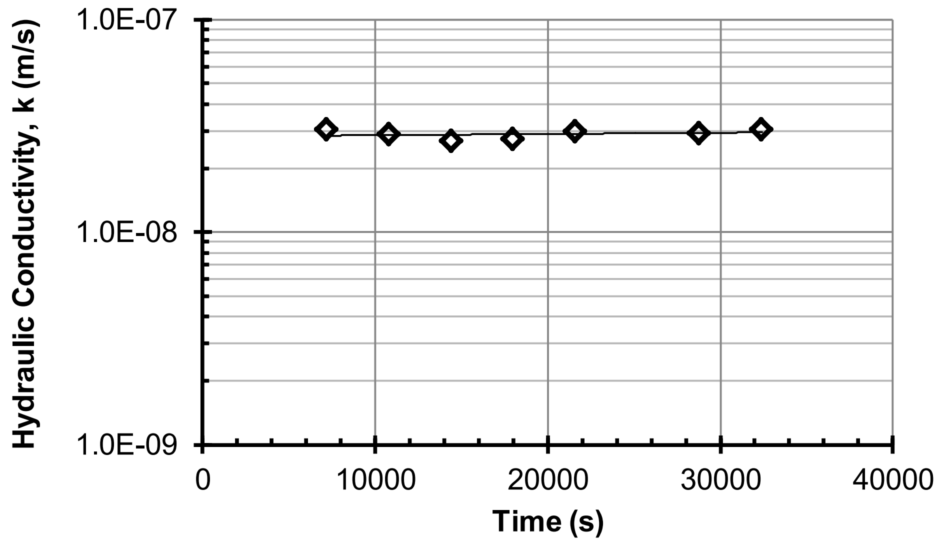


Figure XI-13. Constant head test results at 500 kPa for A5

3.2 Flume A3 Data

Table XI-12. Hydraulic conductivity (k) measurement at 0.4 kPa for A3

| Sample Height = 6.640 cm ; i = 0.1 | | | | | |
|---|---|---|---|---|---|
| Distance (m) | Cumlative Distance (m) | Time (s) | Velocity (m/s) | Flow rate, Q ($m^3$/s) | k (=Q/Ai) (m/s) |
| 0.525 | 0 | 0 | 0 | 0 | 0 |
| 0.520 | 0.005 | 100 | 5.0E-05 | 6.3E-10 | 6.6E-07 |
| 0.515 | 0.010 | 202 | 5.0E-05 | 6.2E-10 | 6.6E-07 |
| 0.510 | 0.015 | 293 | 5.1E-05 | 6.4E-10 | 6.8E-07 |
| 0.505 | 0.020 | 396 | 5.1E-05 | 6.3E-10 | 6.7E-07 |
| 0.500 | 0.025 | 485 | 5.2E-05 | 6.5E-10 | 6.8E-07 |
| 0.495 | 0.030 | 576 | 5.2E-05 | 6.5E-10 | 6.9E-07 |
| 0.490 | 0.035 | 692 | 5.1E-05 | 6.4E-10 | 6.7E-07 |
| 0.485 | 0.040 | 752 | 5.3E-05 | 6.7E-10 | 7.1E-07 |
| 0.480 | 0.045 | 850 | 5.3E-05 | 6.7E-10 | 7.1E-07 |
| 0.475 | 0.050 | 933 | 5.4E-05 | 6.7E-10 | 7.1E-07 |
| 0.470 | 0.055 | 1032 | 5.3E-05 | 6.7E-10 | 7.1E-07 |
| 0.465 | 0.060 | 1119 | 5.4E-05 | 6.7E-10 | 7.1E-07 |
| 0.460 | 0.065 | 1210 | 5.4E-05 | 6.8E-10 | 7.1E-07 |
| 0.455 | 0.070 | 1298 | 5.4E-05 | 6.8E-10 | 7.2E-07 |
| 0.450 | 0.075 | 1389 | 5.4E-05 | 6.8E-10 | 7.2E-07 |
| 0.445 | 0.080 | 1481 | 5.4E-05 | 6.8E-10 | 7.2E-07 |
| 0.440 | 0.085 | 1567 | 5.4E-05 | 6.8E-10 | 7.2E-07 |
| 0.435 | 0.090 | 1655 | 5.4E-05 | 6.8E-10 | 7.2E-07 |
| 0.430 | 0.095 | 1744 | 5.4E-05 | 6.8E-10 | 7.2E-07 |
| 0.425 | 0.100 | 1836 | 5.4E-05 | 6.8E-10 | 7.2E-07 |
| 0.415 | 0.110 | 2007 | 5.5E-05 | 6.9E-10 | 7.3E-07 |
| 0.405 | 0.120 | 2185 | 5.5E-05 | 6.9E-10 | 7.3E-07 |

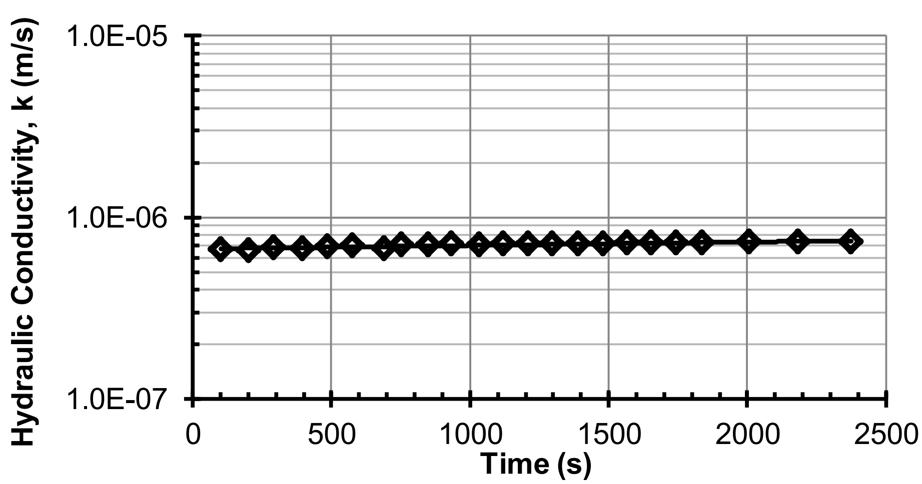


Figure XI-14. Constant head test results at 0.4 kPa for A3

Table XI-13. Hydraulic conductivity (k) measurement at 4.4 kPa for A3

| Sample Height = 6.630 cm ; i = 0.7 | | | | | |
|---|---|---|---|---|---|
| Distance (m) | Cumlative Distance (m) | Time (s) | Velocity (m/s) | Flow rate, Q ($m^3$/s) | k (=Q/Ai) (m/s) |
| 0.535 | 0 | 0 | 0 | 0 | 0 |
| 0.530 | 0.005 | 24 | 2.1E-04 | 2.6E-09 | 4.6E-07 |
| 0.525 | 0.010 | 48 | 2.1E-04 | 2.6E-09 | 4.6E-07 |
| 0.520 | 0.015 | 74 | 2.0E-04 | 2.5E-09 | 4.5E-07 |
| 0.515 | 0.020 | 98 | 2.0E-04 | 2.6E-09 | 4.5E-07 |
| 0.510 | 0.025 | 127 | 2.0E-04 | 2.5E-09 | 4.3E-07 |
| 0.505 | 0.030 | 155 | 1.9E-04 | 2.4E-09 | 4.3E-07 |
| 0.500 | 0.035 | 183 | 1.9E-04 | 2.4E-09 | 4.2E-07 |
| 0.495 | 0.040 | 213 | 1.9E-04 | 2.4E-09 | 4.1E-07 |
| 0.490 | 0.045 | 245 | 1.8E-04 | 2.3E-09 | 4.1E-07 |
| 0.485 | 0.050 | 279 | 1.8E-04 | 2.3E-09 | 4.0E-07 |
| 0.480 | 0.055 | 313 | 1.8E-04 | 2.2E-09 | 3.9E-07 |
| 0.475 | 0.060 | 350 | 1.7E-04 | 2.2E-09 | 3.8E-07 |
| 0.470 | 0.065 | 391 | 1.7E-04 | 2.1E-09 | 3.7E-07 |
| 0.465 | 0.070 | 438 | 1.6E-04 | 2.0E-09 | 3.5E-07 |
| 0.460 | 0.075 | 499 | 1.5E-04 | 1.9E-09 | 3.3E-07 |
| 0.455 | 0.080 | 569 | 1.4E-04 | 1.8E-09 | 3.3E-07 |
| 0.450 | 0.085 | 686 | 1.2E-04 | 1.6E-09 | 2.7E-07 |
| 0.445 | 0.090 | 865 | 1.0E-04 | 1.3E-09 | 2.3E-07 |
| 0.440 | 0.095 | 1297 | 7.3E-05 | 9.2E-10 | 1.6E-07 |
| 0.438 | 0.097 | 1765 | 5.5E-05 | 6.9E-10 | 1.2E-07 |

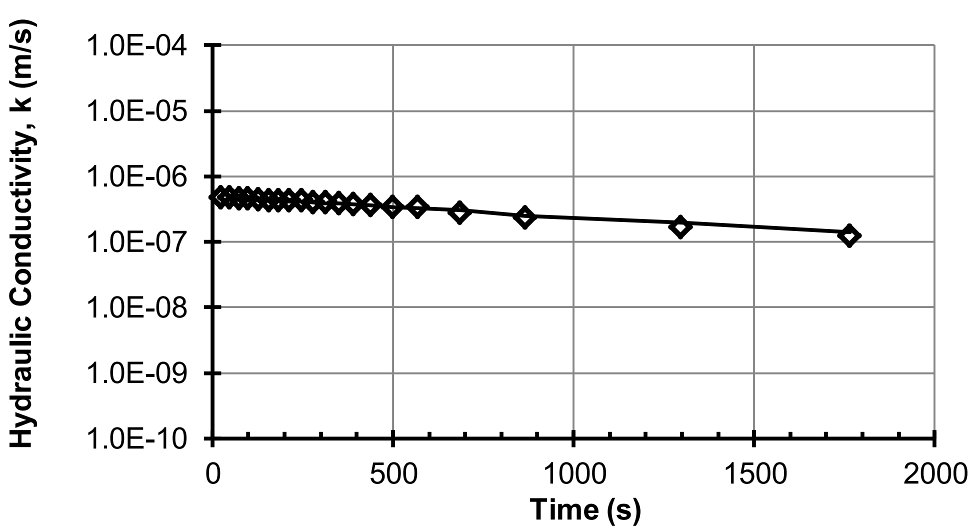


Figure XI-15. Constant head test results at 4.4 kPa for A3

Table XI-14. Hydraulic conductivity (k) measurement at 10 kPa for A3

| Sample Height = 6.626 cm ; i = 1.3 | | | | | |
|---|---|---|---|---|---|
| Distance (m) | Cumlative Distance (m) | Time (s) | Velocity (m/s) | Flow rate, Q ($m^3$/s) | k (=Q/Ai) (m/s) |
| 0.500 | 0.000 | 0 | 0 | 0 | 0 |
| 0.495 | 0.005 | 17 | 2.9E-04 | 3.7E-09 | 3.8E-07 |
| 0.490 | 0.010 | 33 | 3.0E-04 | 3.8E-09 | 3.9E-07 |
| 0.485 | 0.015 | 50 | 3.0E-04 | 3.8E-09 | 3.8E-07 |
| 0.480 | 0.020 | 67 | 3.0E-04 | 3.8E-09 | 3.8E-07 |
| 0.475 | 0.025 | 84 | 3.0E-04 | 3.7E-09 | 3.8E-07 |
| 0.470 | 0.030 | 100 | 3.0E-04 | 3.8E-09 | 3.8E-07 |
| 0.460 | 0.040 | 134 | 3.0E-04 | 3.8E-09 | 3.8E-07 |
| 0.450 | 0.050 | 175 | 2.9E-04 | 3.6E-09 | 3.6E-07 |
| 0.440 | 0.060 | 221 | 2.7E-04 | 3.4E-09 | 3.6E-07 |
| 0.430 | 0.070 | 285 | 2.5E-04 | 3.1E-09 | 3.1E-07 |
| 0.420 | 0.080 | 381 | 2.1E-04 | 2.6E-09 | 2.7E-07 |
| 0.410 | 0.090 | 542 | 1.7E-04 | 2.1E-09 | 2.1E-07 |
| 0.405 | 0.095 | 635 | 1.5E-04 | 1.9E-09 | 1.9E-07 |
| 0.400 | 0.100 | 764 | 1.3E-04 | 1.6E-09 | 1.7E-07 |
| 0.395 | 0.105 | 997 | 1.1E-04 | 1.3E-09 | 1.3E-07 |
| 0.393 | 0.107 | 1181 | 9.1E-05 | 1.1E-09 | 1.3E-07 |
| 0.392 | 0.109 | 1590 | 6.8E-05 | 8.6E-10 | 8.7E-08 |

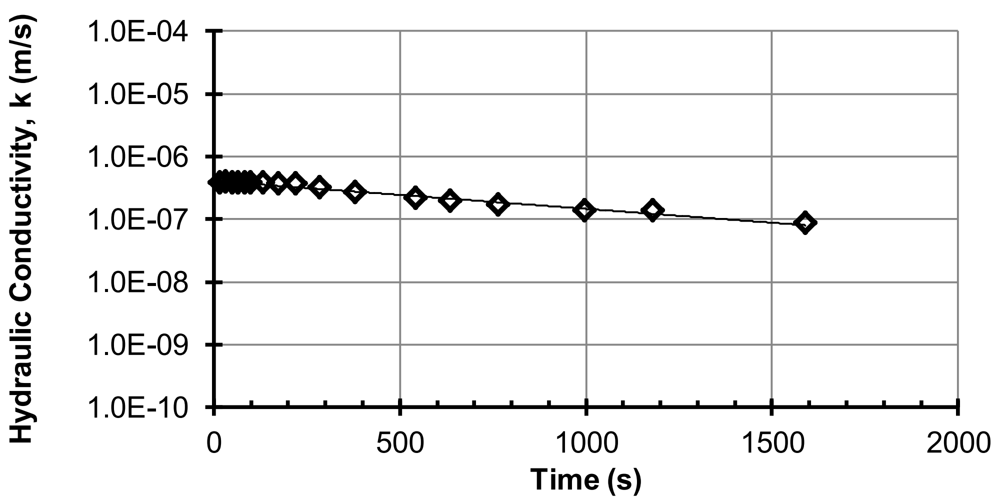


Figure XI-16. Constant head test results at 10 kPa for A3

Table XI-15. Hydraulic conductivity (k) measurements at 40 kPa for A3

| Sample Height = 6.625 cm ; i = 1.6 | | | | | |
|---|---|---|---|---|---|
| Distance (m) | Cumlative Distance (m) | Time (s) | Velocity (m/s) | Flow rate, Q (m3/s) | k (=Q/Ai) (m/s) |
| 0.400 | 0 | 0 | 0 | 0 | 0 |
| 0.395 | 0.005 | 32 | 1.6E-04 | 2.0E-09 | 1.6E-07 |
| 0.390 | 0.010 | 67 | 1.5E-04 | 1.9E-09 | 1.5E-07 |
| 0.385 | 0.015 | 114 | 1.3E-04 | 1.7E-09 | 1.3E-07 |
| 0.380 | 0.020 | 169 | 1.2E-04 | 1.5E-09 | 1.2E-07 |
| 0.375 | 0.025 | 242 | 1.0E-04 | 1.3E-09 | 1.0E-07 |
| 0.370 | 0.030 | 365 | 8.2E-05 | 1.0E-09 | 8.3E-08 |
| 0.365 | 0.035 | 532 | 6.6E-05 | 8.3E-10 | 6.6E-08 |
| 0.360 | 0.040 | 791 | 5.1E-05 | 6.4E-10 | 5.1E-08 |
| 0.355 | 0.045 | 1410 | 3.2E-05 | 4.0E-10 | 5.1E-08 |
| 0.353 | 0.047 | 2010 | 2.3E-05 | 2.9E-10 | 2.4E-08 |
| 0.351 | 0.049 | 2610 | 1.9E-05 | 2.4E-10 | 1.9E-08 |
| 0.349 | 0.051 | 3210 | 1.6E-05 | 2.0E-10 | 1.6E-08 |
| 0.348 | 0.052 | 3603 | 1.4E-05 | 1.8E-10 | 1.5E-08 |
| 0.346 | 0.054 | 3613 | 1.5E-05 | 1.9E-10 | 1.5E-08 |

Table XI-16. Hydraulic conductivity (k) measurement at 80 kPa for A3

| Sample Height = 6.624 cm ; i = 1.8 | | | | | |
|---|---|---|---|---|---|
| Distance (m) | Cumlative Distance (m) | Time (s) | Velocity (m/s) | Flow rate, Q (m3/s) | k (=Q/Ai) (m/s) |
| 0.440 | 0 | 0 | 0 | 0 | 0 |
| 0.430 | 0.010 | 43 | 2.3E-04 | 2.9E-09 | 2.0E-07 |
| 0.420 | 0.020 | 90 | 2.2E-04 | 2.8E-09 | 1.9E-07 |
| 0.415 | 0.025 | 116 | 2.2E-04 | 2.7E-09 | 1.9E-07 |
| 0.410 | 0.030 | 148 | 2.0E-04 | 2.5E-09 | 1.8E-07 |
| 0.383 | 0.057 | 450 | 1.3E-04 | 1.6E-09 | 1.1E-07 |
| 0.371 | 0.069 | 810 | 8.5E-05 | 1.1E-09 | 7.5E-08 |
| 0.362 | 0.078 | 1410 | 5.5E-05 | 7.0E-10 | 4.8E-08 |
| 0.356 | 0.084 | 2010 | 4.2E-05 | 5.3E-10 | 3.7E-08 |
| 0.352 | 0.088 | 2610 | 3.4E-05 | 4.2E-10 | 3.7E-08 |
| 0.349 | 0.091 | 3210 | 2.8E-05 | 3.6E-10 | 2.5E-08 |

Table XI-17. Hydraulic conductivity (k) measurement at 260 kPa for A3

| Sample Height = 6.610 cm ; i = 0.6 | | | | | |
|---|---|---|---|---|---|
| Distance (m) | Cumlative Distance (m) | Time (s) | Velocity (m/s) | Flow rate, Q (m3/s) | k (=Q/Ai) (m/s) |
| 0.540 | 0 | 0 | 0 | 0 | 0 |
| 0.525 | 0.015 | 300 | 5.0E-05 | 6.3E-10 | 1.3E-07 |
| 0.513 | 0.027 | 600 | 4.5E-05 | 5.7E-10 | 1.2E-07 |
| 0.444 | 0.096 | 2185 | 4.4E-05 | 5.5E-10 | 1.2E-07 |
| 0.358 | 0.182 | 4080 | 4.5E-05 | 5.6E-10 | 1.2E-07 |
| 0.270 | 0.270 | 6060 | 4.5E-05 | 5.6E-10 | 1.2E-07 |
| 0.193 | 0.347 | 7219 | 4.8E-05 | 6.0E-10 | 1.3E-07 |

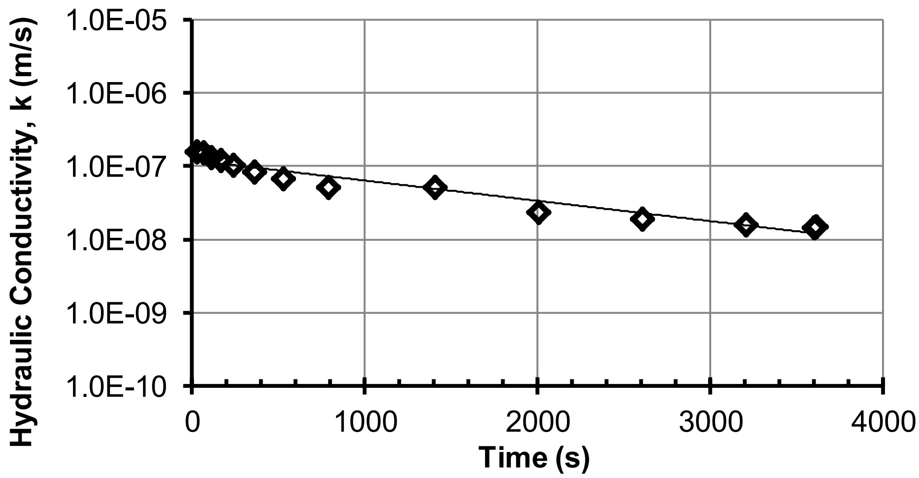


Figure XI-17. Constant head test results at 40 kPa for A3

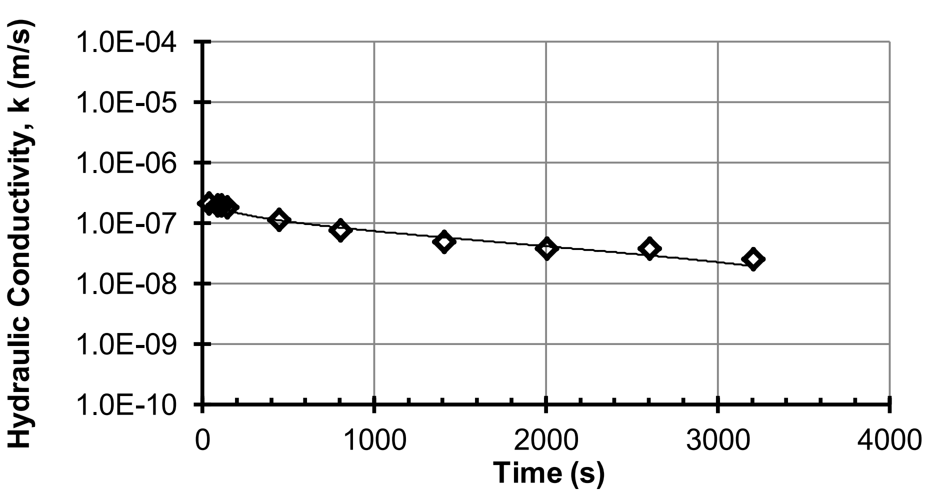


Figure XI-18. Constant head test results at 80 kPa for A3

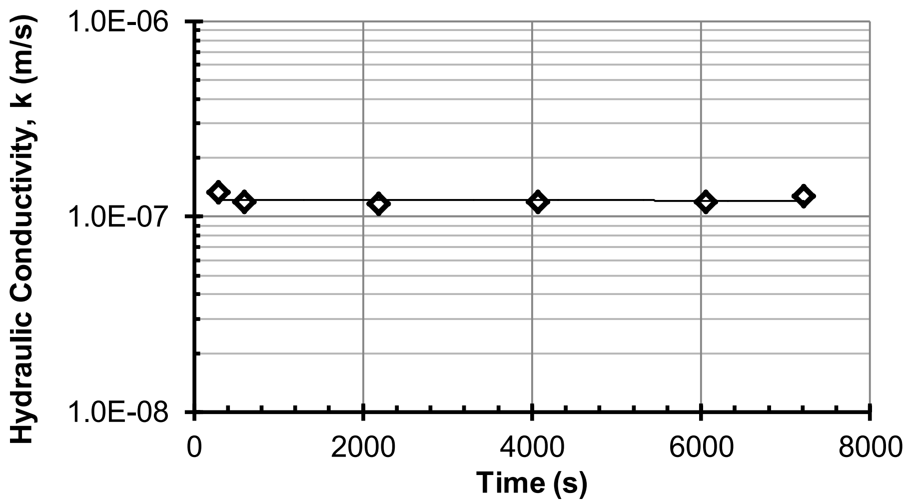

Figure XI-19. Constant head test results at 260 kPa for A3

Table XI-18. Hydraulic conductivity (k) measurement at 360 kPa for A3

| Sample Height = 6.605 cm ; i = 1.1 | | | | | |
|---|---|---|---|---|---|
| Distance (m) | Cumlative Distance (m) | Time (s) | Velocity (m/s) | Flow rate, Q (m3/s) | k (=Q/Ai) (m/s) |
| 0.540 | 0 | 0 | 0 | 0 | 0 |
| 0.530 | 0.010 | 140 | 7.1E-05 | 9.0E-10 | 1.0E-07 |
| 0.518 | 0.022 | 290 | 7.6E-05 | 9.5E-10 | 1.1E-07 |
| 0.510 | 0.030 | 402 | 7.5E-05 | 9.4E-10 | 1.1E-07 |
| 0.500 | 0.040 | 537 | 7.4E-05 | 9.4E-10 | 1.0E-07 |
| 0.490 | 0.050 | 668 | 7.5E-05 | 9.4E-10 | 1.1E-07 |
| 0.480 | 0.060 | 795 | 7.5E-05 | 9.5E-10 | 1.1E-07 |
| 0.469 | 0.071 | 930 | 7.6E-05 | 9.6E-10 | 1.1E-07 |
| 0.460 | 0.080 | 1050 | 7.6E-05 | 9.6E-10 | 1.1E-07 |
| 0.450 | 0.090 | 1170 | 7.7E-05 | 9.7E-10 | 1.1E-07 |
| 0.440 | 0.100 | 1295 | 7.7E-05 | 9.7E-10 | 1.1E-07 |
| 0.430 | 0.110 | 1414 | 7.8E-05 | 9.8E-10 | 1.1E-07 |
| 0.379 | 0.161 | 2042 | 7.9E-05 | 9.9E-10 | 1.1E-07 |
| 0.327 | 0.213 | 2676 | 8.0E-05 | 1.0E-09 | 1.1E-07 |
| 0.277 | 0.263 | 3273 | 8.0E-05 | 1.0E-09 | 1.1E-07 |
| 0.225 | 0.315 | 3840 | 8.2E-05 | 1.0E-09 | 1.2E-07 |
| 0.172 | 0.368 | 4560 | 8.1E-05 | 1.0E-09 | 1.1E-07 |

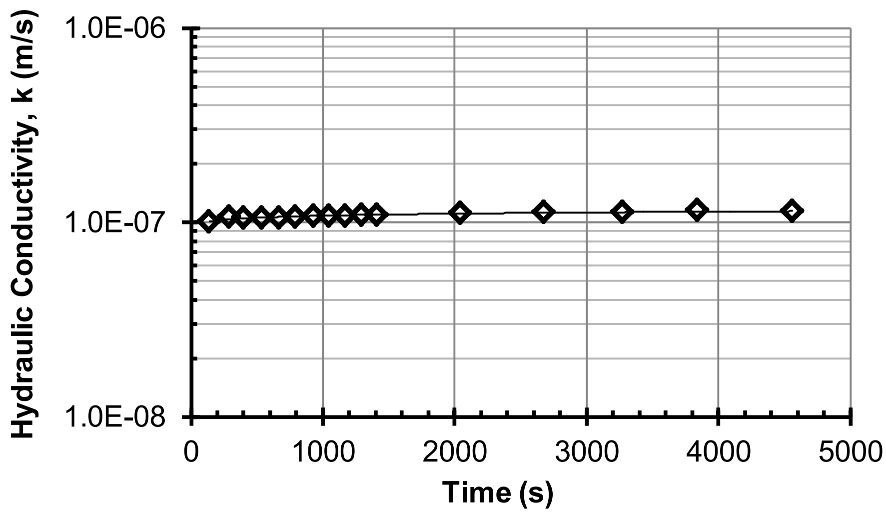


Figure XI-20. Constant head test results at 360 kPa for A3

Table XI-19. Hydraulic conductivity (k) measurement at 500 kPa for A3

| Sample Height = 6.592 cm ; i = 0.4 | | | | | |
|---|---|---|---|---|---|
| Distance (m) | Cumlative Distance (m) | Time (s) | Velocity (m/s) | Flow rate, Q (m3/s) | k (=Q/Ai) (m/s) |
| 0.52 | 0 | 0 | 0 | 0 | 0 |
| 0.47 | 0.05 | 668 | 7.5E-05 | 9.4E-10 | 3.3E-07 |
| 0.46 | 0.06 | 795 | 7.5E-05 | 9.5E-10 | 3.3E-07 |
| 0.45 | 0.07 | 930 | 7.5E-05 | 9.5E-10 | 3.3E-07 |
| 0.44 | 0.08 | 1050 | 7.6E-05 | 9.6E-10 | 3.3E-07 |
| 0.43 | 0.09 | 1170 | 7.7E-05 | 9.7E-10 | 3.3E-07 |
| 0.42 | 0.10 | 1295 | 7.7E-05 | 9.7E-10 | 3.4E-07 |
| 0.41 | 0.11 | 1414 | 7.8E-05 | 9.8E-10 | 3.4E-07 |
| 0.40 | 0.12 | 2042 | 5.9E-05 | 7.4E-10 | 2.6E-07 |
| 0.39 | 0.13 | 2676 | 4.9E-05 | 6.1E-10 | 2.1E-07 |
| 0.38 | 0.14 | 3273 | 4.3E-05 | 5.4E-10 | 1.9E-07 |
| 0.37 | 0.15 | 3840 | 3.9E-05 | 4.9E-10 | 1.7E-07 |
| 0.36 | 0.16 | 4560 | 3.5E-05 | 4.4E-10 | 1.5E-07 |

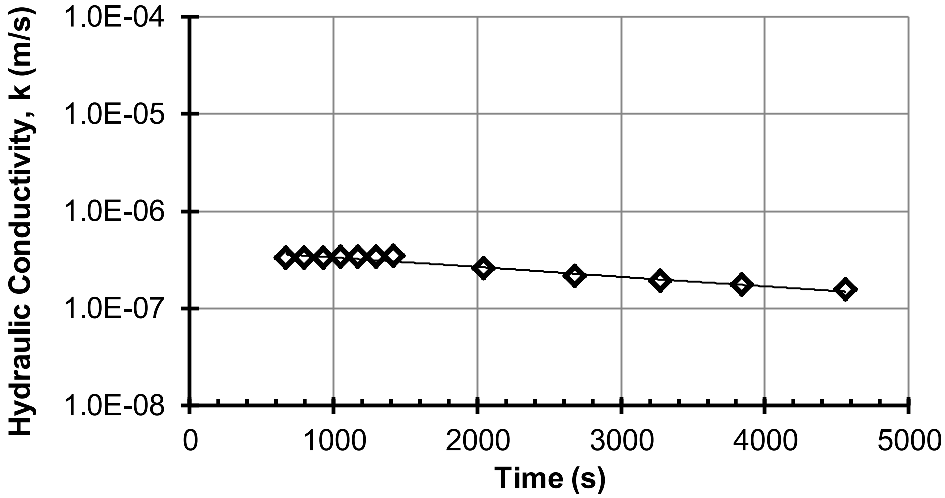

Figure XI-21. Constant head test results at 500 kPa for A3